

Peristaltic flow of Newtonian and Non-Newtonian
fluids in an asymmetric channel



By

Safia Akram



Department of Mathematics
Quaid-i-Azam University
Islamabad, Pakistan
2011

Peristaltic flow of Newtonian and Non-Newtonian
fluids in an asymmetric channel



By

Safia Akram

Supervised By

Dr. Sohail Nadeem

Department of Mathematics

Quaid-i-Azam University

Islamabad, Pakistan

2011

Peristaltic flow of Newtonian and Non-Newtonian
fluids in an asymmetric channel



By

Safia Akram

A Dissertation Submitted in the Partial Fulfillment of the requirements for the degree of

DOCTOR OF PHILOSOPHY

IN

MATHEMATICS

Supervised By

Dr. Sohail Nadeem

Department of Mathematics
Quaid-i-Azam University
Islamabad, Pakistan
2011

CERTIFICATE

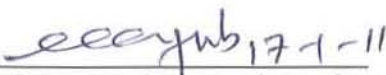
Peristaltic flow of Newtonian and Non-Newtonian fluids in an asymmetric channel

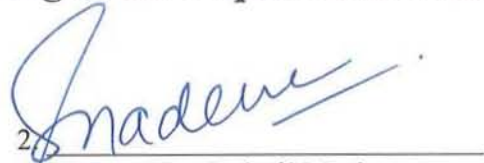
By

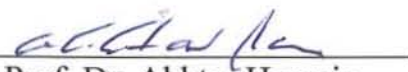
Safia Akram

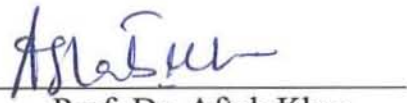
A DISSERTATION SUBMITTED IN THE PARTIAL FULFILLMENT OF THE REQUIREMENTS FOR THE DEGREE OF THE DOCTOR OF PHILOSOPHY

We accept this dissertation as conforming to the required standard

1. 
Prof. Dr. Muhammad Ayub
(Chairman)

2. 
Dr. Sohail Nadeem
(Supervisor)

3. 
Prof. Dr. Akhtar Hussain
(External Examiner)

4. 
Prof. Dr. Aftab Khan
(External Examiner)

Department of Mathematics
Quaid-i-Azam University
Islamabad, Pakistan
2011

Dedicated

To my

FAMILY

And

To My

Most Respected Supervisor

DR. SOHAIL NADEEM

ACKNOWLEDGEMENT

Praise is due to Allah whose worth cannot be described by speakers, whose bounties cannot be counted by calculators and whose claim cannot be satisfied by those who attempt to do so, whom the height of intellectual courage cannot appreciate and the dividing of understanding cannot reach. He for whose description no limit has been laid down, no eulogy exists, no time is ordained and no duration is fixed.

Verily Allah sent Muhammad (S.A.W) when none among the Arabs read the book or claimed prophet hood. He guided the people till he took them to their position and their salvation. So their spears become straight and their conditions settled down. I stand witness that there is no God but Allah the one, there is no partner for him nor is there with him any God other than himself and Muhammad (S.A.W) is his servant and his prophet.

I am heartily thankful to my supervisor *Dr. Sohail Nadeem* whose encouragement, guidance and support from the initial to the final level enabled me to develop an understanding of the subject.

I offer my regards and blessings to all of those teachers who supported me in any respect during the completion of the thesis.

This piece of research was completed on account of prays of my parents. I was unable to accomplish the task without their economic and moral help. I am thankful to my brothers and sisters, *Noman, Waqas, Gul-e-Rana and Ayesha*, whom I always found helpful, friendly and cooperative in every situation.

Last but not the least I am thankful to my friends *Asia Anjum, Tabinda Naz, Noreen Sher Akbar and Sadaf Ashiq* who have never left me alone for the whole academic session in QAU. Special gratitude is expressed to my colleagues *Capt Mariam Kayani, Aimen, Lt. Col. Anwar and Alia* for their valuable assistance and moral support in completion of my thesis work.

SAFIA AKRAM

Preface

Peristalsis pumping is a form of fluid transport which is generated by a progressive wave of area contraction or expansion along the walls of a distensible duct containing liquid. This kind of fluid transport appears in many biological organs such as urine transport from kidney to bladder through the ureter, movement of chyme in the gastrointestinal tract, the movements of spermatozoa in the ducts efferentes of the male reproductive tract and the ovum in the female fallopian tube, the locomotion of some worms, transport of lymph in the lymphatic vessels and vasomotion of small blood vessels such as arterioles, veins, and capillaries involve the peristaltic motion. In addition, peristaltic phenomena is used in industrial engineering, and biomechanical applications like sanitary fluid transport, blood pumps in heart lungs machine, roller and finger pumps and transport of corrosive fluids where the contact of the fluid with the machinery parts is prohibited. In view of these interesting applications, the peristaltic flows with different flow geometries for both Newtonian and non-Newtonian fluids have been reported analytically, numerically and experimentally by number of researchers. Most of these studies have been made under certain simplifying assumptions regarding the magnitudes of the wave amplitude, the wave length, the Reynolds number and the time mean flow. Analytically, these studies are investigated either in a fixed frame of reference or in a wave frame of reference moving with a constant velocity of the wave simplifying the study to a case with stationary wavy walls.

The study of motion of non-Newtonian fluids has applications in many areas. Due to complexity of fluids there are many models of non-Newtonian fluids each exhibits different properties. Only a limited attention has been focused to the study of non-Newtonian fluids in asymmetric channel. Physiologists observed that the intrauterine fluid flow due to myometrial contraction is peristaltic type motion and myometrial contraction may occur in both symmetric and asymmetric directions. Motivated from the applications and importance's highlighted above, the purpose of the present thesis is to discuss the peristaltic flows of Newtonian and non-Newtonian fluids in an asymmetric channel. It is worth mentioning that few new models have been modeled and presented in

this thesis which has not reported for peristaltic flow problems. The thesis has been organized in the following manner:

The literature survey and introduction on the subject is given in chapter zero. Chapter one is devoted to the study of heat transfer in a peristaltic flow of MHD fluid with partial slip. The peristaltic flow of a couple stress fluid under the effect of induced magnetic field in an asymmetric channel has been discussed in chapter two. In chapter three, we have examined the influence of heat transfer and magnetic field on a peristaltic transport of a Jeffrey fluid in an asymmetric channel with partial slip. Chapter four is devoted to the study of influence of induced magnetic field on the peristaltic motion of Jeffrey fluid in an asymmetric channel. The study of slip effects on the peristaltic flow of a Jeffrey fluid in an asymmetric channel under the effects of induced magnetic field is carried out in chapter five. The study of peristaltic flows of some new models such as six constant Jeffrey fluid, Walter's B fluid, hyperbolic tangent fluid and Williamson fluids are presented in chapter six to ten.

Contents

0	Introduction	5
1	Heat Transfer in a peristaltic flow of MHD fluid with partial slip	12
1.1	Introduction	12
1.2	Mathematical formulation	12
1.3	Volume flow rate	17
1.4	Solution of the problem	18
1.4.1	Adomian decomposition method	18
1.5	Results and discussion	21
1.6	Conclusion	22
2	Peristaltic flow of a couple stress fluid under the effect of induced magnetic field in an asymmetric channel	33
2.1	Introduction	33
2.2	Mathematical formulation	34
2.3	Solution of the problem	36
2.3.1	Exact solution	36
2.4	Results and discussion	40
2.5	Conclusion	50
3	Influence of heat transfer and magnetic field on a peristaltic transport of a Jeffrey fluid in an asymmetric channel with partial slip	51
3.1	Introduction	51

3.2	Mathematical formulation	52
3.3	Solution of the problem	55
3.3.1	Exact solution	55
3.3.2	Solution by Adomian decomposition method	56
3.4	Expressions for wave shape	58
3.5	Results and discussion	59
3.6	Conclusion	75
4	Influence of induced magnetic field on the peristaltic motion of a Jeffrey fluid in an asymmetric channel: Closed form solutions	76
4.1	Introduction	76
4.2	Mathematical formulation	77
4.3	Solution of the problem	79
4.3.1	Exact Solution	79
4.3.2	Solution by Adomian decomposition method	80
4.4	Expressions for different wave shape	83
4.5	Results and discussion	84
4.6	Conclusion	100
5	Slip effects on the peristaltic flow of a Jeffrey fluid in an asymmetric channel under the effects of induced magnetic field	101
5.1	Introduction	101
5.2	Mathematical formulation	102
5.3	Solution of the problem	102
5.3.1	Exact Solution	102
5.3.2	Solution by Adomian decomposition method	103
5.4	Expressions for different wave shapes	107
5.5	Results and discussion	107
5.6	Conclusion	121

6	Numerical and analytical solutions of peristaltic transport of a six constant Jeffreys model of fluid in a symmetric or asymmetric channel	123
6.1	Introduction	123
6.2	Mathematical formulation	123
6.3	Solution of the problem	128
6.3.1	Perturbation solution	128
6.3.2	Numerical solution	132
6.4	Results and discussion	134
6.5	Conclusion	147
7	Peristaltic motion of a Walter's B fluid in a symmetric or asymmetric channel	148
7.1	Introduction	148
7.2	Mathematical formulation	148
7.3	Solution of the problem	150
7.3.1	System of order δ^0 :	151
7.3.2	System of order δ^1 :	151
7.3.3	Solution for system of order δ^0	152
7.3.4	Solution for system of order δ^1	152
7.4	Results and discussion	154
7.5	Conclusion	164
8	Peristaltic transport of a hyperbolic tangent fluid model in an asymmetric channel	166
8.1	Introduction	166
8.2	Mathematical formulation	166
8.3	Solution of the problem	169
8.3.1	Perturbation solution	169
8.3.2	System of order We^0	169
8.3.3	System of order We^1	170
8.3.4	Solution for system of order We^0	170
8.3.5	Solution for system of order We^1	170

8.4	Results and discussion	172
8.5	Conclusion	181
9	Effects of partial slip on the peristaltic transport of a hyperbolic tangent fluid model in an asymmetric channel	182
9.1	Introduction	182
9.2	Mathematical formulation	183
9.3	Solution of the problem	183
9.4	Results and discussion	185
9.5	Conclusion	197
10	Peristaltic flow of a Williamson fluid in an asymmetric channel	198
10.1	Introduction	198
10.2	Mathematical formulation	198
10.3	Solution of the problem	201
10.3.1	Perturbation solution	201
10.4	Results and discussion	202
10.5	Conclusion	211

Chapter 0

Introduction

The word "Peristalsis" is derived from the Greek word "Peristalikos" which means clasp and compressing. Peristalsis is basically a mechanism of pumping fluids in tubes when a progressive wave of area contraction or expansion propagates along the length of a distensible tube containing fluid. In general terms it includes propulsive and mixing movements and pumps the fluids against pressure rise. Physiologically, peristalsis is an inherent property of smooth muscle contraction. Applications of peristalsis occur in swallowing food through the esophagus, urine transport from kidney to bladder through the ureter, transport of the spermatozoa in the ducts efferentes of the male reproductive tract, movement of the ovum in the fallopian tube, movement of the chyme in the gastrointestinal tract, the transport of lymph in the lymphatic vessels and the vasomotion in small blood vessels such as arterioles, veins and capillaries. The mechanism of peristaltic transport has been exploited for industrial applications like sanitary fluid transport, blood pumps in heart lung machine, transport of sensitive or corrosive fluids and transport of noxious fluids where the contact of the fluid with the machinery parts is prohibited.

The study of peristalsis in the context of fluid mechanics has received considerable attention in the recent times because of its relevance to biological systems and industrial applications. Peristalsis existed very well in physiology. Its relevance came about mainly through the works of Kill [1] and Boyarsky [2]. Later, several investigators studied the phenomenon both mathematically and experimentally to understand its mechanical aspects, in mechanical and physiological situations under various approximations. Latham [3] was probably the first to investigate the mechanism of peristalsis in relation to mechanical pumping. Burns and Parkes [4] studied the

peristaltic motion of a viscous fluid through a pipe and a channel by considering sinusoidal variation at the walls. Barton and Raynor [5] studied peristaltic flow in tubes using long wave approximation. Barton and Raynor also analyzed the case of low Reynolds number. Shapiro et al [6] studied the peristaltic transport of Newtonian fluid with long wave length and low Reynolds number approximation. They discussed the pressure mechanical efficiency, reflux limit and trapping limit in both two dimensional and axisymmetric cases by assuming infinite length of vessels. An elaborate review of the earlier literature regarding peristalsis is provided by Jaffrin and Shapiro [7]. Bohme and Friedrich [8] have investigated the peristaltic flow of viscoelastic liquids and have assumed that the relevant Reynolds number is small enough to neglect inertia forces and that the ratio of the wavelength and the channel height is large, which implies that the pressure rise is constant over the cross-section. Srivastava and Srivastava [9] have investigated the effects of power-law fluid in uniform and non-uniform tubes under zero Reynolds number and long wave length approximations. Takabatake et al. [10] have studied numerically the influence of finite wavelength and Reynolds number on the efficiency of peristaltic pumping.

Physiologists observed that the intra-uterine fluid flow due to myometrial contractions in peristaltic type motion and the myometrial contractions may occur in both symmetric and asymmetric directions. Several works have considered the peristaltic flows in asymmetric channel for the viscous fluid. Eytan et al. [11] have observed that the characterization of non-pregnant women uterine contractions is very complicated as they are composed of variable amplitude, frequencies and wave-lengths. It was observed that the width of the sagittal cross-section of the uterine cavity increases towards the fundus and the cavity is not fully occluded during the contractions. Recently, Eytan and Elad [12] have developed a mathematical model of wall-induced peristaltic fluid flow in a two dimensional channel with wave trains having a phase difference moving independently on the upper and lower walls to stimulate intra-uterine fluid motion in a sagittal cross-section of the uterus. They have obtained a time-dependent flow solution in a fixed frame by using lubrication theory. These results have been used to evaluate fluid flow pattern in a non-pregnant uterus. They have also calculated the possible particle trajectories to understand the transport of embryo before it gets implanted at the uterine wall. On the other hand, numerical technique using boundary integral method has been developed by Pozrikidis

[13] to investigate peristaltic transport in an asymmetric channel under Stokes flow conditions to understand the fluid dynamics involved. He has studied the stream line patterns and mean flow rate due to different amplitudes and phases of the wall deformation. Very few investigations dealing with the peristaltic flow in an asymmetric channel are available for viscous fluids. Very recently, Mishra and Rao [14] have discussed the peristalsis of a viscous fluid in an asymmetric channel under long wave length and low Reynolds number approximations. In another paper, Rao and Mishra [15] examined the effects of curvature on the peristaltic transport of a viscous fluid in an asymmetric channel by using wave number as the perturbation parameter. Haroun [16] has studied the effect of wall compliance on peristaltic transport of a Newtonian fluid in an asymmetric channel. A number of studies containing peristaltic flow in an asymmetric channel for viscous fluid have been investigated in Refs [17 – 18].

The study of non-Newtonian fluids has been an important subject in the field of chemical, biomedical and environmental engineering science. Undoubtedly, the mechanics of non-Newtonian fluids presents special challenges to engineers, physicists, modelers and mathematicians. This is due to the fact that non-linearity manifests itself in a variety of ways. The flows of non-Newtonian fluids are not only important because of their technological significance but also in the interesting mathematical features presented by the equations governing the flow. It is well known that such fluids cannot be described by the classical Navier-Stokes equations. Numerous models have been proposed to describe response characteristics of non-Newtonian fluids. These models can be classified as fluid of differential, rate and integral type. The constitutive equations in these fluid models are very complex due to a number of parameters. It has now been accepted that most of the physiological fluids behave like a non-Newtonian fluids. However, only a few recent studies have considered this aspect of the problem since the initial investigation by Raju and Devanathan [19]. Siddiqui and Schwarz [20] analyzed the mechanics of peristaltic pumping for non-Newtonian fluid through an axi-symmetric conduit. Quite a good number of studies pertaining to peristaltic flow of the non-Newtonian fluids have been carried out in the past [21 – 31] to analyze the rheological effects on the flow characteristics. In most of the mentioned studies, at least one of the parameters, namely the amplitude ratio, the ratio of the channel width to the wave length and the Reynolds number is assumed to be small. In all of the above studies the effects of an asymmetric channel have been neglected. There

is hardly an attempt available in the literature which deals with the peristaltic mechanism of non-Newtonian fluid in an asymmetric channel [32 – 41].

It is known that research of MHD flows has important applications in metallurgical industry, such as the cooling of continuous strips and filaments drawn through a quiescent fluid and the purification of molten metals from non-metallic inclusions. The MHD flows have numerous applications in bioengineering and medical sciences. Magnetic wound or cancer tumor treatment causing hyperthermia, bleeding reducing during surgeries and targeted transport of drugs using magnetic particles as drug carriers are few such examples. In living creature, blood is a biomagnetic fluid because of complex interaction of the intra cellular protein, cell membrane and the hemoglobin. The magnetohydrodynamic (MHD) flow of a fluid in a channel with elastic, rhythmically contracting walls is of interest in connection with certain problems of the movement of conductive physiological fluids e.g. the blood and with the need for theoretical research on the operation of a peristaltic MHD compressor. The effect of a moving magnetic field on blood flow was studied by stud et al. [42]. They observed that the effects of a suitable moving magnetic field accelerate the speed of blood. Srivastava and Agrawal [43] consider the blood as an electrically conducting fluid that constitutes a suspension of red cells in plasma. Agrawal and Anwaruddin [44] studied the effect of magnetic field on blood flow by taking a simple mathematical model for blood through an equally branched channel with flexible walls executing peristaltic waves using long wave length approximation method and observed for the flow of blood in arteries with arterial disease like arterial stenosis or arterio sclerosis, that the influence of magnetic field may be utilized as a blood pump in carrying out cardiac operations. Mekheimer [45] analyzed the MHD flow of a conducting couple stress fluid in a slit channel with rhythmically contracting walls. More recently, Kothandapani and Srinivas [46] have studied the influence of wall properties in the MHD peristaltic transport with heat transfer and porous medium. In all of these studies the effect of the induced magnetic field has been neglected.

The first investigation of the effect of the induced magnetic field on peristaltic flow was studied by Vishnyakov and Pavlov [47] where they considered the peristaltic MHD flow of a conductive Newtonian fluid by using the asymptotic narrow-band method to solve the problem. But they only obtained the velocity profiles in certain channel cross-sections for definite parameters values, and little attention was given to the induced magnetic field. Mention may

be made to the works of [48 – 50].

Heat transfer analysis can be used to obtain information about the properties of tissues. There are complicated temperature sensing systems in each organism. Heat stimulation influence life system greatly, and heat transfer in biological tissues involves complicated processes such as heat conduction in tissues, heat convection due to blood flow through the pores of tissues, and radiation heat transfer between surface and its environment and there is also mass transfer in these processes. Research on bioheat transfer studies heat and mass transfer in organisms. Research interest on flow and heat transfer phenomena in a channel/ tube has increased substantially in recent years due to developments in the electronic industry, micro-fabrication technologies, biomedical engineering etc. Moreover, with the investigative studies of the interaction between peristalsis and heat transfer where the thermodynamic aspects of blood have become significant in processes like oxygenation and hemodialysis. Radhakrishnamurthy et al. [51] and Varjavelu et al. [52] have investigated flow through vertical porous tube with peristalsis and heat transfer. Some interesting investigations related to this topic are given in Refs. [53 – 57]. Again, the available study eschews the effect of heat transfer on peristaltic flow in an asymmetric channel. Only limited attention is given to this type of flows [58 – 61].

Motivated by the extensive literature regarding the peristaltic flows of Newtonian and non-Newtonian fluids with different geometries, the aim of the present thesis is to analyze peristaltic flows of Newtonian and non-Newtonian fluids in an asymmetric channels. This thesis consists of eleven chapters, Chapter zero deals with basic literature survey and the other ten chapters are arranged as follows:

In chapter one, the effects of heat transfer and magnetic field on the peristaltic flow of a viscous fluid in an asymmetric channel under the assumptions of long wave length and low Reynolds number have been discussed. The problem is solved analytically and closed form solutions are computed with the help of Adomian decomposition method. The contents of this chapter have been published in **Communications in Nonlinear Science and Numerical Simulation** 15(2010)312-321.

Chapter two is devoted to the study of peristaltic flow of a couple stress fluid under the effects of induced magnetic field in an asymmetric channel. Making the assumptions of long wave length and low Reynolds number, the exact solution of the problem has been computed

and discussed. The contents of this chapter have been published in *Archive of Applied Mechanics*.

The influence of heat transfer and magnetic field on a peristaltic transport of a Jeffrey fluid in an asymmetric channel with partial slip condition has been examined in chapter three. The contents of this chapter have been accepted for publication in *Zeitschrift für Naturforschung A*.

In chapter four, we have examined the peristaltic motion of a two dimensional Jeffrey fluid in an asymmetric channel in the presence of induced magnetic field. An exact and closed form Adomian solution have been computed and discussed for different wave shapes. The work of this chapter is submitted for publication in *Zeitschrift für Naturforschung A*.

Chapter five described the slip and induced magnetic field effects on the peristaltic flow of a Jeffrey fluid in an asymmetric channel for different wave shapes. The closed form Adomian solution and exact solution have been found and discussed. The contents of this chapter have been published in *International journal for numerical methods in fluids*.

In chapter six, we have presented the peristaltic flow of a six constant Jeffrey fluid in an asymmetric channel. The governing equation of six constant Jeffrey fluid for two dimensional flow are modeled and then solved numerically and analytically. The work of this chapter is submitted in *Zeitschrift für Naturforschung A* for publication.

Chapter seven described the peristaltic motion of Walter's fluid model in an asymmetric channel. An analytical solution has been presented using regular perturbation method. The contents of this chapter have been submitted to *Chinese Physics Letter* for publication.

The peristaltic transport of a hyperbolic tangent fluid model in an asymmetric channel has been given in chapter eight. The governing equations of hyperbolic tangent fluid model are first modeled and then solved analytically. The contents of this chapter have been published in *Zeitschrift für Naturforschung A* 64a (2009)559-567.

In chapter nine, we have extended the idea of pervious chapter for partial slip boundary conditions. The contents of this chapter have been submitted to *Chinese physics Letter* for publication.

Chapter ten is devoted to the study of peristaltic flow of a Williamson fluid in an asymmetric channel. The modeling of Williamson fluid is given and the problem is solved analytically. This

chapter has been published in *Communications in Nonlinear Science and Numerical Simulation* 15(2010)1705-1716.

Chapter 1

Heat Transfer in a peristaltic flow of MHD fluid with partial slip

1.1 Introduction

In this chapter the effects of heat transfer and MHD on the peristaltic flow of a Newtonian fluid in an asymmetric channel is presented. The governing two dimensional equations are simplified using the assumption of long wave length and low Reynolds number. The reduced equations of motion and energy are solved analytically by Adomian decomposition method and found a closed form solution. The expression for pressure rise is computed using numerical integration recipe. At the end, the behavior of velocity, pressure rise, temperature and stream function are shown pictorially for different physical parameters of interest.

1.2 Mathematical formulation

We consider MHD flow of an electrically conducting viscous fluid in an asymmetric channel through porous medium in a two dimensional channel of width $d_1 + d_2$. The flow is generated by a sinusoidal wave trains propagating with constant speed c along the channel walls. We choose the rectangular coordinate system for the channel with X along the centerline of the channel and Y is transverse to it. The lower wall of the channel is maintained at temperature T_1 while the upper wall has temperature T_0 .

We assume that the fluid is subject to a constant transverse magnetic field B_0 . A very small magnetic Reynold number is assumed and hence the induced magnetic field can be neglected. When the fluid moves into magnetic field two major physical effects arise. The first one is that an electric field \mathbf{E} is induced in the flow. We shall assume that there is no excess charge density and therefore, $\nabla \cdot \mathbf{B} = 0$. Neglecting the induced magnetic field implies that $\nabla \times \mathbf{E} = 0$ and therefore, the induced electric field is negligible. The second effect is dynamically in nature, i.e., a Lorentz force ($\mathbf{J} \times \mathbf{B}$), where \mathbf{J} is the current density, this force acts on the fluid and modifies its motion. This results in the transfer of energy from the electromagnetic field to the fluid. In present study, the relativistic effects are neglected and the current density \mathbf{J} is given by the Ohm's law as

$$\mathbf{J} = \sigma (\mathbf{V} \times \mathbf{B}).$$

Since we are considering asymmetric channel therefore, the channel flow is produced due to different amplitudes and phases of the peristaltic waves on the channel. It is also assumed that the fluid particles near the walls are not same it means we are considering the partial slip conditions instead of usual no slip boundary conditions. A schematic diagram of the geometry of the problem under consideration is shown in Fig. (1.1).

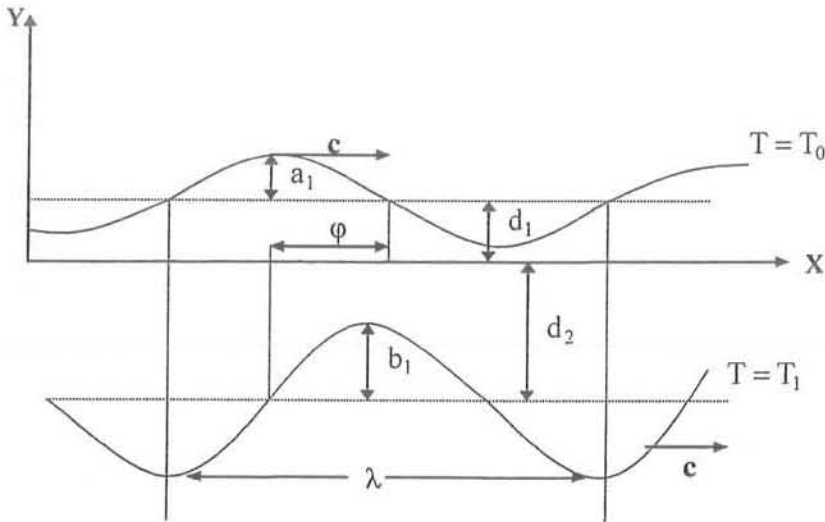


Fig.(1.1) : Schematic diagram of a two-dimensional asymmetric channel.

The geometry of the wall surface is defined as

$$\begin{aligned} Y &= H_1(X, t) = d_1 + a_1 \cos \left[\frac{2\pi}{\lambda} (X - ct) \right], \\ Y &= H_2(X, t) = -d_2 - b_1 \cos \left[\frac{2\pi}{\lambda} (X - ct) + \phi \right], \end{aligned} \quad (1.1)$$

where a_1 and b_1 are the amplitudes of the waves, λ is the wave length, $d_1 + d_2$ is the width of the channel, c is the velocity of propagation, t is the time and X is the direction of wave propagation. The phase difference ϕ varies in the range $0 \leq \phi \leq \pi$, in which $\phi = 0$ corresponds to symmetric channel with waves out of phase and $\phi = \pi$ the waves are in phase; further more, a_1, b_1, d_1, d_2 and ϕ satisfies the condition

$$a_1^2 + b_1^2 + 2a_1b_1 \cos \phi \leq (d_1 + d_2)^2.$$

The equations governing the flow of a are given by

(i) The continuity equation

$$\nabla \cdot \mathbf{V} = 0, \quad (1.2)$$

(ii) The equation of motion

$$\rho \left(\frac{\partial \mathbf{V}}{\partial t} + (\mathbf{V} \cdot \nabla) \mathbf{V} \right) = \text{div } \boldsymbol{\tau} + \mathbf{J} \times \mathbf{B} + \mathbf{R}, \quad (1.3)$$

where $\boldsymbol{\tau}$ for Newtonian fluid is defined as

$$\boldsymbol{\tau} = -P\mathbf{I} + \mu\mathbf{A}_1, \quad (1.4)$$

(iii) The energy equation

$$\rho \frac{de}{dt} = \boldsymbol{\tau} \cdot \mathbf{L}_1 - \text{div } \mathbf{Q}_1 + \rho \mathbf{r}. \quad (1.5)$$

In the above equation \mathbf{V} is the velocity vector, μ is the viscosity of the fluid, P is the pressure, \mathbf{J} is the current density, \mathbf{L}_1 is the velocity gradient, \mathbf{A}_1 is the first Rivlin-Ericksen tensor, $\mathbf{Q}_1 = (-K' \text{div } T, K'$ being the thermal conductivity) is the heat flux vector, \mathbf{r} is the internal heat generation (radial heating) taken here to be zero, and $e = (C'T, C'$ being specific heat) is the

specific internal energy.

We seek the velocity field for the two dimensional and two directional flow of the form

$$\mathbf{V} = (U(X, Y, t), V(X, Y, t), 0). \quad (1.6)$$

For the two dimensional incompressible flow, the governing equations of motion (including MHD and Darcy term) and energy are

$$\frac{\partial U}{\partial X} + \frac{\partial V}{\partial Y} = 0, \quad (1.7)$$

$$\frac{\partial U}{\partial t} + U \frac{\partial U}{\partial X} + V \frac{\partial U}{\partial Y} = -\frac{1}{\rho} \frac{\partial P}{\partial X} + \nu \left(\frac{\partial^2 U}{\partial X^2} + \frac{\partial^2 U}{\partial Y^2} \right) - \frac{\nu}{K} U - \sigma B_0^2 U, \quad (1.8)$$

$$\frac{\partial V}{\partial t} + U \frac{\partial V}{\partial X} + V \frac{\partial V}{\partial Y} = -\frac{1}{\rho} \frac{\partial P}{\partial Y} + \nu \left(\frac{\partial^2 V}{\partial X^2} + \frac{\partial^2 V}{\partial Y^2} \right) - \frac{\nu}{K} V, \quad (1.9)$$

$$C' \left[\frac{\partial T}{\partial t} + U \frac{\partial T}{\partial X} + V \frac{\partial T}{\partial Y} \right] = \frac{K'}{\rho} \nabla^2 T + \nu \phi_1, \quad (1.10)$$

where

$$\nabla^2 = \frac{\partial^2}{\partial X^2} + \frac{\partial^2}{\partial Y^2}, \quad \phi_1 = \left[2 \left(\frac{\partial U}{\partial X} \right)^2 + 2 \left(\frac{\partial V}{\partial X} \right)^2 + \left(\frac{\partial U}{\partial Y} + \frac{\partial V}{\partial X} \right)^2 \right],$$

U, V are the velocities in X and Y directions in fixed frame, ρ is constant density, ν is the kinematic viscosity, σ is the electrical conductivity, K is the permeability parameter, C' is the specific heat and T is the temperature.

Introducing a wave frame (x, y) moving with velocity c away from the fixed frame (X, Y) by the transformation

$$x = X - ct, \quad y = Y, \quad u = U - c, \quad v = V, \quad p(x) = P(X, t). \quad (1.11)$$

Define the following non-dimensional quantities

$$\begin{aligned}\bar{x} &= \frac{x}{\lambda}, \quad \bar{y} = \frac{y}{d_1}, \quad \bar{u} = \frac{u}{c}, \quad \bar{v} = \frac{v}{c}, \quad \delta = \frac{d_1}{\lambda}, \quad d = \frac{d_2}{d_1}, \quad \bar{p} = \frac{d_1^2 p}{\mu c \lambda}, \quad \bar{t} = \frac{ct}{\lambda}, \\ h_1 &= \frac{H_1}{d_1}, \quad h_2 = \frac{H_2}{d_2}, \quad a = \frac{a_1}{d_1}, \quad b = \frac{b_1}{d_1}, \quad \text{Re} = \frac{cd_1}{\nu}, \quad \bar{\Psi} = \frac{\Psi}{cd_1}, \quad \bar{K} = \frac{K}{d_1^2}, \\ \theta &= \frac{T - T_0}{T_1 - T_0}, \quad E_c = \frac{c^2}{C'(T_1 - T_0)}, \quad P_r = \frac{\rho \nu C'}{K'}, \quad M = \sqrt{\frac{\sigma}{\mu}} B_0 d_1.\end{aligned}\quad (1.12)$$

Using the transformation (1.11) and non-dimensional quantities (1.12), Eqs. (1.7) to (1.10) in terms of stream function $\Psi(u = \frac{\partial \Psi}{\partial y}, v = -\delta \frac{\partial \Psi}{\partial x})$ after dropping bars) can be written as

$$\text{Re} \delta (\Psi_y \Psi_{xy} - \Psi_x \Psi_{yy}) = -\frac{\partial p}{\partial x} + (\Psi_{yyy} + \delta^2 \Psi_{yxx}) - \left(M^2 + \frac{1}{K}\right) (\Psi_y + 1), \quad (1.13)$$

$$\text{Re} \delta^3 (\Psi_x \Psi_{xy} - \Psi_y \Psi_{xy}) = -\frac{\partial p}{\partial y} - (\delta^4 \Psi_{xxx} + \delta^2 \Psi_{xyy}) + \frac{\delta^2}{K} \Psi_x, \quad (1.14)$$

$$\text{Re} \delta (\theta_x \Psi_y - \theta_y \Psi_x) = \frac{\delta^2}{P_r} \theta_{xx} + \frac{1}{P_r} \theta_{yy} + E_c \left(4\delta^2 (\Psi_{xy})^2 + (\Psi_{yy} - \delta^2 \Psi_{xx})^2\right). \quad (1.15)$$

Under the assumptions of long wave length and low Reynolds number, Eqs. (1.13) to (1.15) become

$$\frac{\partial p}{\partial x} = \Psi_{yyy} - \frac{1}{K} (\Psi_y + 1) - M^2 (\Psi_y + 1), \quad (1.16)$$

$$\frac{\partial p}{\partial y} = 0, \quad (1.17)$$

$$\frac{1}{P_r} \theta_{yy} + E_c \Psi_{yy}^2 = 0. \quad (1.18)$$

Elimination of pressure between Eqs. (1.16) and (1.17) leads to the following governing equations

$$\Psi_{yyy} - \frac{1}{K} \Psi_{yy} - M^2 \Psi_{yy} = 0, \quad (1.19)$$

$$\frac{1}{P_r} \theta_{yy} + E_c \Psi_{yy}^2 = 0. \quad (1.20)$$

Since we are considering the partial slip on the wall, therefore, the corresponding non-dimensional

boundary conditions for the present problem can be written as

$$\begin{aligned}
 \Psi &= \frac{q}{2} \text{ at } y = h_1 = 1 + a \cos 2\pi x, \\
 \Psi &= -\frac{q}{2} \text{ at } y = h_2 = -d - b \cos(2\pi x + \phi), \\
 \frac{\partial \Psi}{\partial y} + L \frac{\partial^2 \Psi}{\partial y^2} &= -1 \text{ at } y = h_1, \\
 \frac{\partial \Psi}{\partial y} - L \frac{\partial^2 \Psi}{\partial y^2} &= -1 \text{ at } y = h_2,
 \end{aligned} \tag{1.21}$$

$$\begin{aligned}
 \theta &= 0 \text{ at } y = h_1, \\
 \theta &= 1 \text{ at } y = h_2,
 \end{aligned} \tag{1.22}$$

where q is the flux in the wave frame, L is the slip parameter, a , b , ϕ and d satisfy the relation

$$a^2 + b^2 + 2ab \cos \phi \leq (1 + d)^2.$$

1.3 Volume flow rate

The instantaneous volume flow rate in the fixed frame is given by

$$F^* = \int_{H_1}^{H_2} U(X, Y, t) dY, \tag{1.23}$$

where H_1 and H_2 are function of X and t .

The rate of volume flow in the wave frame is given by

$$f = \int_{h_1}^{h_2} u(x, y) dy, \tag{1.24}$$

where h_1 and h_2 are function of x alone. With the help of Eqs. (1.11), (1.23) and (1.24), we find that the two rates of volume flow are related through

$$F^* = f + ch_1 - ch_2. \tag{1.25}$$

The time mean flow over a period T^* at a fixed position X is defined as

$$\bar{F} = \frac{1}{T^*} \int_0^{T^*} F^* dt. \quad (1.26)$$

Substituting Eq. (1.25) into Eq. (1.26), and integrating, we get

$$\bar{F} = f + cd_1 + cd_2. \quad (1.27)$$

Defining the dimensionless time-mean flows Q and q in the fixed and wave frame respectively as

$$Q = \frac{\bar{F}}{cd_1} \quad \text{and} \quad q = \frac{f}{cd_1}. \quad (1.28)$$

Using Eq. (1.28) in Eq. (1.27), we get

$$Q = q + 1 + d. \quad (1.29)$$

1.4 Solution of the problem

1.4.1 Adomian decomposition method

According to Adomian decomposition method [62 – 65], we write Eq. (1.19) in the operator form as

$$\hat{L}_{yyyy} \Psi = \left(\frac{1}{K} + M^2 \right) \Psi_{yy}. \quad (1.30)$$

Applying the inverse operator $\hat{L}_{yyyy}^{-1} = \int \int \int \int [\cdot] dy dy dy dy$, we can write Eq. (1.30) as

$$\Psi = C_0 + C_1 y + C_2 \frac{y^2}{2!} + C_3 \frac{y^3}{3!} + \frac{1}{A} \hat{L}_{yyyy}^{-1} (\Psi_{yy}), \quad (1.31)$$

where

$$\frac{1}{A} = \frac{1}{K} + M^2,$$

C_0, C_1, C_2, C_3 are functions of x . Now we decompose Ψ as

$$\Psi = \sum_{n=0}^{\infty} \Psi_n. \quad (1.32)$$

Substituting Ψ into Eq. (1.31), we obtain

$$\begin{aligned}\Psi_0 &= C_0 + C_1 y + C_2 \frac{y^2}{2!} + C_3 \frac{y^3}{3!}, \\ \Psi_{n+1} &= \frac{1}{A} \int \int \int \int (\Psi_n)_{yy} dy dy dy dy, n \geq 0.\end{aligned}\tag{1.33}$$

Therefore,

$$\begin{aligned}\Psi_1 &= \frac{1}{A} \left(C_2 \frac{y^4}{4!} + C_3 \frac{y^5}{5!} \right), \\ \Psi_2 &= \frac{1}{A^2} \left(C_2 \frac{y^6}{6!} + C_3 \frac{y^7}{7!} \right), \\ &\vdots \\ \Psi_n &= \frac{1}{A^n} \left(C_2 \frac{y^{2n+2}}{(2n+2)!} + C_3 \frac{y^{2n+3}}{(2n+3)!} \right), n > 0.\end{aligned}\tag{1.34}$$

According to (1.32), the closed form of Ψ can be written as

$$\Psi = C_0 + C_1 y + AC_2 \left(\cosh \frac{y}{\sqrt{A}} - 1 \right) + A\sqrt{A}C_3 \left(\sinh \frac{y}{\sqrt{A}} - \frac{y}{\sqrt{A}} \right).$$

The above equation can be put in the simplest form as

$$\Psi = F_0 + F_1 y + F_2 \cosh \frac{y}{\sqrt{A}} + F_3 \sinh \frac{y}{\sqrt{A}},\tag{1.35}$$

where F_0, F_1, F_2, F_3 are functions of x . These constants are calculated using the boundary conditions (1.21) and are defined as

$$\begin{aligned}
F_0 &= \frac{-(h_1 + h_2) \left[q + \left(\frac{qL+2A}{\sqrt{A}} \right) \tanh \left[\frac{h_1-h_2}{2\sqrt{A}} \right] \right]}{2(h_1 - h_2) - 2 \left(\frac{L(h_2-h_1)+2A}{\sqrt{A}} \right) \tanh \left[\frac{h_1-h_2}{2\sqrt{A}} \right]}, \\
F_1 &= \frac{q + \left(\frac{qL+2A}{\sqrt{A}} \right) \tanh \left[\frac{h_1-h_2}{2\sqrt{A}} \right]}{(h_1 - h_2) - \left(\frac{L(h_2-h_1)+2A}{\sqrt{A}} \right) \tanh \left[\frac{h_1-h_2}{2\sqrt{A}} \right]}, \\
F_2 &= \frac{-\sqrt{A}(q + h_1 - h_2) \sec h \left[\frac{h_1-h_2}{2\sqrt{A}} \right] \sinh \left[\frac{h_1+h_2}{2\sqrt{A}} \right]}{(h_2 - h_1) + \left(\frac{L(h_2-h_1)+2A}{\sqrt{A}} \right) \tanh \left[\frac{h_1-h_2}{2\sqrt{A}} \right]}, \\
F_3 &= \frac{\sqrt{A}(q + h_1 - h_2) \sec h \left[\frac{h_1-h_2}{2\sqrt{A}} \right] \cosh \left[\frac{h_1+h_2}{2\sqrt{A}} \right]}{(h_2 - h_1) + \left(\frac{L(h_2-h_1)+2A}{\sqrt{A}} \right) \tanh \left[\frac{h_1-h_2}{2\sqrt{A}} \right]}. \tag{1.36}
\end{aligned}$$

Substituting Eq. (1.35) in Eq. (1.16), we get the axial pressure gradient as

$$\frac{dp}{dx} = \frac{(h_2 - h_1 - q) \left[1 + \frac{L}{\sqrt{A}} \tanh \left[\frac{h_1-h_2}{2\sqrt{A}} \right] \right]}{A \left(h_1 - h_2 - \left(\frac{L(h_2-h_1)+2A}{\sqrt{A}} \right) \tanh \left[\frac{h_1-h_2}{2\sqrt{A}} \right] \right)}. \tag{1.37}$$

Integrating (1.37) over one wavelength, we get

$$\Delta p = \int_0^1 \frac{dp}{dx} dx. \tag{1.38}$$

The axial velocity component in the fixed frame is given as

$$\begin{aligned}
U(X, Y, t) &= 1 + \Psi_y \\
&= \frac{2(h_1 - h_2 + q) \sinh \left[\frac{h_1-Y}{2\sqrt{A}} \right] \sinh \left[\frac{h_2-Y}{2\sqrt{A}} \right] - \frac{L(h_1-h_2+q)}{\sqrt{A}} \sinh \left[\frac{h_1-h_2}{2\sqrt{A}} \right]}{\left(\frac{L(h_2-h_1)+2A}{\sqrt{A}} \right) \sinh \left[\frac{h_1-h_2}{2\sqrt{A}} \right] - (h_1 - h_2) \cosh \left[\frac{h_1-h_2}{2\sqrt{A}} \right]}, \tag{1.39}
\end{aligned}$$

where

$$h_1 = 1 + a \cos [2\pi (X - t)] \quad \text{and} \quad h_2 = -d - b \cos [2\pi (X - t) + \phi].$$

It is noticed here that when $M = 0$, the solution of Hayat et al [18] is recovered and when $M = L = 0$, the solution of Elshehawey et al [17] is recovered.

Making use of Eq. (1.35), the solution of Eq. (1.20) satisfying the boundary conditions (1.22) can be written as

$$\begin{aligned} \theta = & -E_c P_r \left(\frac{F_2^2}{2A^2} Y^2 + \frac{1}{8A} (F_2^2 + F_3^2) \cosh 2 \left(\frac{Y}{\sqrt{A}} \right) - \frac{Y^2}{4A^2} (F_2^2 + F_3^2) \right. \\ & \left. + \frac{F_2 F_3}{4A} \sinh 2 \left(\frac{Y}{\sqrt{A}} \right) \right) + c_1 Y + c_2, \end{aligned} \quad (1.40)$$

where

$$\begin{aligned} c_1 = & \frac{-1}{(h_1 - h_2)} + \frac{E_c P_r}{(h_1 - h_2)} \left(\frac{F_2^2}{2A^2} (h_1^2 - h_2^2) - \frac{(h_1^2 - h_2^2)}{4A^2} (F_2^2 + F_3^2) \right. \\ & \left. + \frac{1}{8A} (F_2^2 + F_3^2) \left[\cosh 2 \left(\frac{h_1}{\sqrt{A}} \right) - \cosh 2 \left(\frac{h_2}{\sqrt{A}} \right) \right] \right. \\ & \left. + \frac{F_2 F_3}{4A} \left[\sinh 2 \left(\frac{h_1}{\sqrt{A}} \right) - \sinh 2 \left(\frac{h_2}{\sqrt{A}} \right) \right] \right), \\ c_2 = & E_c P_r \left(\frac{F_2^2}{2A^2} h_1^2 + \frac{1}{8A} (F_2^2 + F_3^2) \cosh 2 \left(\frac{h_1}{\sqrt{A}} \right) - \frac{h_1^2}{4A^2} (F_2^2 + F_3^2) \right. \\ & \left. + \frac{F_2 F_3}{4A} \sinh 2 \left(\frac{h_1}{\sqrt{A}} \right) \right) - c_1 h_1. \end{aligned} \quad (1.41)$$

1.5 Results and discussion

In this section results are presented and discussed for different physical quantities of interest. Pressure rise is important physical measures in peristaltic mechanism. Therefore, Figs. 1.2 to 1.4 are plotted to see the effects of partial slip L , magnetic field M , amplitude ratio ϕ on pressure rise. Fig. 1.2a represents the average pressure rise Δp against Q (the time average mean flow rate) for different values of slip parameter L . It is observed that pressure rise Δp increases ($\Delta p > 0$) for $Q < 1$ and for $Q > 1$, Δp has an opposite behavior ($\Delta p < 0$). The maximum pressure rise occur at $Q = -1$ and $\Delta p = 21$ for $K = 0.1$. Similar behavior of pressure rise is shown in Fig. 1.2b for $K = 1000$. But we observe here that for very large value of K the maximum pressure is $\Delta p = 6$. Thus we conclude that as we increase the value of K

the maximum pressure rise decreases. The effects of magnetic parameter M on Δp are shown in Figs. 1.3(a, b) for small and large K . It is seen that Δp increases for $Q < 0.6$ and after that Δp decreases. Figs. 1.4(a, b) show that Δp decreases when $Q < 2.4$ with an increase in ϕ and it increases when $Q > 2.4$. Figs. 1.5 and 1.6 are prepared to discuss the pressure gradient for different values of M and L . It is observed that pressure is maximum at $x = 0.5$ for $M = 1.5$ and $L = 0.04$. The velocity field for various values of K and M are plotted in Figs. 1.7 and 1.8. It is depicted from the Fig. 1.7 that for small value of K , the velocity represents a rectangular shape but as we increased the value of K its amplitude increases and finally it seems to be like a parabola. It is observed from Fig. 1.8 that with an increase in M , the amplitude of the velocity decreases in the center and near the channel wall the velocity increases. The temperature field for different values of L , P_r , M and E_c are shown in Figs. 1.9 to 1.12. It is observed from the figures that the increase in L and M the temperature field decreases while with an increase in P_r and E_c , the temperature field increases. Trapping is another interesting phenomena in peristaltic motion. It is basically the formation of an internally circulating bolus of fluid by closed streamlines. This trapped bolus pushed a head along with the peristaltic wave. Fig. 1.13 illustrate the streamline graphs for different values of L . It is observed that with an increase in slip parameter L the size of trapped bolus decreases. The streamlines for different values of mean flow rate Q are shown in Fig. 1.14. It is evident from the figures that the size of the trapped bolus increases by increasing Q . It is also observed that the number of trapped bolus decreases. The streamlines for different values of amplitude ratio ϕ are shown in Fig. 1.15. It is observed that with an increase in ϕ , the size and number of trapped bolus decreases.

1.6 Conclusion

This chapter presents the influence of heat transfer and magnetic field on the peristaltic flow of a Newtonian fluid with partial slip. The governing two dimensional equations have been modeled and then simplified using long wave length approximation. The results are discussed through graphs. The main finding can be summarized as follows:

1. In the peristaltic pumping region the pressure rise increases with an increase in L and M , and decreases with an increase in ϕ .

2. The pressure gradient decreases with an increase in both M and L .
3. The velocity field increases with an increase in K and decreases with an increase in M .
4. The temperature field decreases with an increase in L and magnetic field M , while with an increase in P_r and E_c , the temperature field increases.
5. The size of the trapping bolus decreases by increasing L .
6. The size of the trapping bolus increases and number of the trapping bolus decreases by increasing Q .
7. The size and number of the trapping bolus decreases by increasing ϕ .
8. If $M = 0$ the solution of Hayat et al [18] is recovered and when $M = L = 0$, the solution of Elshehawey et al [17] are recovered as a special case of our analysis.

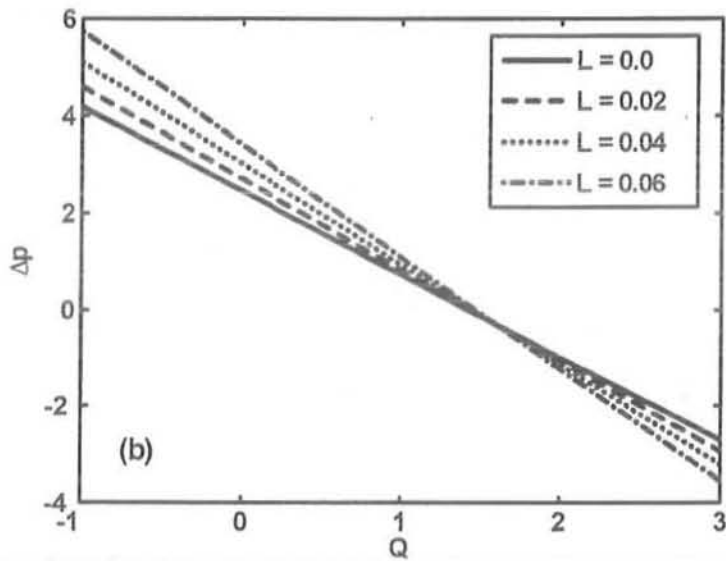
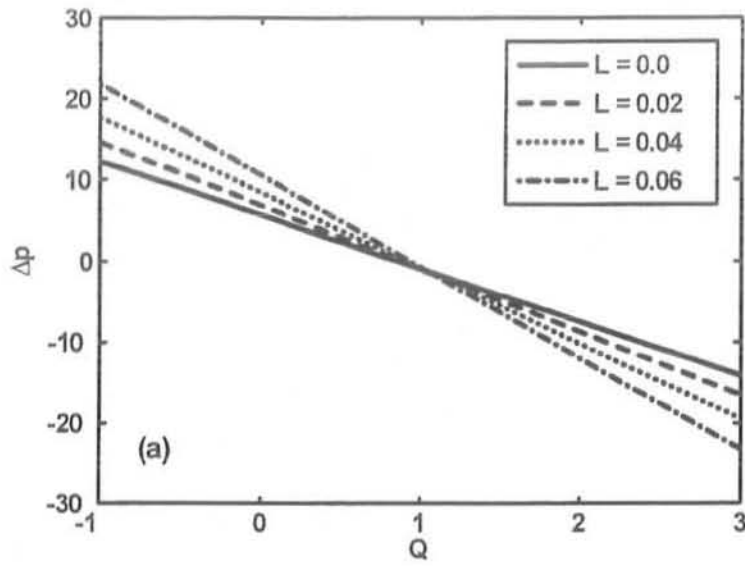


Fig.(1.2) : Variation of Q with Δp for different values of L at $a = 0.7$, $b = 1.2$, $d = 2$, $M = 0.1$, $\phi = \frac{\pi}{6}$ and (a) $K = 0.1$ (b) $K = 1000$.

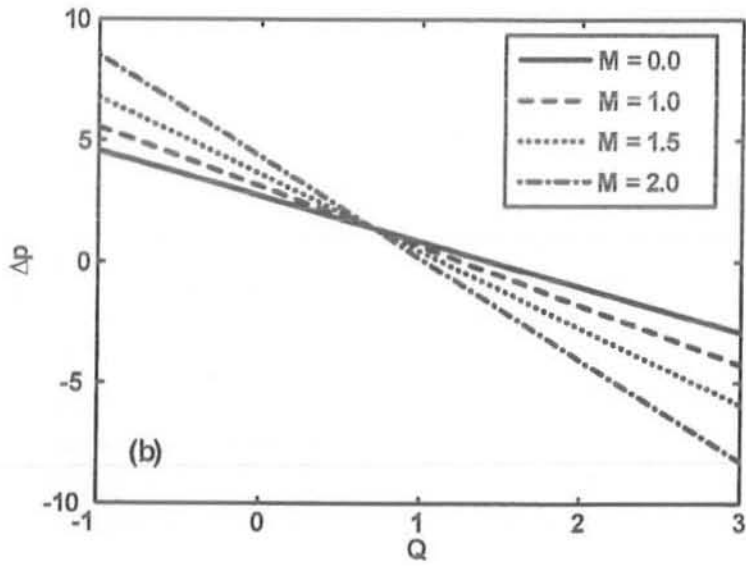
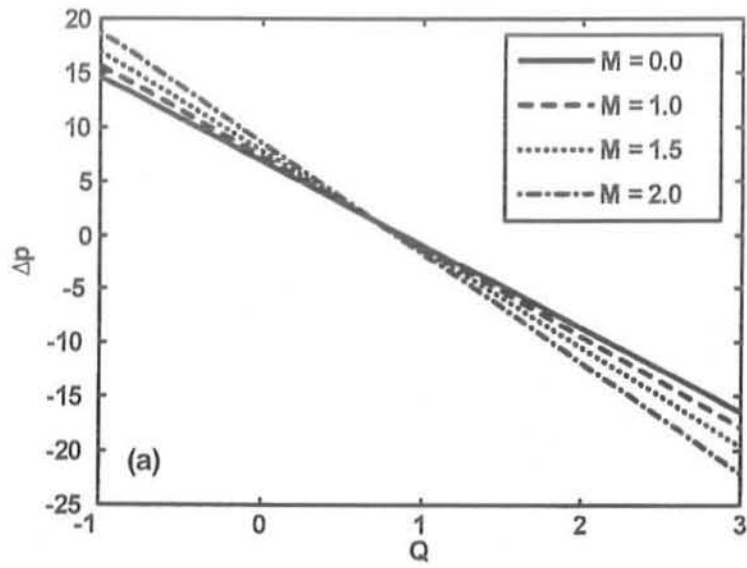


Fig.(1.3) : Variation of Q with Δp for different values of M at $a = 0.7$, $b = 1.2$, $d = 2$, $L = 0.02$, $\phi = \frac{\pi}{6}$ and (a) $K = 0.1$ (b) $K = 1000$.

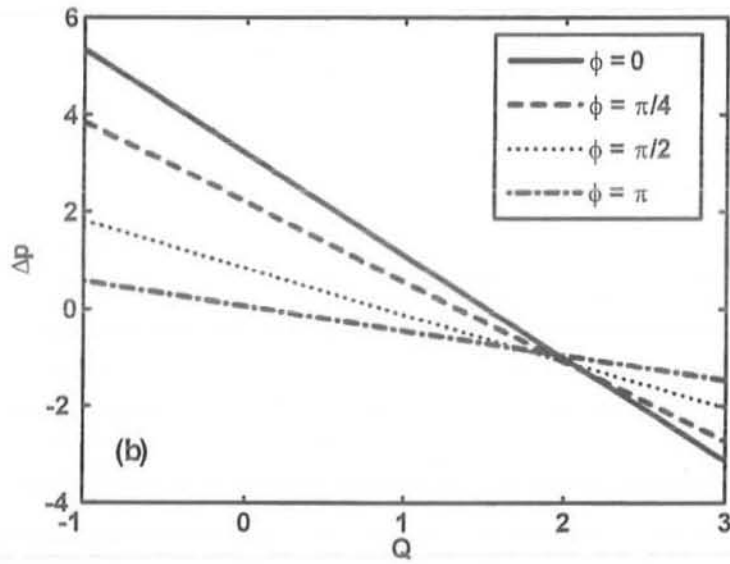
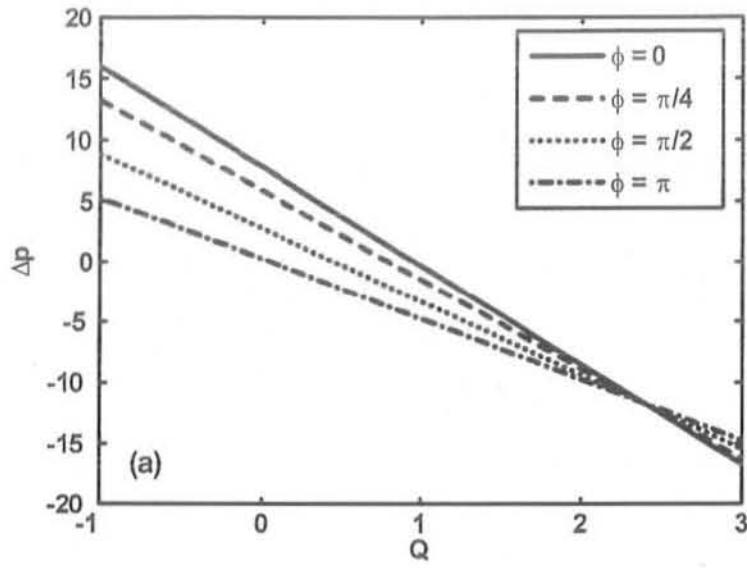


Fig.(1.4) : Variation of Q with Δp for different values of ϕ at $a = 0.7$, $b = 1.2$, $d = 2$, $M = 0.1$, $\phi = \frac{\pi}{6}$ and (a) $K = 0.1$ (b) $K = 1000$.

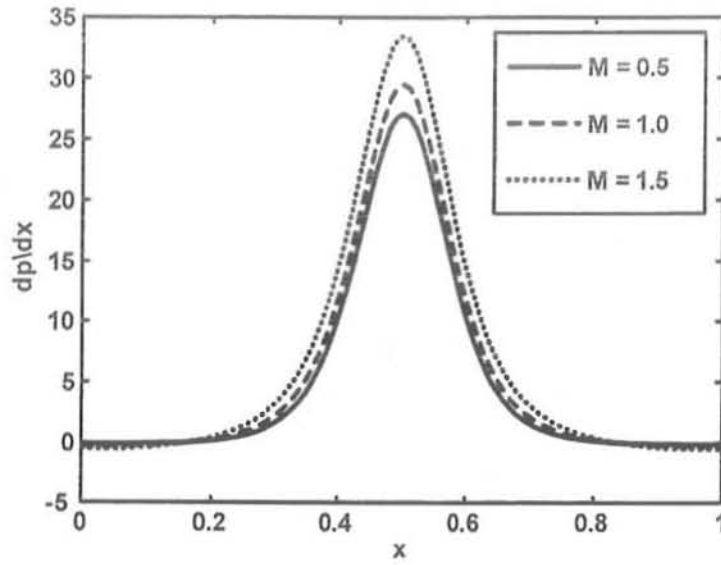


Fig. (1.5) : Variation of $\frac{dp}{dx}$ with x for different values of M at $a = 0.7$, $b = 1.2$, $d = 2$, $K = 1000$, $L = 0.001$, $Q = -1$, $\phi = 0.001$.

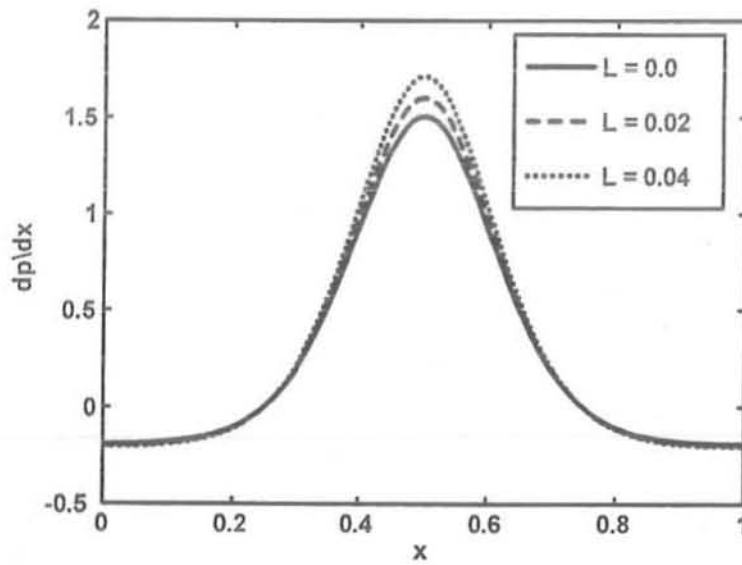


Fig. (1.6) : Variation of $\frac{dp}{dx}$ with x for different values of L at $a = 0.5$, $b = 0.5$, $d = 2$, $K = 1000$, $M = 0.1$, $Q = 0$, $\phi = 0.001$.

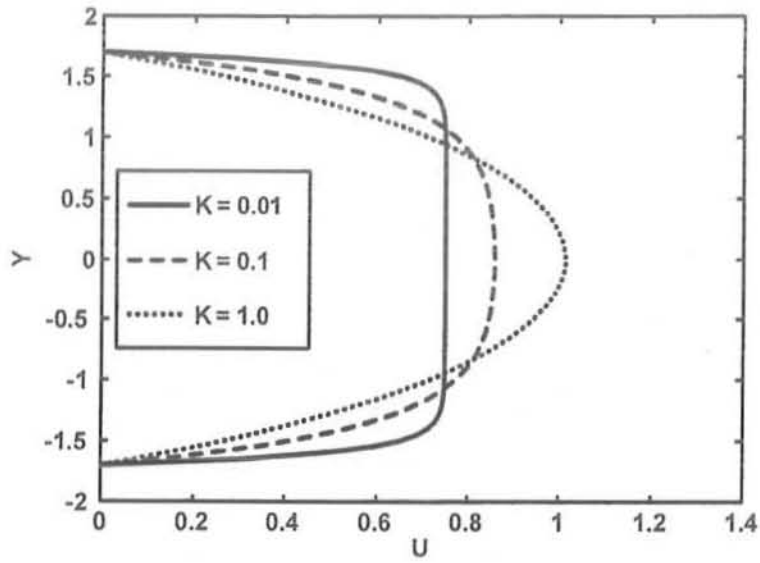


Fig. (1.7) : Velocity profile for different values of K at $a = 0.7, b = 0.7, d = 1.7, M = 0.1, X = 1, t = 1, L = 0.001, Q = 1.7, \phi = \frac{\pi}{2}$.

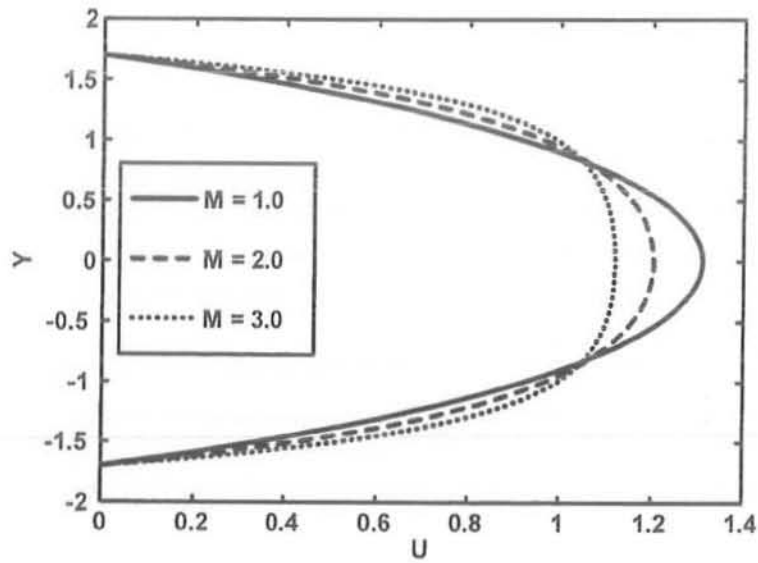


Fig. (1.8) : Velocity profile for different values of M at $a = 0.7, b = 0.7, d = 1.7, L = 0.02, X = 1, t = 1, L = 0.001, Q = 1.7, \phi = \frac{\pi}{2}$.

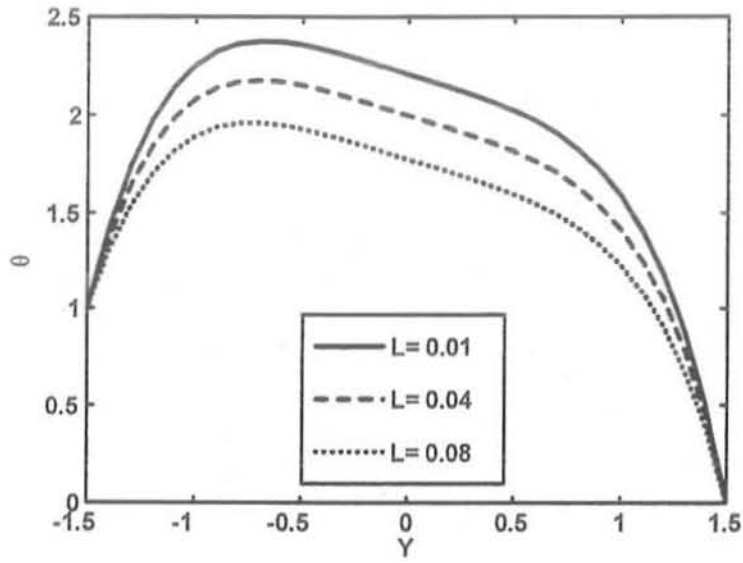


Fig. (1.9) : Temperature profile θ for different values of L at $a = 0.5$, $b = 1.2$, $Q = -0.5$, $\phi = \frac{\pi}{2}$, $X = 1$, $t = 1$, $d = 1.5$, $M = 1$, $K = 1000$, $E_c = 1$, $P_r = 1$.

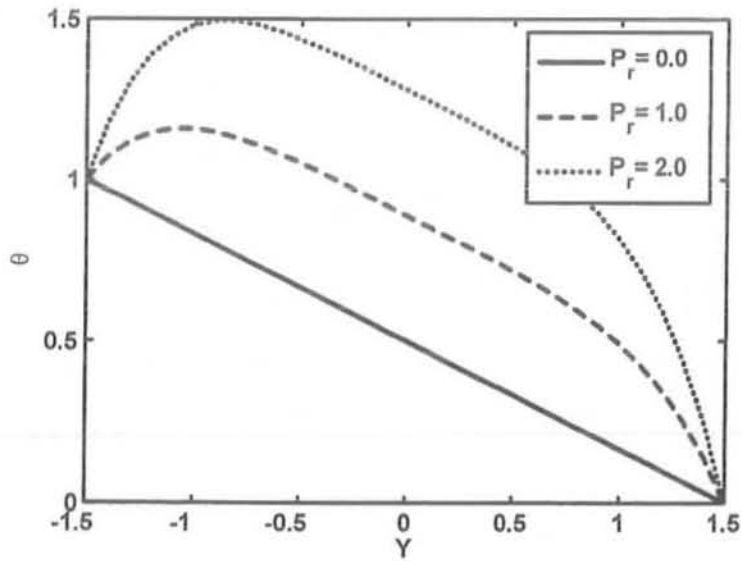


Fig. (1.10) : Temperature profile θ for different values of P_r at $a = 0.5$, $b = 1.2$, $Q = -0.5$, $\phi = \frac{\pi}{2}$, $X = 1$, $t = 1$, $d = 1.5$, $M = 1$, $K = 1000$, $E_c = 1$, $L = 0.5$.

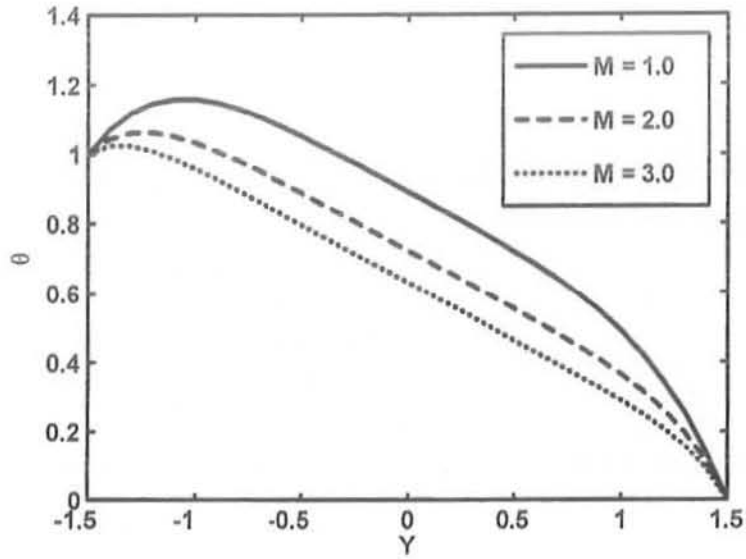


Fig. (1.11) : Temperature profile θ for different values of M at $a = 0.5$, $b = 1.2$, $Q = -0.5$, $\phi = \frac{\pi}{2}$, $X = 1$, $t = 1$, $d = 1.5$, $P_r = 1$, $K = 1000$, $E_c = 1$, $L = 0.5$.

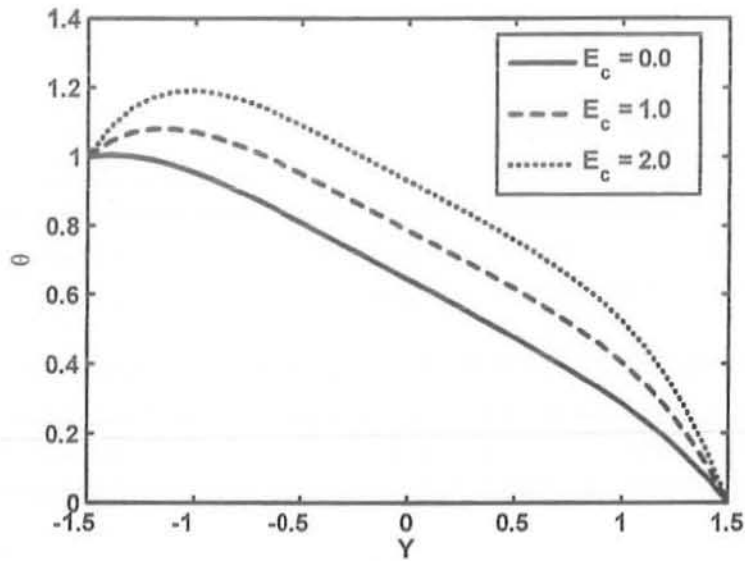
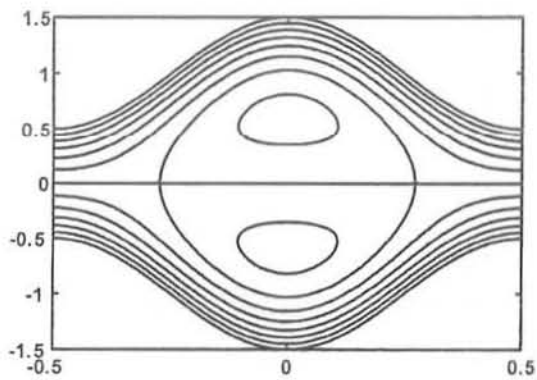
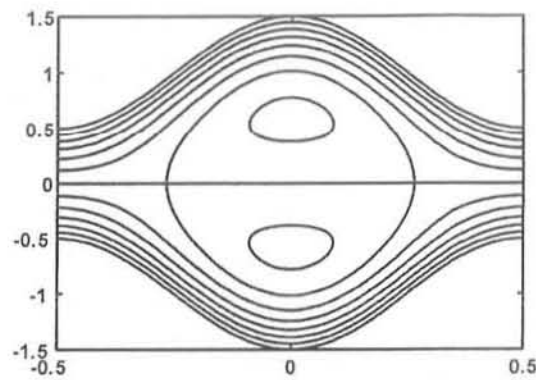


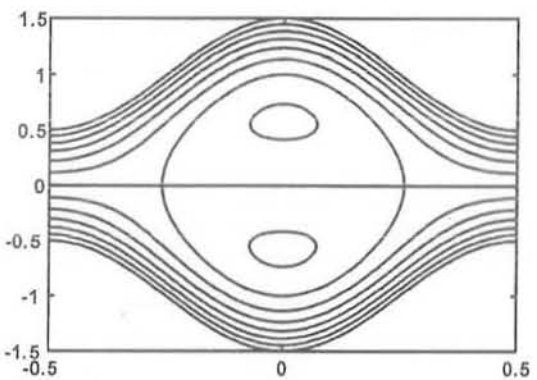
Fig. (1.12) : Temperature profile θ for different values of E_c at $a = 0.5$, $b = 1.2$, $Q = -0.5$, $\phi = \frac{\pi}{2}$, $X = 1$, $t = 1$, $d = 1.5$, $P_r = 1$, $K = 1000$, $L = 0.5$



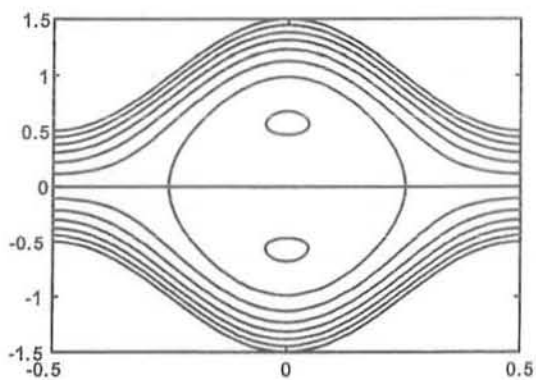
(a)



(b)



(c)



(d)

Fig.(1.13) : Stream lines for four different values of L . (a) for $L = 0$, (b) for $L = 0.01$, (c) for $L = 0.02$ and (d) for $L = 0.03$. The other physical parameters are $Q = 1.4$, $a = 0.5$, $b = 0.5$, $d = 1.0$, $M = 2$, $K = 0.2$, $\phi = 0$.

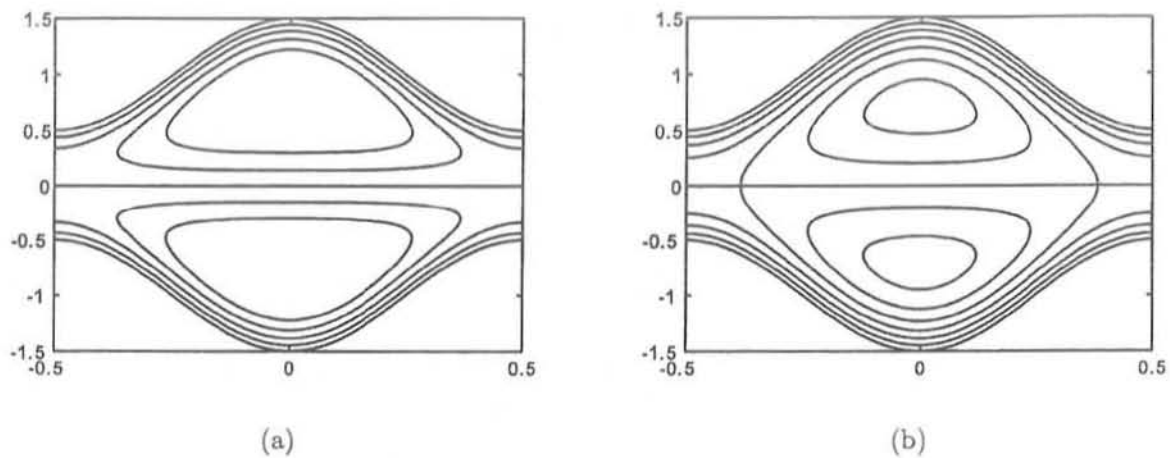


Fig. (1.14) : Stream lines for two different values of Q . (a) for $Q = 1.8$, (b) for $Q = 1.6$. The other physical parameters are $a = 0.5$, $b = 0.5$, $d = 1.0$, $M = 2$, $K = 0.2$, $\phi = 0$, $L = 0.01$.

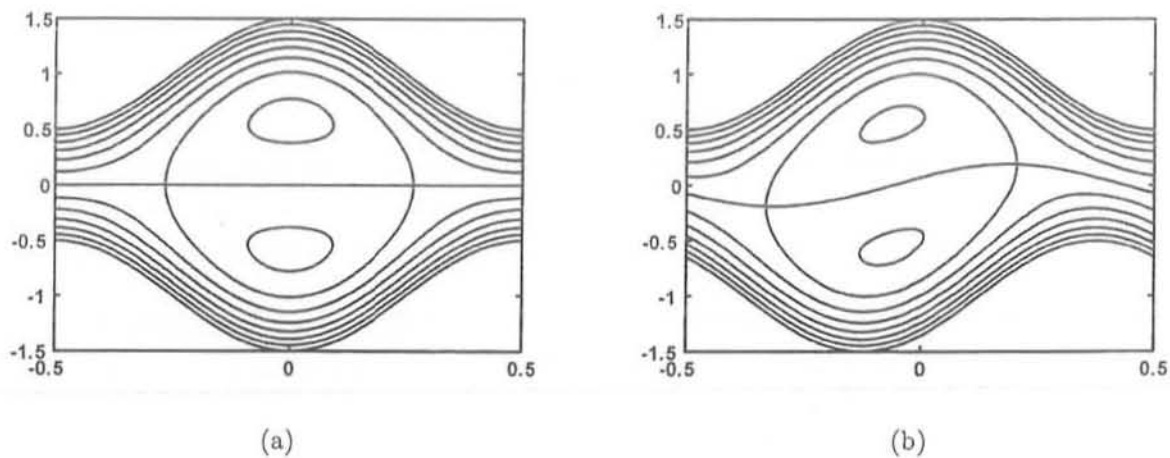


Fig.(1.15) : Stream lines for four different values of ϕ . (a) for $\phi = 0$, (b) for $\phi = \frac{\pi}{4}$. The other physical parameters are $Q = 1.4$, $a = 0.5$, $b = 0.5$, $d = 1.0$, $M = 2$, $K = 0.2$.

Chapter 2

Peristaltic flow of a couple stress fluid under the effect of induced magnetic field in an asymmetric channel

2.1 Introduction

This chapter deals with the peristaltic flow of a couple stress fluid under the effects of induced magnetic field in an asymmetric channel. The governing coupled nonlinear partial differential equations are simplified by using long wave length and low Reynolds number assumptions. The exact solutions of reduced equations are found for velocity, stream function, pressure gradient, current density distribution and magnetic potential Φ . The expression for pressure rise is computed using numerical integration. The physical features of various parameters are discussed through graphs.

2.2 Mathematical formulation

Let us consider the peristaltic flow of an incompressible, electrically conducting couple stress fluid in a two dimensional channel of width $d_1 + d_2$. The flow is generated by sinusoidal wave trains propagating with constant speed c along the channel walls. We choose rectangular coordinate system for the channel with X along the centerline of the channel and Y is transverse to it. An external transverse uniform constant magnetic field H_0 , induced magnetic field $H(h_X(X, Y, t), H_0 + h_Y(X, Y, t), 0)$ and the total magnetic field $H^+(h_X(X, Y, t), H_0 + h_Y(X, Y, t), 0)$ are taken into account. Finally, the channel walls are considered to be non-conductive and the geometry of the wall surface is defined in previous chapter but for the sake of simplicity we define it again

$$Y = H_1(X, t) = d_1 + a_1 \cos\left(\frac{2\pi}{\lambda}(X - ct)\right), \quad Y = H_2(X, t) = -d_2 - b_1 \cos\left(\frac{2\pi}{\lambda}(X - ct) + \phi\right). \quad (2.1)$$

Equation of continuity is defined in Eq. (1.2) and the other equations which governs the MHD flow of a couple stress fluid are given as

(i) Maxwell's equation

$$\nabla \cdot \mathbf{H} = 0, \quad \nabla \cdot \mathbf{E} = 0, \quad (2.2)$$

$$\nabla \wedge \mathbf{H} = \mathbf{J}, \quad \text{with } \mathbf{J} = \sigma\{\mathbf{E} + \mu_e(\mathbf{V} \wedge \mathbf{H})\}, \quad (2.3)$$

$$\nabla \wedge \mathbf{E} = -\mu_e \frac{\partial \mathbf{H}}{\partial t}. \quad (2.4)$$

(ii) The equations of motion

$$\rho \left(\frac{\partial \mathbf{V}}{\partial t} + (\mathbf{V} \cdot \nabla) \mathbf{V} \right) = -\nabla \left(p + \frac{1}{2} \mu_e (\mathbf{H}^+)^2 \right) + \mu \nabla^2 \mathbf{V} - \eta \nabla^4 \mathbf{V} - \mu_e (\mathbf{H}^+ \cdot \nabla) \mathbf{H}^+. \quad (2.5)$$

In the above equation \mathbf{E} is an induced electric field, \mathbf{J} is the current density, μ_e is the magnetic permeability and σ is the electric conductivity.

Combining Eqs. (2.2) to (2.4), we obtain the induction equation as follows

$$\frac{\partial \mathbf{H}^+}{\partial t} = \nabla \wedge (\mathbf{V} \wedge \mathbf{H}^+) + \frac{1}{\xi} \nabla^2 \mathbf{H}^+, \quad (2.6)$$

where $\xi = \frac{1}{\sigma\mu_e}$ is the magnetic diffusivity.

Defining the scales

$$\begin{aligned}
\bar{x} &= \frac{x}{\lambda}, \quad \bar{y} = \frac{y}{d_1}, \quad \bar{u} = \frac{u}{c}, \quad \bar{v} = \frac{v}{c}, \quad \delta = \frac{d_1}{\lambda}, \quad d = \frac{d_2}{d_1}, \quad \bar{p} = \frac{d_1^2 p}{\mu c \lambda}, \quad \bar{t} = \frac{ct}{\lambda}, \\
h_1 &= \frac{H_1}{d_1}, \quad h_2 = \frac{H_2}{d_2}, \quad a = \frac{a_1}{d_1}, \quad b = \frac{b_1}{d_1}, \quad \text{Re} = \frac{cd_1}{v}, \quad \bar{\Psi} = \frac{\Psi}{cd_1}, \quad \bar{\Phi} = \frac{\Phi}{H_0 d_1}, \\
u &= \frac{\partial \psi}{\partial y}, \quad v = -\frac{\partial \psi}{\partial x}, \quad h_x = \frac{\partial \Phi}{\partial y}, \quad h_y = -\delta \frac{\partial \Phi}{\partial x}, \quad R_m = \sigma \mu_e a c, \quad \gamma = \sqrt{\frac{\mu}{\eta}} d_1, \\
p_m &= p + \frac{1}{2} \text{Re} \delta \frac{\mu_e (H^+)^2}{\rho c^2}, \quad S = \frac{H_0}{c} \sqrt{\frac{\mu_e}{\rho}}, \quad \nabla^2 = \delta^2 \frac{\partial^2}{\partial x^2} + \frac{\partial^2}{\partial y^2}.
\end{aligned} \tag{2.7}$$

With the help of Eq. (1.6), the transformations (1.11) and the non-dimensional quantities (2.7), Eqs. (1.7), (2.5) and (2.6) for a couple stress fluid in wave frame (after dropping bars) take the following form

$$\frac{\partial u}{\partial x} + \frac{\partial v}{\partial y} = 0, \tag{2.8}$$

$$\begin{aligned}
\text{Re} \delta \left(u \frac{\partial}{\partial x} + v \frac{\partial}{\partial y} \right) u &= -\frac{\partial p_m}{\partial x} + \nabla^2 u - \frac{1}{\gamma^2} \nabla^4 u + \text{Re} S_1^2 \frac{\partial (h_x)}{\partial y} \\
&\quad + \text{Re} S_1^2 \delta \left(h_x \frac{\partial}{\partial x} + h_y \frac{\partial}{\partial y} \right) h_x,
\end{aligned} \tag{2.9}$$

$$\begin{aligned}
\text{Re} \delta^3 \left(u \frac{\partial}{\partial x} + v \frac{\partial}{\partial y} \right) v &= -\frac{\partial p_m}{\partial y} + \delta^2 \nabla^2 v - \frac{\delta^2}{\gamma^2} \nabla^2 v + \text{Re} S_1^2 \delta^2 \frac{\partial (h_y)}{\partial y} \\
&\quad + \text{Re} S_1^2 \delta^3 \left(h_x \frac{\partial}{\partial x} + h_y \frac{\partial}{\partial y} \right) h_y,
\end{aligned} \tag{2.10}$$

$$u + \delta (u h_y - v h_x) + \frac{1}{R_m} \left(\frac{\partial (h_x)}{\partial y} - \delta^2 \frac{\partial (h_y)}{\partial x} \right) = E. \tag{2.11}$$

The corresponding dimensionless boundary conditions are

$$\begin{aligned}
u &= -1, \quad v = \frac{dh_1}{dx}, \\
-\left(\delta^4 \frac{\partial^2 v}{\partial x^2} - \delta^2 \frac{\partial^2 u}{\partial x \partial y} \right) \frac{dh_1}{dx} + \delta^2 \frac{\partial^2 v}{\partial x \partial y} - \frac{\partial^2 u}{\partial y^2} &= 0 \quad \text{at } y = h_1,
\end{aligned} \tag{2.12}$$

$$\begin{aligned}
u &= -1, \quad v = \frac{dh_2}{dx}, \\
-\left(\delta^4 \frac{\partial^2 v}{\partial x^2} - \delta^2 \frac{\partial^2 u}{\partial x \partial y} \right) \frac{dh_2}{dx} + \delta^2 \frac{\partial^2 v}{\partial x \partial y} - \frac{\partial^2 u}{\partial y^2} &= 0 \quad \text{at } y = h_2.
\end{aligned} \tag{2.13}$$

Using the assumption of long wave length and low but finite Reynolds number consideration, Eqs. (2.8) to (2.13) reduce to

$$\frac{\partial p}{\partial x} = \frac{\partial^2 u}{\partial y^2} - \frac{1}{\gamma^2} \frac{\partial^4 u}{\partial y^4} + \text{Re } S_1^2 \frac{\partial(h_x)}{\partial y}, \quad (2.14)$$

$$\frac{\partial p}{\partial y} = 0, \quad (2.15)$$

$$u + \frac{1}{R_m} \frac{\partial(h_x)}{\partial y} = E, \quad (2.16)$$

$$u = -1, \quad v = \frac{dh_1}{dx}, \quad \frac{\partial^2 u}{\partial y^2} = 0 \quad \text{at } y = h_1 = 1 + a \cos 2\pi x, \quad (2.17)$$

$$u = -1, \quad v = \frac{dh_2}{dx}, \quad \frac{\partial^2 u}{\partial y^2} = 0 \quad \text{at } y = h_2 = -d - b \cos(2\pi x + \phi). \quad (2.18)$$

With the help of Eqs. (2.14) and (2.16), we obtain

$$\frac{\partial p}{\partial x} = \frac{\partial^2 u}{\partial y^2} - \frac{1}{\gamma^2} \frac{\partial^4 u}{\partial y^4} + \text{Re } S_1^2 (E - u) R_m. \quad (2.19)$$

The dimensionless mean flow Q is defined in chapter one and is straight forward written as

$$Q = q + 1 + d,$$

where

$$q = \int_{h_1}^{h_2} u dy. \quad (2.20)$$

2.3 Solution of the problem

2.3.1 Exact solution

Eq. (2.19) is linear, non-homogeneous fourth order differential equation whose exact solution can be written as

$$u = A_2 \cosh(m_1 y) + A_3 \sinh(m_1 y) + A_4 \cosh(m_2 y) + A_5 \sinh(m_2 y) + E - \frac{1}{M^2} \frac{dp}{dx}, \quad (2.21)$$

where A_2 to A_5 are constants, $M^2 = \text{Re } S_1^2 R_m$ and $m_{1,2} = \frac{\gamma}{\sqrt{2}} \left(1 \pm \sqrt{1 - \frac{4M^2}{\gamma^2}}\right)^{\frac{1}{2}}$.

Invoking the boundary conditions we get

$$\begin{aligned}
 A_2 &= \frac{1}{M^2(m_1^2 - m_2^2)} \left[\sec h \left(\frac{m_1(h_1 - h_2)}{2} \right) \left(m_2^2 \left(M^2 - \frac{dp}{dx} + M^2 E \right) \cosh \left(\frac{m_1(h_1 + h_2)}{2} \right) \right) \right], \\
 A_3 &= -\frac{1}{M^2(m_1^2 - m_2^2)} \left[\sec h \left(\frac{m_1(h_1 - h_2)}{2} \right) \left(m_2^2 \left(M^2 - \frac{dp}{dx} + M^2 E \right) \sinh \left(\frac{m_1(h_1 + h_2)}{2} \right) \right) \right], \\
 A_4 &= -\frac{1}{M^2(m_1^2 - m_2^2)} \left[\sec h \left(\frac{m_2(h_1 - h_2)}{2} \right) \left(m_1^2 \left(M^2 - \frac{dp}{dx} + M^2 E \right) \cosh \left(\frac{m_2(h_1 + h_2)}{2} \right) \right) \right], \\
 A_5 &= -\frac{1}{M^2(m_1^2 - m_2^2)} \left[\sec h \left(\frac{m_2(h_1 - h_2)}{2} \right) \left(m_1^2 \left(-M^2 + \frac{dp}{dx} - M^2 E \right) \sinh \left(\frac{m_2(h_1 + h_2)}{2} \right) \right) \right].
 \end{aligned} \tag{2.22}$$

The corresponding stream function is defined as

$$\psi = \frac{A_2}{m_1} \sinh(m_1 y) + \frac{A_3}{m_1} \cosh(m_1 y) + \frac{A_4}{m_2} \sinh(m_2 y) + \frac{A_5}{m_2} \cosh(m_2 y) + \left(E - \frac{1}{M^2} \frac{dp}{dx} \right) y, \tag{2.23}$$

where constants A_2 to A_5 are defined in Eq. (2.22).

From Eqs. (2.20) to (2.22), the expression for pressure gradient is defined as

$$\frac{dp}{dx} = \frac{M^2 m_1 m_2 (m_1^2 - m_2^2)}{d_{10}} (q - E(h_1 - h_2) + d_{01} + d_{02} + d_{03} + d_{04}), \tag{2.24}$$

where

$$\begin{aligned}
 d_{01} &= -\frac{\left(m_2^2 (1 + E) \cosh \left(\frac{m_1(h_1 + h_2)}{2} \right) \sec h \left(\frac{m_1(h_1 - h_2)}{2} \right) (\sinh(h_1 m_1) - \sinh(h_2 m_1)) \right)}{m_1 (m_1^2 - m_2^2)}, \\
 d_{02} &= \frac{\left(m_2^2 (1 + E) \sinh \left(\frac{m_1(h_1 + h_2)}{2} \right) \sec h \left(\frac{m_1(h_1 - h_2)}{2} \right) (\cosh(h_1 m_1) - \cosh(h_2 m_1)) \right)}{m_1 (m_1^2 - m_2^2)}, \\
 d_{03} &= \frac{\left(m_1^2 (1 + E) \cosh \left(\frac{m_2(h_1 + h_2)}{2} \right) \sec h \left(\frac{m_2(h_1 - h_2)}{2} \right) (\sinh(h_1 m_2) - \sinh(h_2 m_2)) \right)}{m_2 (m_1^2 - m_2^2)},
 \end{aligned}$$

$$d_{04} = -\frac{\left(m_1^2(1+E)\sinh\left(\frac{m_2(h_1+h_2)}{2}\right)\operatorname{sech}h\left(\frac{m_2(h_1-h_2)}{2}\right)(\cosh(h_1m_2)-\cosh(h_2m_2))\right)}{m_2(m_1^2-m_2^2)},$$

$$d_{05} = m_1^3m_2(h_2-h_1)+m_2^3m_1(h_1-h_2),$$

$$d_{06} = m_2^3\cosh\left(\frac{m_1(h_1+h_2)}{2}\right)\operatorname{sech}h\left(\frac{m_1(h_1-h_2)}{2}\right)(\sinh(h_2m_1)-\sinh(h_1m_1)),$$

$$d_{07} = m_2^3\sinh\left(\frac{m_1(h_1+h_2)}{2}\right)\operatorname{sech}h\left(\frac{m_1(h_1-h_2)}{2}\right)(\cosh(h_1m_1)-\cosh(h_2m_1)),$$

$$d_{08} = m_1^3\cosh\left(\frac{m_2(h_1+h_2)}{2}\right)\operatorname{sech}h\left(\frac{m_2(h_1-h_2)}{2}\right)(\sinh[h_1m_2]-\sinh(h_2m_2)),$$

$$d_{09} = m_1^3\sinh\left(\frac{m_2(h_1+h_2)}{2}\right)\operatorname{sech}h\left(\frac{m_2(h_1-h_2)}{2}\right)(\cosh(h_2m_2)-\cosh(h_1m_2)),$$

$$d_{10} = d_{05}+d_{06}+d_{07}+d_{08}+d_{09}. \quad (2.25)$$

The non-dimensional expression for the pressure rise per wavelength Δp , is defined as

$$\Delta p = \int_0^1 \left(\frac{dp}{dx}\right) dx. \quad (2.26)$$

With the help of Eq. (2.16), we get the magnetic force function of the form

$$\frac{\partial^2\Phi}{\partial y^2} = (E-u)R_m, \quad (2.27)$$

with the corresponding boundary conditions are

$$\Phi = 0 \quad \text{at } y = h_1 \quad \text{and } y = h_2. \quad (2.28)$$

Using Eq. (2.21), the exact solution of Eq. (2.27) satisfying the *boundary conditions* (2.28) can

be written as

$$\begin{aligned}\Phi = & -R_m \left(\frac{A_2}{m_1^2} \cosh(m_1 y) + \frac{A_3}{m_1^2} \sinh(m_1 y) + \frac{A_4}{m_2^2} \cosh(m_2 y) + \frac{A_5}{m_2^2} \sinh(m_2 y) \right) \\ & + \frac{R_m}{M^2} \frac{dp}{dx} \frac{y^2}{2} + c_3 y + c_4,\end{aligned}\quad (2.29)$$

where

$$c_3 = \frac{-R_m}{2(h_2 - h_1)M^2 m_1^2 m_2^2} \left(\frac{dp}{dx} (h_2^2 - h_1^2) m_1^2 m_2^2 + b_0 \right),$$

$$c_4 = \frac{-R_m}{2(h_1 - h_2)M^2 m_1^2 m_2^2} \left(\frac{dp}{dx} (h_2^2 h_1 - h_2 h_1^2) m_1^2 m_2^2 + b_1 \right),$$

$$\begin{aligned}b_0 = & 2A_2 M^2 m_2^2 (\cosh(h_1 m_1) - \cosh(h_2 m_1)) + 2A_3 M^2 m_2^2 (\sinh(h_1 m_1) - \sinh(h_2 m_1)) \\ & + 2A_4 M^2 m_1^2 (\cosh(h_1 m_2) - \cosh(h_2 m_2)) + 2A_5 M^2 m_1^2 (\sinh(h_1 m_2) - \sinh(h_2 m_2)),\end{aligned}$$

$$\begin{aligned}b_1 = & 2A_2 M^2 m_2^2 (h_2 \cosh(h_1 m_1) - h_1 \cosh(h_2 m_1)) + 2A_3 M^2 m_2^2 (h_2 \sinh(h_1 m_1) - h_1 \sinh(h_2 m_1)) \\ & + 2A_4 M^2 m_1^2 (h_2 \cosh(h_1 m_2) - h_1 \cosh(h_2 m_2)) + 2A_5 M^2 m_1^2 (h_2 \sinh(h_1 m_2) - h_1 \sinh(h_2 m_2)),\end{aligned}$$

A_2 to A_5 are defined in Eq. (2.22).

The expression of axial induced magnetic field is calculated from Eq. (2.29) by using ($h_x = \frac{\partial \Phi}{\partial y}$), we have

$$\begin{aligned}h_x(x, y) = & -R_m \left(\frac{A_2}{m_1} \sinh(m_1 y) + \frac{A_3}{m_1} \cosh(m_1 y) + \frac{A_4}{m_2} \sinh(m_2 y) + \frac{A_5}{m_2} \cosh(m_2 y) \right) \\ & + \frac{R_m}{M^2} \frac{dp}{dx} y + c_3.\end{aligned}\quad (2.30)$$

Also the current density distribution takes the following form

$$J_z(x, y) = \frac{R_m}{M^2} \frac{dp}{dx} - R_m (A_2 \cosh(m_1 y) + A_3 \sinh(m_1 y) + A_4 \cosh(m_2 y) + A_5 \sinh(m_2 y)).\quad (2.31)$$

2.4 Results and discussion

In this section, the graphical results of the problem under consideration is discussed. The expression for pressure rise is calculated numerically using a mathematics software. The pressure rise Δp for different values of couple stress parameter γ and Hartmann number M are plotted in Figs. 2.1 to 2.2. It is observed from Fig. 2.1, that the pressure rise increases for small values of Q ($-1 \leq Q \leq 1$) with an increase in γ and for large Q ($1 \leq Q \leq 3$) the pressure rise decreases. From Fig. 2.2 it is observed that with an increase in M , the pressure rise increase for small values of Q , and at the end the behavior is reversed. The pressure gradient for different values of γ and Q against x are plotted in Figs. 2.3 and 2.4. It is depicted from the figures that for $x \in [0, 0.15]$ and $x \in [0.8, 1]$, the pressure rise is small i.e. the flow can easily pass without the imposition of large pressure gradient, while in the narrow part of the channel $x \in [0.15, 0.8]$, to retain the same flux large pressure gradient is required. This phenomena is physically valid. Moreover, in the narrow part of the channel, the pressure gradient increases with an increase in couple stress parameter γ and decreases with an increase in Q (flow rate). The velocity u for different values of E and M are shown in Figs. 2.5 and 2.6. We observed that the magnitude value of velocity profile decreases with an increase in E (see Fig. 2.5). The effect of M on the velocity is almost opposite as compared to the case of E . Here the velocity profile increases with an increase of M . The magnetic force function Φ for different values of R_m , M and Q (volume flow rate) are shown in Figs. 2.7 to 2.9. It is observed from Fig. 2.7 that the magnitude value of the magnetic force function increases with an increase in magnetic Reynolds number R_m . The effect of Hartmann number M and volume flow rate Q is opposite as compared to the case of R_m . In this case the magnetic force function decreases with an increase in Hartmann number M and volume flow rate Q . The induced magnetic field h_x against y for different values of magnetic Reynold number R_m is plotted in Fig. 2.10. It is observed that with an increase in R_m , h_x increases in upper half of the channel while in the lower half the behavior is opposite. The current density distribution J_z for different values of volume flow rate Q and Hartmann number M are plotted in Figs. 2.11 and 2.12. It is illustrated in Fig. 2.11 that the current density distribution J_z decreases with an increase in flow rate Q . The effects of M on the J_z are shown in Fig. 2.12. It is observed that the behavior of J_z is monotonically increasing and decreasing.

Trapping phenomena

Another interesting phenomena in peristaltic motion is trapping. It is basically the formation of an internally circulating bolus of fluid by closed stream lines. This trapped bolus pushed a head along a peristaltic waves. Figs. 2.13 and 2.14 illustrate the stream lines for different values of γ , M and Q . The effect of the couple stress parameter γ and Hartmann number M on the trapping are illustrated in Fig. 2.13. It is observed that with an increase in γ and M , the size of the trapping bolus decreases. It is concluded from Fig. 2.14 that with an increase in Q the size of the trapped bolus decreases.

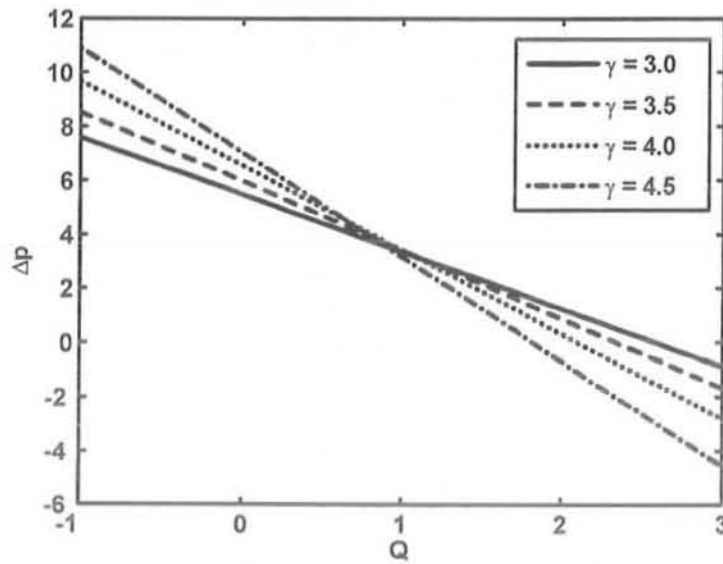


Fig.(2.1) : Variation of Δp with Q for different values of γ at $a = 0.7$, $b = 1.2$, $d = 2$, $\phi = \frac{\pi}{4}$, $M = 1$, $E = 6$.

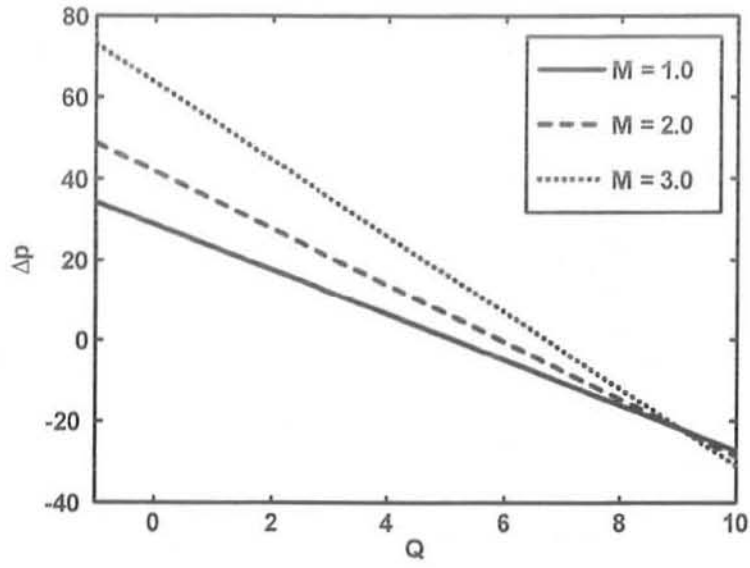


Fig.(2.2) : Variation of Δp with Q for different values of M at $a = 0.7$, $b = 1.2$, $d = 2$, $\phi = \frac{\pi}{4}$, $\gamma = 3$, $E = 6$.

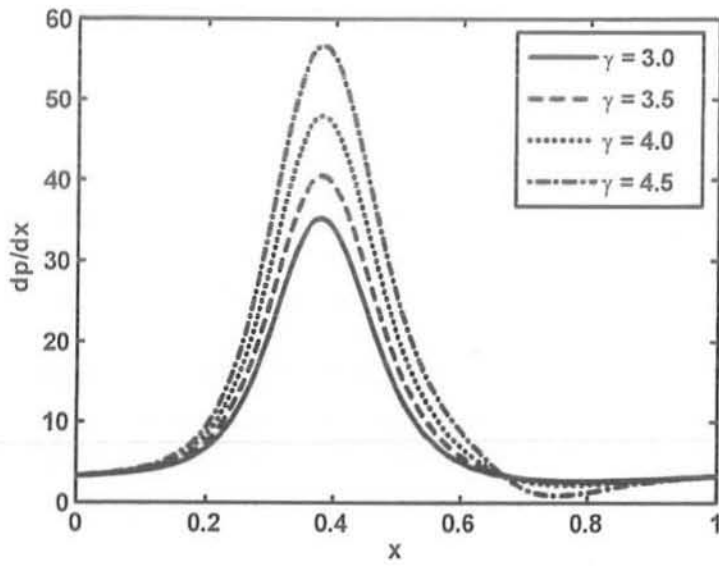


Fig.(2.3) : Variation of $\frac{dp}{dx}$ with x for different values of γ at $a = 0.7$, $b = 1.2$, $d = 2$, $\phi = \frac{\pi}{4}$, $M = 1$, $E = 5$, $Q = -2$.

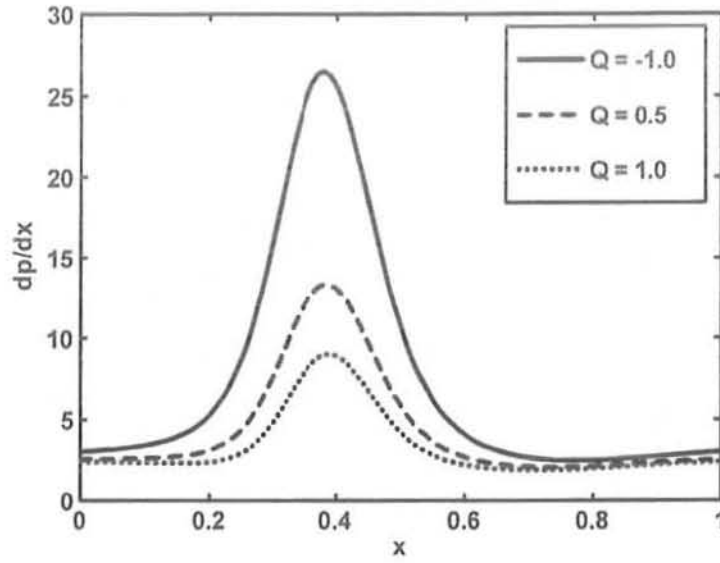


Fig. (2.4) : Variation of $\frac{dp}{dx}$ with x for different values of Q at $a = 0.7, b = 1.2, d = 2, \phi = \frac{\pi}{4}, M = 1, E = 5, \gamma = 3$.

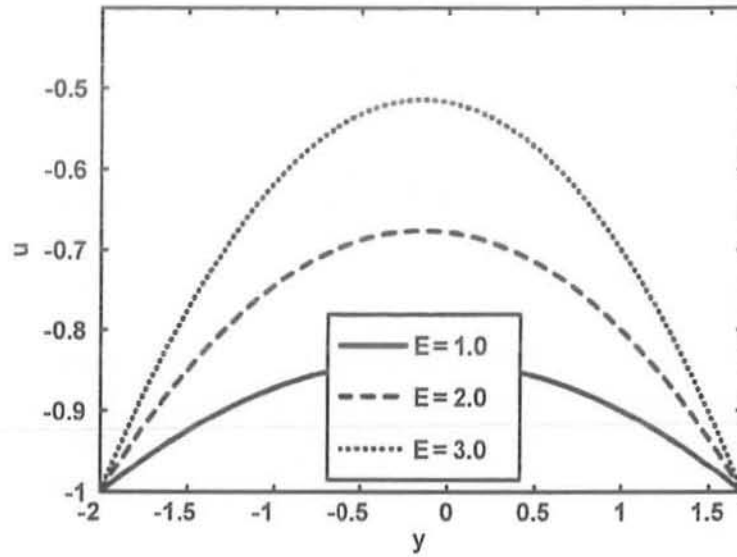


Fig.(2.5) : Velocity profile for different values of E at $a = 0.7, b = 1.2, d = 2, \phi = \frac{\pi}{2}, M = 1, R_m = 2, Q = 2, \gamma = 6$.

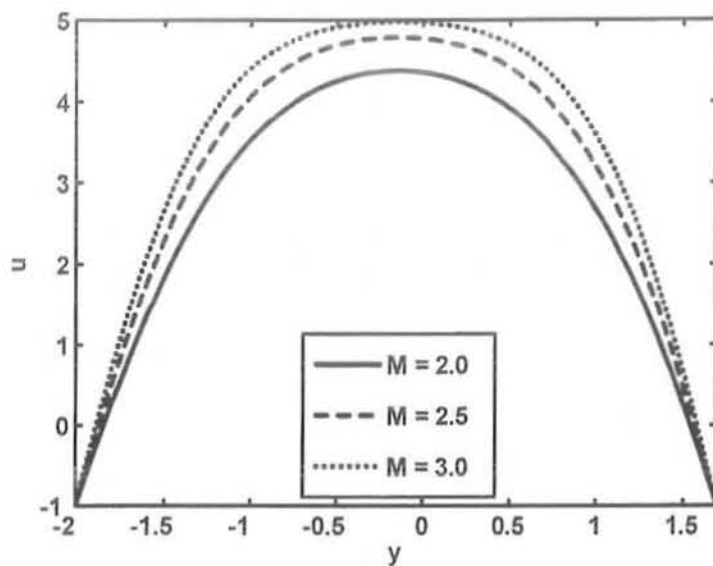


Fig.(2.6) : Velocity profile for different values of M at $a = 0.7$, $b = 1.2$, $d = 2$, $\phi = \frac{\pi}{2}$, $E = 4$, $\gamma = 2$, $R_m = 2$, $Q = 2$, $\gamma = 6$.

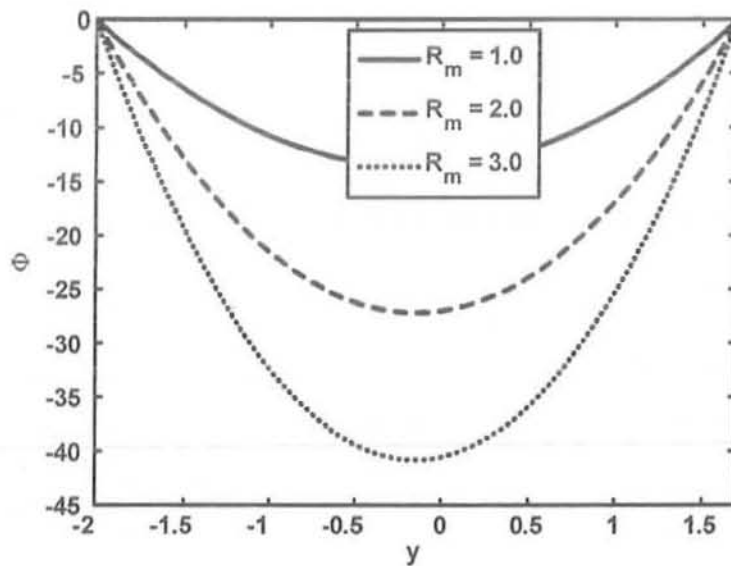


Fig.(2.7) : Profile of magnetic force function Φ for different values of magnetic Reynolds number R_m at $a = 0.7$, $b = 1.2$, $d = 2$, $\phi = \frac{\pi}{2}$, $M = 4$, $x = 0$, $E = 4$, $Q = 2$, $\gamma = 3$.

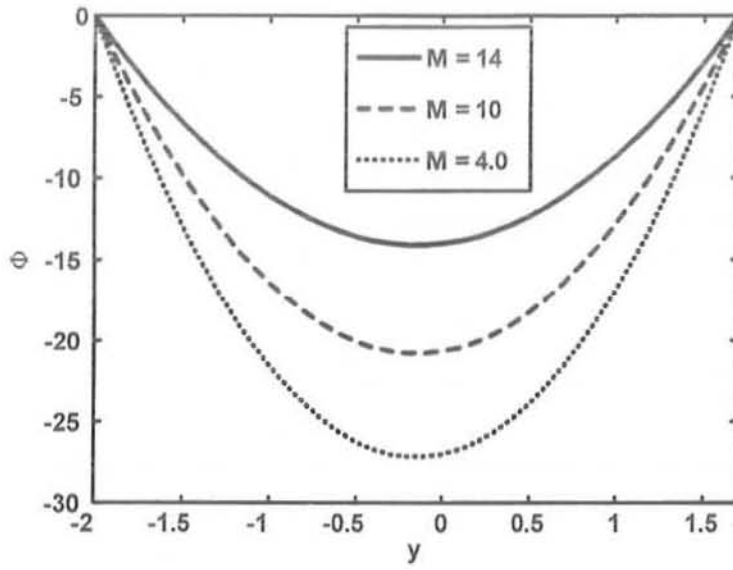


Fig.(2.8) : Profile of magnetic force function Φ for different values of M at $a = 0.7$, $b = 1.2$, $d = 2$, $\phi = \frac{\pi}{2}$, $R_m = 2$, $Q = 2$, $\gamma = 3$.

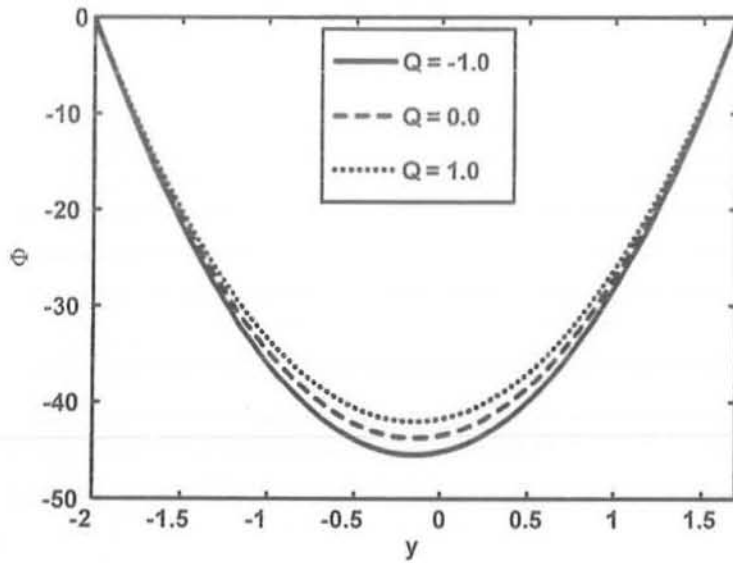


Fig.(2.9) : Profile of magnetic force function Φ for different values of Q at $a = 0.7$, $b = 1.2$, $d = 2$, $\phi = \frac{\pi}{2}$, $R_m = 2$, $M = 2$, $\gamma = 3$.

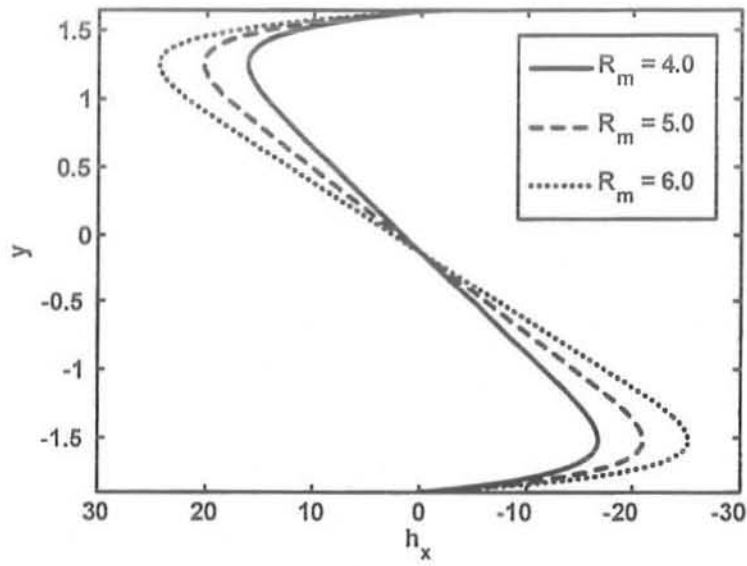


Fig.(2.10) : Variation of axial induced magnetic field h_x for different values of R_m at $a = 0.7$, $b = 1.2$, $d = 2$, $\phi = \frac{\pi}{2}$, $M = 3$, $E = 6$, $Q = 3$, $\gamma = 6$.

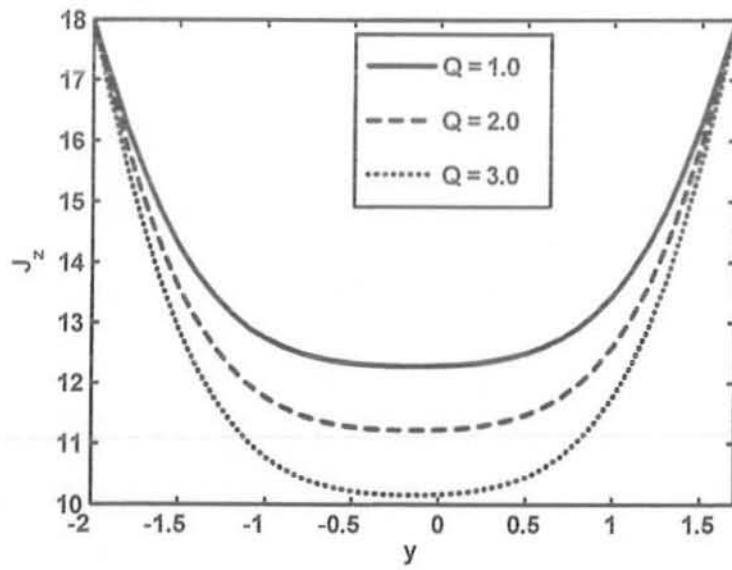


Fig.(2.11) : Profile of current density distribution J_z for different values of volume flow rate Q at $a = 0.7$, $b = 1.2$, $d = 2$, $\phi = \frac{\pi}{2}$, $M = 4$, $E = 2$, $R_m = 3$, $\gamma = 3$.

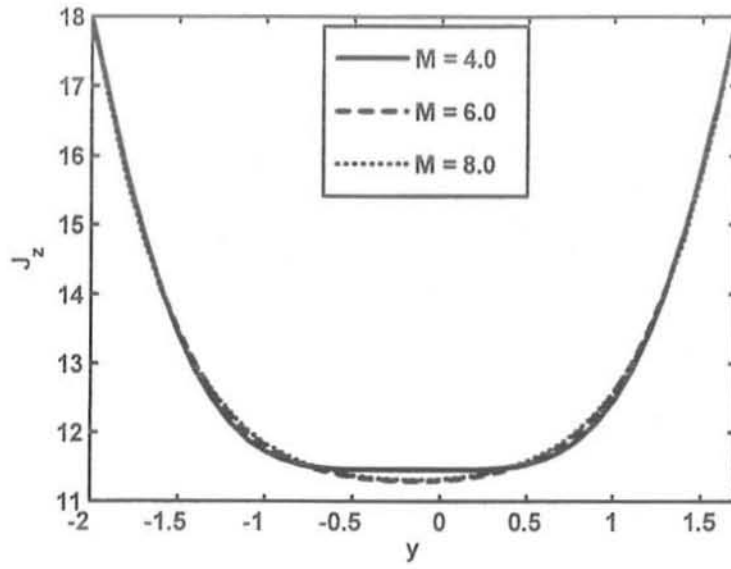
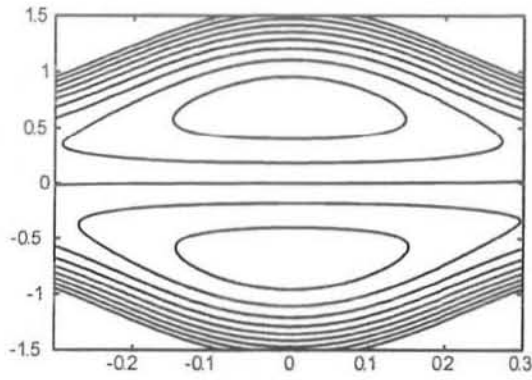
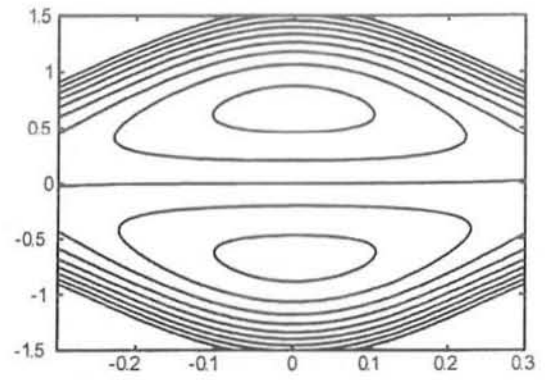


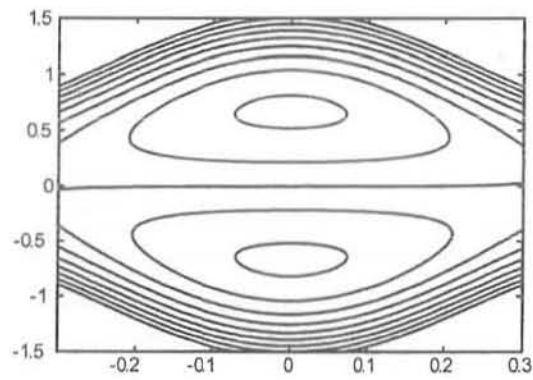
Fig.(2.12) : Profile of current density distribution J_z for different values M at $a = 0.7$, $b = 1.2$, $d = 2$, $\phi = \frac{\pi}{2}$, $E = 2$, $R_m = 3$, $Q = 2$, $\gamma = 2$.



(a)

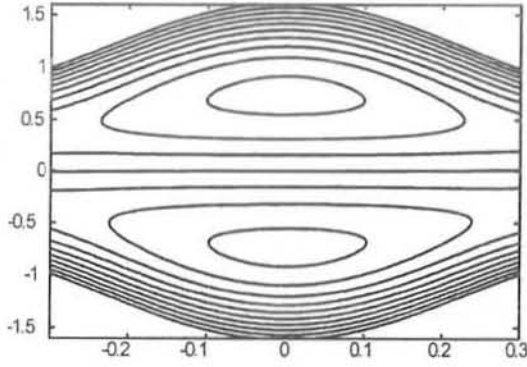


(b)

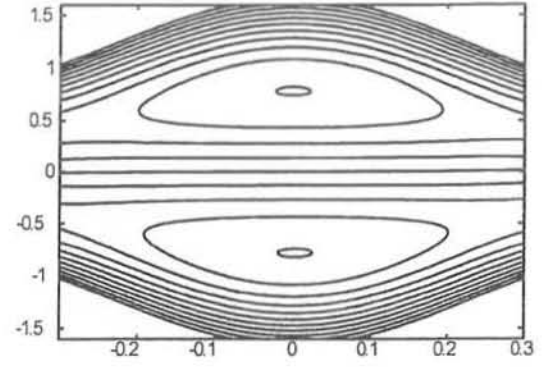


(c)

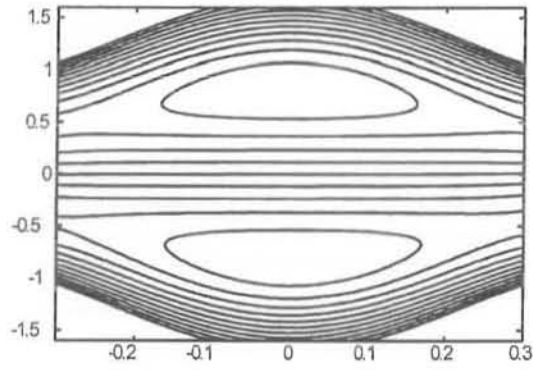
Fig.(2.13) : Stream lines for different values of M and γ . (a) for $\gamma = 3.5$, $M = 1$, (b) for $\gamma = 5$, $M = 2$, (c) for $\gamma = 8$, $M = 3$. The other parameters are $Q = 1.6$, $b = 0.5$, $d = 1$, $E = 4$, $a = 0.5$, $\phi = 0.02$.



(a)



(b)



(c)

Fig.(2.14) : Stream lines for different values of Q . (a) for $Q = 1.6$, (b) for $Q = 1.7$, (c) for $Q = 1.8$. The other parameters are $\gamma = 3.5$, $b = 0.5$, $d = 1$, $E = 4$, $a = 0.5$, $\phi = 0.02$, $E = 4$, $M = 1$.

2.5 Conclusion

This chapter presents the peristaltic flow of a couple stress fluid under the effect of induced magnetic field in an asymmetric channel. The governing two dimensional equations are simplified using long wave length approximation. The exact solution of simplified equations are calculated. The results are discussed through graphs. The main finding can be summarized as follows:

1. It is observed that in the peristaltic pumping region, the pressure rise increases with an increase in couple stress parameter γ and Hartmann number M .
2. The pressure gradient increases with an increase in couple stress parameter γ and decreases with an increase in Q (flow rate).
3. The velocity field decreases with an increase in E and increases with an increase in M .
4. The magnetic force function increases with an increase in magnetic Reynolds number R_m and decreases with an increase in Hartmann number M and volume flow rate Q .
5. The axial induced magnetic field increases in the upper half of the channel while in the lower half the behavior is opposite with an increase in magnetic Reynolds number R_m .
6. The current density distribution J_z decreases with an increase in flow rate Q . It is also observed that the behavior of J_z is monotonically increasing and decreasing with an increase in M .
7. The size of the trapping bolus decreases with an increase in couple stress parameter γ , Hartmann number M and volume flow rate Q .

Chapter 3

Influence of heat transfer and magnetic field on a peristaltic transport of a Jeffrey fluid in an asymmetric channel with partial slip

3.1 Introduction

This chapter deals with the influence of heat transfer and magnetic field on a peristaltic transport of a Jeffrey fluid in an asymmetric channel with partial slip. The complicated Jeffrey fluid equations are simplified using the long wave length and low Reynolds number assumptions. In the wave frame of reference, an exact and closed form Adomian solution is presented. The expressions for pressure drop, pressure rise, stream function and temperature field have been calculated. The behavior of different physical parameters have been discussed graphically. The pumping and trapping phenomena of various wave forms (sinusoidal, multisinusoidal, square, triangular and trapezoidal) are also studied.

3.2 Mathematical formulation

We consider MHD flow of an electrically conducting Jeffrey fluid in an asymmetric channel. The lower wall of the channel is maintained at temperature T_1 while the upper wall has temperature T_0 . We assume that the fluid is subject to a constant transverse magnetic field B_0 . A very small magnetic Reynolds number is assumed and hence the induced magnetic field can be neglected. When the fluid moves into magnetic field two major physical effects arise. The first one is that an electric field \mathbf{E} is induced in the flow. We shall assume that there is no excess charge density and therefore, $\nabla \cdot \mathbf{B} = 0$. Neglecting the induced magnetic field implies that $\nabla \times \mathbf{E} = 0$ and therefore, the induced electric field is negligible. The second effect is dynamically in nature, i.e., a Lorentz force ($\mathbf{J} \times \mathbf{B}$), where \mathbf{J} is the current density, this force acts on the fluid and modifies its motion. This results in the transfer of energy from the electromagnetic field to the fluid. In present study, the relativistic effects are neglected and the current density \mathbf{J} is given by the Ohm's law as

$$\mathbf{J} = \sigma (\mathbf{V} \times \mathbf{B}).$$

Since we are considering asymmetric channel therefore, the channel flow is produced due to different amplitudes and phases of the peristaltic waves on the channel. The geometry of the wall surface is defined in Eq. (2.1). The continuity and energy equations are defined in Eqs. (1.2) and (1.5), however the momentum equation is defined as

$$\rho \left(\frac{\partial \mathbf{V}}{\partial t} + (\mathbf{V} \cdot \nabla) \mathbf{V} \right) = \text{div } \boldsymbol{\tau} + \mathbf{J} \times \mathbf{B}, \quad (3.1)$$

where

$$\boldsymbol{\tau} = -P\mathbf{I} + \mathbf{S}, \quad (3.2)$$

in which the extra stress tensor \mathbf{S} for Jeffrey fluid is defined as [35]

$$\mathbf{S} = \frac{\mu}{1 + \lambda_1} (\dot{\boldsymbol{\gamma}} + \lambda_2 \ddot{\boldsymbol{\gamma}}), \quad (3.3)$$

where λ_1 is the ratio of relaxation to retardation times, $\dot{\boldsymbol{\gamma}}$ is the shear rate, λ_2 the retardation time and dots denote differentiation with respect to time.

With the help of Eq. (1.6), Eqs. (1.2), (1.5) and (3.1) to (3.3) take the following form

$$\frac{\partial U}{\partial X} + \frac{\partial V}{\partial Y} = 0, \quad (3.4)$$

$$\rho \left(\frac{\partial U}{\partial t} + U \frac{\partial U}{\partial X} + V \frac{\partial U}{\partial Y} \right) = -\frac{\partial P}{\partial X} + \frac{\partial}{\partial X} (S_{XX}) + \frac{\partial}{\partial Y} (S_{XY}) - \sigma B_0^2 U, \quad (3.5)$$

$$\rho \left(\frac{\partial V}{\partial t} + U \frac{\partial V}{\partial X} + V \frac{\partial V}{\partial Y} \right) = -\frac{\partial P}{\partial Y} + \frac{\partial}{\partial X} (S_{YX}) + \frac{\partial}{\partial Y} (S_{YY}), \quad (3.6)$$

$$C' \left[\frac{\partial T}{\partial t} + U \frac{\partial T}{\partial X} + V \frac{\partial T}{\partial Y} \right] = \frac{K'}{\rho} \nabla^2 T + \nu \phi_2, \quad (3.7)$$

where

$$\begin{aligned} S_{XX} &= \frac{2\mu}{1+\lambda_1} \left(1 + \lambda_2 \left(\frac{\partial}{\partial t} + U \frac{\partial}{\partial X} + V \frac{\partial}{\partial Y} \right) \right) \frac{\partial U}{\partial X}, \\ S_{XY} &= \frac{\mu}{1+\lambda_1} \left(1 + \lambda_2 \left(\frac{\partial}{\partial t} + U \frac{\partial}{\partial X} + V \frac{\partial}{\partial Y} \right) \right) \left(\frac{\partial U}{\partial Y} + \frac{\partial V}{\partial X} \right), \\ S_{YY} &= \frac{2\mu}{1+\lambda_1} \left(1 + \lambda_2 \left(\frac{\partial}{\partial t} + U \frac{\partial}{\partial X} + V \frac{\partial}{\partial Y} \right) \right) \frac{\partial V}{\partial Y}, \\ \phi_2 &= \frac{1}{1+\lambda_1} \left[1 + \lambda_2 \left(\frac{\partial}{\partial t} + U \frac{\partial}{\partial X} + V \frac{\partial}{\partial Y} \right) \right] \left[2 \left(\frac{\partial U}{\partial X} \right)^2 + 2 \left(\frac{\partial V}{\partial Y} \right)^2 + \left(\frac{\partial U}{\partial Y} + \frac{\partial V}{\partial X} \right)^2 \right]. \end{aligned} \quad (3.8)$$

Defining

$$\begin{aligned} \bar{x} &= \frac{x}{\lambda}, \quad \bar{y} = \frac{y}{d_1}, \quad \bar{u} = \frac{u}{c}, \quad \bar{v} = \frac{v}{c}, \quad \delta = \frac{d_1}{\lambda}, \quad d = \frac{d_2}{d_1}, \quad \bar{p} = \frac{d_1^2 p}{\mu c \lambda}, \quad \bar{t} = \frac{ct}{\lambda}, \quad h_1 = \frac{H_1}{d_1}, \\ h_2 &= \frac{H_2}{d_2}, \quad a = \frac{a_1}{d_1}, \quad b = \frac{b_1}{d_1}, \quad Re = \frac{cd_1}{\nu}, \quad \bar{\Psi} = \frac{\Psi}{cd_1}, \quad \theta = \frac{T - T_0}{T_1 - T_0}, \quad \bar{S} = \frac{Sd_1}{\mu c}, \\ E_c &= \frac{c^2}{C'(T_1 - T_0)}, \quad Pr = \frac{\rho \nu C'}{K'}, \quad M = \sqrt{\frac{\sigma}{\nu}} B_0 d. \end{aligned} \quad (3.9)$$

Using the transformation defined in Eqs. (1.11) and (3.9) into Eqs. (3.4) to (3.8), the resulting equations in terms of stream function Ψ (dropping the bars, $u = \frac{\partial \Psi}{\partial y}$, $v = -\delta \frac{\partial \Psi}{\partial x}$) can be written

as

$$\operatorname{Re} \delta [\Psi_y \Psi_{xy} - \Psi_x \Psi_{yy}] = -\frac{\partial p}{\partial x} + \delta \frac{\partial}{\partial x} (S_{xx}) + \frac{\partial}{\partial y} (S_{xy}) - M^2 (\Psi_y + 1), \quad (3.10)$$

$$\operatorname{Re} \delta^3 [\Psi_x \Psi_{xy} - \Psi_y \Psi_{xx}] = -\frac{\partial p}{\partial y} + \delta^2 \frac{\partial}{\partial x} (S_{yx}) + \delta \frac{\partial}{\partial y} (S_{yy}), \quad (3.11)$$

$$\begin{aligned} \operatorname{Re} \delta [\Psi_y \theta_x - \Psi_x \theta_y] &= \frac{1}{P_r} [\theta_{yy} + \delta^2 \theta_{xx}] \\ &+ \frac{E_c}{(1 + \lambda_1)} \left[1 + \frac{\lambda_2 c \delta}{d_1} \left(\Psi_y \frac{\partial}{\partial x} - \Psi_x \frac{\partial}{\partial y} \right) \right] \\ &\left[4\delta^2 \Psi_{xy}^2 + (\Psi_{yy} - \delta^2 \Psi_{xx})^2 \right], \end{aligned} \quad (3.12)$$

where

$$\begin{aligned} S_{xx} &= \frac{2\delta}{1 + \lambda_1} \left[1 + \frac{\lambda_2 c \delta}{d_1} \left(\Psi_y \frac{\partial}{\partial x} - \Psi_x \frac{\partial}{\partial y} \right) \right] \Psi_{xy}, \\ S_{xy} &= \frac{1}{1 + \lambda_1} \left[1 + \frac{\lambda_2 c \delta}{d_1} \left(\Psi_y \frac{\partial}{\partial x} - \Psi_x \frac{\partial}{\partial y} \right) \right] [\Psi_{yy} - \delta^2 \Psi_{xx}], \\ S_{yy} &= -\frac{2\delta}{1 + \lambda_1} \left[1 + \frac{\lambda_2 c \delta}{d_1} \left(\Psi_y \frac{\partial}{\partial x} - \Psi_x \frac{\partial}{\partial y} \right) \right] \Psi_{xy}. \end{aligned} \quad (3.13)$$

Under the assumption of long wave length $\delta \ll 1$ and low Reynolds number, Eqs. (3.10) to (3.13) become

$$-\frac{\partial p}{\partial x} + \frac{\partial}{\partial y} \left[\frac{1}{1 + \lambda_1} \frac{\partial^2 \Psi}{\partial y^2} \right] - M^2 (\Psi_y + 1) = 0, \quad (3.14)$$

$$\frac{\partial p}{\partial y} = 0, \quad (3.15)$$

$$\frac{1}{P_r} \theta_{yy} + \frac{E_c}{(1 + \lambda_1)} \Psi_{yy}^2 = 0. \quad (3.16)$$

Elimination of pressure from Eqs. (3.14) and (3.16), yield

$$\frac{\partial^2}{\partial y^2} \left[\frac{1}{1 + \lambda_1} \frac{\partial^2 \Psi}{\partial y^2} \right] - M^2 \Psi_{yy} = 0, \quad (3.17)$$

$$\frac{1}{P_r} \theta_{yy} + \frac{E_c}{(1 + \lambda_1)} \Psi_{yy}^2 = 0. \quad (3.18)$$

The corresponding non dimensional boundary conditions are

$$\begin{aligned}\Psi &= \frac{q}{2} \text{ at } y = h_1 = 1 + a \cos 2\pi x, \\ \Psi &= -\frac{q}{2} \text{ at } y = h_2 = -d - b \cos(2\pi x + \phi), \\ \frac{\partial \Psi}{\partial y} + \frac{L}{(1 + \lambda_1)} \frac{\partial^2 \Psi}{\partial y^2} &= -1 \text{ at } y = h_1, \\ \frac{\partial \Psi}{\partial y} - \frac{L}{(1 + \lambda_1)} \frac{\partial^2 \Psi}{\partial y^2} &= -1 \text{ at } y = h_2,\end{aligned}\tag{3.19}$$

$$\begin{aligned}\theta &= 0 \text{ at } y = h_1, \\ \theta &= 1 \text{ at } y = h_2,\end{aligned}\tag{3.20}$$

where q is the flux in the wave frame, L represents the partial slip parameter.

3.3 Solution of the problem

3.3.1 Exact solution

The exact solution of Eq. (3.17) can be written as

$$\Psi = F_4 + F_5 y + F_6 \cosh \frac{y}{\sqrt{B}} + F_7 \sinh \frac{y}{\sqrt{B}},\tag{3.21}$$

where F_4, F_5, F_6, F_7 are functions of x and can be calculated using boundary conditions (3.19)

$$\begin{aligned}F_4 &= \frac{-(h_1 + h_2) \left[q + \left(\frac{qL + 2B(1 + \lambda_1)}{\sqrt{B}(1 + \lambda_1)} \right) \tanh \left[\frac{h_1 - h_2}{2\sqrt{B}} \right] \right]}{2(h_1 - h_2) - 2 \left(\frac{L(h_2 - h_1) + 2B(1 + \lambda_1)}{\sqrt{B}(1 + \lambda_1)} \right) \tanh \left[\frac{h_1 - h_2}{2\sqrt{B}} \right]}, \\ F_5 &= \frac{q + \left(\frac{qL + 2B(1 + \lambda_1)}{\sqrt{B}(1 + \lambda_1)} \right) \tanh \left[\frac{h_1 - h_2}{2\sqrt{B}} \right]}{(h_1 - h_2) - \left(\frac{L(h_2 - h_1) + 2B(1 + \lambda_1)}{\sqrt{B}(1 + \lambda_1)} \right) \tanh \left[\frac{h_1 - h_2}{2\sqrt{B}} \right]}, \\ F_6 &= \frac{-\sqrt{B}(q + h_1 - h_2) \sec h \left[\frac{h_1 - h_2}{2\sqrt{B}} \right] \sinh \left[\frac{h_1 + h_2}{2\sqrt{B}} \right]}{(h_2 - h_1) + \left(\frac{L(h_2 - h_1) + 2B(1 + \lambda_1)}{\sqrt{B}(1 + \lambda_1)} \right) \tanh \left[\frac{h_1 - h_2}{2\sqrt{B}} \right]},\end{aligned}$$

$$F_7 = \frac{\sqrt{B}(q + h_1 - h_2) \sec h \left[\frac{h_1 - h_2}{2\sqrt{B}} \right] \cosh \left[\frac{h_1 + h_2}{2\sqrt{B}} \right]}{(h_2 - h_1) + \left(\frac{L(h_2 - h_1) + 2B(1 + \lambda_1)}{\sqrt{B}(1 + \lambda_1)} \right) \tanh \left[\frac{h_1 - h_2}{2\sqrt{B}} \right]}. \quad (3.22)$$

3.3.2 Solution by Adomian decomposition method

In this section, the Adomian solutions will be determined for the velocity field [62 – 65]. According to Adomian decomposition method, we write Eq. (3.17) in the operator form as

$$\hat{L}_{yyyy}\Psi = M^2(1 + \lambda_1)\Psi_{yy}. \quad (3.23)$$

Applying the inverse operator $\hat{L}_{yyyy}^{-1} = \int \int \int \int [\cdot] dydydydy$, we can write Eq. (3.23) as

$$\Psi = C_4 + C_5y + C_6\frac{y^2}{2!} + C_7\frac{y^3}{3!} + \frac{1}{B}\hat{L}_{yyyy}^{-1}(\Psi_{yy}), \quad (3.24)$$

where

$$\frac{1}{B} = M^2(1 + \lambda_1),$$

C_4, C_5, C_6, C_7 are functions of x . Now we decompose Ψ as

$$\Psi = \sum_{n=0}^{\infty} \Psi_n. \quad (3.25)$$

Substituting Ψ into Eq. (3.24), we obtain

$$\begin{aligned} \Psi &= C_4 + C_5y + C_6\frac{y^2}{2!} + C_7\frac{y^3}{3!}, \\ \Psi_{n+1} &= \frac{1}{B} \int \int \int \int (\Psi_n)_{yy} dydydydy, n \geq 0. \end{aligned} \quad (3.26)$$

Therefore,

$$\begin{aligned}
\Psi_1 &= \frac{1}{B} \left(C_6 \frac{y^4}{4!} + C_7 \frac{y^5}{5!} \right), \\
\Psi_2 &= \frac{1}{B^2} \left(C_6 \frac{y^6}{6!} + C_7 \frac{y^7}{7!} \right), \\
&\vdots \\
\Psi_n &= \frac{1}{B^n} \left(C_6 \frac{y^{2n+2}}{(2n+2)!} + C_7 \frac{y^{2n+3}}{(2n+3)!} \right), \quad n > 0.
\end{aligned} \tag{3.27}$$

Using Eq. (3.25), the closed form of Ψ can be written as

$$\Psi = C_4 + C_5 y + BC_6 \left(\cosh \frac{y}{\sqrt{B}} - 1 \right) + B\sqrt{B}C_7 \left(\sinh \frac{y}{\sqrt{B}} - \frac{y}{\sqrt{B}} \right).$$

The above equation in simplest form can be written as

$$\Psi = F_4 + F_5 y + F_6 \cosh \frac{y}{\sqrt{B}} + F_7 \sinh \frac{y}{\sqrt{B}}. \tag{3.28}$$

Now the Adomian solution (3.28) and exact solution (3.21) are exactly same in which F_i ($i = 4$ to 7) are calculated using boundary conditions which are defined in Eq. (3.22).

The pressure gradient is obtained from the dimensionless momentum equation for the axial velocity as

$$\frac{dp}{dx} = \frac{1}{(1 + \lambda_1)} \left[\Psi_{yyy} - \frac{1}{B} \Psi_y - \frac{1}{B} \right]. \tag{3.29}$$

Substituting the values of Ψ into (3.29), we obtain

$$\frac{dp}{dx} = \frac{-(h_1 - h_2 + q) \left[1 + \frac{L}{B(1+\lambda_1)} \tanh \left[\frac{h_1 - h_2}{2\sqrt{B}} \right] \right]}{B(1 + \lambda_1) \left(h_1 - h_2 - \left(\frac{L(h_2 - h_1) + 2B(1+\lambda_1)}{\sqrt{B}(1+\lambda_1)} \right) \tanh \left[\frac{h_1 - h_2}{2\sqrt{B}} \right] \right)}. \tag{3.30}$$

Integrating (3.30) over one wavelength, we get

$$\Delta p = \int_0^1 \left(\frac{dp}{dx} \right) dx. \tag{3.31}$$

The axial velocity component in the fixed frame (non-dimensional form) is given by

$$\begin{aligned}
 U(X, Y, t) &= 1 + \Psi_y \\
 &= \frac{2(h_1 - h_2 + q) \sinh\left[\frac{h_1 - Y}{2\sqrt{B}}\right] \sinh\left[\frac{h_2 - Y}{2\sqrt{B}}\right] - \frac{L(h_1 - h_2 + q)}{\sqrt{B}(1 + \lambda_1)} \sinh\left[\frac{h_1 - h_2}{2\sqrt{B}}\right]}{\left(\frac{L(h_2 - h_1) + 2B(1 + \lambda_1)}{\sqrt{B}(1 + \lambda_1)}\right) \sinh\left[\frac{h_1 - h_2}{2\sqrt{B}}\right] - (h_1 - h_2) \cosh\left[\frac{h_1 - h_2}{2\sqrt{B}}\right]}, \quad (3.32)
 \end{aligned}$$

where

$$h_1 = 1 + a \cos[2\pi(X - t)] \quad \text{and} \quad h_2 = -d - b \cos[2\pi(X - t) + \phi].$$

Using solution (3.21) into Eq. (3.16), the exact solution of the energy equation in fixed frame satisfying the boundary conditions can be written as

$$\begin{aligned}
 \theta &= -\frac{E_c P_r}{(1 + \lambda_1)} \left(\frac{F_6^2}{2B^2} Y^2 + \frac{1}{8B} (F_6^2 + F_7^2) \cosh 2\left(\frac{Y}{\sqrt{B}}\right) - \frac{Y^2}{4B^2} (F_6^2 + F_7^2) + \frac{F_6 F_7}{4B} \sinh 2\left(\frac{Y}{\sqrt{B}}\right) \right) \\
 &\quad + c_5 Y + c_6, \quad (3.33)
 \end{aligned}$$

where

$$\begin{aligned}
 c_5 &= \frac{-1}{(h_1 - h_2)} + \frac{E_c P_r}{(1 + \lambda_1)(h_1 - h_2)} \left(\frac{F_6^2}{2B^2} (h_1^2 - h_2^2) - \frac{(h_1^2 - h_2^2)}{4B^2} (F_6^2 + F_7^2) \right. \\
 &\quad \left. + \frac{1}{8B} (F_6^2 + F_7^2) \left[\cosh 2\left(\frac{h_1}{\sqrt{B}}\right) - \cosh 2\left(\frac{h_2}{\sqrt{B}}\right) \right] + \frac{F_6 F_7}{4B} \left[\sinh 2\left(\frac{h_1}{\sqrt{B}}\right) - \sinh 2\left(\frac{h_2}{\sqrt{B}}\right) \right] \right), \\
 c_6 &= \frac{E_c P_r}{(1 + \lambda_1)} \left(\frac{F_6^2}{2B^2} h_1^2 + \frac{F_6 F_7}{4B} \sinh 2\left(\frac{h_1}{\sqrt{B}}\right) - \frac{h_1^2}{4B^2} (F_6^2 + F_7^2) + \frac{1}{8B} (F_6^2 + F_7^2) \cosh 2\left(\frac{h_1}{\sqrt{B}}\right) \right) \\
 &\quad - c_5 h_1. \quad (3.34)
 \end{aligned}$$

It is noticed that in the absence of heat transfer and slip parameter L the results of Kothandapani and Srinivas [35] can be recovered as a special case of our problem. Moreover the results of Mishra and Rao [14] can be recovered if $\lambda_1 \rightarrow 0$, $L \rightarrow 0$ and in the absence of heat transfer.

3.4 Expressions for wave shape

The non-dimensional expressions for the five considered wave forms are defined as follow

1. Sinusoidal wave

$$h_1(x) = 1 + a \sin 2\pi x, \quad h_2(x) = -d - b \sin(2\pi x + \phi).$$

2. Multisinusoidal wave

$$h_1(x) = 1 + a \sin 2\pi x n, \quad h_2(x) = -d - b \sin(2\pi x n + \phi).$$

3. Square wave

$$h_1(x) = 1 + a \left[\frac{4}{\pi} \sum_{m=1}^{\infty} \frac{(-1)^{m+1}}{(2m-1)} \cos[2(2m-1)\pi x] \right],$$

$$h_2(x) = -d - b \left[\frac{4}{\pi} \sum_{m=1}^{\infty} \frac{(-1)^{m+1}}{(2m-1)} \cos[2(2m-1)\pi x + \phi] \right].$$

4. Triangular wave

$$h_1(x) = 1 + a \left[\frac{8}{\pi^3} \sum_{m=1}^{\infty} \frac{(-1)^{m+1}}{(2m-1)^2} \sin[2(2m-1)\pi x] \right],$$

$$h_2(x) = -d - b \left[\frac{8}{\pi^3} \sum_{m=1}^{\infty} \frac{(-1)^{m+1}}{(2m-1)^2} \sin[2(2m-1)\pi x + \phi] \right].$$

5. Trapezoidal wave

$$h_1(x) = 1 + a \left[\frac{32}{\pi^2} \sum_{m=1}^{\infty} \frac{\sin\left[\frac{\pi}{8}(2m-1)\right]}{(2m-1)^2} \sin[2(2m-1)\pi x] \right],$$

$$h_2(x) = -d - b \left[\frac{32}{\pi^2} \sum_{m=1}^{\infty} \frac{\sin\left[\frac{\pi}{8}(2m-1)\right]}{(2m-1)^2} \sin[2(2m-1)\pi x + \phi] \right].$$

3.5 Results and discussion

In this section, the graphical results are displayed. The integration which appears to compute pressure rise Δp is calculated numerically using a mathematics software. The pressure rise Δp for different values of slip parameter L , magnetic parameter M and amplitude ratio ϕ are

plotted in Figs. 3.1 to 3.3. Fig. 3.1 illustrate the pressure rise for different values of L . It is shown that Δp decreases for small values of Q with an increase in L , however, Δp increases for large values of Q with an increase in L . Thus we say that Δp and Q has inversely linear relation between each other. Fig. 3.2 represents the variation of Δp with Q for different values of M . It is observed that the pressure rise increases with an increase in M for small Q whereas for large Q , Δp decreases with an increase in M . The effects of the amplitude ratio ϕ on the pressure rise are shown in Fig. 3.3. It is observed that for $Q \in [-1, 2]$, the pressure rise decreases with an increase in ϕ , whereas for $Q \in [2, 3]$, the pressure rise increases. The pressure gradient for different value of M and L against x is plotted in Figs. 3.4 and 3.5. It is depicted that for $x \in [0, 0.2]$ and $x \in [0.8, 1]$, the pressure gradient is small i.e., the flow can easily pass, while in the region $x \in [0.2, 0.8]$, pressure gradient increases with an increase in M and decreases with an increase in L and much pressure gradient is required to maintain the flux to pass. The velocity field for several values of M , λ_1 and Q are shown in Figs. 3.6 to 3.8. It is seen from Figs. 3.6 and 3.7 that for $Y \in [-1.65, -1]$ and $[1, 1.65]$, the velocity field show slight increase with an increase in M , while $Y \in [-1, 1]$ with an increase in M and λ_1 , the velocity decreases and the maximum value of velocity is at the center of the channel. Velocity profile for different values of Q is shown in Fig. 3.8. It is observed that the velocity profile increases with an increase in Q . The temperature profile for several values of L , P_r , M , and λ_1 are shown in Figs. 3.9 to 3.12. It is observed that temperature field decreases with an increase of L , M and λ_1 , while it is increases with an increase in P_r . The pressure rise Δp for different types of waves are presented in Fig. 3.13. It is observed that Δp in trapezoidal wave is greater than sinusoidal wave which is greater than triangular wave. The temperature field for different waves form are presented in Fig. 3.14. It is observed that temperature field for sinusoidal wave is greater than trapezoidal wave and the temperature field for triangular wave is greater than sinusoidal wave.

Trapping phenomena

Another interesting phenomena in peristaltic motion is trapping. It is basically the formation of an internally circulating bolus of fluid by closed stream lines. This trapped bolus pushed a head along a peristaltic waves. Figs. 3.15 to 3.17, illustrate the stream lines for different values of L , Q , and M for both symmetric and asymmetric channel. It is observed that for a symmetric channel the trapping bolus is symmetric about the centre line of the channel (see

panels (a) and (c)), while in case of asymmetric channel the bolus tends to shift towards left side of the channel due to phase angle (see panels (b) and (d)). Fig. 3.15 shows the stream lines for different values of slip parameter L . It is observed that with an increase in L , the size of the trapping bolus decreases. Moreover, it is also observed that the size of the trapping bolus is small in asymmetric channel as compared with the symmetric channel. It is also observed from Fig. 3.16 that with an increase in Q , the size and the number of the trapped bolus increases. The size of the trapped bolus increases with an increase in M (see Fig. 3.17). Stream lines for different waves forms are presented in Fig. 3.18. It is observed that the size of the trapped bolus is smaller in case of triangular wave when compared with other wave forms.

Table 3.1 and 3.2 show the comparison of present solution with those available in the literature when some of parameters are replaced to be zero in our problem.

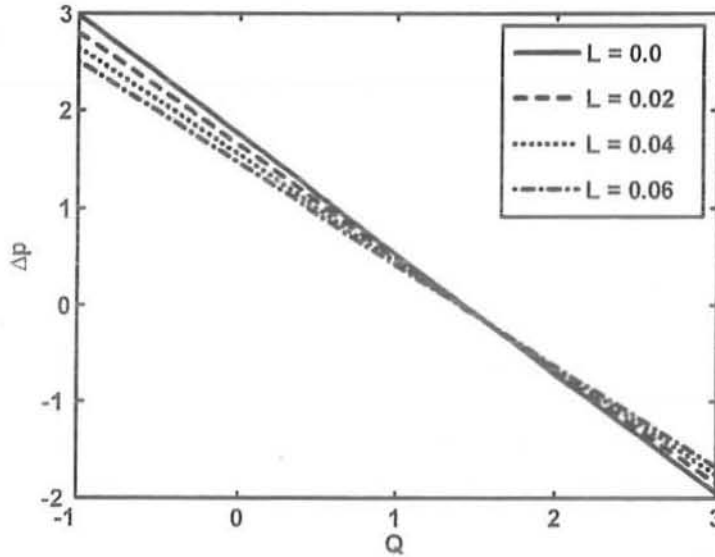


Fig.(3.1) : Variation of Δp with Q for different values of L at $a = 0.7$, $b = 1.2$, $d = 2$, $M = 0.1$, $\phi = \frac{\pi}{6}$, $\lambda_1 = 0.4$.

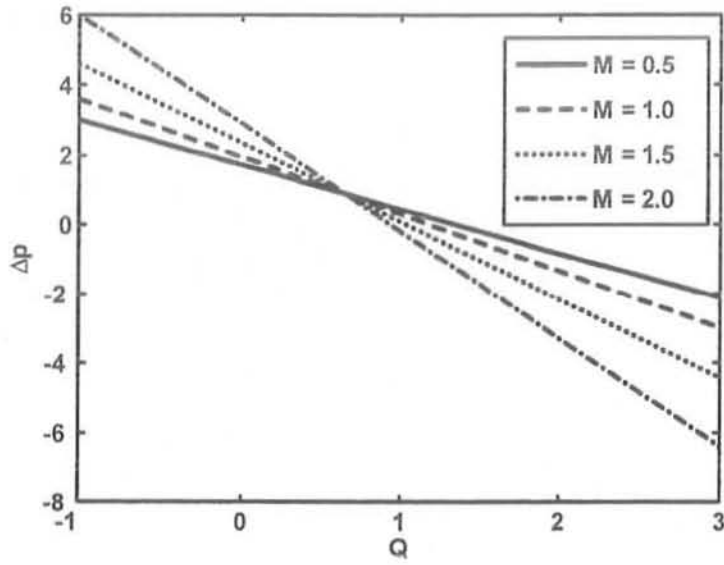


Fig.(3.2) : Variation of Δp with Q for different values of M at $a = 0.7$, $d = 2$, $b = 1.2$, $L = 0.02$, $\phi = \frac{\pi}{6}$, $\lambda_1 = 0.4$.

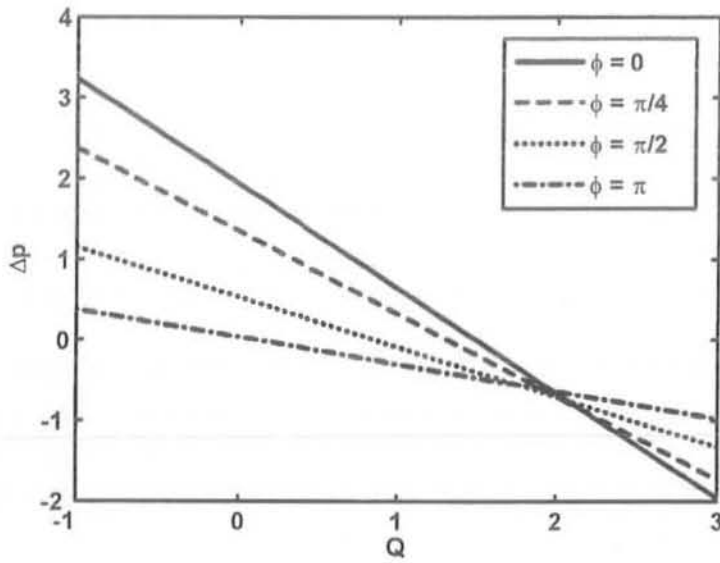


Fig.(3.3) : Variation of Δp with Q for different values of ϕ at $a = 0.7$, $d = 2$, $b = 1.2$, $M = 0.1$, $L = 0.02$, $\lambda_1 = 0.4$.

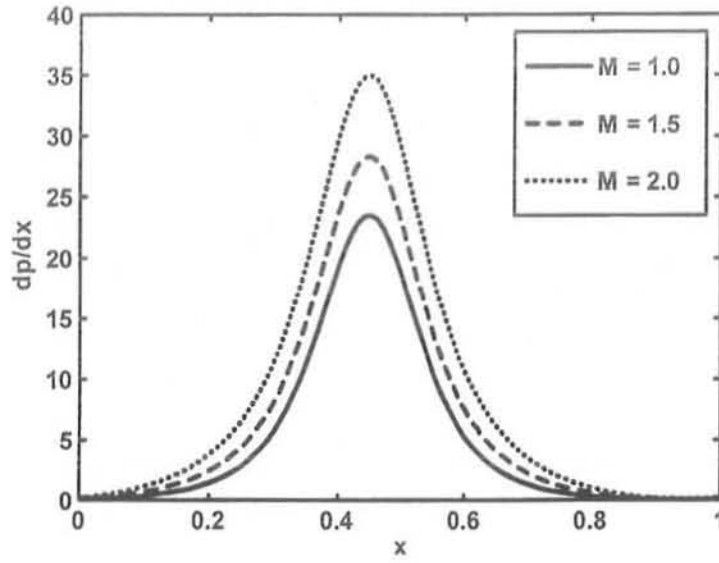


Fig.(3.4) : Variation of $\frac{dp}{dx}$ with x for different values of M at $a = 0.7$, $b = 1.2$, $d = 2$, $L = 0.02$, $Q = -1$, $\phi = \frac{\pi}{6}$, $\lambda_1 = 0.4$.

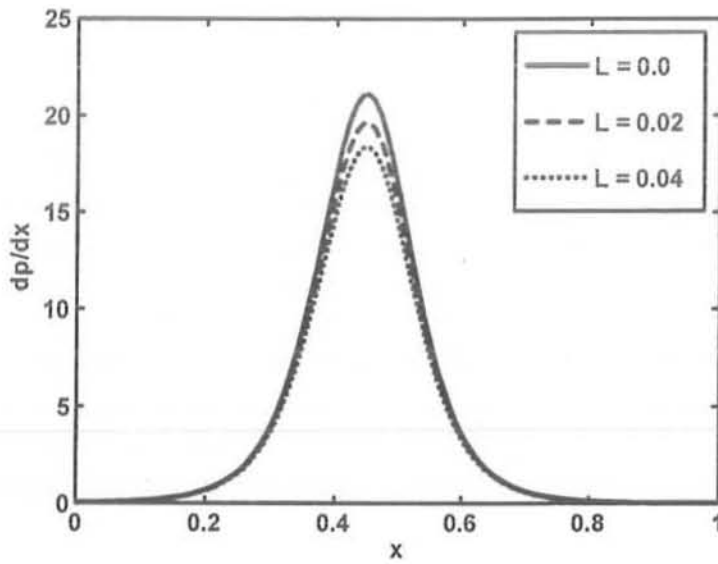


Fig.(3.5) : Variation of $\frac{dp}{dx}$ with x for different values of L at $a = 0.7$, $b = 1.2$, $d = 2$, $M = 0.1$, $Q = -1$, $\phi = \frac{\pi}{6}$, $\lambda_1 = 0.4$.

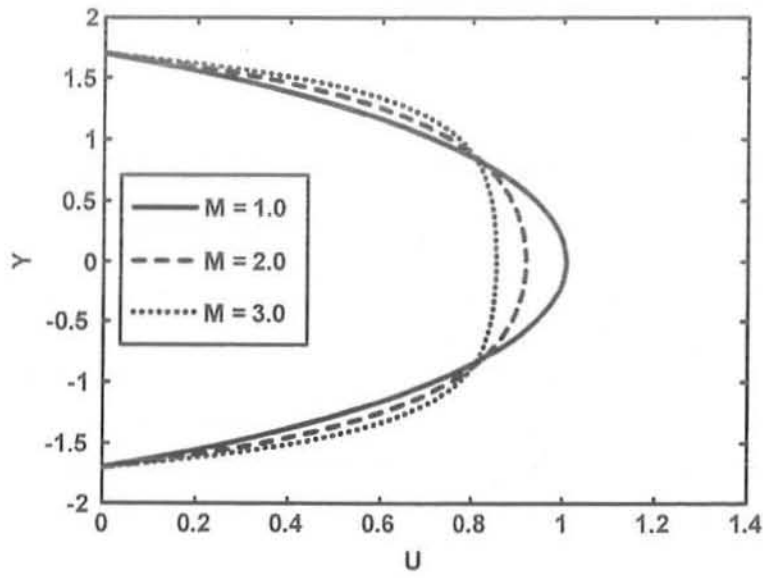


Fig.(3.6) : Velocity profile for different values of M at $a = 0.7, b = 0.7, d = 1.7, Q = 1.7, L = 0.001, X = 1, t = 1, \phi = \frac{\pi}{2}$.

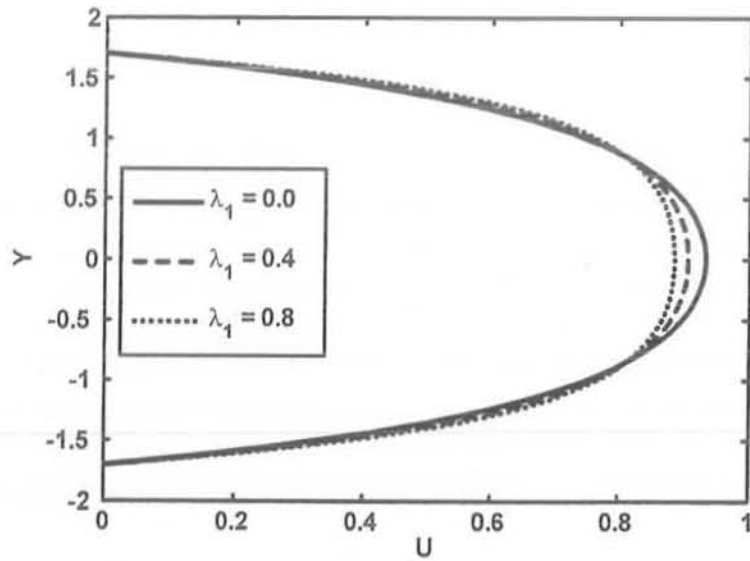


Fig.(3.7) : Velocity profile for different values of λ_1 at $a = 0.7, b = 0.7, d = 1.7, L = 0.001, Q = 1.7, X = 1, t = 1, \phi = \frac{\pi}{2}$.

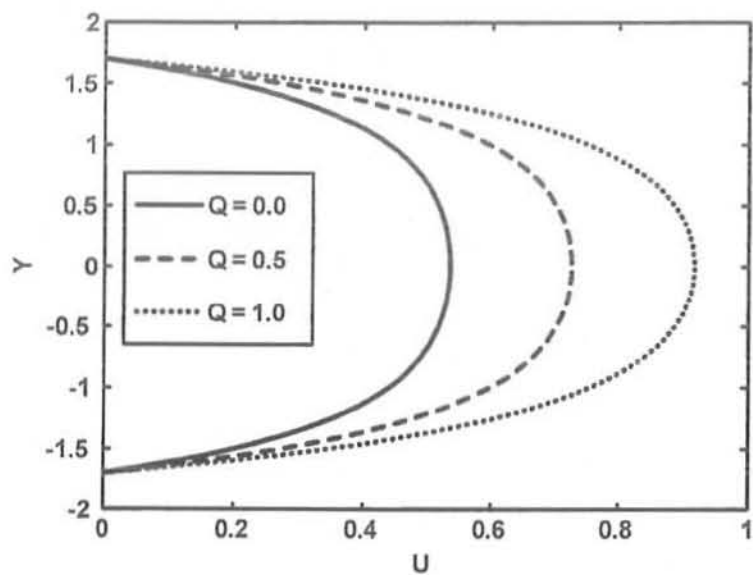


Fig.(3.8) : Velocity profile for different values of Q of at $a = 0.7, b = 0.7, d = 1.7, L = 0.001, X = 1, t = 1, \phi = \frac{\pi}{2}$.

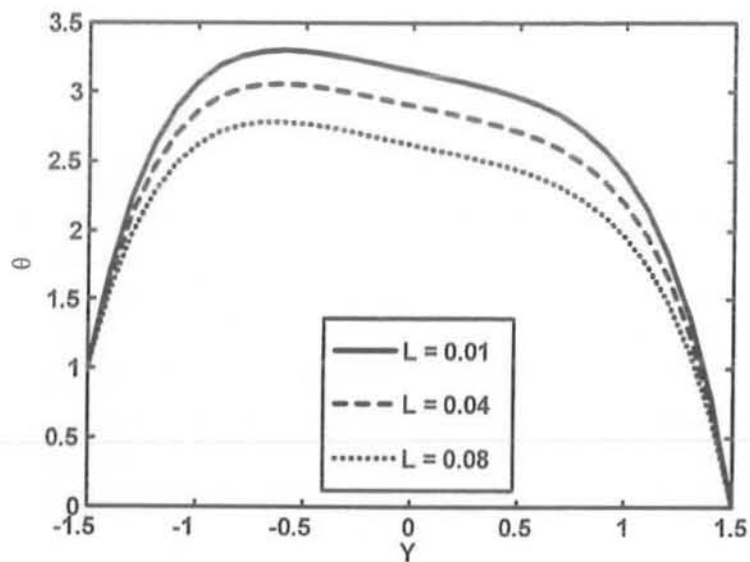


Fig.(3.9) : Temperature profile θ for different values of L at $a = 0.5, b = 1.2, d = 1.5, Q = -2, M = 0.1, \lambda_1 = 0.4, E_r = 1, P_r = 1, X = 1, t = 1, \phi = \frac{\pi}{2}$.

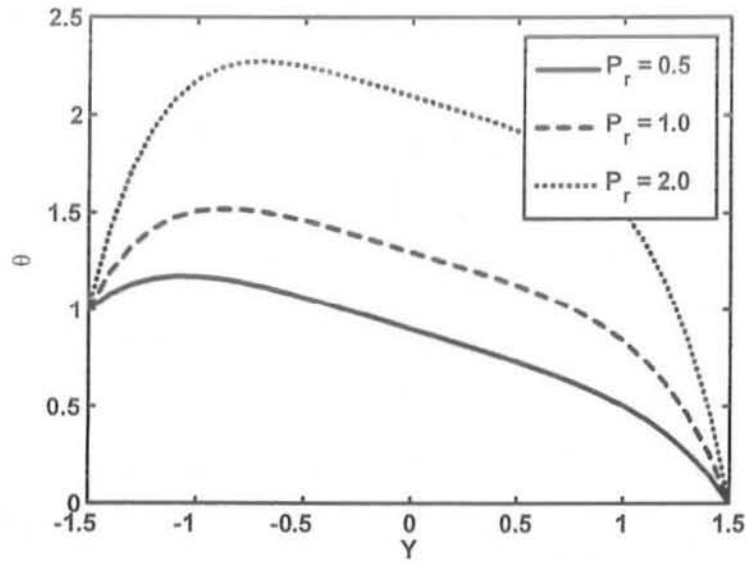


Fig.(3.10) : Temperature profile θ for different values of P_r at $a = 0.5, b = 1.2, d = 1.5, Q = -1, M = 0.1, \lambda_1 = 0.4, E_r = 1, L = 0.02, X = 1, t = 1, \phi = \frac{\pi}{2}$.

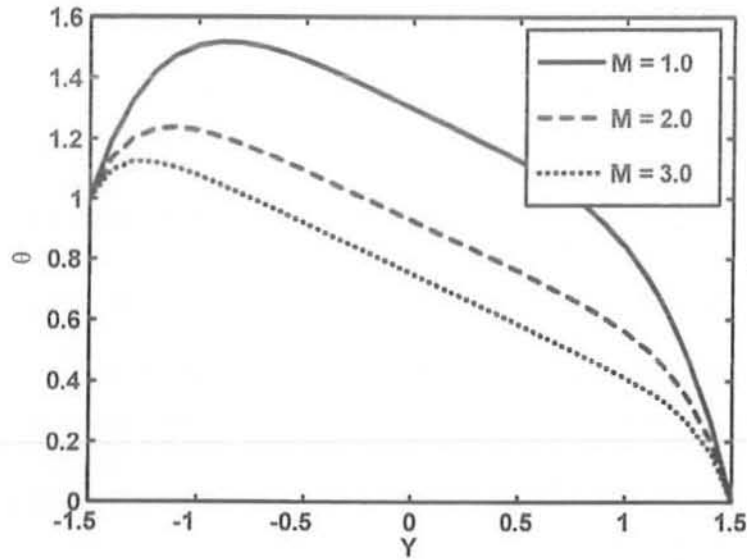


Fig.(3.11) : Temperature profile θ for different values of M at $a = 0.5, b = 1.2, d = 1.5, Q = -2, L = 0.02, \lambda_1 = 0.4, E_r = 1, P_r = 1, X = 1, t = 1, \phi = \frac{\pi}{2}$.

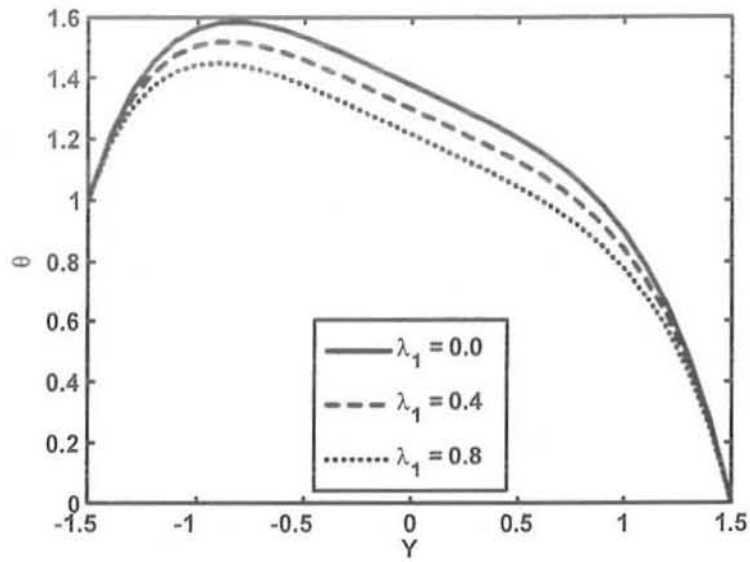


Fig.(3.12) : Temperature profile θ for different values of λ_1 at $a = 0.5, b = 1.2, d = 1.5, Q = -2, M = 0.1, L = 0.02, E_r = 1, P_r = 1, X = 1, t = 1, \phi = \frac{\pi}{2}$.

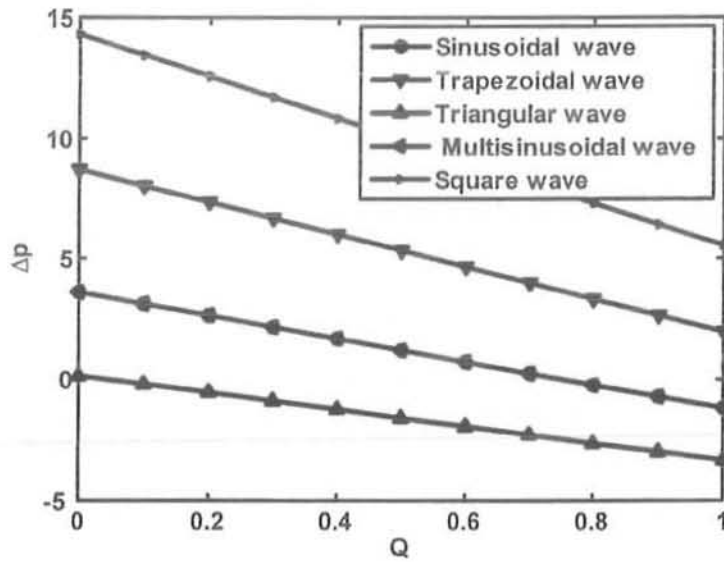


Fig.(3.13): Variation of Δp with Q for different wave form at $a = 0.7, b = 1.2, d = 2, M = 3, L = 0.02, \lambda_1 = 2, \phi = \frac{\pi}{6}$.

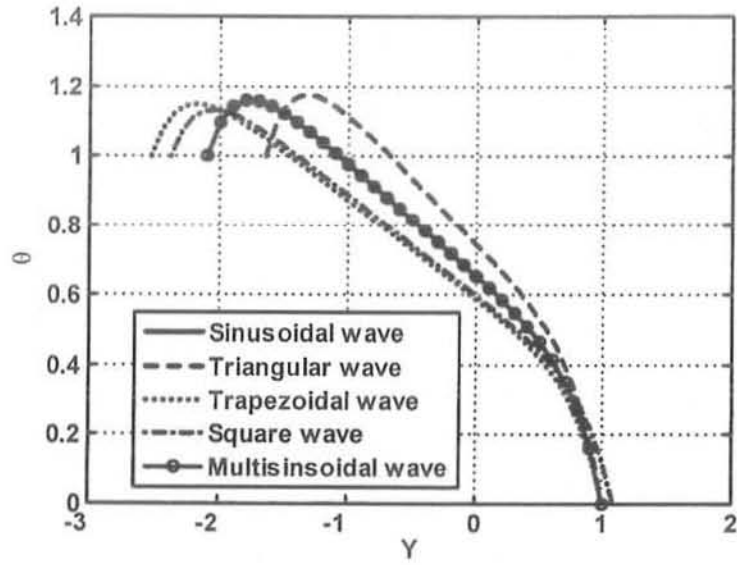
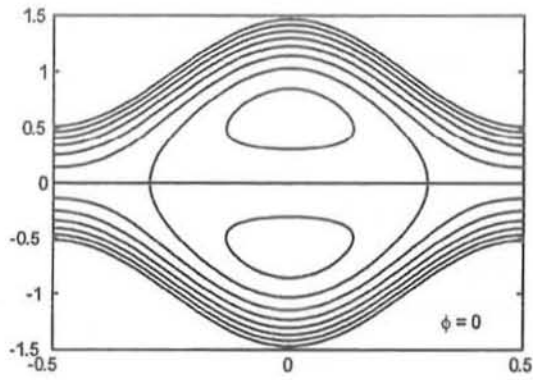
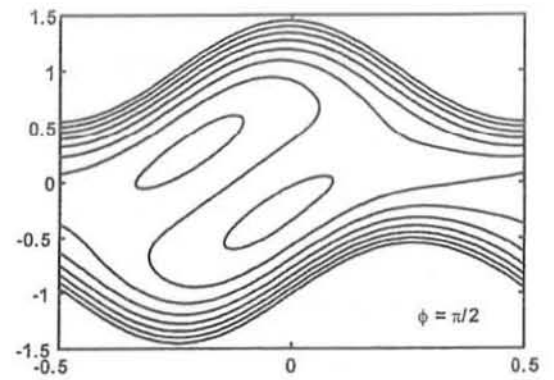


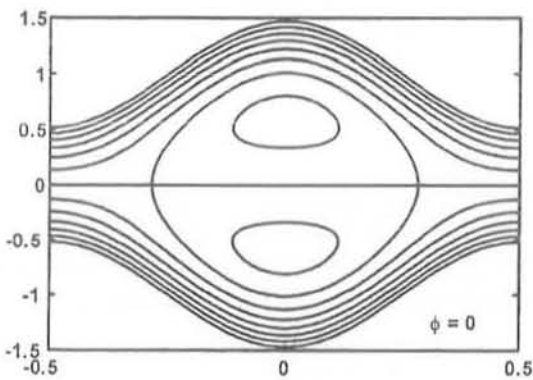
Fig.(3.14) : Temperature profile θ for different wave forms at $a = 0.7$, $b = 1.2$, $d = 1.5$, $Q = -2$, $M = 2$, $L = 0.5$, $E_r = 1$, $P_r = 1$, $\phi = \frac{\pi}{6}$, $X = 1$, $t = 1$, $\lambda_1 = 0.4$.



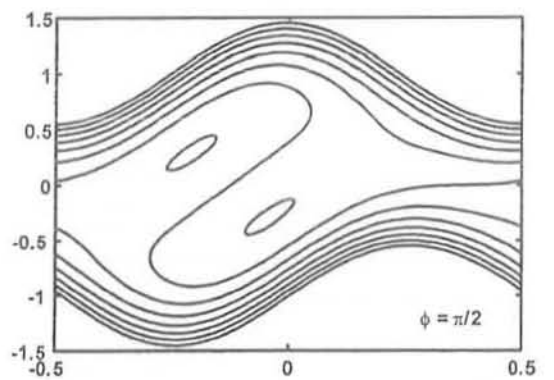
(a)



(b)

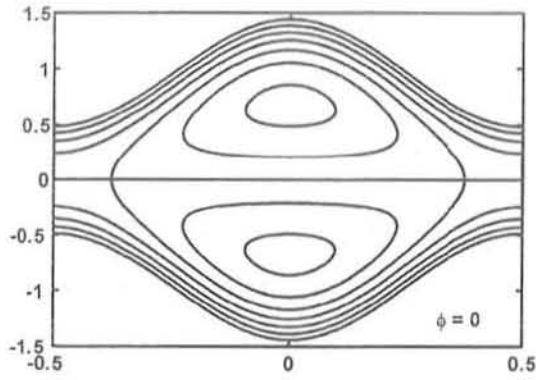


(c)

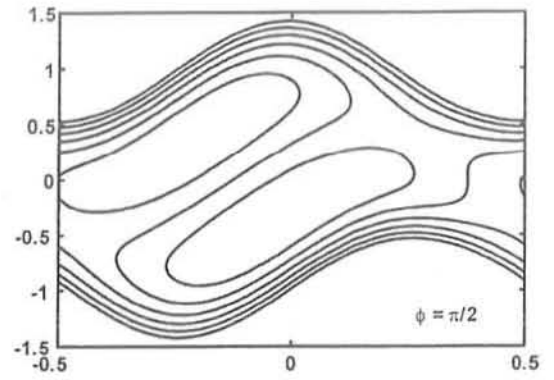


(d)

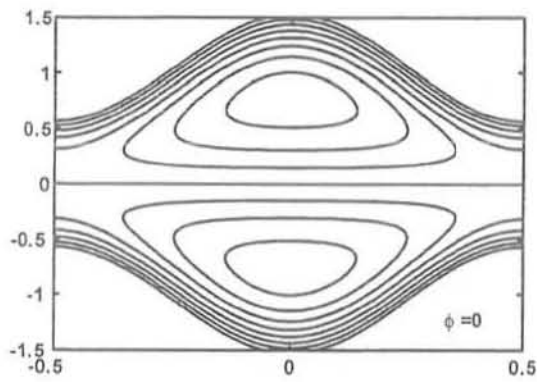
Fig.(3.15) : Stream lines for two different values of L . (a) and (b) for $L = 0.01$, (c) and (d) for $L = 0.03$. The other parameters are chosen as $a = 0.5$, $b = 0.5$, $d = 1.0$, $Q = 1.45$, $\lambda_1 = 0.1$, $M = 1$.



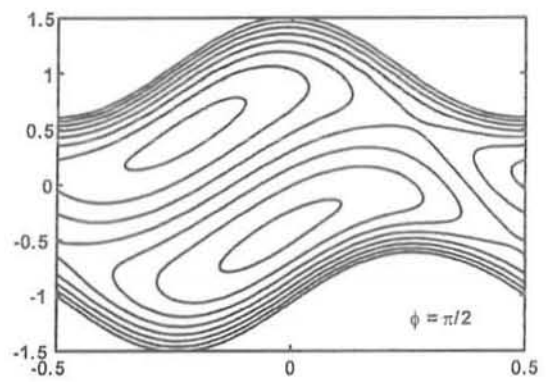
(a)



(b)

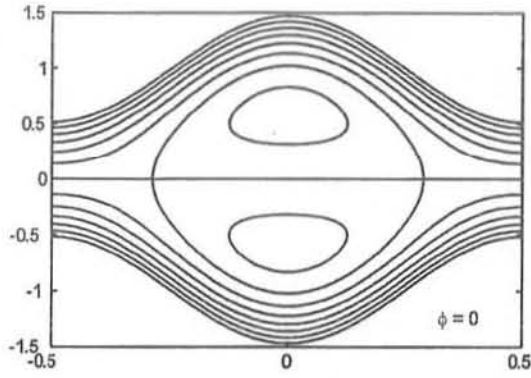


(c)

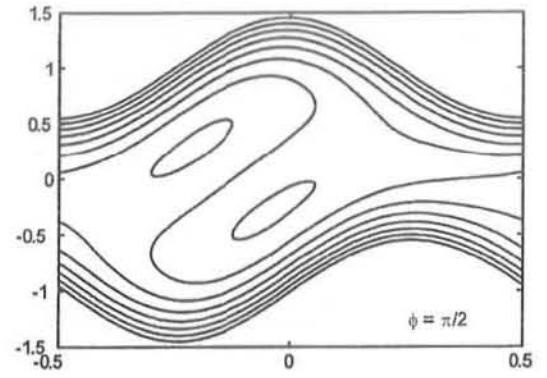


(d)

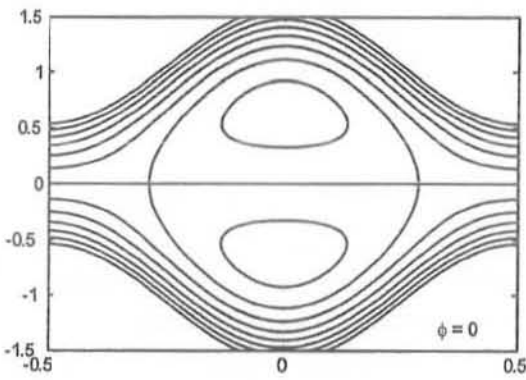
Fig.(3.16) : Stream lines for two different values of Q . (a) and (b) for $Q = 1.8$, (c) and (d) for $Q = 2.0$. The other parameters are chosen as $a = 0.5$, $b = 0.5$, $d = 1.0$, $L = 0.02$, $\lambda_1 = 0.2$, $M = 1$.



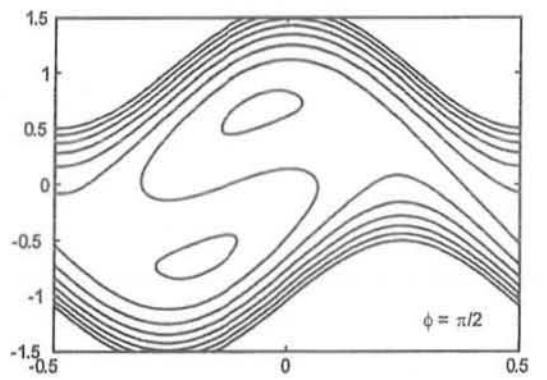
(a)



(b)

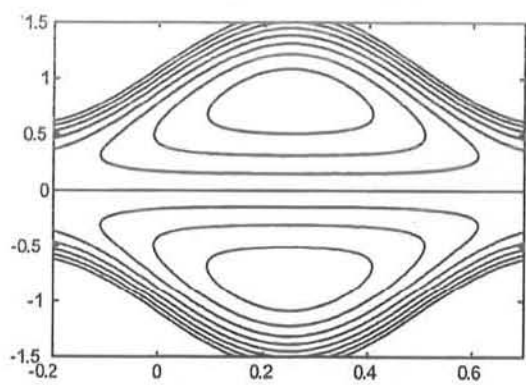


(c)

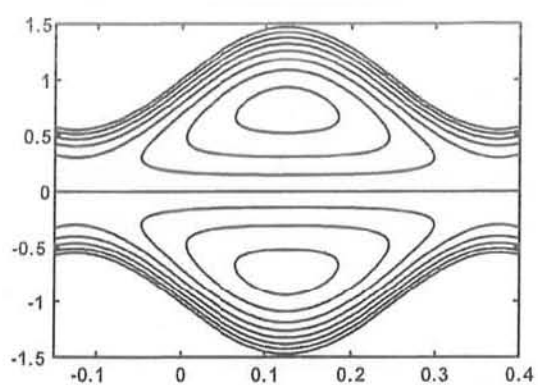


(d)

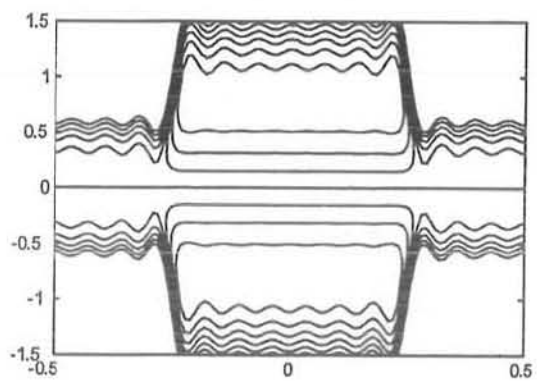
Fig.(3.17) : Stream lines for two different values of M . (a) and (b) for $M = 1.0$, (c) and (d) for $M = 1.1$. The other parameters are chosen as $a = 0.5$, $b = 0.5$, $d = 1.0$, $L = 0.02$, $\lambda_1 = 0.2$, $Q = 1.45$.



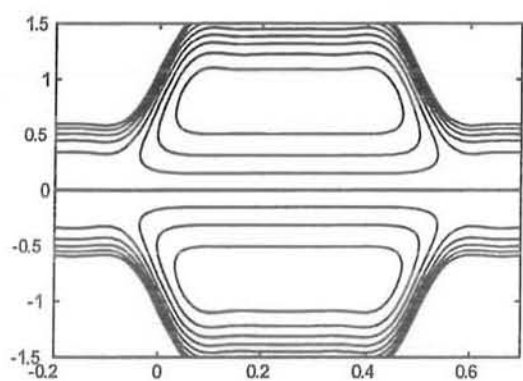
(a)



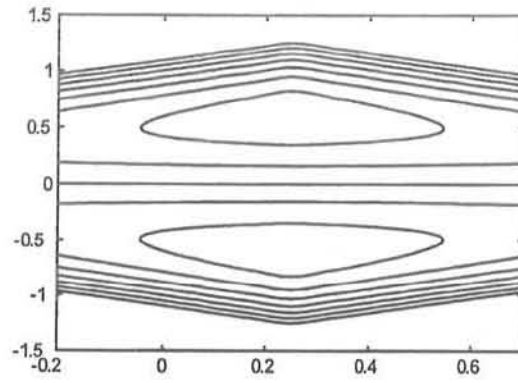
(b)



(c)



(d)



(e)

Fig.(3.18): Stream lines for different wave shape for fixed $a = 0.5$, $b = 0.5$, $d = 1.0$, $M = 1$, $L = 0.02$, $\lambda_1 = 0.2$, $Q = 1.8$, $\phi = 0$: (a) sinusoidal wave (b) multisinusoidal wave (c) square wave (d) trapezoidal wave (e) triangular wave.

Table 3.1: Pressure rise with volume flow rate for fixed $a = 0.7$, $b = 1.2$, $d = 2$, $M = 0.1$, $\phi = \frac{\pi}{6}$, $\lambda_1 = 0.4$.

Q	M. Kothandapani et al [35] when $L = 0$	Present work when $L = 0.02$
-1	2.98239	2.80332
-0.5	2.36653	2.22225
0	1.75066	1.64118
0.5	1.13479	1.06011
1	0.518927	0.479047
1.5	-0.09694	-0.10202
2	-0.712807	-0.683087
2.5	-1.32867	-1.26415
3	-1.94454	-1.84522

Table 3.2: Velocity profile for fixed $a = 0.7$, $b = 0.7$, $d = 1$, $X = 1$, $t = 1$, $\phi = 0$.

Y	M. Kothandapani et al [35] when $L = 0$	Present work when $L = 0.02$
-1.7	0	0
-1.3	0.5619	0.574951
-0.9	0.794255	0.786245
-0.5	0.887231	0.870794
-0.1	0.916923	0.897794
0.1	0.916923	0.897794
0.5	0.887231	0.870794
0.9	0.794255	0.786245
1.3	0.5619	0.574951
1.7	0	0

3.6 Conclusion

This chapter presents the effects of heat transfer and magnetic field on a peristaltic transport of a Jeffrey fluid in an asymmetric channel with partial slip. The governing two dimensional equations are simplified using long wave length approximation. In the wave frame of reference, an exact and closed form Adomian solution is presented. The results are discussed through graphs. The main finding can be summarized as follows:

1. It is observed that the pressure rise Δp and volume flow rate Q has inversely linear relation between each other.
2. The pressure gradient increases with an increase in Hartmann number M and decreases with an increase in slip parameter L .
3. The velocity field show slight increase with an increase in M and λ_1 when $Y \in [-1.65, -1]$, while it decreases with an increase in M and λ_1 when $Y \in [-1, 1]$ and the maximum value of the velocity is at the center of the channel.
4. The temperature field decreases with an increase in L , M and λ_1 , while it is increases with an increase in P_r .
5. The pressure rise in trapezoidal wave is greater than sinusoidal wave which is greater than triangular wave.
6. The temperature field for sinusoidal wave is grater than trapezoidal wave and the temperature field for triangular wave is greater than sinusoidal wave.
7. The size of the trapping bolus decreases with an increase in L .
8. The number of the trapping bolus increases with an increase in Q .
9. The size of the trapping bolus increases with an increase in M .

Chapter 4

Influence of induced magnetic field on the peristaltic motion of a Jeffrey fluid in an asymmetric channel: Closed form solutions

4.1 Introduction

This chapter deals with the peristaltic motion of a two dimensional Jeffrey fluid in an asymmetric channel under the effects of induced magnetic field. The problem is simplified by using long wave length and low Reynolds number approximations. An exact and closed form Adomian solutions have been presented. The expressions for velocity, stream function, magnetic force function, temperature, pressure gradient and pressure rise have been computed. The results of pertinent parameters have been discussed graphically. Finally, the trapping phenomena for different wave shape have also been discussed. It is observed that the pressure rise for sinusoidal wave is less than trapezoidal wave and greater than triangular in a Jeffrey fluid.

4.2 Mathematical formulation

Let us consider the peristaltic flow of an incompressible, electrically conducting non-Newtonian fluid (Jeffrey fluid) in a two dimensional channel of width $d_1 + d_2$. The lower wall of the channel is maintained at temperature T_1 while the upper wall has temperature T_0 . The flow is generated by sinusoidal wave trains propagating with constant speed c along the channel walls. We choose a rectangular coordinate system for the channel with X along the centerline of the channel and Y is transverse to it. An external transverse uniform constant magnetic field H_0 , induced magnetic field $H(h_X(X, Y, t), H_0 + h_Y(X, Y, t), 0)$ and the total magnetic field $H^+(h_X(X, Y, t), H_0 + h_Y(X, Y, t), 0)$ are taken into account. The geometry of the asymmetric channel is defined in Eq. (1.1), the continuity, energy, Maxwell and induction equations are defined in Eqs. (1.2), (1.5), (2.2) to (2.4) and (2.6), however the momentum equation in the presence of induced magnetic field is defined as

$$\rho \left(\frac{\partial \mathbf{V}}{\partial t} + (\mathbf{V} \cdot \nabla) \mathbf{V} \right) = \text{div } \boldsymbol{\tau} - \nabla \left(\frac{1}{2} \mu_e (\mathbf{H}^+)^2 \right) - \mu_e (\mathbf{H}^+ \cdot \nabla) \mathbf{H}^+, \quad (4.1)$$

where the extra stress tensor \mathbf{S} for Jeffrey fluid is defined in Eq. (3.3).

Defining

$$\begin{aligned} \bar{x} &= \frac{x}{\lambda}, \quad \bar{y} = \frac{y}{d_1}, \quad \bar{u} = \frac{u}{c}, \quad \bar{v} = \frac{v}{c}, \quad \delta = \frac{d_1}{\lambda}, \quad d = \frac{d_2}{d_1}, \quad p = \frac{d_1^2 P}{\mu c \lambda}, \quad \bar{t} = \frac{ct}{\lambda}, \quad h_1 = \frac{H_1}{d_1}, \\ h_2 &= \frac{H_2}{d_2}, \quad a = \frac{a_1}{d_1}, \quad b = \frac{b_1}{d_1}, \quad \text{Re} = \frac{cd_1}{\nu}, \quad \bar{\Psi} = \frac{\Psi}{cd_1}, \quad \bar{\Phi} = \frac{\Phi}{H_0 d_1}, \\ p_m &= p + \frac{1}{2} \text{Re} \delta \frac{\mu_e (H^+)^2}{\rho c^2}, \quad R_m = \sigma \mu_e d_1 c, \quad S_1 = \frac{H_0}{c} \sqrt{\frac{\mu_e}{\rho}}, \quad \theta = \frac{T - T_0}{T_1 - T_0}, \\ E_c &= \frac{c^2}{C' (T_1 - T_0)}, \quad P_r = \frac{\rho \nu C'}{K'}, \quad \bar{S} = \frac{S d_1}{\mu c}. \end{aligned} \quad (4.2)$$

With the help of Eqs. (1.6), (1.11) and (4.2), Eqs. (1.2), (1.5), (2.6) and (4.1) in terms of the stream function $\Psi(x, y)$ and magnetic-force function $\Phi(x, y)$ (dropping the bars and using

$u = \frac{\partial \Psi}{\partial y}, v = -\delta \frac{\partial \Psi}{\partial x}, h_x = \frac{\partial \Phi}{\partial y}, h_y = -\delta \frac{\partial \Phi}{\partial x}$ take the form

$$\begin{aligned} \operatorname{Re} \delta (\Psi_y \Psi_{xy} - \Psi_x \Psi_{yy}) &= -\frac{\partial p_m}{\partial x} + \delta \frac{\partial}{\partial x} (S_{xx}) + \frac{\partial}{\partial y} (S_{xy}) \\ &\quad + \operatorname{Re} S_1^2 \Phi_{yy} + \operatorname{Re} S_1^2 \delta (\Phi_y \Phi_{xy} - \Phi_x \Phi_{yy}), \end{aligned} \quad (4.3)$$

$$\begin{aligned} \operatorname{Re} \delta^3 (\Psi_x \Psi_{xy} - \Psi_y \Psi_{xx}) &= -\frac{\partial p_m}{\partial y} + \delta^2 \frac{\partial}{\partial x} (S_{yx}) + \delta \frac{\partial}{\partial y} (S_{yy}) \\ &\quad - \operatorname{Re} \delta^2 S_1^2 \Phi_{xy} - \operatorname{Re} S_1^2 \delta^3 (\Phi_y \Phi_{xx} - \Phi_x \Phi_{xy}), \end{aligned} \quad (4.4)$$

$$\begin{aligned} \operatorname{Re} \delta (\Psi_y \theta_x - \Psi_x \theta_y) &= \frac{1}{P_r} (\theta_{yy} + \delta^2 \theta_{xx}) + \\ &\quad \frac{E_c}{(1 + \lambda_1)} \left(1 + \frac{\lambda_2 c \delta}{d_1} \left(\Psi_y \frac{\partial}{\partial x} - \Psi_x \frac{\partial}{\partial y} \right) \right) \\ &\quad \left(4\delta^2 \Psi_{xy}^2 + (\Psi_{yy} - \delta^2 \Psi_{xx})^2 \right), \end{aligned} \quad (4.5)$$

$$\Psi_y - \delta (\Psi_y \Phi_x - \Psi_x \Phi_y) + \frac{1}{R_m} (\Phi_{yy} + \delta^2 \Phi_{xx}) = E, \quad (4.6)$$

where

$$\begin{aligned} S_{xx} &= \frac{2\delta}{1 + \lambda_1} \left(1 + \frac{\lambda_2 c \delta}{d_1} \left(\Psi_y \frac{\partial}{\partial x} - \Psi_x \frac{\partial}{\partial y} \right) \right) \Psi_{xy}, \\ S_{xy} &= \frac{1}{1 + \lambda_1} \left(1 + \frac{\lambda_2 c \delta}{d_1} \left(\Psi_y \frac{\partial}{\partial x} - \Psi_x \frac{\partial}{\partial y} \right) \right) (\Psi_{yy} - \delta^2 \Psi_{xx}), \\ S_{yy} &= -\frac{2\delta}{1 + \lambda_1} \left(1 + \frac{\lambda_2 c \delta}{d_1} \left(\Psi_y \frac{\partial}{\partial x} - \Psi_x \frac{\partial}{\partial y} \right) \right) \Psi_{xy}. \end{aligned} \quad (4.7)$$

Under the assumption of long wave length $\delta \ll 1$ and low Reynold number neglecting the terms of order δ and higher, Eqs. (4.3) to (4.7) take the form

$$-\frac{\partial p}{\partial x} + \frac{\partial}{\partial y} \left(\frac{1}{1 + \lambda_1} \frac{\partial^2 \Psi}{\partial y^2} \right) + \operatorname{Re} S_1^2 \Phi_{yy} = 0, \quad (4.8)$$

$$\frac{\partial p}{\partial y} = 0, \quad (4.9)$$

$$\frac{1}{P_r} \theta_{yy} + \frac{E_c}{(1 + \lambda_1)} \Psi_{yy}^2 = 0, \quad (4.10)$$

$$\Phi_{yy} = R_m \left(E - \frac{\partial \Psi}{\partial y} \right). \quad (4.11)$$

Elimination of pressure from Eqs. (4.8) and (4.9) yields

$$\frac{\partial^2}{\partial y^2} \left(\frac{1}{1 + \lambda_1} \frac{\partial^2 \Psi}{\partial y^2} \right) + \text{Re } S_1^2 \Phi_{yyy} = 0. \quad (4.12)$$

Combining Eq. (4.11) and (4.12) yields

$$\frac{\partial^3 \Psi}{\partial y^3} + M^2(1 + \lambda_1) \left(E - \frac{\partial \Psi}{\partial y} \right) = F_{11}, \quad (4.13)$$

where F_{11} is a constant, $M^2 = R_m \text{Re} S_1^2$, Re is the Reynolds number, S_1 is the Strommer's number (magnetic force number) and R_m is the magnetic Reynolds number.

The corresponding dimensionless boundary conditions are

$$\begin{aligned} \Psi &= \frac{q}{2}, & \text{at } y = h_1 = 1 + a \cos 2\pi x, \\ \Psi &= -\frac{q}{2}, & \text{at } y = h_2 = -d - b \cos(2\pi x + \phi), \\ \frac{\partial \Psi}{\partial y} &= -1, & \text{at } y = h_1 \text{ and } y = h_2, \end{aligned} \quad (4.14)$$

$$\begin{aligned} \theta &= 0, & \text{at } y = h_1, \\ \theta &= 1, & \text{at } y = h_2, \end{aligned} \quad (4.15)$$

$$\Phi = 0, \quad \text{at } y = h_1 \text{ and } y = h_2. \quad (4.16)$$

4.3 Solution of the problem

4.3.1 Exact Solution

The exact solution of Eq. (4.13) can be written as

$$\Psi = F_8 + F_9 \cosh(m_3 y) + F_{10} \sinh(m_3 y) + Ey - \frac{F_{11}}{m_3^2} y, \quad (4.17)$$

where

$$m_3 = M \sqrt{(1 + \lambda_1)},$$

and F_8, F_9, F_{10} and F_{11} are functions of x only which has been calculated with the help of boundary conditions (4.14) as

$$\begin{aligned}
F_8 &= \frac{qm_3(h_1 + h_2) + 2(h_2 + h_1) \tanh \left[m_3 \left(\frac{h_1 - h_2}{2} \right) \right]}{2(h_2 - h_1)m_3 + 4 \tanh \left[m_3 \left(\frac{h_1 - h_2}{2} \right) \right]}, \\
F_9 &= \frac{(q + h_1 - h_2) \operatorname{sech} \left[m_3 \left(\frac{h_1 - h_2}{2} \right) \right] \sinh \left[m_3 \left(\frac{h_1 + h_2}{2} \right) \right]}{(h_1 - h_2)m_3 - 2 \tanh \left[m_3 \left(\frac{h_1 - h_2}{2} \right) \right]}, \\
F_{10} &= \frac{(q + h_1 - h_2) \operatorname{sech} \left[m_3 \left(\frac{h_1 - h_2}{2} \right) \right] \cosh \left[m_3 \left(\frac{h_1 + h_2}{2} \right) \right]}{(h_2 - h_1)m_3 + 2 \tanh \left[m_3 \left(\frac{h_1 - h_2}{2} \right) \right]}, \\
F_{11} &= \frac{m_3^3(q - h_1E + Eh_2) + 2m_3^2(E + 1) \tanh \left[m_3 \left(\frac{h_1 - h_2}{2} \right) \right]}{(h_2 - h_1)m_3 + 2 \tanh \left[m_3 \left(\frac{h_1 - h_2}{2} \right) \right]}. \tag{4.18}
\end{aligned}$$

4.3.2 Solution by Adomian decomposition method

In this section, the Adomian solutions will be determined for the stream function. According to Adomian decomposition method, we rewrite Eq. (4.13) in the operator form as

$$\hat{L}_{yyy}\Psi = (F_{11} - m_3^2E) + m_3^2\Psi_y. \tag{4.19}$$

Applying the inverse operator $\hat{L}_{yyy}^{-1} = \int \int \int [\cdot] dydydy$, we can write Eq. (4.19) as

$$\Psi = C_8 + C_9y + C_{10}\frac{y^2}{2!} + (F_{11} - m_3^2E)\frac{y^3}{3!} + m_3^2L_{yyy}^{-1}(\Psi_y), \tag{4.20}$$

where

$$m_3^2 = M^2(1 + \lambda_1),$$

and C_8, C_9, C_{10}, F_{11} are functions of x . Now we decompose Ψ as

$$\Psi = \sum_{n=0}^{\infty} \Psi_n. \tag{4.21}$$

Substituting Ψ into Eq. (4.20), we obtain

$$\begin{aligned}\Psi_0 &= C_8 + C_9 y + C_{10} \frac{y^2}{2!} + (F_{11} - m_3^2 E) \frac{y^3}{3!}, \\ \Psi_{n+1} &= m_3^2 \int \int \int (\Psi_n)_y dy dy dy, n \geq 0.\end{aligned}\quad (4.22)$$

Therefore,

$$\begin{aligned}\Psi_1 &= m_3^2 \left(C_9 \frac{y^3}{3!} + C_{10} \frac{y^4}{4!} + (F_{11} - m_3^2 E) \frac{y^5}{5!} \right), \\ \Psi_2 &= m_3^4 \left(C_9 \frac{y^5}{5!} + C_{10} \frac{y^6}{6!} + (F_{11} - m_3^2 E) \frac{y^7}{7!} \right), \\ &\vdots \\ \Psi_n &= m_3^{2n} \left(C_9 \frac{y^{2n+1}}{(2n+1)!} + C_{10} \frac{y^{2n+2}}{(2n+2)!} + (F_{11} - m_3^2 E) \frac{y^{2n+3}}{(2n+3)!} \right), \quad n > 0.\end{aligned}\quad (4.23)$$

With the help of Eq. (4.21), the closed form of Ψ can be written as

$$\Psi = C_8 + \sinh(m_3 y) \left(\frac{C_9}{m_3} + \frac{1}{m_3} (F_{11} - m_3^2 E) \right) + \frac{C_{10}}{m_3^2} (\cosh(m_3 y) - 1) - \frac{1}{m_3^2} (F_{11} - m_3^2 E) y.$$

The simplest form of above equation can be written as

$$\Psi = F_8 + F_9 \cosh(m_3 y) + F_{10} \sinh(m_3 y) + E y - \frac{F_{11}}{m_3^2} y. \quad (4.24)$$

Now the Adomian solution (4.24) and exact solution (4.17) are exactly same in which $F_i (i = 8$ to 11) are calculated using boundary conditions which are defined in Eq. (4.18).

Making use of Eq. (4.17), the exact solution of Eq. (4.10) in fixed frame satisfying the boundary condition can be written as

$$\begin{aligned}\theta &= -\frac{E_c P_r}{(1 + \lambda_1)} \left(\frac{F_9^2}{2} m_3^4 Y^2 + \frac{1}{8} (F_9^2 + F_{10}^2) m_3^2 \cosh 2(m_3 Y) + \frac{1}{4} F_9 F_{10} m_3^2 \sinh 2(m_3 Y) \right. \\ &\quad \left. - \frac{1}{4} (F_9^2 + F_{10}^2) m_3^4 Y^2 \right) + c_7 Y + c_8,\end{aligned}\quad (4.25)$$

where

$$\begin{aligned}
c_7 &= \frac{-1}{(h_1 - h_2)} + \frac{E_c P_r}{(1 + \lambda_1)(h_1 - h_2)} \left(\frac{1}{2} F_9^2 m_3^4 (h_1^2 - h_2^2) - \frac{1}{4} (F_9^2 + F_{10}^2) m_3^4 (h_1^2 - h_2^2) \right. \\
&\quad \left. + \frac{1}{8} (F_9^2 + F_{10}^2) m_3^2 (\cosh 2(m_3 h_1) - \cosh 2(m_3 h_2)) \right. \\
&\quad \left. + \frac{1}{4} F_9 F_{10} m_3^2 (\sinh 2(m_3 h_1) - \sinh 2(m_3 h_2)) \right), \\
c_8 &= \frac{E_c P_r}{(1 + \lambda_1)} \left(\frac{1}{2} F_9^2 m_3^4 h_1^2 + \frac{1}{4} F_9 F_{10} m_3^2 \sinh 2(m_3 h_1) + \frac{1}{8} (F_9^2 + F_{10}^2) m_3^2 \cosh 2(m_3 h_1) \right. \\
&\quad \left. - \frac{1}{4} (F_9^2 + F_{10}^2) m_3^4 h_1^2 \right) - c_7 h_1. \tag{4.26}
\end{aligned}$$

With the help of Eq. (4.17) the solution of Eq. (4.11) can be straightforward written as

$$\Phi = c_9 y + c_{10} + \frac{F_{11} R_m y^2}{m_3^2} - R_m \left(\frac{F_9}{m_3} \sinh(m_3 y) + \frac{F_{10}}{m_3} \cosh(m_3 y) \right), \tag{4.27}$$

where c_9 and c_{10} are calculated using boundary condition (4.16), which are as follow

$$\begin{aligned}
c_9 &= \frac{R_m}{2} (h_1 + h_2) \left(\frac{m_3 (q - h_1 E + h_2 E) + 2(E + 1) \tanh \left[m_3 \left(\frac{h_1 - h_2}{2} \right) \right]}{(h_1 - h_2) m_3 - 2 \tanh \left[m_3 \left(\frac{h_1 - h_2}{2} \right) \right]} \right), \\
c_{10} &= \frac{R_m}{2} \left(h_1 h_2 (1 + E) + \frac{(2 + h_1 h_2 m_3^2) (h_1 - h_2 + q)}{m_3 \left((h_2 - h_1) m_3 + 2 \tanh \left[m_3 \left(\frac{h_1 - h_2}{2} \right) \right] \right)} \right). \tag{4.28}
\end{aligned}$$

The expression for axial induced magnetic field can be obtained with the help of $h_x = \frac{\partial \Phi}{\partial y}$, which are as follows

$$h_x(x, y) = \frac{R_m \left(\begin{aligned} &2(q + h_1 - h_2) \sec h \left[m_3 \left(\frac{h_1 - h_2}{2} \right) \right] \sinh \left[m_3 \left(\frac{h_1 + h_2}{2} - y \right) \right] \\ &+ (2y - h_1 - h_2) \left(m_3 (q - h_1 E + h_2 E) + 2(E + 1) \tanh \left[m_3 \left(\frac{h_1 - h_2}{2} \right) \right] \right) \end{aligned} \right)}{2(h_2 - h_1) m_3 + 4 \tanh \left[m_3 \left(\frac{h_1 - h_2}{2} \right) \right]}. \tag{4.29}$$

Also the current density distribution takes the following form

$$J_z = \frac{R_m \left(\begin{array}{l} 2m_3 (q + h_1 - h_2) \operatorname{sech} \left[m_3 \left(\frac{h_1 - h_2}{2} \right) \right] \cosh \left[m_3 \left(\frac{h_1 + h_2}{2} - y \right) \right] \\ -2 \left(m_3 (q - h_1 E + h_2 E) + 2(E + 1) \tanh \left[m_3 \left(\frac{h_1 - h_2}{2} \right) \right] \right) \end{array} \right)}{2(h_1 - h_2)m_3 - 4 \tanh \left[m_3 \left(\frac{h_1 - h_2}{2} \right) \right]} \quad (4.30)$$

The pressure gradient is obtained from the dimensionless momentum equation for the axial velocity as

$$\frac{dp}{dx} = \frac{1}{(1 + \lambda_1)} \Psi_{yyy} + M^2 (E - \Psi_y). \quad (4.31)$$

Substituting the value of Ψ given in Eq. (4.17), Eq. (4.31) takes the form

$$\frac{dp}{dx} = \frac{m_3^3 (q - h_1 E + h_2 E) + 2m_3^2 (E + 1) \tanh \left[m_3 \left(\frac{h_1 - h_2}{2} \right) \right]}{(1 + \lambda_1) \left((h_2 - h_1) m_3 + 2 \tanh \left[m_3 \left(\frac{h_1 - h_2}{2} \right) \right] \right)} \quad (4.32)$$

For one wavelength, the integration of Eq. (4.32), yields

$$\Delta p = \int_0^1 \frac{m_3^3 (q - h_1 E) + 2m_3^2 (E + 1) \tanh \left[m_3 \left(\frac{h_1 - h_2}{2} \right) \right]}{(1 + \lambda_1) \left((h_2 - h_1) m_3 + 2 \tanh \left[m_3 \left(\frac{h_1 - h_2}{2} \right) \right] \right)} dx. \quad (4.33)$$

The axial velocity component in fixed frame is calculated as

$$\begin{aligned} U(X, Y, t) &= 1 + \Psi_y \\ &= \frac{m_3 (h_1 - h_2 + q) \left(-1 + \operatorname{sech} \left[m_3 \left(\frac{h_1 - h_2}{2} \right) \right] \cosh \left[m_3 \left(\frac{h_1 + h_2}{2} - Y \right) \right] \right)}{(h_2 - h_1) m_3 + 2 \tanh \left[m_3 \left(\frac{h_1 - h_2}{2} \right) \right]}. \end{aligned} \quad (4.34)$$

4.4 Expressions for different wave shape

The non- dimensional expressions for three considered wave form for the present case are given as

1. Sinusoidal wave

$$h_1(x) = 1 + a \sin 2\pi x, \quad h_2(x) = -d - b \sin(2\pi x + \phi).$$

2. Triangular wave

$$h_1(x) = 1 + a \left[\frac{8}{\pi^3} \sum_{m=1}^{\infty} \frac{(-1)^{m+1}}{(2m-1)^2} \sin(2\pi(2m-1)x) \right],$$

$$h_2(x) = -d - b \left[\frac{8}{\pi^3} \sum_{m=1}^{\infty} \frac{(-1)^{m+1}}{(2m-1)^2} \sin(2\pi(2m-1)x + \phi) \right].$$

3. Trapezoidal wave

$$h_1(x) = 1 + a \left[\frac{32}{\pi^2} \sum_{m=1}^{\infty} \frac{\sin \frac{\pi}{8}(2m-1)}{(2m-1)^2} \sin(2\pi(2m-1)x) \right],$$

$$h_2(x) = -d - b \left[\frac{32}{\pi^2} \sum_{m=1}^{\infty} \frac{\sin \frac{\pi}{8}(2m-1)}{(2m-1)^2} \sin(2\pi(2m-1)x + \phi) \right].$$

4.5 Results and discussion

The exact and closed form Adomian solutions of the Eq. (4.13) subject to the boundary conditions (4.14) have been computed. The graphical results of pressure rise, velocity, magnetic force function, axial induced magnetic field, current density and temperature are displayed in Figs. 4.1 to 4.16. Figs. 4.1 and 4.2 are prepared for pressure rise Δp against volume flow rate Q for different values of Jeffrey parameter λ_1 and amplitude ratio ϕ . It is observed from both the figures that the relation between pressure rise and volume flow rate are inversely proportional to each other. It means that pressure rise give larger values for small volume flow rate and it gives smaller values for large Q . Moreover, the peristaltic pumping occurs in the region $-1 \leq Q < 1.6$ for λ_1 and $-1 \leq Q \leq 1.8$ for ϕ , other wise augmented pumping occurs. The velocity U for different values of λ_1 and M are shown in Figs. 4.3 and 4.4 which describe the effects of λ_1 and M on the velocity field. We observed that near the channel walls the velocity increases but in the middle of the channel the velocity decreases with an increases in λ_1 (see Fig. 4.3). It is observed from Fig. 4.4 that the velocity field increases near the channel walls but in the middle of the channel the velocity decreases and is maximum for small values of M at the center. The magnetic force function Φ for different values of E , λ_1 , M , R_m , and Q are shown in Figs. 4.5 to 4.9. It is observed from Figs. 4.5 to 4.8 that the magnitude of the magnetic force function increases with an increase in E , λ_1 , M and R_m . It is observed from

Fig. 4.9 that with an increase in Q , the magnitude of the magnetic force function decreases. The expression for axial induced magnetic field h_x against space variable y for different values of magnetic Reynold number R_m and E are shown in Figs. 4.10 and 4.11. It is observed that the relation between h_x and y are inversely proportional to each other, with an increase in R_m and E in the region $-2 \leq y \leq 0$, h_x decreases, while in the region $0 \leq y \leq 2$, h_x increases with an increase in R_m and E . The current density distribution function J_z with space variable y for different values of M and λ_1 are shown in Figs. 4.12 and 4.13. It is observed from both the figures that the current density decreases in the middle of the channel. The temperature field for different values of λ_1, P_r and E_c against space variable Y in fixed frame are displayed in Figs. 4.14 to 4.16. It is depicted that with an increases in λ_1 the temperature field decreases while the temperature field increases with an increases in P_r and E_c .

The pressure rise for different kinds of wave shape are presented in Fig. 4.17. It is observed that the pressure rise for sinusoidal wave is less than trapezoidal wave and greater than triangular wave. The temperature field θ for different wave shape are shown in Fig. 4.18. It is seen that the temperature field for triangular wave is greater than sinusoidal wave and sinusoidal wave is greater than trapezoidal wave. The magnetic force function Φ for different wave shape are shown in Fig. 4.19. It is observed that the magnitude value of the magnetic force function Φ for trapezoidal wave is greater than sinusoidal and triangular waves.

The trapping phenomena for different values of λ_1, E and Q are shown in Figs. 4.20 to 4.23. It is observed from Fig. 4.20 that the volume of the trapped bolus in the lower half channel is smaller as compared to the upper half of the channel, moreover, the size of the trapped bolus decreases with an increase in λ_1 and finally the number of trapped bolus reduces. It is depicted from Fig. 4.21 that with an increase in E the size of the trapped bolus decreases. The stream lines for different values of Q are plotted in Figs. 4.22. It is observed that the number and size of the trapped bolus increases with an increases in Q . The stream lines for different wave shape such as sinusoidal wave, triangular wave and trapezoidal wave are shown in Figs. 4.23.

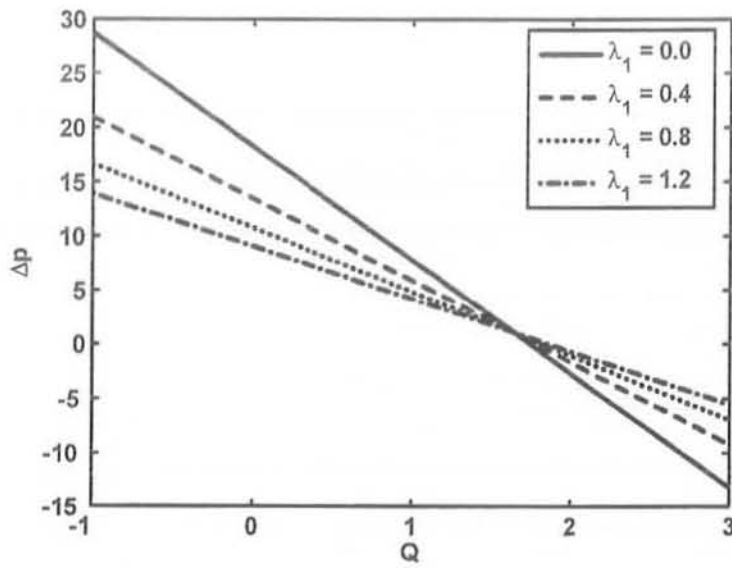


Fig. (4.1) : Variation of Δp with Q for different values of λ_1 at $a = 0.7$, $b = 1.2$, $d = 1.4$, $E = 4$, $M = 0.5$, $\phi = \frac{\pi}{6}$.

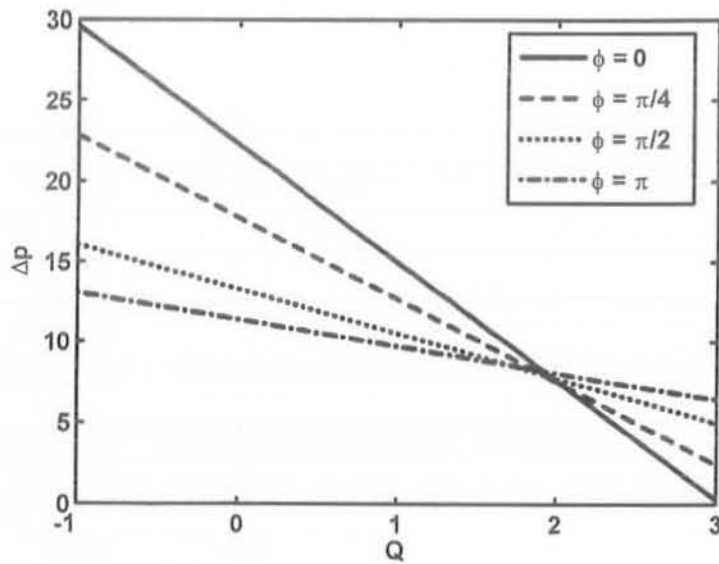


Fig. (4.2) : Variation of Δp with Q for different values of ϕ at $a = 0.7$, $b = 1.2$, $d = 1.5$, $E = 4$, $M = 1.5$, $\lambda_1 = 0.5$.

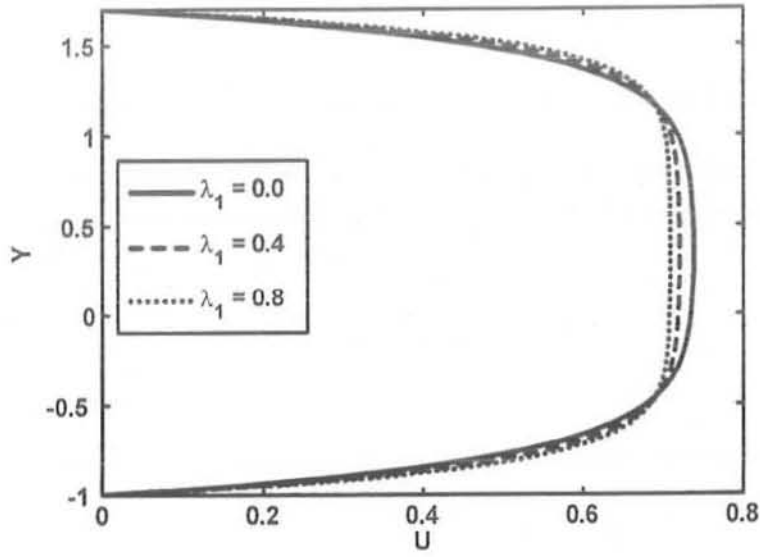


Fig. (4.3) : Velocity profile for different values of λ_1 at $a = 0.7, b = 0.7, d = 1, X = 1, t = 1, Q = 1, M = 5, \phi = \frac{\pi}{2}$.

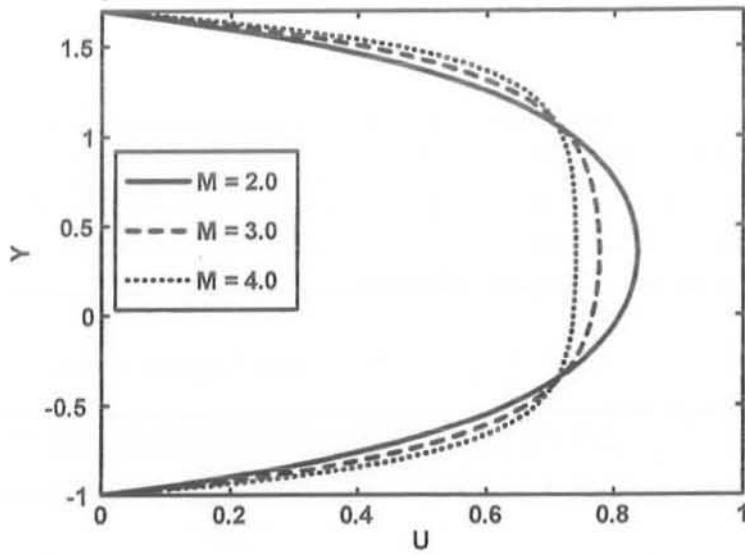


Fig. (4.4) : Velocity profile for different values of M at $a = 0.7, b = 0.7, d = 1, X = 1, t = 1, Q = 1, \lambda_1 = 0.5, \phi = \frac{\pi}{2}$.

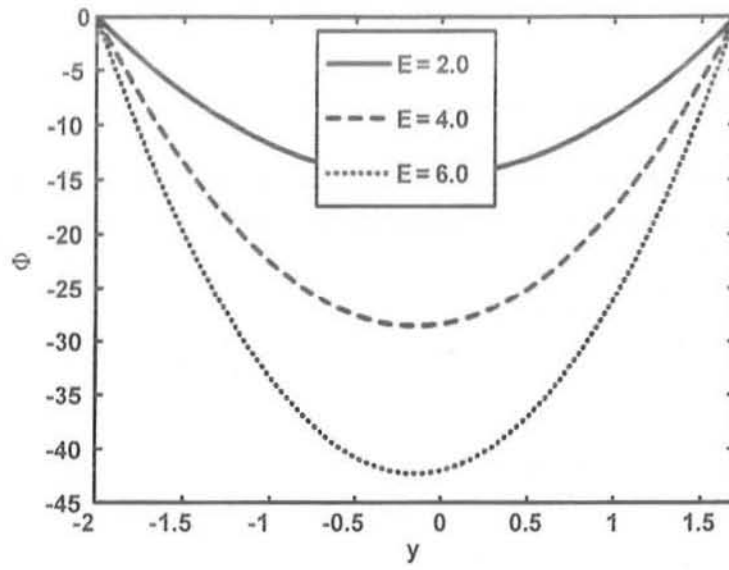


Fig. (4.5) : Profile of magnetic force function Φ for different values of E at $a = 0.7$, $b = 1.2$, $d = 2$, $x = 0$, $R_m = 4$, $Q = 2$, $M = 2$, $\lambda_1 = 2$, $\phi = \frac{\pi}{2}$.

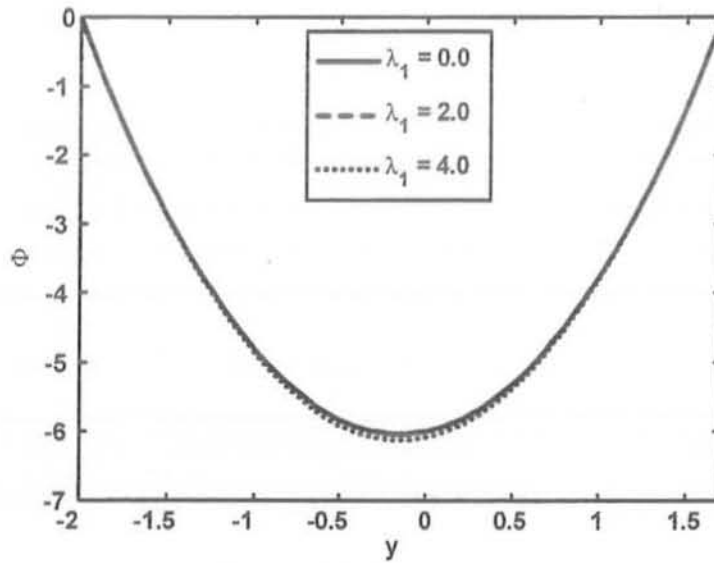


Fig. (4.6) : Profile of magnetic force function Φ for different values of λ_1 at $a = 0.7$, $b = 1.2$, $d = 2$, $x = 0$, $R_m = 3$, $Q = 2$, $M = 2$, $E = 1$, $\phi = \frac{\pi}{2}$.

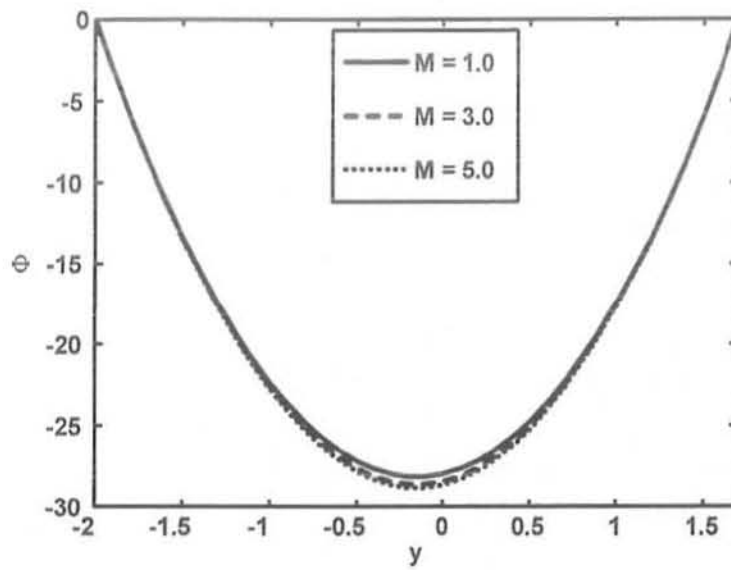


Fig. (4.7) : Profile of magnetic force function Φ for different values of M at $a = 0.7$, $b = 1.2$, $d = 2$, $x = 0$, $R_m = 4$, $Q = 2$, $\lambda_1 = 0.5$, $E = 4$, $\phi = \frac{\pi}{2}$.

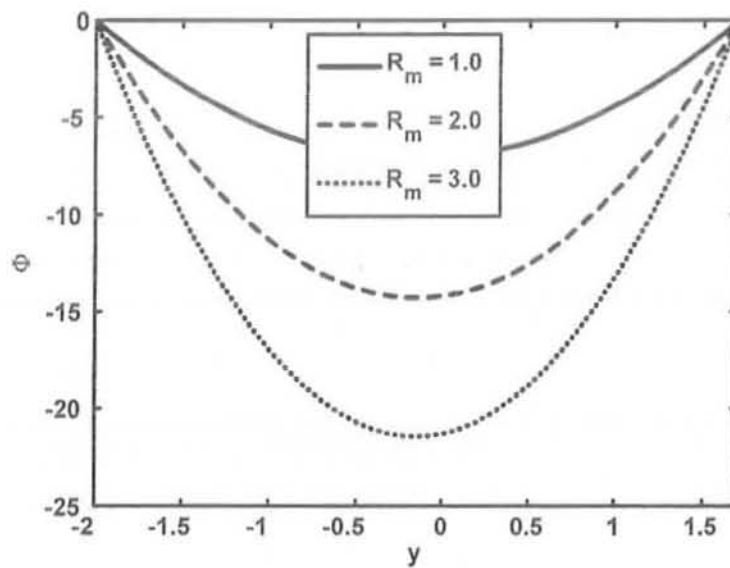


Fig. (4.8) : Profile of magnetic force function Φ for different values of R_m at $a = 0.7$, $b = 1.2$, $d = 2$, $x = 0$, $M = 2$, $Q = 2$, $\lambda_1 = 2$, $E = 4$, $\phi = \frac{\pi}{2}$.

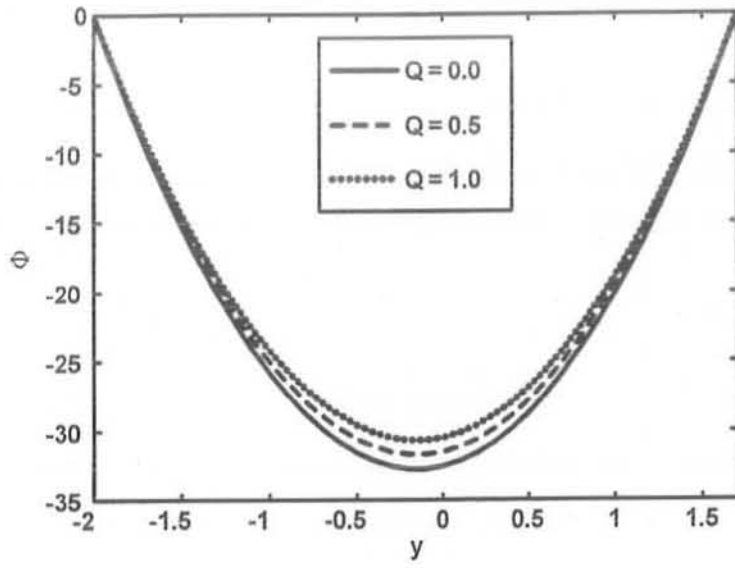


Fig. (4.9) : Profile of magnetic force function Φ for different values of Q at $a = 0.7$, $b = 1.2$, $d = 2$, $x = 0$, $M = 2$, $R_m = 4$, $\lambda_1 = 2$, $E = 4$, $\phi = \frac{\pi}{2}$.

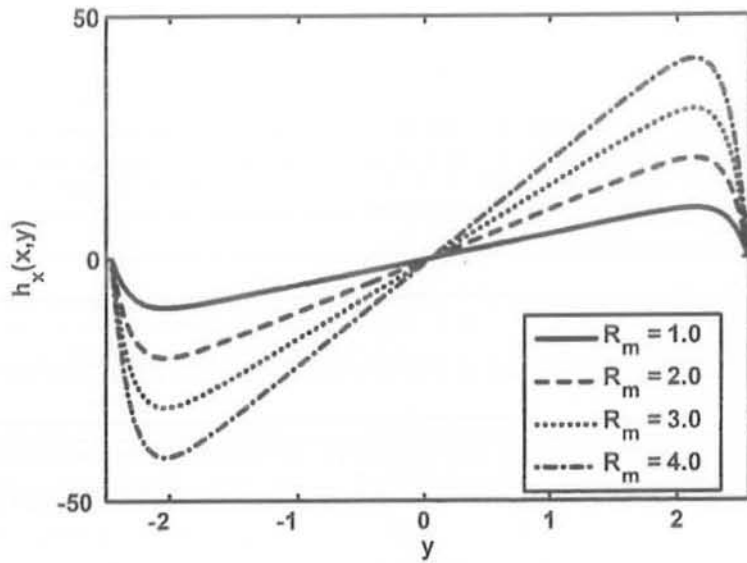


Fig. (4.10) : Variation of axial induced magnetic field h_x for different values of R_m at $a = 0.7$, $b = 0.7$, $Q = -0.85$, $\phi = \pi$, $d = 2.3$, $E = 4$, $M = 3$, $x = 0$, $\lambda_1 = 4$.

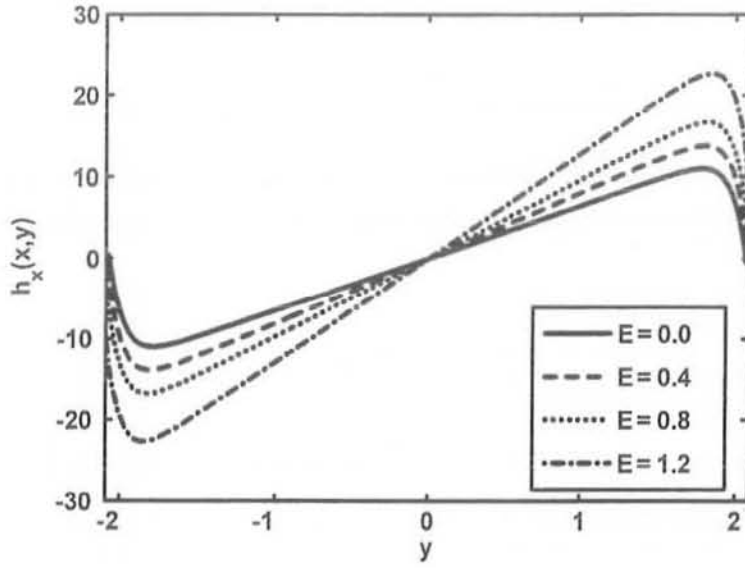


Fig. (4.11) : Variation of axial induced magnetic field h_x for different values of E at $a = 0.7$, $b = 0.7$, $Q = -2.0$, $\phi = \pi$, $d = 2.4$, $R_m = 4$, $M = 5$, $x = 0$, $\lambda_1 = 4$.

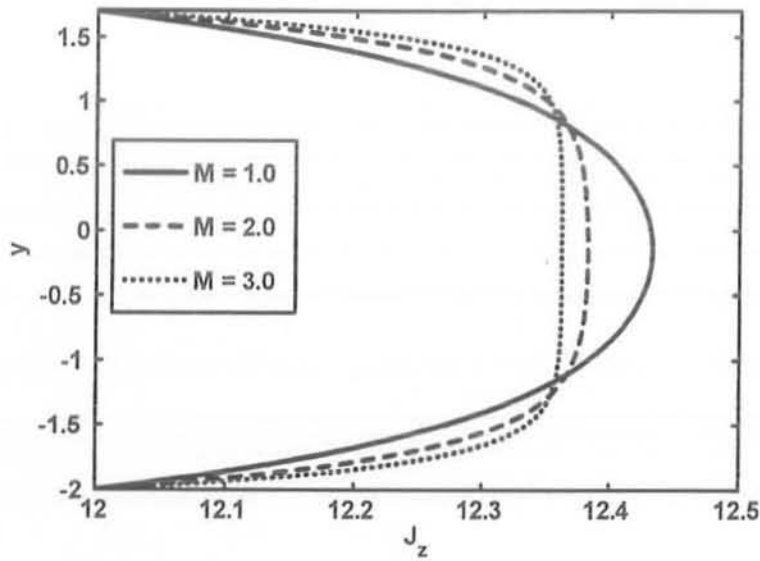


Fig. (4.12) : Profile of current density distribution J_z for different values of M at $a = 0.7$, $b = 1.2$, $Q = -1.0$, $\phi = \frac{\pi}{2}$, $d = 2.0$, $R_m = 4$, $E = 2$, $x = 0$, $\lambda_1 = 2$.

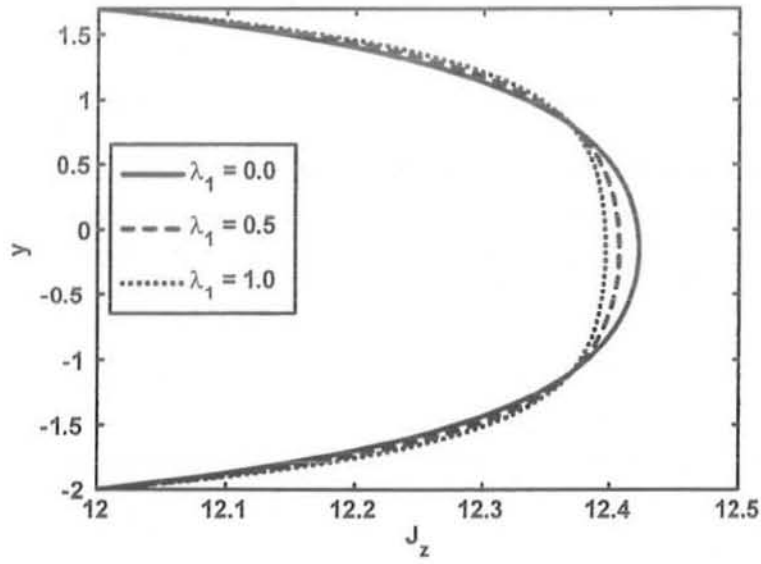


Fig. (4.13) : Profile of current density distribution J_z for different values of λ_1 at $a = 0.7$, $b = 1.2$, $Q = -1.0$, $\phi = \frac{\pi}{2}$, $d = 2.4$, $R_m = 4$, $M = 2$, $x = 0$, $E = 2$.

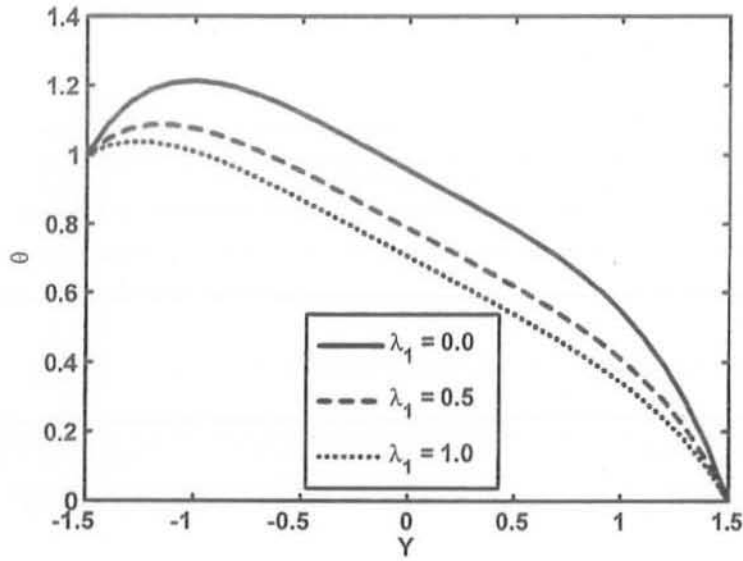


Fig. (4.14) : Temperature profile θ for different values of λ_1 at $a = 0.5$, $b = 1.2$, $d = 1.5$, $E = 4$, $M = 1$, $P_r = 1$, $E_c = 1$, $X = 1$, $t = 1$, $Q = 2$, $\phi = \frac{\pi}{2}$.

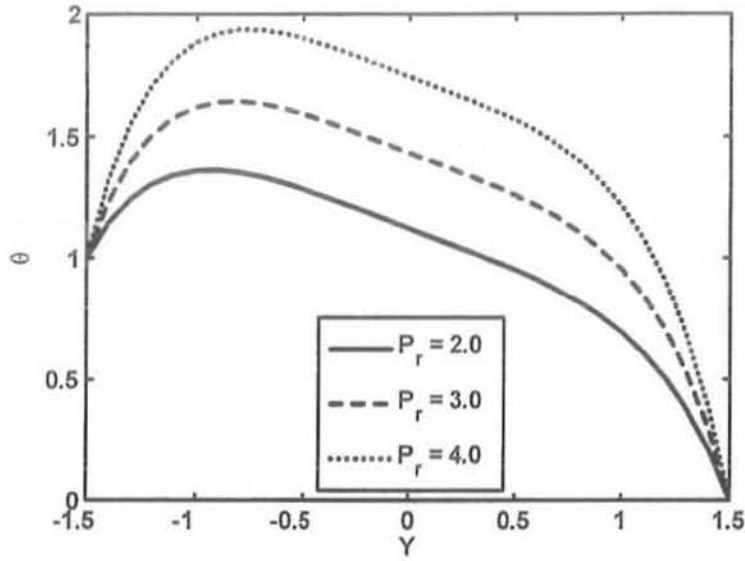


Fig. (4.15) : Temperature profile θ for different values of P_r at $a = 0.5$, $b = 1.2$, $d = 1.5$, $E = 4$, $M = 1$, $\lambda_1 = 0.4$, $Q = 2$, $t = 1$, $X = 1$, $E_c = 1$, $\phi = \frac{\pi}{2}$.

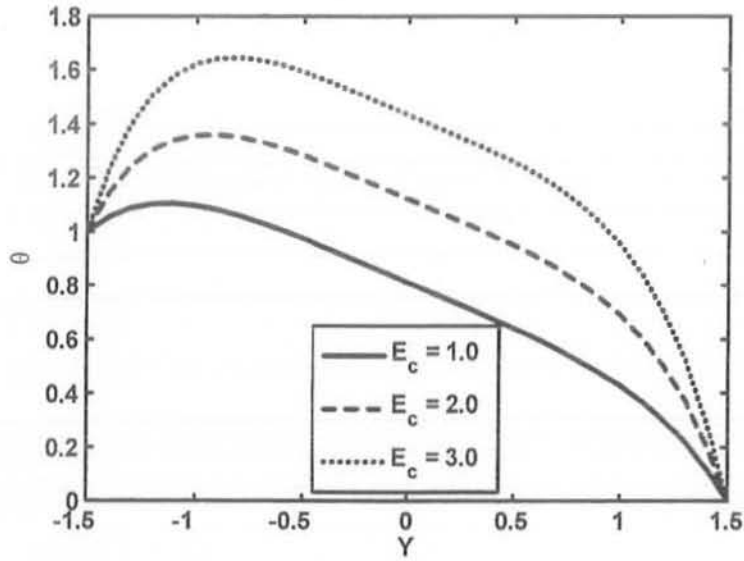


Fig. (4.16) : Temperature profile θ for different values of E_c at $a = 0.5$, $b = 1.2$, $d = 1.5$, $E = 4$, $Q = 2$, $t = 1$, $X = 1$, $M = 1$, $P_r = 1$, $\lambda_1 = 0.4$, $\phi = \frac{\pi}{2}$.

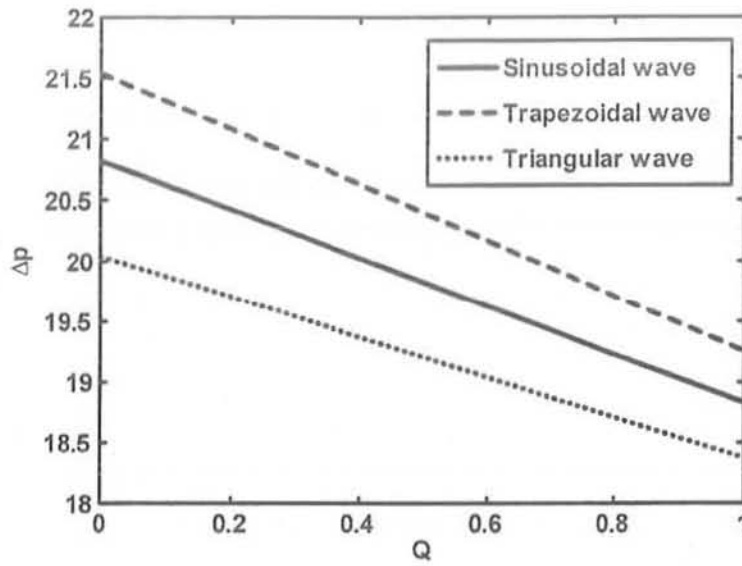


Fig. (4.17) : Variation of Δp with Q for different wave forms at $a = 0.7$, $b = 0.7$, $d = 2$, $\phi = \frac{\pi}{6}$, $E = 4$, $M = 2$, $\lambda_1 = 2$.

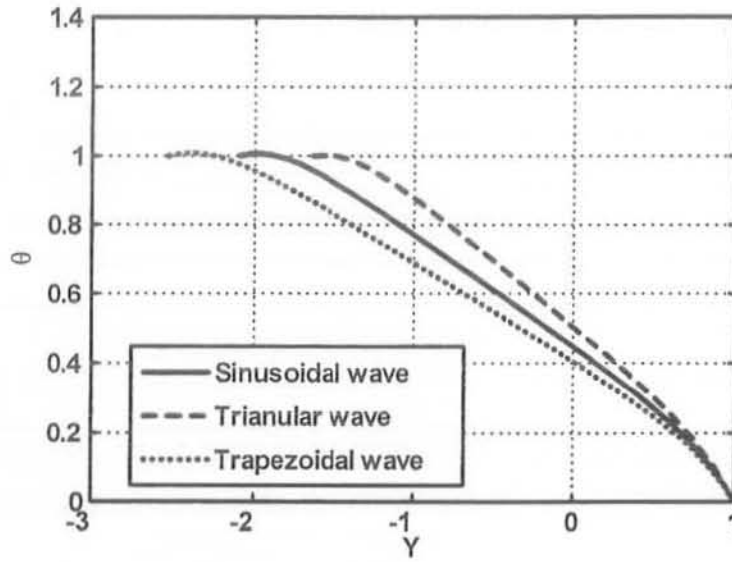


Fig. (4.18) : Temperature profile θ for different wave forms at $a = 0.5$, $b = 1.2$, $d = 1.5$, $Q = 2$, $\phi = \frac{\pi}{6}$, $E = 4$, $E_c = 1$, $X = 1$, $t = 1$, $P_r = 1$, $M = 1$, $\lambda_1 = 2$.

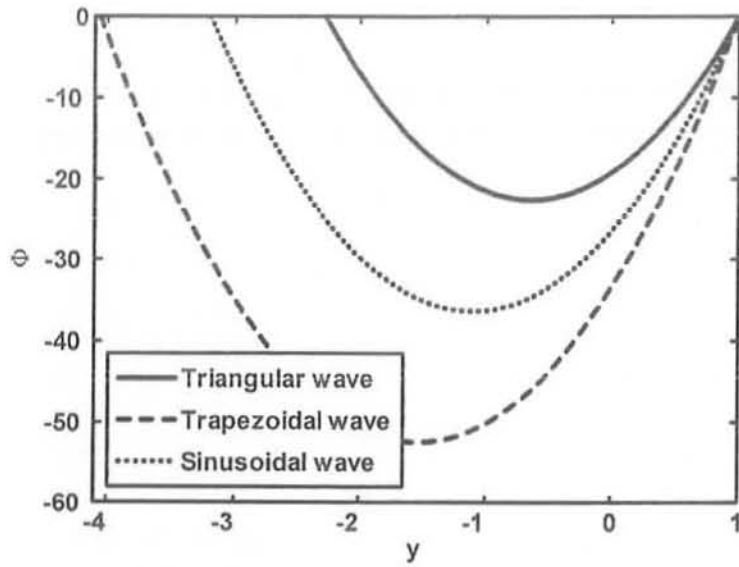
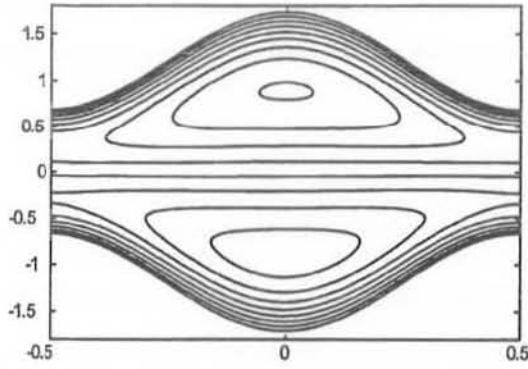
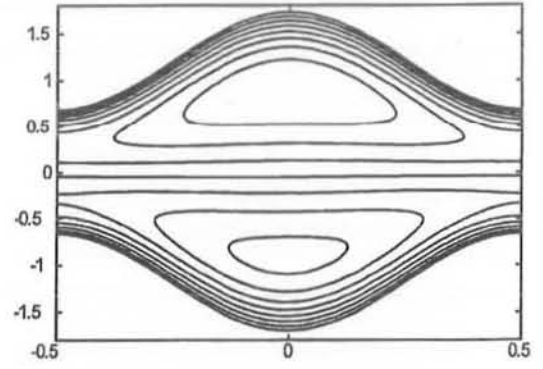


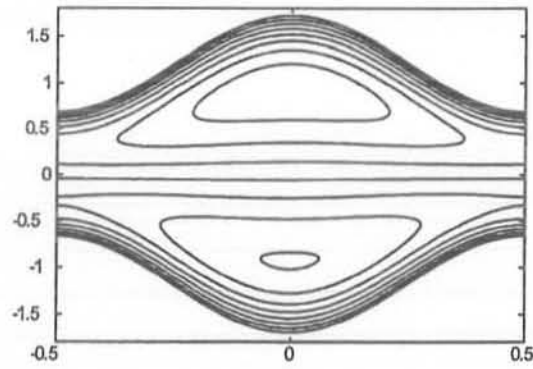
Fig. (4.19) : Profile of magnetic force function Φ for different wave forms at $a = 0.7$, $b = 1.2$, $d = 2$, $Q = 2$, $\phi = \frac{\pi}{2}$, $E = 4$, $R_m = 4$, $x = 0$, $M = 2$, $\lambda_1 = 0.5$.



(a)

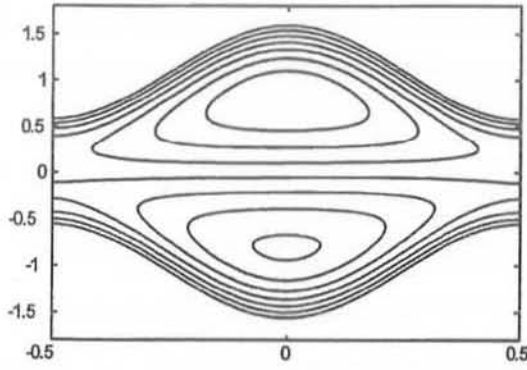


(b)

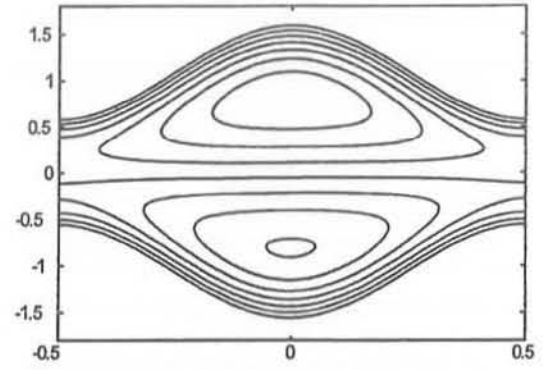


(c)

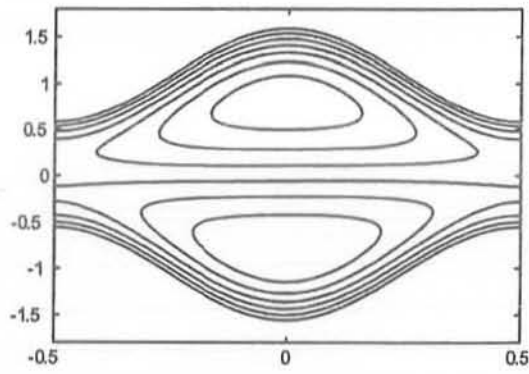
Fig. (4.20) : Stream lines for different values of λ_1 . (a) for $\lambda_1 = 0.5$, (b) for $\lambda_1 = 1.0$, (c) for $\lambda_1 = 1.5$. The other parameters are $a = 0.5$, $b = 0.5$, $E = 1.5$, $M = 0.1$, $d = 1.0$, $\phi = 0.02$, $Q = 2$.



(a)

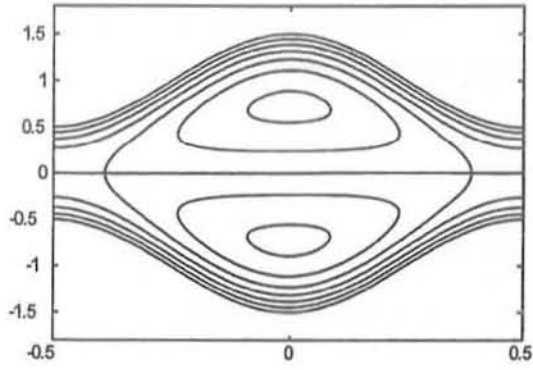


(b)

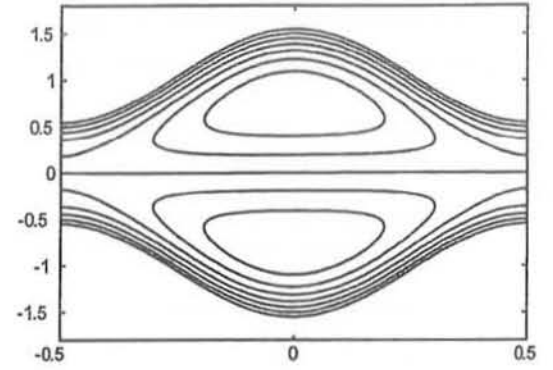


(c)

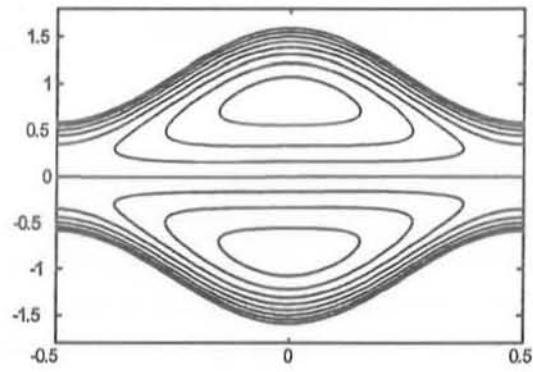
Fig. (4.21) : Stream lines for different values of E . (a) for $E = 0.5$, (b) for $E = 0.7$, (c) for $E = 0.9$. The other parameters are $a = 0.5$, $b = 0.5$, $M = 0.1$, $\lambda_1 = 0.9$, $d = 1.0$, $\phi = 0.02$, $Q = 1.8$.



(a)

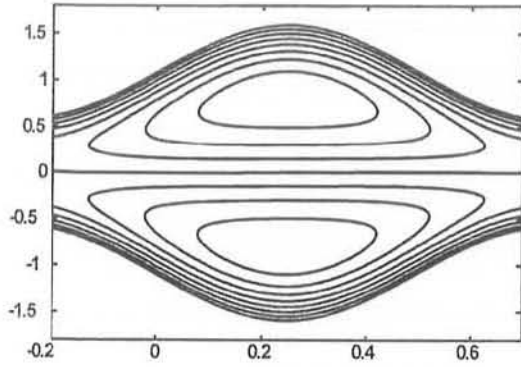


(b)

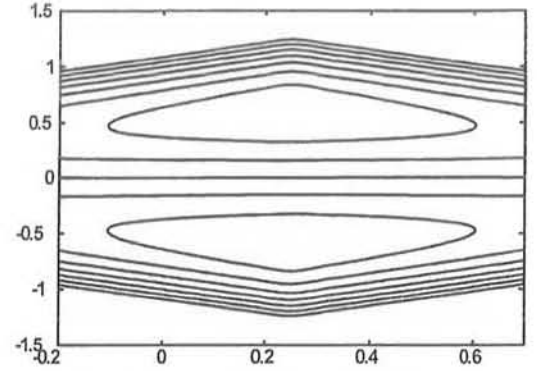


(c)

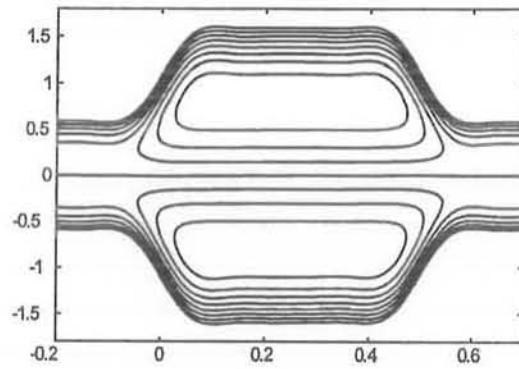
Fig.(4.22) : Stream lines for different values of Q . (a) for $Q = 1.6$, (b) for $Q = 1.7$, (c) for $Q = 1.8$. The other parameters are $a = 0.5$, $b = 0.5$, $E = 1.5$, $\lambda_1 = 0.9$, $d = 1.0$, $\phi = 0.02$, $M = 0.1$.



(a)



(b)



(c)

Fig. (4.23) : Stream lines for different wave forms. (a) for sinusoidal wave, (b) for triangular wave, (c) for trapezoidal wave. The parameters are $a = 0.5$, $b = 0.5$, $E = 1.5$, $\lambda_1 = 0.9$, $d = 1.0$, $\phi = 0.02$, $M = 0.1$, $Q = 1.8$.

4.6 Conclusion

This chapter presents the peristaltic flow of a Jeffrey fluid in an asymmetric channel under the effects of induced magnetic field. The problem is simplified under long wave length and low Reynolds number assumptions. An exact and closed form solution of the problem have been presented. The results are discussed through graphs. The main finding can be summarized as follows:

1. It is observed that pressure rise give larger values for small volume flow rate and it gives smaller values for large Q . Moreover, the peristaltic pumping occurs in the region $-1 \leq Q < 1.6$ for λ_1 and $-1 \leq Q \leq 1.8$ for ϕ , other wise augmented pumping occurs.
2. It is observed that the magnitude of the magnetic force function increases with an increase in E , λ_1 M and R_m , but the behavior is quite opposite with an increase in Q .
3. The axial induced magnetic field h_x decreases with an increase in R_m and E in the region $-2 \leq y \leq 0$, while in the region $0 \leq y \leq 2$, h_x increases with an increase in R_m and E .
4. The temperature field decreases with an increase in λ_1 , while the temperature field increases with an increases in P_r and E_c .
5. It is observed that the pressure rise for sinusoidal wave is less than trapezoidal wave and greater than triangular wave.
6. The temperature field θ in triangular wave is greater than sinusoidal wave and sinusoidal wave is greater than trapezoidal wave.
7. The magnitude value of magnetic force function Φ for trapezoidal wave is greater than sinusoidal and triangular waves.
8. The size of the trapped bolus decreases with an increase in λ_1 and E , but the number and size of the trapped bolus increases with an increases in Q .

Chapter 5

Slip effects on the peristaltic flow of a Jeffrey fluid in an asymmetric channel under the effects of induced magnetic field

5.1 Introduction

This chapter deals with the effects of slip and induced magnetic field on the peristaltic flow of a Jeffrey fluid in an asymmetric channel. The governing two dimensional equations for momentum, magnetic force function and energy are simplified by using the assumptions of long wave length and low but finite Reynolds number. The reduced problem has been solved by Adomian decomposition method (ADM) and a closed form solutions have been presented. Further, the exact solution of the proposed problem has also been computed and the mathematical comparison show that both solutions are almost same. The effects of pertinent parameters on the pressure rise per wave length are investigated using numerical integration. The expressions for pressure rise, friction force, velocity, temperature, magnetic force function and the stream lines against various physical parameters of interest are shown graphically. Moreover, the behavior of different kind of wave shape are also discussed.

5.2 Mathematical formulation

Let us consider the peristaltic flow of an incompressible, electrically conducting non-Newtonian fluid (Jeffrey fluid) in a two dimensional channel of width $d_1 + d_2$. The lower wall of the channel is maintained at temperature T_1 while the upper wall has temperature T_0 . The flow is generated by sinusoidal wave trains propagating with constant speed c along the channel walls. We are considering a rectangular coordinate system for the channel in which $X - axis$ is taken along the centerline of the channel and $Y - axis$ is transverse to it. An external transverse uniform constant magnetic field H_0 , induced magnetic field $H(h_X(X, Y, t), H_0 + h_Y(X, Y, t), 0)$ and the total magnetic field $H^+(h_X(X, Y, t), H_0 + h_Y(X, Y, t), 0)$ are taken into account. The geometry of wall surface is defined in Eq. (1.1). The governing equations are defined in previous chapter (Eqs. (4.8) to (4.13)) however, in the presence of slip parameter, the boundary conditions in non-dimension form are defined as

$$\begin{aligned} \Psi &= \frac{q}{2}, & \text{at } y &= h_1 = 1 + a \cos 2\pi x, \\ \Psi &= -\frac{q}{2}, & \text{at } y &= h_2 = -d - b \cos(2\pi x + \phi), \\ \frac{\partial \Psi}{\partial y} + \frac{L}{(1 + \lambda_1)} \frac{\partial^2 \Psi}{\partial y^2} &= -1, & \text{at } y &= h_1, \\ \frac{\partial \Psi}{\partial y} - \frac{L}{(1 + \lambda_1)} \frac{\partial^2 \Psi}{\partial y^2} &= -1, & \text{at } y &= h_2, \end{aligned} \tag{5.1}$$

$$\begin{aligned} \theta &= 0, & \text{at } y &= h_1, \\ \theta &= 1, & \text{at } y &= h_2, \end{aligned} \tag{5.2}$$

$$\Phi = 0, \quad \text{at } y = h_1 \text{ and } y = h_2. \tag{5.3}$$

5.3 Solution of the problem

5.3.1 Exact Solution

The exact solution of Eq. (4.13) can be written as

$$\Psi = F_{12} + F_{13} \cosh(m_3 y) + F_{14} \sinh(m_3 y) + Ey - \frac{F_{15}}{m_3^2} y, \tag{5.4}$$

where

$$m_3 = M \sqrt{(1 + \lambda_1)},$$

and F_{12} , F_{13} , F_{14} and F_{15} are functions of x only and can be calculated using boundary conditions (5.1)

$$\begin{aligned} F_{12} &= \frac{qm_3(h_2 + h_1) + \left(\frac{2(h_2 + h_1) + qm_3^2 \frac{L}{(1+\lambda_1)}(h_2 + h_1)}{2(h_2 - h_1)m_3 + 2\left(2 + m_3^2 \frac{L}{(1+\lambda_1)}(h_2 - h_1)\right) \tanh\left[m_3\left(\frac{h_1 - h_2}{2}\right)\right]} \right) \tanh\left[m_3\left(\frac{h_1 - h_2}{2}\right)\right]}{2(h_2 - h_1)m_3 + 2\left(2 + m_3^2 \frac{L}{(1+\lambda_1)}(h_2 - h_1)\right) \tanh\left[m_3\left(\frac{h_1 - h_2}{2}\right)\right]}, \\ F_{13} &= \frac{(q + h_1 - h_2) \sec h\left[m_3\left(\frac{h_1 - h_2}{2}\right)\right] \sinh\left[m_3\left(\frac{h_1 + h_2}{2}\right)\right]}{(h_1 - h_2)m_3 - \left(2 + m_3^2 \frac{L}{(1+\lambda_1)}(h_2 - h_1)\right) \tanh\left[m_3\left(\frac{h_1 - h_2}{2}\right)\right]}, \\ F_{14} &= \frac{(q + h_1 - h_2) \sec h\left[m_3\left(\frac{h_1 - h_2}{2}\right)\right] \cosh\left[m_3\left(\frac{h_1 + h_2}{2}\right)\right]}{(h_2 - h_1)m_3 + \left(2 + m_3^2 \frac{L}{(1+\lambda_1)}(h_2 - h_1)\right) \tanh\left[m_3\left(\frac{h_1 - h_2}{2}\right)\right]}, \\ F_{15} &= \frac{m_3^3(q - h_1E + Eh_2) + \left(\frac{2m_3^2(E + 1) + m_3^4(q - h_1E + Eh_2) \frac{L}{(1+\lambda_1)}}{(h_2 - h_1)m_3 + \left(2 + m_3^2 \frac{L}{(1+\lambda_1)}(h_2 - h_1)\right) \tanh\left[m_3\left(\frac{h_1 - h_2}{2}\right)\right]} \right) \tanh\left[m_3\left(\frac{h_1 - h_2}{2}\right)\right]}{(h_2 - h_1)m_3 + \left(2 + m_3^2 \frac{L}{(1+\lambda_1)}(h_2 - h_1)\right) \tanh\left[m_3\left(\frac{h_1 - h_2}{2}\right)\right]}. \end{aligned} \quad (5.5)$$

5.3.2 Solution by Adomian decomposition method

According to Adomian decomposition method, we rewrite Eq.(4.13) in the operator form as

$$\hat{L}_{yyy}\Psi = (F_{15} - m_3^2E) + m_3^2\Psi_y. \quad (5.6)$$

Applying the inverse operator $\hat{L}_{yyy}^{-1} = \int \int \int [\cdot] dydydy$, we can write Eq. (5.6) as

$$\Psi = C_{11} + C_{12}y + C_{13} \frac{y^2}{2!} + (F_{15} - m_3^2E) \frac{y^3}{3!} + m_3^2 L_{yyy}^{-1}(\Psi_y), \quad (5.7)$$

where

$$m_3^2 = M^2(1 + \lambda_1),$$

and $C_{11}, C_{12}, C_{13}, F_{15}$ are functions of x . Now we decompose Ψ as

$$\Psi = \sum_{n=0}^{\infty} \Psi_n. \quad (5.8)$$

Substituting Ψ into Eq.(5.7), we obtain

$$\begin{aligned} \Psi_0 &= C_{11} + C_{12}y + C_{13}\frac{y^2}{2!} + (F_{15} - m_3^2 E)\frac{y^3}{3!}, \\ \Psi_{n+1} &= m_3^2 \int \int \int (\Psi_n)_y dy dy dy, n \geq 0. \end{aligned} \quad (5.9)$$

Therefore,

$$\begin{aligned} \Psi_1 &= m_3^2 \left(C_{12}\frac{y^3}{3!} + C_{13}\frac{y^4}{4!} + (F_{15} - m_3^2 E)\frac{y^5}{5!} \right), \\ \Psi_2 &= m_3^4 \left(C_{12}\frac{y^5}{5!} + C_{13}\frac{y^6}{6!} + (F_{15} - m_3^2 E)\frac{y^7}{7!} \right), \\ &\vdots \\ \Psi_n &= m_3^{2n} \left(C_{12}\frac{y^{2n+1}}{(2n+1)!} + C_{13}\frac{y^{2n+2}}{(2n+2)!} + (F_{15} - m_3^2 E)\frac{y^{2n+3}}{(2n+3)!} \right), n > 0. \end{aligned} \quad (5.10)$$

Using (5.8), the closed form of Ψ can be written as

$$\Psi = C_{11} + \sinh(m_3 y) \left(\frac{C_{12}}{m_3} + \frac{1}{m_3^3} (F_{15} - m_3^2 E) \right) + \frac{C_{13}}{m_3^2} (\cosh(m_3 y) - 1) - \frac{1}{m_3^2} (F_{15} - m_3^2 E) y,$$

which can be put in the simplest form as

$$\Psi = F_{12} + F_{13} \cosh(m_3 y) + F_{14} \sinh(m_3 y) + Ey - \frac{F_{15}}{m_3^2} y. \quad (5.11)$$

Now the Adomian solution (5.11) and exact solution (5.4) are exactly same in which $F_i (i = 12$ to 15) are calculated using boundary conditions which are defined in Eq. (5.5).

Making use of Eq.(5.4), the exact solution of Eq. (4.10) satisfying the boundary conditions

(5.2) can be written as

$$\theta = -\frac{E_c P_r}{(1 + \lambda_1)} \left(\begin{aligned} &\frac{F_{13}^2}{2} m_3^4 Y^2 + \frac{1}{8} (F_{13}^2 + F_{14}^2) m_3^2 \cosh 2(m_3 Y) - \frac{1}{4} (F_{13}^2 + F_{14}^2) m_3^4 Y^2 \\ &+ \frac{1}{4} F_{13} F_{14} m_3^2 \sinh 2(m_3 Y) \end{aligned} \right) + c_{11} Y + c_{12}, \quad (5.12)$$

where

$$\begin{aligned} c_{11} &= \frac{-1}{(h_1 - h_2)} + \\ &\frac{E_c P_r}{(1 + \lambda_1)(h_1 - h_2)} \left(\begin{aligned} &\frac{1}{2} F_{13}^2 m_3^4 (h_1^2 - h_2^2) - \frac{1}{4} (F_{13}^2 + F_{14}^2) m_3^4 (h_1^2 - h_2^2) \\ &+ \frac{1}{8} (F_{13}^2 + F_{14}^2) m_3^2 (\cosh 2(m_3 h_1) - \cosh 2(m_3 h_2)) \\ &+ \frac{1}{4} F_{13} F_{14} m_3^2 (\sinh 2(m_3 h_1) - \sinh 2(m_3 h_2)) \end{aligned} \right), \\ c_{12} &= \frac{E_c P_r}{(1 + \lambda_1)} \left(\begin{aligned} &\frac{1}{2} F_{13}^2 m_3^4 h_1^2 + \frac{1}{4} F_{13} F_{14} m_3^2 \sinh 2(m_3 h_1) \\ &+ \frac{1}{8} (F_{13}^2 + F_{14}^2) m_3^2 \cosh 2(m_3 h_1) - \frac{1}{4} (F_{13}^2 + F_{14}^2) m_3^4 h_1^2 \end{aligned} \right) - c_{11} h_1. \end{aligned} \quad (5.13)$$

The exact solution of Eq. (4.11) is defined as

$$\Phi = c_{13} y + c_{14} + \frac{F_{15} R_m y^2}{m_3^2} - R_m \left(\frac{F_{13}}{m_3} \sinh(m_3 y) + \frac{F_{14}}{m_3} \cosh(m_3 y) \right), \quad (5.14)$$

where c_{13} and c_{14} are calculated using boundary condition (5.3) and are defined as

$$\begin{aligned} c_{13} &= \frac{R_m}{2} (h_1 + h_2) \left(\frac{m_3 (q - h_1 E + E h_2) + \left(\frac{2(E+1) + \frac{L}{(1+\lambda_1)} m_3^2 (q - h_1 E + E h_2)}{\tanh \left[m_3 \left(\frac{h_1 - h_2}{2} \right) \right]} \right) \tanh \left[m_3 \left(\frac{h_1 - h_2}{2} \right) \right]}{(h_1 - h_2) m_3 - \left(2 + m_3^2 \frac{L}{(1+\lambda_1)} (h_2 - h_1) \right) \tanh \left[m_3 \left(\frac{h_1 - h_2}{2} \right) \right]} \right), \\ c_{14} &= \frac{R_m}{m_3} \left(\frac{2(q + h_1 - h_2) + m_3^2 h_1 h_2 (q - h_1 E + E h_2) + m_3 h_1 h_2 \left(2(E+1) + \frac{L}{(1+\lambda_1)} m_3^2 (q - h_1 E + E h_2) \right) \tanh \left[m_3 \left(\frac{h_1 - h_2}{2} \right) \right]}{2(h_2 - h_1) m_3 + 2 \left(2 + m_3^2 \frac{L}{(1+\lambda_1)} (h_2 - h_1) \right) \tanh \left[m_3 \left(\frac{h_1 - h_2}{2} \right) \right]} \right). \end{aligned} \quad (5.15)$$

The expression for axial induced magnetic field can be obtained with the help of $h_x = \frac{\partial \Phi}{\partial y}$,

which are as follows

$$h_x(x, y) = \frac{R_m \left(\begin{array}{c} 2(q + h_1 - h_2) \sec h \left[m_3 \left(\frac{h_1 - h_2}{2} \right) \right] \sinh \left[m_3 \left(\frac{h_1 + h_2}{2} - y \right) \right] + \\ m_3(q - h_1 E + h_2 E) + \\ \left(2(E + 1) + \frac{L}{(1 + \lambda_1)} m_3^2 (q - h_1 E + h_2 E) \right) \tanh \left[m_3 \left(\frac{h_1 - h_2}{2} \right) \right] \end{array} \right) (2y - h_1 - h_2)}{2(h_2 - h_1) m_3 + 2 \left(2 + m_3^2 \frac{L}{(1 + \lambda_1)} (h_2 - h_1) \right) \tanh \left[m_3 \left(\frac{h_1 - h_2}{2} \right) \right]} \quad (5.16)$$

In the above solution when $\lambda_1 \rightarrow 0$ and $M \rightarrow 0$, the solutions of Mishra and Rao [14] can be recovered as a special case of our problem. Moreover, the Jeffrey problem with induced magnetic field has not been discussed so far.

The pressure gradient is obtained from the dimensionless momentum equation for the axial velocity

$$\frac{dp}{dx} = \frac{1}{(1 + \lambda_1)} \Psi_{yyy} + M^2 (E - \Psi_y). \quad (5.17)$$

Substituting the value of Ψ given in (5.4), Eq. (5.17) takes the form

$$\frac{dp}{dx} = \frac{m_3^3 (q - h_1 E + h_2 E) + \left(2m_3^2 (E + 1) + \frac{L}{(1 + \lambda_1)} m_3^4 (q - h_1 E + h_2 E) \right) \tanh \left[m_3 \left(\frac{h_1 - h_2}{2} \right) \right]}{(1 + \lambda_1) \left((h_2 - h_1) m_3 + \left(2 + m_3^2 \frac{L}{(1 + \lambda_1)} (h_2 - h_1) \right) \tanh \left[m_3 \left(\frac{h_1 - h_2}{2} \right) \right] \right)} \quad (5.18)$$

For one wavelength, the integration of Eq. (5.18), yields

$$\Delta p = \int_0^1 \left(\frac{dp}{dx} \right) dx. \quad (5.19)$$

The expression for frictional force is defined as

$$F = - \int_0^1 \left(\frac{dp}{dx} \right) dx, \quad (5.20)$$

where the expression for dp/dx is defined in Eq. (5.18).

The axial velocity component in fixed frame is calculated as

$$\begin{aligned}
 U(X, Y, t) &= 1 + \Psi_y \\
 &= \frac{m_3 (h_1 - h_2 + q) \left(\begin{array}{c} -1 + \sec h \left[m_3 \left(\frac{h_1 - h_2}{2} \right) \right] \\ \cosh \left[m_3 \left(\frac{h_1 + h_2}{2} - Y \right) \right] \end{array} \right) + m_3^2 \frac{L}{(1 + \lambda_1)} (h_2 - h_1 - q) \tanh \left[m_3 \left(\frac{h_1 - h_2}{2} \right) \right]}{(h_2 - h_1) m_3 + \left(2 + m_3^2 \frac{L}{(1 + \lambda_1)} \right) (h_2 - h_1) \tanh \left[m_3 \left(\frac{h_1 - h_2}{2} \right) \right]}, \quad (5.21)
 \end{aligned}$$

where

$$h_1 = 1 + a \cos [2\pi (X - t)] \quad \text{and} \quad h_2 = -d - b \cos [2\pi (X - t) + \phi].$$

The expression for the Nusselt number for the upper wall is defined as

$$Nu = -\frac{\partial \theta}{\partial y} \Big|_{y=h_1}, \quad (5.22)$$

where θ is defined in Eq. (5.12).

5.4 Expressions for different wave shapes

The non-dimensional expressions for three considered wave form are defined in previous chapter, which will be helpful for finding the solutions of these wave shapes which are discussed and shown graphically proceeding in the sections.

5.5 Results and discussion

In this section, the graphical results are displayed to see the effects of various physical parameters on the pressure rise, frictional force, velocity, temperature, magnetic force function and stream lines. The expression for pressure rise and frictional force are calculated numerically using a mathematics software. The graphical results of pressure rise, frictional force, velocity, magnetic force function and temperature are displayed in Figs. 5.1 to 5.15. Figs. 5.1 to 5.3 are prepared for pressure rise Δp against volume flow rate Q for different values of Jeffrey parameter λ_1 , amplitude ratio ϕ and slip parameter L . It is observed that the relation between pressure

rise and volume flow rate is inversely proportional to each other. It means that pressure rise gives larger values for small volume flow rate and it gives smaller values for large Q . Moreover, the peristaltic pumping occurs in the region $-1 \leq Q < 1.5$ for λ_1 , $-1 \leq Q \leq 1.7$ for ϕ , and $-1 \leq Q < 1.5$ for L , other wise augmented pumping occurs. The frictional forces F against flow rate Q for different values of λ_1 , ϕ , and L are shown in Figs. 5.4 to 5.6. It is observed from the figures that frictional forces have opposite behavior as compare to the pressure rise. The velocity U for different values of λ_1 and M are shown in Figs. 5.7 and 5.8. We observed that the velocity profile decreases with the decrease in λ_1 (see Fig. 5.7). The effect of M on the velocity is almost opposite as compared to the case of λ_1 . Here the velocity profile increases with an increase of M . The temperature field for different values of λ_1, P_r and L against space variable Y are displayed in Figs. 5.9 to 5.11. It is depicted that with an increase in λ_1 and L the temperature field decreases while the temperature field increases with an increase in P_r . The expression for axial induced magnetic field h_x against space variable y for different values of magnetic Reynold number R_m and slip parameter L are shown in Fig. 5.12 to 5.13. It is observed that with an increases in R_m and slip parameter L , h_x increases in the upper half of the channel while in the lower half the behavior is opposite.

The pressure rise for different kinds of wave shape are presented in Fig. 5.14. It is observed that the pressure rise for sinusoidal wave is less than trapezoidal wave and greater than triangular wave. The temperature field θ for different wave shape are shown in Fig. 5.15. It is seen that the temperature field for triangular wave is greater than sinusoidal wave and sinusoidal wave is greater than trapezoidal wave.

The trapping phenomena for different values of λ_1, M and L are shown in Figs. 5.16 to 5.18. It is observed from Fig. 5.16 that the volume of the trapped bolus in the lower half channel is smaller as compared to the upper half of the channel, Moreover, the size of the trapped bolus decreases in the lower half of the channel with an increase in λ_1 . It is depicted from Fig. 5.17 that with an increase in M the size of the trapped bolus increases. The stream lines for different values of L are plotted in Fig. 5.18. It is observed that the number and size of the trapped bolus decreases in the lower half of the channel and increases in the upper half of the channel with an increase in L . The stream lines for different wave shape such as sinusoidal wave, triangular wave and trapezoidal wave are shown in Fig. 5.19. Table 5.1 is prepared to

see the behavior of Nusselt number for different values of physical parameters. The table shows that with an increase in L , λ_1 , and d the Nusselt number decreases while with an increase in Prandtl number P_r , the Nusselt number increases.

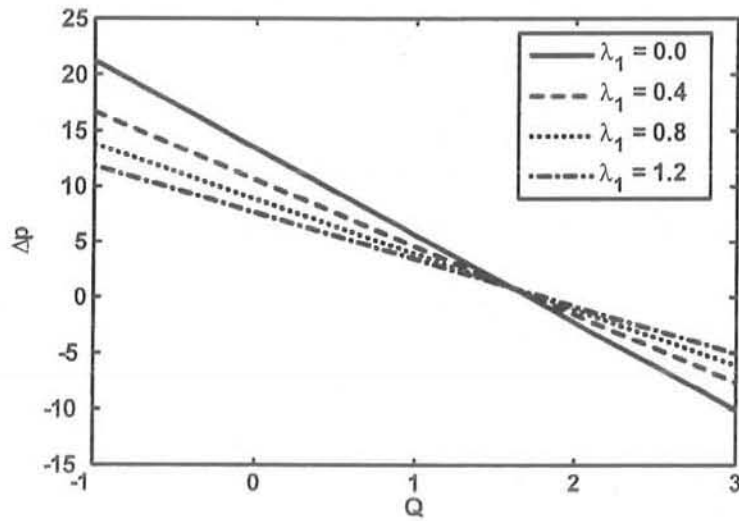


Fig. (5.1) : Variation of Δp with Q for different values of λ_1 at $a = 0.7$, $b = 1.2$, $d = 1.4$, $E = 4$, $M = 0.5$, $\phi = \frac{\pi}{6}$, $L = 0.04$. (Sinusoidal wave).

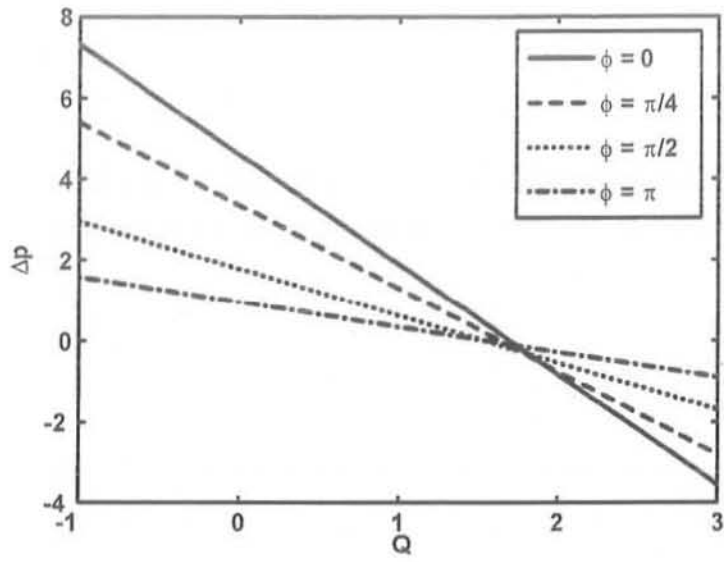


Fig.(5.2) : Variation of Δp with Q for different values of ϕ at $a = 0.7, b = 1.2, d = 1.5, E = 4, M = 1.5, \lambda_1 = 0.5, L = 0.04$. (Sinusoidal wave).

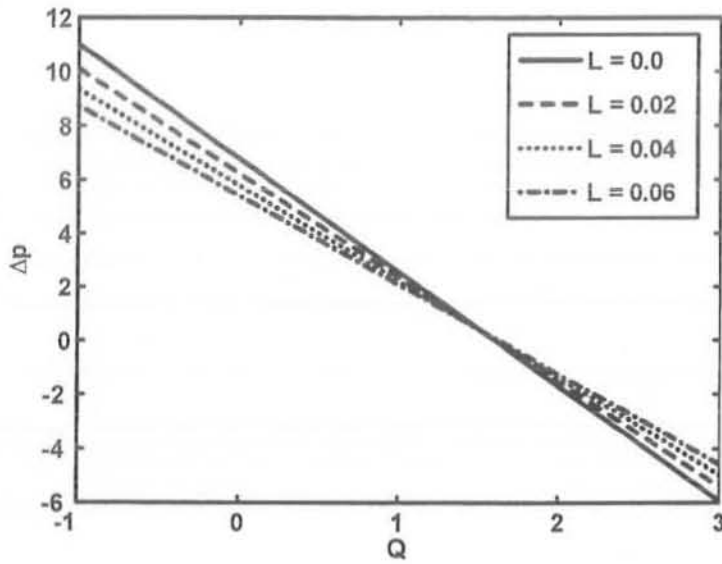


Fig.(5.3) : Variation of Δp with Q for different values of L at $a = 0.7, b = 1.2, d = 1.4, E = 4, M = 0.5, \lambda_1 = 0.5, \phi = \frac{\pi}{6}$. (Sinusoidal wave).

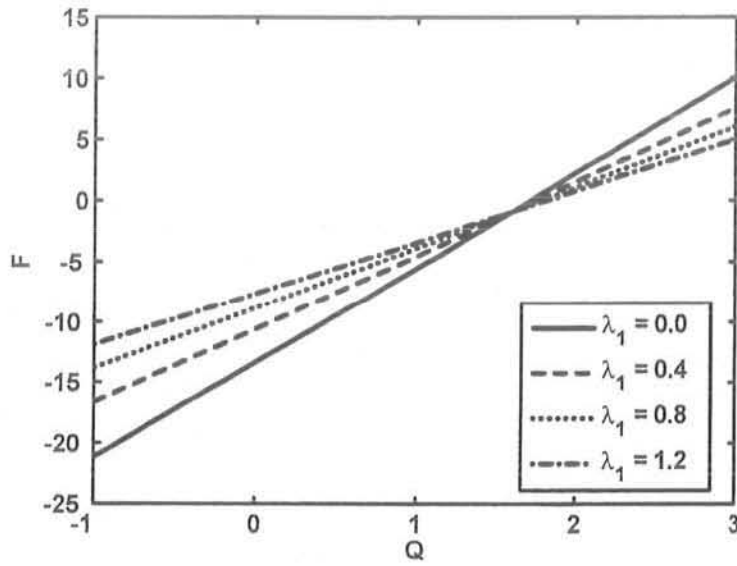


Fig.(5.4) : Variation of F with Q for different values of λ_1 at $a = 0.7, b = 1.2, d = 1.4, E = 4, M = 0.5, \phi = \frac{\pi}{6}, L = 0.04$. (Sinusoidal wave).

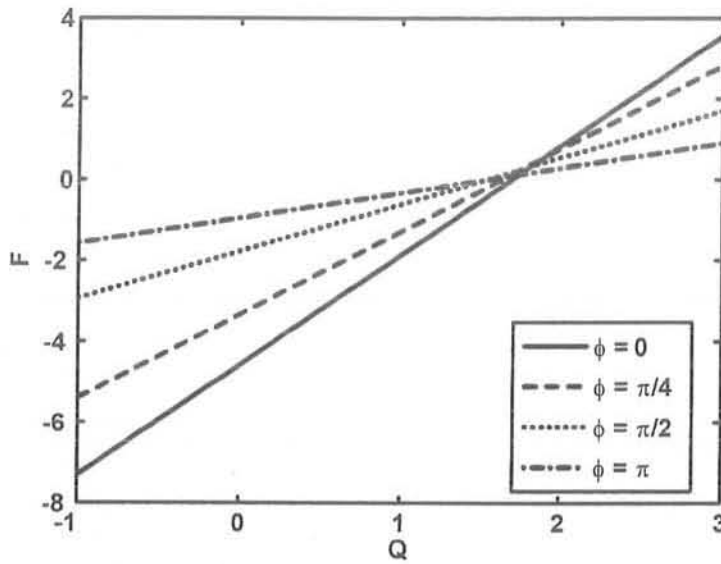


Fig.(5.5) : Variation of F with Q for different values of ϕ at $a = 0.7, b = 1.2, d = 1.5, E = 4, M = 1.5, \lambda_1 = 0.5, L = 0.04$. (Sinusoidal wave).

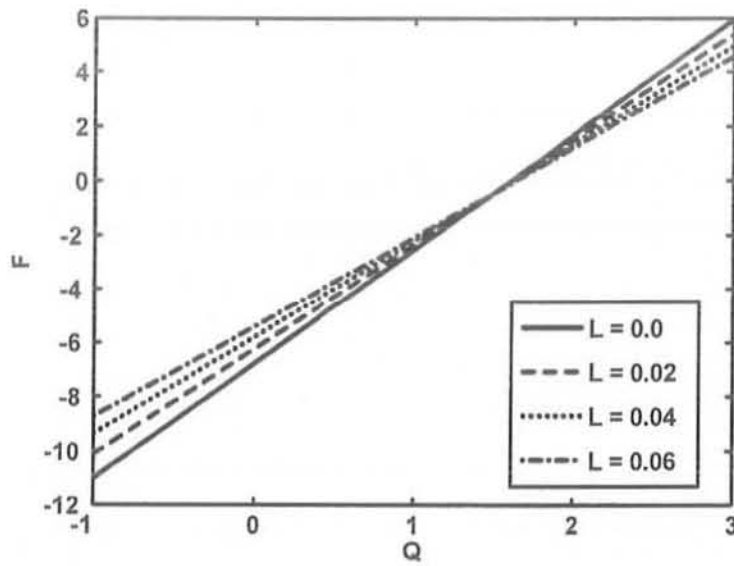


Fig. (5.6) : Variation of F with Q for different values of L at $a = 0.7$, $b = 1.2$, $d = 1.4$, $E = 4$, $M = 0.5$, $\lambda_1 = 0.5$, $\phi = \frac{\pi}{6}$. (Sinusoidal wave).

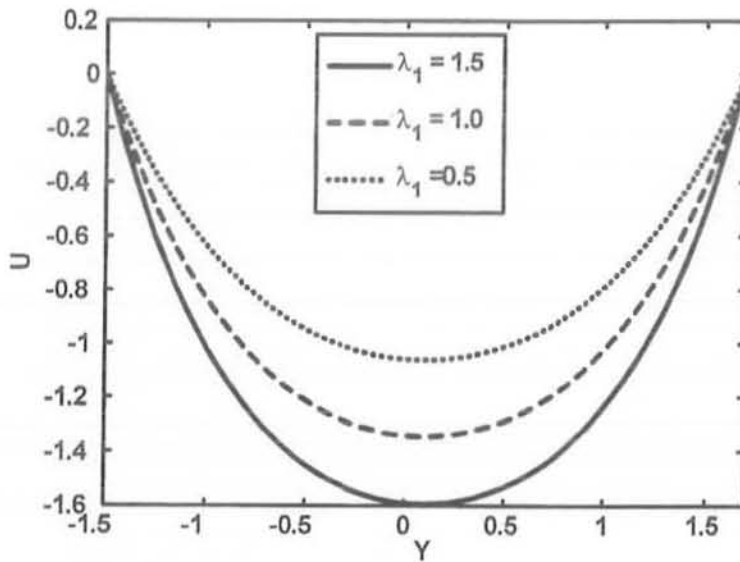


Fig.(5.7) : Velocity profile for different values of λ_1 at $a = 0.7$, $b = 1.2$, $d = 1.5$, $X = 1$, $t = 1$, $Q = 0.5$, $E = 4$, $M = 1$, $\phi = \frac{\pi}{2}$, $L = 0.04$. (Sinusoidal wave).

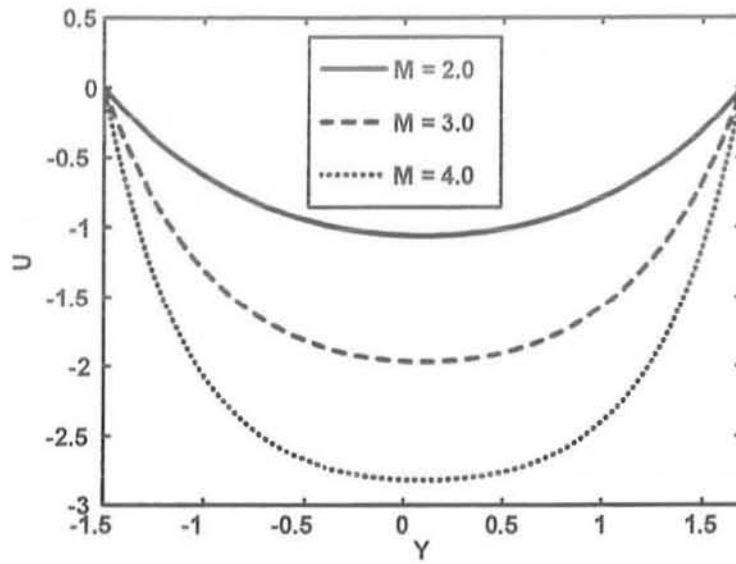


Fig. (5.8) : Velocity profile for different values of M at $a = 0.7, b = 1.2, d = 1.5, X = 1, t = 1, Q = 0.5, E = 4, \lambda_1 = 0.5, \phi = \frac{\pi}{2}, L = 0.04$. (Sinusoidal wave).

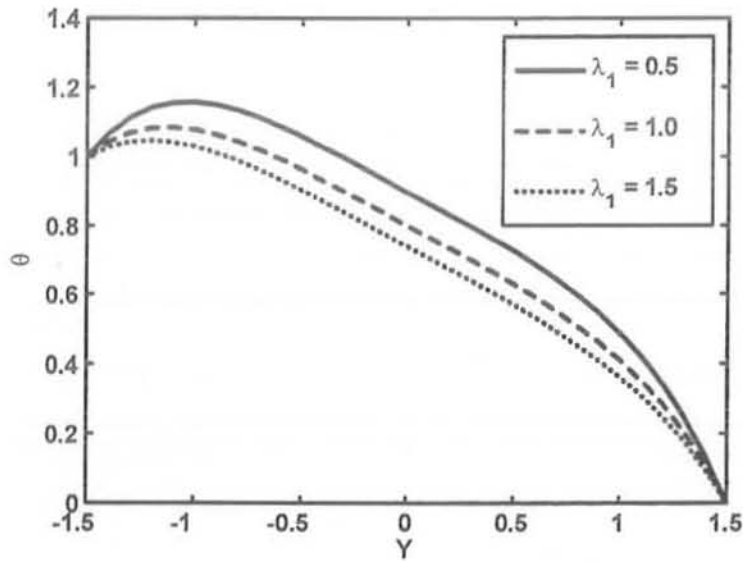


Fig.(5.9) : Temperature profile θ for different values of λ_1 at $a = 0.5, b = 1.2, d = 1.5, E = 4, M = 1, P_r = 1, E_c = 1, Q = 2.4, \phi = \frac{\pi}{2}, L = 0.04$. (Sinusoidal wave).

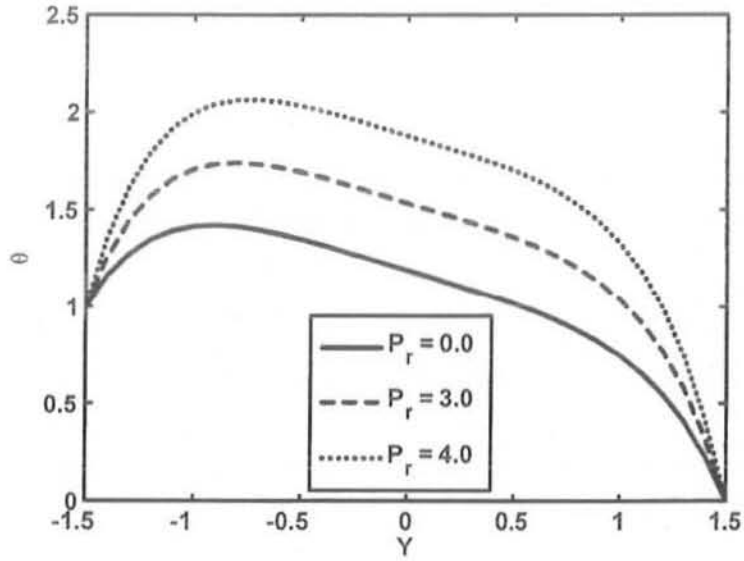


Fig.(5.10) : Temperature profile θ for different values of P_r at $a = 0.5$, $b = 1.2$, $d = 1.5$, $E = 4$, $M = 1$, $\lambda_1 = 0.4$, $Q = 2.4$, $t = 1$, $X = 1$, $E_c = 1$, $\phi = \frac{\pi}{2}$, $L = 0.04$. (Sinusoidal wave).

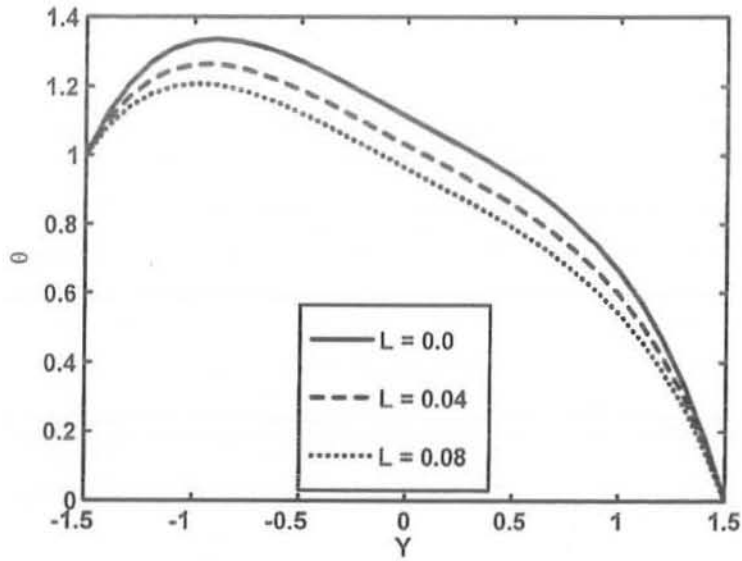


Fig.(5.11) : Temperature profile θ for different values of L at $a = 0.5$, $b = 1.2$, $d = 1.5$, $E = 4$, $M = 1$, $\lambda_1 = 0.4$, $Q = 2.4$, $t = 1$, $X = 1$, $E_c = 1$, $\phi = \frac{\pi}{2}$, $P_r = 1$. (Sinusoidal wave).

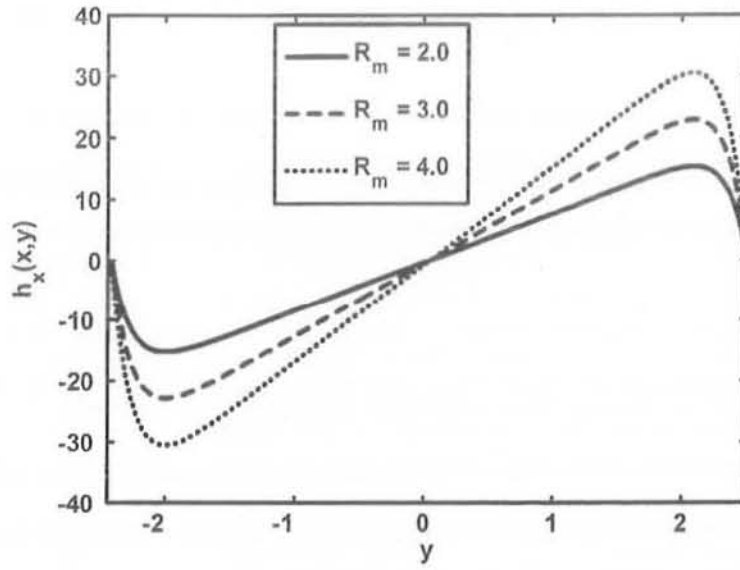


Fig.(5.12) : Variation of axial induced magnetic field h_x for different values of R_m at $a = 0.7$, $b = 0.7$, $Q = -0.9$, $L = 0.04$, $\phi = \pi$, $d = 2.3$, $E = 4$, $M = 3$, $\lambda_1 = 4$, $x = 0$. (Sinusoidal wave).

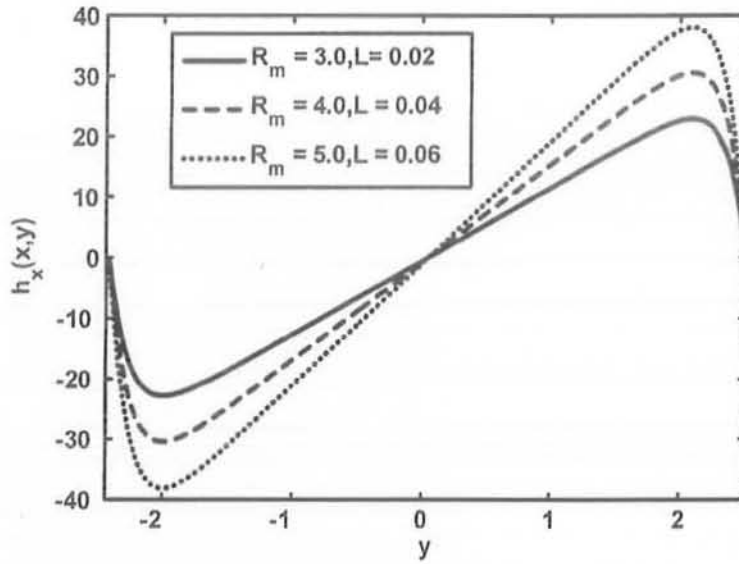


Fig.(5.13) : Variation of axial induced magnetic field h_x for different values of R_m and L at $a = 0.7$, $b = 0.7$, $Q = -0.9$, $\phi = \pi$, $d = 2.3$, $E = 4$, $M = 3$, $\lambda_1 = 4$, $x = 0$. (Sinusoidal wave).

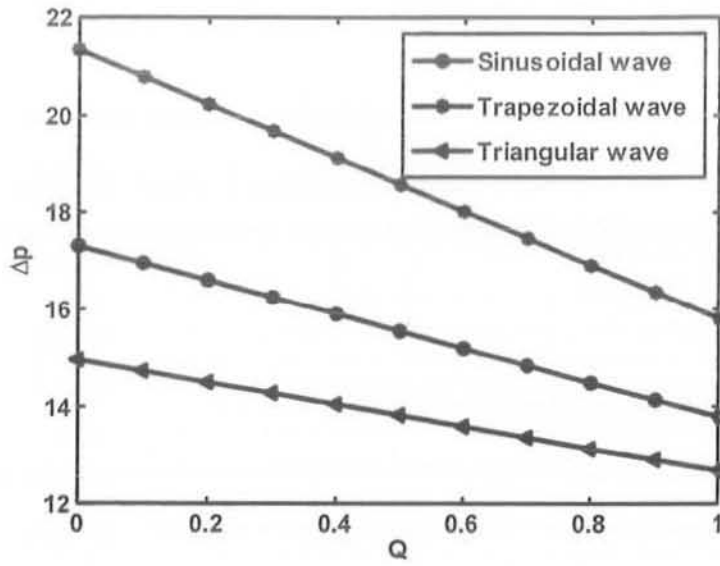


Fig.(5.14) : Variation of Δp with Q for different wave forms at $a = 0.7, b = 1.2, d = 1.4, \phi = \pi, E = 4, M = 2, \lambda_1 = 0.8$.

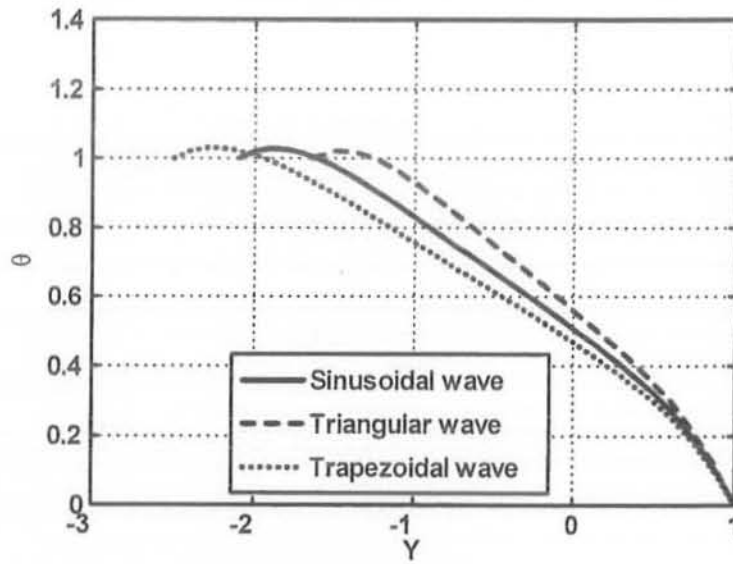
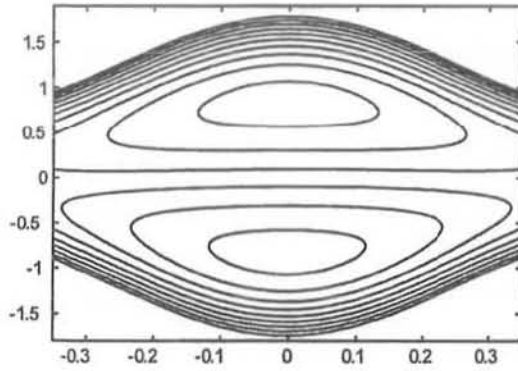
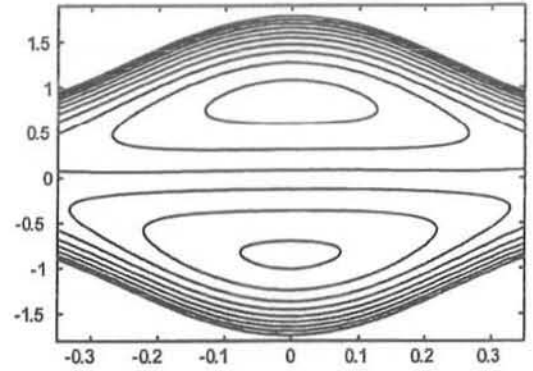


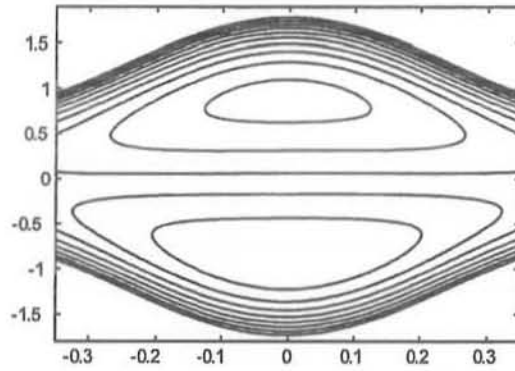
Fig.(5.15) : Temperature profile θ for different wave forms at $a = 0.5, b = 1.2, d = 1.5, \phi = \frac{\pi}{6}, E = 4, E_c = 1, Pr = 1, M = 1, \lambda_1 = 1, L = 0.04$.



(a)

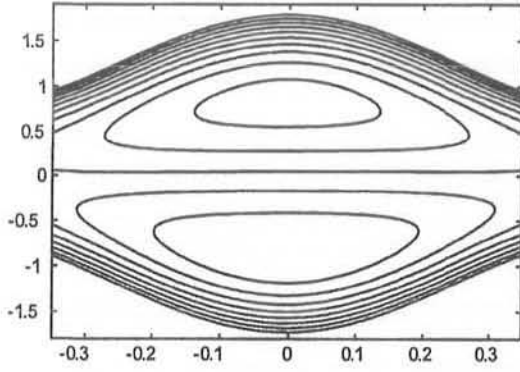


(b)

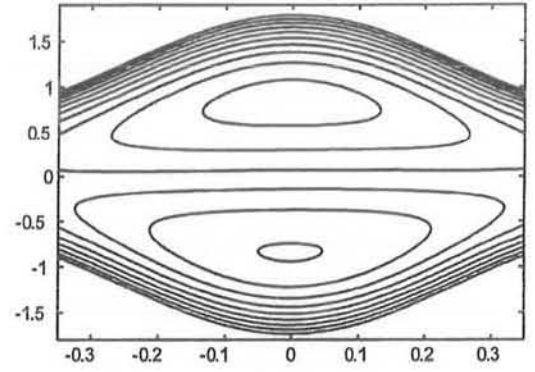


(c)

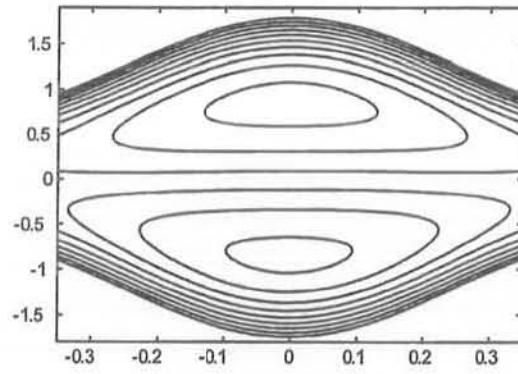
Fig.(5.16) : Stream lines for different values of λ_1 . (a) for $\lambda_1 = 0.7$, (b) for $\lambda_1 = 0.8$, (c) for $\lambda_1 = 0.9$. The other parameters are $a = 0.5$, $b = 0.5$, $E = 1.5$, $M = 0.06$, $L = 0.01$, $d = 1.0$, $\phi = 0.02$, $Q = 1.6$.



(a)

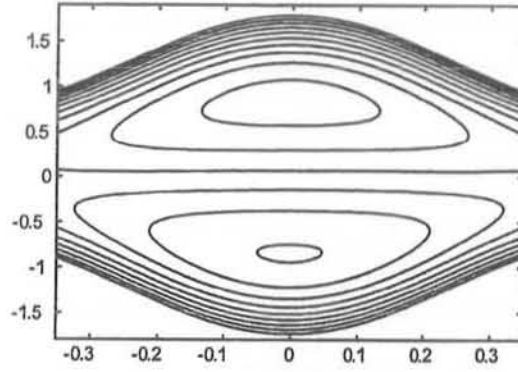


(b)

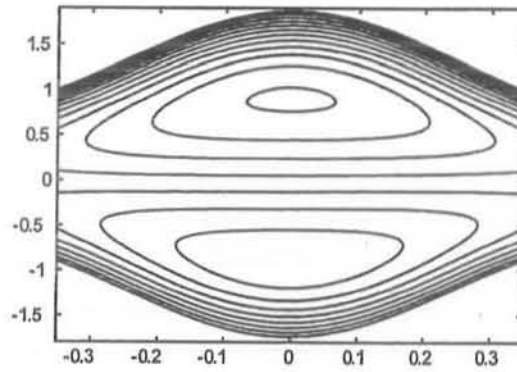


(c)

Fig. (5.17) : Stream lines for different values of M . (a) for $M = 0.06$, (b) for $M = 0.07$, (c) for $M = 0.08$. The other parameters are $a = 0.5$, $b = 0.5$, $E = 1.5$, $\lambda_1 = 0.8$, $L = 0.01$, $d = 1.0$, $\phi = 0.02$, $Q = 1.6$.

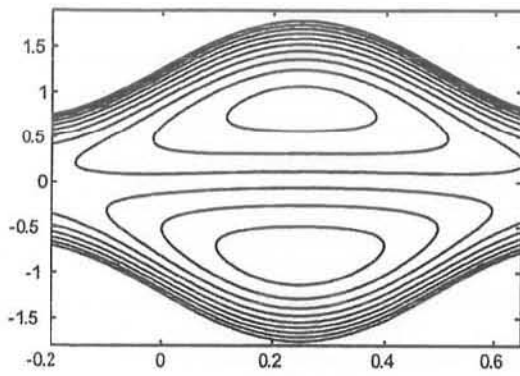


(a)

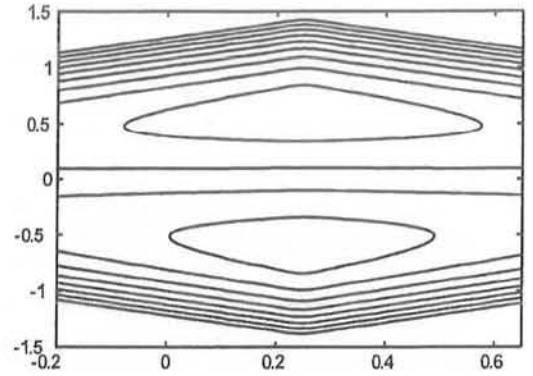


(b)

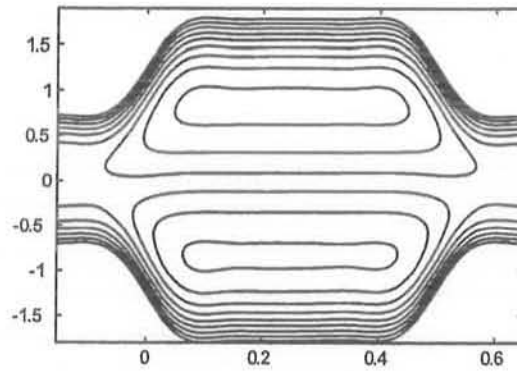
Fig.(5.18) : Stream lines for different values of L . (a) for $L = 0.01$, (b) for $L = 0.02$. The other parameters are $a = 0.5$, $b = 0.5$, $E = 1.5$, $\lambda_1 = 0.8$, $d = 1.0$, $\phi = 0.02$, $Q = 1.6$.



(a)



(b)



(c)

Fig.(5.19) : Stream lines for different wave forms. (a) for sinusoidal wave, (b) for triangular wave, (c) for trapezoidal wave. The parameters are $a = 0.5$, $b = 0.5$, $E = 1$, $\lambda_1 = 0.8$, $d = 1.0$, $\phi = 0.02$, $Q = 1.6$, $L = 0.01$.

Table 5.1: Values of Nusselt number for different values of L (slip parameter), λ_1 (ratio of relaxation to retardation times), d (width of the channel), and P_r (Prandtl number). The other parameters are $a = 0.5$, $b = 1.2$, $E_c = 1$, $x = 1$, $t = 1$, $M = 1$, $\phi = \frac{\pi}{2}$.

L	Nu	λ_1	Nu	d	Nu	P_r	Nu
0.0	3.04216	0.0	3.77918	0.0	6.29996	0.0	0.333333
0.01	2.95211	0.2	3.25119	0.2	3.44381	0.4	0.839961
0.02	2.86647	0.4	2.86647	0.4	2.86647	0.8	1.34659
0.03	2.78497	0.6	2.57392	0.6	2.49755	1.2	1.85322
0.04	2.70733	0.8	2.34411	0.8	2.17929	1.6	2.35984
0.05	2.6333	1.0	2.15892	1.0	1.9118	2.0	2.86647

5.6 Conclusion

This chapter presents the slip effects on the peristaltic flow of a Jeffrey fluid in an asymmetric channel under the effects of induced magnetic field. The governing two dimensional equations are simplified under long wave length and low Reynolds number approximation. An exact and closed form solution of the problem has been presented. The results are discussed through graphs. The main finding can be summarized as follows:

1. It is observed that with an increase in Jeffrey parameter λ_1 , amplitude ratio ϕ and slip parameter L pressure rise decreases in the peristaltic pumping and retrograde pumping regions, while in augmented pumping region the pressure rise increases with an increase in Jeffrey parameter λ_1 , amplitude ratio ϕ and slip parameter L .
2. The frictional forces have opposite behavior as compare to the pressure rise.
3. The magnitude value of the velocity decreases with the decrease in Jeffrey parameter λ_1 , while it increases with an increase in Hartmann number M .
4. The temperature decreases with an increase in Jeffrey parameter λ_1 and slip parameter L , while it increases with an increase in Prandtl number P_r .

5. With an increase in magnetic Reynolds number R_m and slip parameter L the axial induced magnetic field increases in the upper half of the channel while in the lower half, the behavior is opposite.
6. The pressure rise for sinusoidal wave is less than trapezoidal wave and greater than triangular wave.
7. The temperature field for triangular wave is greater than sinusoidal wave and sinusoidal wave is greater than trapezoidal wave.
8. The volume of the trapped bolus in the lower half channel is smaller as compared to the upper half of the channel with an increase in Jeffrey parameter λ_1 .
9. The size of the trapped bolus increases with an increase in Hartmann number M .
10. The number and size of the trapped bolus decreases in the lower half of the channel and increases in the upper half of the channel with an increase in slip parameter L .
11. The Nusselt number decreases with an increase in slip parameter L , Jeffrey parameter λ_1 and width of the channel d , while with an increase in Prandtl number P_r , the Nusselt number increases.

Chapter 6

Numerical and analytical solutions of peristaltic transport of a six constant Jeffreys model of fluid in a symmetric or asymmetric channel

6.1 Introduction

This chapter deals with the peristaltic flow of an incompressible six constant Jeffreys model of fluid in an asymmetric channel. The flow is investigated in a wave frame of reference moving with the velocity of the wave. We have modeled the governing equations of a two dimensional six constant Jeffreys model of fluid. The analytical and numerical solutions of the proposed problem are discussed. The expression for the pressure rise is calculated using numerical integration. The graphical results are presented to interpret various physical parameters of interest.

6.2 Mathematical formulation

Let us consider the peristaltic transport of an incompressible six constant Jeffreys model of fluid in a two dimensional channel of width $d_1 + d_2$. The flow is generated by sinusoidal wave trains

propagating with constant speed c along the channel walls. The geometry of the problem is same as discussed in chapter one. For the sake of simplicity the momentum equation is defined as

$$\rho \left(\frac{\partial \mathbf{V}}{\partial t} + (\mathbf{V} \cdot \nabla) \mathbf{V} \right) = \text{div } \boldsymbol{\tau}, \quad (6.1)$$

where

$$\boldsymbol{\tau} = -P\mathbf{I} + \mathbf{S}, \quad (6.2)$$

The constitutive equation for the extra stress tensor \mathbf{S} is [66]

$$\begin{aligned} & \mathbf{S} + \lambda_1 \left[\frac{d\mathbf{S}}{dt} - \mathbf{W}\mathbf{S} + \mathbf{S}\mathbf{W} + \check{\alpha}(\mathbf{S}\mathbf{D} + \mathbf{D}\mathbf{S}) + \check{b}\mathbf{S} : \mathbf{D}\mathbf{I} + \check{c}\mathbf{D}\text{tr}\mathbf{S} \right] \\ & = 2\mu \left[\mathbf{D} + \lambda_2 \left(\frac{d\mathbf{D}}{dt} - \mathbf{W}\mathbf{D} + \mathbf{D}\mathbf{W} + 2\check{\alpha}\mathbf{D}\mathbf{D} + \check{b}\mathbf{D} : \mathbf{D}\mathbf{I} \right) \right]. \end{aligned} \quad (6.3)$$

In above equations λ_1 is the relaxation time, $\mathbf{D} = (\nabla\mathbf{v}^t + \nabla\mathbf{v})/2$ is the symmetric part of $\nabla\mathbf{v}$, $\mathbf{W} = (\nabla\mathbf{v} - \nabla\mathbf{v}^t)/2$ is the antisymmetric part of $\nabla\mathbf{v}$, $\check{\alpha}, \check{b}, \check{c}$ are arbitrary material constants and λ_2 is the delay time, \mathbf{V} is the velocity vector, μ is the viscosity of the fluid and P is the pressure.

With the help of Eq. (1.6), Eqs. (1.2) and (6.3) take the following form

$$\frac{\partial U}{\partial X} + \frac{\partial V}{\partial Y} = 0, \quad (6.4)$$

$$\rho \left(\frac{\partial U}{\partial t} + U \frac{\partial U}{\partial X} + V \frac{\partial U}{\partial Y} \right) = -\frac{\partial P}{\partial X} + \frac{\partial}{\partial X} (S_{XX}) + \frac{\partial}{\partial Y} (S_{XY}), \quad (6.5)$$

$$\rho \left(\frac{\partial V}{\partial t} + U \frac{\partial V}{\partial Y} + V \frac{\partial V}{\partial Y} \right) = -\frac{\partial P}{\partial Y} + \frac{\partial}{\partial X} (S_{YX}) + \frac{\partial}{\partial Y} (S_{YY}). \quad (6.6)$$

The extra stress components are defined as follow

$$\begin{aligned}
& S_{XX} + \lambda_1 \left[\left(\frac{\partial}{\partial t} + U \frac{\partial}{\partial X} + V \frac{\partial}{\partial Y} \right) S_{XX} + S_{XY} \left(\frac{\partial V}{\partial X} - \frac{\partial U}{\partial Y} \right) + \check{a} \left\{ 2 \frac{\partial U}{\partial X} S_{XX} + S_{XY} \left(\frac{\partial V}{\partial X} + \frac{\partial U}{\partial Y} \right) \right\} \right. \\
& \left. + \check{b} \left\{ \frac{\partial U}{\partial X} S_{XX} + S_{XY} \left(\frac{\partial V}{\partial X} + \frac{\partial U}{\partial Y} \right) + S_{YY} \frac{\partial V}{\partial Y} \right\} + \check{c} (S_{XX} + S_{YY} + S_{ZZ}) \frac{\partial U}{\partial X} \right] \\
= & 2\mu \left[\frac{\partial U}{\partial X} + \lambda_2 \left[\left(\frac{\partial}{\partial t} + U \frac{\partial}{\partial X} + V \frac{\partial}{\partial Y} \right) \frac{\partial U}{\partial X} + \frac{1}{2} \left(\left(\frac{\partial V}{\partial X} \right)^2 - \left(\frac{\partial U}{\partial Y} \right)^2 \right) \right. \right. \\
& \left. \left. + 2\check{a} \left\{ \left(\frac{\partial U}{\partial X} \right)^2 + \frac{1}{4} \left(\frac{\partial U}{\partial Y} + \frac{\partial V}{\partial X} \right)^2 \right\} + \check{b} \left\{ \left(\frac{\partial U}{\partial X} \right)^2 + \left(\frac{\partial V}{\partial Y} \right)^2 + \frac{1}{2} \left(\frac{\partial V}{\partial X} + \frac{\partial U}{\partial Y} \right)^2 \right\} \right] \right], \quad (6.7)
\end{aligned}$$

$$\begin{aligned}
& S_{XY} + \lambda_1 \left[\left(\frac{\partial}{\partial t} + U \frac{\partial}{\partial X} + V \frac{\partial}{\partial Y} \right) S_{XY} + \frac{1}{2} \left(\frac{\partial U}{\partial Y} - \frac{\partial V}{\partial X} \right) (S_{XX} - S_{YY}) \right. \\
& \left. + \frac{\check{c}}{2} (S_{XX} + S_{YY} + S_{ZZ}) \left(\frac{\partial U}{\partial Y} + \frac{\partial V}{\partial X} \right) + \check{a} \left\{ \frac{1}{2} S_{XX} \left(\frac{\partial U}{\partial Y} + \frac{\partial V}{\partial X} \right) + S_{XY} \left(\frac{\partial V}{\partial Y} + \frac{\partial U}{\partial X} \right) \right. \right. \\
& \left. \left. + \frac{1}{2} S_{YY} \left(\frac{\partial U}{\partial Y} + \frac{\partial V}{\partial X} \right) \right\} \right] \\
= & 2\mu \left[\frac{1}{2} \left(\frac{\partial U}{\partial Y} + \frac{\partial V}{\partial X} \right) + \lambda_2 \left[\frac{1}{2} \left(\frac{\partial}{\partial t} + U \frac{\partial}{\partial X} + V \frac{\partial}{\partial Y} \right) \left(\frac{\partial U}{\partial Y} + \frac{\partial V}{\partial X} \right) + \frac{1}{2} \left(\frac{\partial U}{\partial Y} - \frac{\partial V}{\partial X} \right) \left(\frac{\partial U}{\partial X} - \frac{\partial V}{\partial Y} \right) \right. \right. \\
& \left. \left. + 2\check{a} \left\{ \frac{1}{2} \left(\frac{\partial U}{\partial Y} + \frac{\partial V}{\partial X} \right) \left(\frac{\partial U}{\partial X} + \frac{\partial V}{\partial Y} \right) \right\} \right] \right], \quad (6.8)
\end{aligned}$$

$$S_{XZ} + \lambda_1 \left[\left(\frac{\partial}{\partial t} + U \frac{\partial}{\partial X} + V \frac{\partial}{\partial Y} \right) S_{XZ} - \frac{1}{2} \left(\frac{\partial U}{\partial Y} - \frac{\partial V}{\partial X} \right) S_{YZ} + \check{a} \left\{ S_{XZ} \frac{\partial U}{\partial X} + \frac{1}{2} S_{YZ} \left(\frac{\partial U}{\partial Y} + \frac{\partial V}{\partial X} \right) \right\} \right] = 0, \quad (6.9)$$

$$\begin{aligned}
& S_{YY} + \lambda_1 \left[\left(\frac{\partial}{\partial t} + U \frac{\partial}{\partial X} + V \frac{\partial}{\partial Y} \right) S_{YY} + \left(\frac{\partial U}{\partial Y} - \frac{\partial V}{\partial X} \right) S_{XY} + \check{a} \left\{ S_{XY} \left(\frac{\partial U}{\partial Y} + \frac{\partial V}{\partial X} \right) + 2S_{YY} \frac{\partial V}{\partial Y} \right\} \right. \\
& \left. + \check{b} \left\{ S_{XX} \frac{\partial U}{\partial X} + S_{YX} \left(\frac{\partial U}{\partial Y} + \frac{\partial V}{\partial X} \right) + S_{YY} \frac{\partial V}{\partial Y} \right\} + \check{c} (S_{XX} + S_{YY} + S_{ZZ}) \frac{\partial V}{\partial Y} \right] \\
= & 2\mu \left[\frac{\partial V}{\partial Y} + \lambda_2 \left[\left(\frac{\partial}{\partial t} + U \frac{\partial}{\partial X} + V \frac{\partial}{\partial Y} \right) \frac{\partial V}{\partial Y} + \frac{1}{2} \left(\left(\frac{\partial U}{\partial Y} \right)^2 - \left(\frac{\partial V}{\partial X} \right)^2 \right) \right. \right. \\
& \left. \left. + 2\check{a} \left\{ \left(\frac{\partial V}{\partial Y} \right)^2 + \frac{1}{4} \left(\frac{\partial U}{\partial Y} + \frac{\partial V}{\partial X} \right)^2 \right\} + \check{b} \left\{ \left(\frac{\partial U}{\partial X} \right)^2 + \left(\frac{\partial V}{\partial Y} \right)^2 + \frac{1}{2} \left(\frac{\partial V}{\partial X} + \frac{\partial U}{\partial Y} \right)^2 \right\} \right] \right], \quad (6.10)
\end{aligned}$$

$$S_{YZ} + \lambda_1 \left[\left(\frac{\partial}{\partial t} + U \frac{\partial}{\partial X} + V \frac{\partial}{\partial Y} \right) S_{YZ} + \frac{1}{2} \left(\frac{\partial U}{\partial Y} - \frac{\partial V}{\partial X} \right) S_{XZ} + \check{a} \left\{ S_{YZ} \frac{\partial V}{\partial Y} + \frac{1}{2} S_{XZ} \left(\frac{\partial U}{\partial Y} + \frac{\partial V}{\partial X} \right) \right\} \right] = 0, \quad (6.11)$$

$$\begin{aligned} & S_{ZZ} + \lambda_1 \left[\left(\frac{\partial}{\partial t} + U \frac{\partial}{\partial X} + V \frac{\partial}{\partial Y} \right) S_{ZZ} + \check{b} \left\{ S_{XX} \frac{\partial U}{\partial X} + S_{YX} \left(\frac{\partial U}{\partial Y} + \frac{\partial V}{\partial X} \right) + S_{YY} \frac{\partial V}{\partial Y} \right\} \right] \\ &= 2\mu\lambda_2\check{b} \left[\left(\frac{\partial U}{\partial X} \right)^2 + \left(\frac{\partial V}{\partial Y} \right)^2 + \frac{1}{2} \left(\frac{\partial V}{\partial X} + \frac{\partial U}{\partial Y} \right)^2 \right]. \end{aligned} \quad (6.12)$$

Define the following non dimensional quantities

$$\begin{aligned} \bar{x} &= \frac{x}{\lambda}, & \bar{y} &= \frac{y}{d_1}, & \bar{u} &= \frac{u}{c}, & \bar{v} &= \frac{v}{c}, & \delta &= \frac{d_1}{\lambda}, & d &= \frac{d_2}{d_1}, & \bar{p} &= \frac{d_1^2 p}{\mu c \lambda}, & \bar{t} &= \frac{ct}{\lambda}, \\ h_1 &= \frac{H_1}{d_1}, & h_2 &= \frac{H_2}{d_2}, & a &= \frac{a_1}{d_1}, & b &= \frac{b_1}{d_1}, & R_e &= \frac{cd_1}{\nu}, & \bar{\Psi} &= \frac{\Psi}{cd_1}, & \bar{\lambda}_1 &= \frac{\lambda_1 c}{d_1}, \\ \bar{\lambda}_2 &= \frac{\lambda_2 c}{d_1}, & \bar{S}_{\bar{x}\bar{x}} &= \frac{S_{xx} \lambda}{\mu c}, & \bar{S}_{\bar{x}\bar{y}} &= \frac{S_{xy} d_1}{\mu c}, & \bar{S}_{\bar{y}\bar{y}} &= \frac{S_{yy} d_1}{\mu c}. \end{aligned} \quad (6.13)$$

Using the transformation (1.11) and (6.13) Eqs. (6.5) and (6.6) in terms of stream function Ψ (dropping the bars, $u = \frac{\partial \Psi}{\partial y}$, $v = -\delta \frac{\partial \Psi}{\partial x}$) take the form

$$\delta \operatorname{Re} \left[\left(\frac{\partial \Psi}{\partial y} \frac{\partial}{\partial x} - \frac{\partial \Psi}{\partial x} \frac{\partial}{\partial y} \right) \frac{\partial \Psi}{\partial y} \right] = -\frac{\partial p}{\partial x} + \delta^2 \frac{\partial S_{xx}}{\partial x} + \frac{\partial S_{xy}}{\partial y}, \quad (6.14)$$

$$-\delta^3 \operatorname{Re} \left[\left(\frac{\partial \Psi}{\partial y} \frac{\partial}{\partial x} - \frac{\partial \Psi}{\partial x} \frac{\partial}{\partial y} \right) \frac{\partial \Psi}{\partial x} \right] = -\frac{\partial p}{\partial y} + \delta^2 \frac{\partial S_{xy}}{\partial x} + \delta \frac{\partial S_{yy}}{\partial y}. \quad (6.15)$$

Under the assumption of long wave length and low Reynolds number Eq. (6.14) and (6.15) take the form

$$\frac{\partial S_{xy}}{\partial y} = \frac{\partial p}{\partial x}, \quad (6.16)$$

$$\frac{\partial p}{\partial y} = 0, \quad (6.17)$$

$$S_{xy} = \frac{\Psi_{yy} \left(1 - \frac{\lambda_1 \lambda_2}{2} \alpha (\Psi_{yy})^2 \right)}{\left(1 - \frac{\lambda_1^2}{2} \alpha (\Psi_{yy})^2 \right)}, \quad (6.18)$$

where

$$\alpha = \check{c}\check{b} + (-1 + \check{a} + \check{c}) (1 + \check{a} + \check{b}). \quad (6.19)$$

Eliminating pressure from Eqs. (6.16) and (6.17), we get

$$\frac{\partial^2 S_{xy}}{\partial y^2} = 0. \quad (6.20)$$

Making use of Eq. (6.18), Eqs. (6.20) and (6.16) become

$$\frac{\partial^2}{\partial y^2} \left[\frac{\Psi_{yy} \left(1 - \frac{\lambda_1 \lambda_2}{2} \alpha (\Psi_{yy})^2 \right)}{\left(1 - \frac{\lambda_1^2}{2} \alpha (\Psi_{yy})^2 \right)} \right] = 0, \quad (6.21)$$

$$\frac{dp}{dx} = \frac{\partial}{\partial y} \left[\frac{\Psi_{yy} \left(1 - \frac{\lambda_1 \lambda_2}{2} \alpha (\Psi_{yy})^2 \right)}{\left(1 - \frac{\lambda_1^2}{2} \alpha (\Psi_{yy})^2 \right)} \right]. \quad (6.22)$$

Applying the binomial expansion with α small, Eqs. (6.21) and (6.22) reduce to

$$\frac{\partial^4 \Psi}{\partial y^4} + \alpha C \frac{\partial^2}{\partial y^2} (\Psi_{yy})^3 + \alpha^2 \frac{\partial^2}{\partial y^2} (\Psi_{yy})^5 D = 0, \quad (6.23)$$

$$\frac{dp}{dx} = \frac{\partial}{\partial y} \left(\Psi_{yy} + \alpha C (\Psi_{yy})^3 + \alpha^2 (\Psi_{yy})^5 D \right), \quad (6.24)$$

where

$$C = \left(\frac{\lambda_1^2}{2} - \frac{\lambda_1 \lambda_2}{2} \right), \quad D = -\frac{\lambda_1^3 \lambda_2}{4}. \quad (6.25)$$

The dimensionless boundary conditions are defined as

$$\begin{aligned} \Psi &= \frac{q}{2}, \quad \frac{\partial \Psi}{\partial y} = -1 \quad \text{for } y = h_1(x), \\ \Psi &= -\frac{q}{2}, \quad \frac{\partial \Psi}{\partial y} = -1 \quad \text{for } y = h_2(x). \end{aligned} \quad (6.26)$$

The dimensionless mean flow Q is defined in Eq. (1.29).

6.3 Solution of the problem

6.3.1 Perturbation solution

Since, Eq. (6.23) is a highly non linear equation, we employ the well known regular perturbation method to determine the solution. For the perturbation solution, we expand Ψ , q and p as

$$\Psi = \Psi_0 + \alpha\Psi_1 + \alpha^2\Psi_2 + O(\alpha^3), \quad (6.27)$$

$$q = q_0 + \alpha q_1 + \alpha^2 q_2 + O(\alpha^3), \quad (6.28)$$

$$p = p_0 + \alpha p_1 + \alpha^2 p_2 + O(\alpha^3). \quad (6.29)$$

Substituting above expressions in Eqs. (6.23), (6.24) and boundary conditions (6.26), we get the following system

System of order α^0

$$\frac{\partial^4 \Psi_0}{\partial y^4} = 0, \quad (6.30)$$

$$\frac{\partial p_0}{\partial x} = \frac{\partial^3 \Psi_0}{\partial y^3}, \quad (6.31)$$

$$\Psi_0 = \frac{q_0}{2}, \quad \frac{\partial \Psi_0}{\partial y} = -1 \quad \text{on} \quad y = h_1(x), \quad (6.32)$$

$$\Psi_0 = -\frac{q_0}{2}, \quad \frac{\partial \Psi_0}{\partial y} = -1 \quad \text{on} \quad y = h_2(x). \quad (6.33)$$

System of order α^1

$$\frac{\partial^4 \Psi_1}{\partial y^4} = -C \frac{\partial^2}{\partial y^2} \left(\frac{\partial^2 \Psi_0}{\partial y^2} \right)^3, \quad (6.34)$$

$$\frac{\partial p_1}{\partial x} = \frac{\partial^3 \Psi_1}{\partial y^3} + C \frac{\partial}{\partial y} \left(\frac{\partial^2 \Psi_0}{\partial y^2} \right)^3, \quad (6.35)$$

$$\Psi_1 = \frac{q_1}{2}, \quad \frac{\partial \Psi_1}{\partial y} = 0 \quad \text{on} \quad y = h_1(x), \quad (6.36)$$

$$\Psi_1 = -\frac{q_1}{2}, \quad \frac{\partial \Psi_1}{\partial y} = 0 \quad \text{on} \quad y = h_2(x). \quad (6.37)$$

System of order α^2

$$\frac{\partial^4 \Psi_2}{\partial y^4} = -D \frac{\partial^2}{\partial y^2} \left(\frac{\partial^2 \Psi_0}{\partial y^2} \right)^5 - 3C \frac{\partial^2}{\partial y^2} \left(\frac{\partial^2 \Psi_1}{\partial y^2} \left(\frac{\partial^2 \Psi_0}{\partial y^2} \right)^2 \right), \quad (6.38)$$

$$\frac{\partial p_2}{\partial x} = \frac{\partial^3 \Psi_2}{\partial y^3} + 3C \frac{\partial}{\partial y} \left(\frac{\partial^2 \Psi_1}{\partial y^2} \left(\frac{\partial^2 \Psi_0}{\partial y^2} \right)^2 \right) + D \frac{\partial}{\partial y} \left(\frac{\partial^2 \Psi_0}{\partial y^2} \right)^5, \quad (6.39)$$

$$\Psi_2 = \frac{q_2}{2}, \quad \frac{\partial \Psi_2}{\partial y} = 0 \quad \text{on} \quad y = h_1(x), \quad (6.40)$$

$$\Psi_2 = -\frac{q_2}{2}, \quad \frac{\partial \Psi_2}{\partial y} = 0 \quad \text{on} \quad y = h_2(x). \quad (6.41)$$

Solution for system of order α^0

The solution of Eq. (6.30) satisfying the boundary conditions (6.32) and (6.33) can be written as

$$\begin{aligned} \Psi_0 = & \frac{q_0 + h_1 - h_2}{(h_2 - h_1)^3} (2y^3 - 3(h_1 + h_2)y^2 + 6h_1h_2y) - y \\ & + \frac{1}{(h_2 - h_1)^3} \left(\left(\frac{q_0}{2} + h_1 \right) (h_2^3 - 3h_1h_2^2) - \left(h_2 - \frac{q_0}{2} \right) (h_1^3 - 3h_2h_1^2) \right). \end{aligned} \quad (6.42)$$

The axial pressure gradient for this order is

$$\frac{dp_0}{dx} = \frac{12(q_0 + h_1 - h_2)}{(h_2 - h_1)^3}. \quad (6.43)$$

For one wavelength the integration of Eq. (6.43), yields

$$\Delta p = \int_0^1 \frac{dp_0}{dx} dx. \quad (6.44)$$

Solution for system of order α^1

Substituting the zeroth-order solution (6.42) into Eq. (6.34), the solution of the resulting problem satisfying the boundary conditions takes the following form

$$\Psi_1 = \frac{\left\{ \begin{aligned} & -((h_1 + h_2 - 2y)(432C(h_1 - h_2 + q_0)^3(h_1 - y)^2(h_2 - y)^2 + \\ & 5(h_1 - h_2)^6 q_1(h_1^2 - 4h_1h_2 + h_2^3 + 2(h_1 + h_2)y - 2y^2))) \end{aligned} \right\}}{10(h_1 - h_2)^9}. \quad (6.45)$$

The axial pressure gradient for this order is

$$\frac{dp_1}{dx} = \frac{-12(108C(h_1 - h_2 + q_0)^3 + 5(h_1 - h_2)^4 q_1)}{5(h_1 - h_2)^7}. \quad (6.46)$$

Integrating Eq. (6.46) over one wavelength we obtain

$$\Delta p = \int_0^1 \frac{dp_1}{dx} dx, \quad (6.47)$$

Solution for system of order α^2

Substituting Eqs. (6.42) and (6.45) into Eq. (6.38), the solution of the resulting problem satisfying the boundary conditions takes the following form

$$\begin{aligned} \Psi_2 = & \frac{-1}{350(h_1 - h_2)^{15}} ((h_1 + h_2 - 2y)(45360C(h_1 - h_2)^6(h_1 - h_2 + q_0)^2 q_1 (h_1 - y)^2 (h_2 - y)^2 \\ & - 15552C^2(h_1 - h_2 + q_0)^5 (h_1 - y)^2 (h_2 - y)^2 (87h_1^2 + 26h_1 h_2 + 87h_2^2 - 200(h_1 + h_2)y \\ & + 200)y^2 + 25(7(h_1 - h_2)^{12} q_2 (h_1^2 - 4h_1 h_2 + h_2^2 + 2(h_1 + h_2)y - 2y^2) + 10368D(h_1 - y)^2 \\ & (h_1 - h_2 + q_0)^5 (h_2 - y)^2 (3h_1^2 - 2h_1 h_2 + 3h_2^2 - 4(h_1 + h_2)y + 4y^2))) \end{aligned} \quad (6.48)$$

The axial pressure gradient for this order is

$$\begin{aligned} \frac{dp_2}{dx} = & \frac{-1}{175(h_1 - h_2)^{11}} (12(-46656C^2(h_1 - h_2 + q_0)^5 + 11340C(h_1 - h_2)^4 (h_1 - h_2 + q_0)^2 q_1 \\ & + 25(3888D(h_1 - h_2 + q_0)^5 + 7(h_1 - h_2)^8 q_2))). \end{aligned} \quad (6.49)$$

Integrating Eq. (6.49) over one wavelength we obtain

$$\Delta p = \int_0^1 \frac{dp_2}{dx} dx, \quad (6.50)$$

Summarizing the perturbation results up to second order for Ψ , dp/dx , and Δp

$$\Psi = \Psi_0 + \alpha\Psi_1 + \alpha^2\Psi_2, \quad (6.51)$$

$$\frac{dp}{dx} = \frac{dp_0}{dx} + \alpha\frac{dp_1}{dx} + \alpha^2\frac{dp_2}{dx}, \quad (6.52)$$

$$\Delta p = \Delta p_0 + \alpha\Delta p_1 + \alpha^2\Delta p_2, \quad (6.53)$$

Defining

$$q = q_0 + \alpha q_1 + \alpha^2 q_2. \quad (6.54)$$

Insert $q_0 = q - \alpha q_1 - \alpha^2 q_2$ and then neglecting the terms greater than $O(\alpha^2)$, the results given by Eq. (6.51) to Eq. (6.53) are expressed up to α^2 .

$$\begin{aligned} \Psi = & \frac{1}{350(h_1 - h_2)^{15}} ((h_1 + h_2 - 2y)(350h_1^{14}h_2 - 4550h_1^{13}h_2^2 + 27300h_1^{12}h_2^3 - 100100h_1^{11}h_2^4 \\ & + 250250h_1^{10}h_2^5 - 450450h_1^9h_2^6 + 600600h_1^8h_2^7 - 600600h_1^7h_2^8 + 450450h_1^6h_2^9 - 175h_1^{14}q \\ & - 250250h_1^5h_2^{10} + 100100h_1^4h_2^{11} - 27300h_1^3h_2^{12} + 4550h_1^2h_2^{13} - 350h_1h_2^{14} + 2800h_1^{13}h_2q \\ & - 20125h_2^2h_1^{12}q + 86800h_1^{11}h_2^3q - 252175h_1^{10}h_2^4q + 523600h_1^9h_2^5q - 802725h_1^8h_2^6q \\ & + 924000h_1^7h_2^7q - 802725h_1^6h_2^8q + 523600h_1^5h_2^9q - 252175h_1^4h_2^{10}q + 86800h_1^3h_2^{11}q \\ & - 20125h_1^2h_2^{12}q + 2800h_1h_2^{13}q - 175h_2^{14}q - 350h_1^{14}y + 4200h_1^{13}h_2y - 22750h_1^{12}h_2^2y \\ & + 72800h_1^{11}h_2^3y - 150150h_1^{10}h_2^4y + 200200h_1^9h_2^5y - 150150h_1^8h_2^6y + 150150h_1^6h_2^8y \\ & - 200200h_1^5h_2^9y + 150150h_1^4h_2^{10}y - 72800h_1^3h_2^{11}y + 22750h_1^2h_2^{12}y + 3850h_1^{12}h_2qy \\ & - 4200h_1h_2^{13}y350h_2^{14}y - 350h_1^{13}qy - 18900h_1^{11}h_2^2qy + 53900h_1^{10}h_2^3qy - 96250h_1^9h_2^4qy \\ & + 103950h_1^8h_2^5qy - 46200h_1^7h_2^6qy - 46200h_1^6h_2^7qy + 103950h_1^5h_2^8qy - 96250h_1^4h_2^9qy \\ & + 53900h_1^3h_2^{10}qy - 18900h_1^2h_2^{11}qy + 3850h_1h_2^{12}qy - 350h_2^{13}qy + 250250h_1^9h_2^4y^2 \\ & + 350h_1^{13}y^2 - 4550h_1^{12}h_2y^2 + 27300h_1^{11}h_2^2y^2 - 100100h_1^{10}h_2^3y^2 - 450450h_1^8h_2^5y^2 \\ & - 350h_2^{13}y^2 + 600600h_1^7h_2^6y^2 - 600600h_1^6h_2^7y^2 + 450450h_1^5h_2^8y^2 - 250250h_1^4h_2^9y^2 \\ & + 100100h_1^3h_2^{10}y^2 - 27300h_1^2h_2^{11}y^2 + 4550h_1h_2^{12}y^2 + 350h_1^{12}qy^2 - 4200h_1^{11}h_2qy^2 \\ & + 23100h_1^{10}h_2^2qy^2 - 77000h_1^9h_2^3qy^2 + 173250h_1^8h_2^4qy^2 - 277200h_1^7h_2^5qy^2 \\ & + 3234000h_1^6h_2^6qy^2 - 277200h_1^5h_2^7qy^2 + 173250h_1^4h_2^8qy^2 - 77000h_1^3h_2^9qy^2 \\ & + 23100h_1^2h_2^{10}qy^2 - 15120C\alpha(h_1 - h_2)^6(h_1 - h_2 + q)^3(h_1 - y)^2(h_2 - y)^2 \\ & + 5184(h_1 - h_2 + q)^5(h_1 - y)^2(h_2 - y)^2(50D(-3h_1^2 + 2h_1h_2 - 3h_2^2 + 4(h_1 + h_2)y \\ & - 4y^2) + 350h_2^{12}qy^2 - 4200h_1h_2^{11}qy^2 + 3C^2(87h_1^2 + 26h_1h_2 + 87h_2^2 \\ & - 200(h_1 + h_2)y + 200y^2)\alpha^2)). \end{aligned} \quad (6.55)$$

$$\frac{dp}{dx} = \frac{-1}{175(h_1 - h_2)^{11}} (12(h_1 - h_2 + q)(175(h_1 - h_2)^8 + 3780C\alpha(h_1 - h_2)^4(h_1 - h_2 + q)^2 - 3888\alpha^2(12C^2 - 25D)(h_1 - h_2 + q)^4)). \quad (6.56)$$

6.3.2 Numerical solution

The present problem consisting of equations (6.23) and (6.24) are also solved numerically by employing shooting method. The numerical results are also compared with the perturbation results.

Case.1 : ($\alpha = 0.3$)

Table 6.1: The comparison of Numerical and perturbation solutions.

y	Numerical sol	Perturbation sol	Error
1.0	-1.00000	-1.00000	0.00000
0.6	-1.48100	-1.48076	0.00016
0.2	-1.72114	-1.72151	0.00021
0.0	-1.75115	-1.75159	0.00014
-0.2	-1.72114	-1.72151	0.00021
-0.6	-1.48100	-1.48076	0.00016
-1.0	-1.00000	-1.00000	0.00000

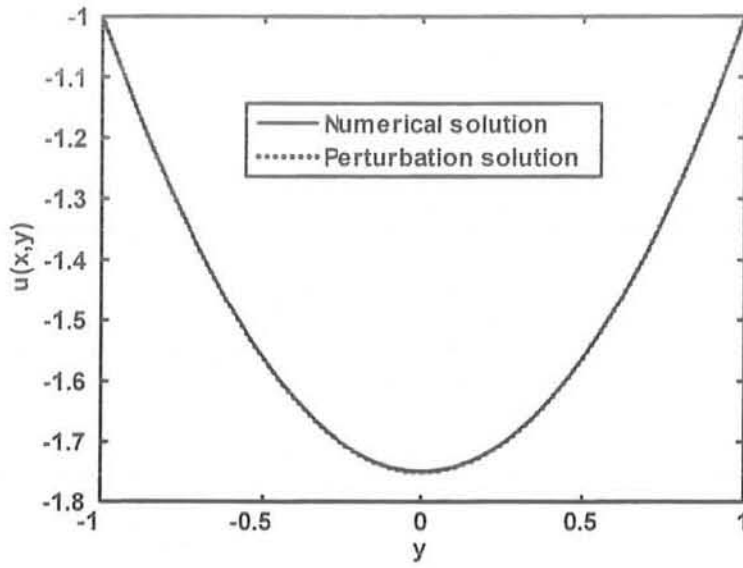


Fig.(6.a) : Comparison of velocity field for $a = 0.1$, $b = 0.1$, $d = 1.1$, $dp/dx = 1.5$, $\phi = \frac{\pi}{2}$, $\lambda_1 = 0.2$, $\lambda_2 = 0.3$, $\alpha = 0.3$, $x = 0.25$.

Case.2 : ($\alpha = 0.9$)

Table 6.2: The comparison of Numerical and perturbation solutions.

y	Numerical sol	Perturbation sol	Error
1.0	-1.00000	-1.00000	0.00000
0.6	-1.48881	-1.48248	0.00426
0.4	-1.64174	-1.63358	0.00499
0.2	-1.73365	-1.72151	0.00705
0.0	-1.76432	-1.75159	0.00726
-0.2	-1.73365	-1.72151	0.00705
-0.4	-1.64174	-1.63126	0.00642
-0.6	-1.48881	-1.48076	0.00543
-1.0	-1.00000	-1.00000	0.00000

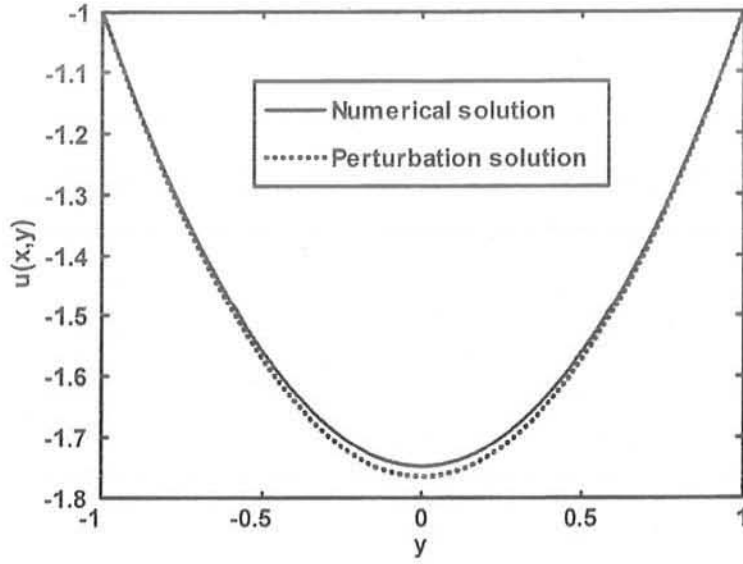


Fig.(6.b) : Comparison of velocity field for $a = 0.1$, $b = 0.1$, $d = 1.1$, $dp/dx = 1.5$, $\phi = \frac{\pi}{2}$, $\lambda_1 = 0.2$, $\lambda_2 = 0.3$, $\alpha = 0.9$, $x = 0.25$.

6.4 Results and discussion

In this section we have present the graphical results of the solution. The expression for the pressure rise is calculated numerically using a mathematics software Mathematica. The pressure rise Δp for different values of the width of the channel d , parameter α , relaxation time λ_1 and delay time λ_2 are plotted in Fig. 6.1 to 6.5. It is observed from Fig. 6.1, that the pressure rise decreases for small values of Q ($0 \leq Q \leq 1.4$) with an increase in width of the channel d and for large Q the pressure rise increases. From Fig. 6.2, it is observed that with an increase in α , the pressure rise decreases for small values of Q , and for large values of Q , the behavior is almost same. It is observed from Figs. 6.3 to 6.5 that the pressure rise decreases with an increase in λ_1 , λ_2 and ϕ . Figs. 6.6 to 6.10 are prepared to discuss the pressure gradient for different values of ϕ , α , d , λ_1 and λ_2 . It is seen from the figures that for $x \in [0, 0.2]$ and $x \in [0.8, 1]$, the pressure rise is small i.e. the flow can easily pass without the imposition of large pressure gradient, while in the narrow part of the channel $x \in [0.2, 0.8]$, to retain the same flux large pressure gradient is required. Moreover, in the narrow part of the channel, the pressure gradient decreases with

an increase in α , d , λ_1 and λ_2 . The velocity profile for different values of α , relaxation time λ_1 , delay time λ_2 and volume flow rate Q are plotted in Figs. 6.11 to 6.14. It is depicted from the Figs. 6.11 to 6.13 that with an increase in α , λ_1 and λ_2 the amplitude of the velocity decreases in the center and near the channel wall the velocity increases. From Fig. 6.14 it is observed that with an increase in volume flow rate Q the velocity profile decreases. Fig. 6.15 shows the comparison of Newtonian and six constant Jeffreys model of fluid. The comparison shows that the velocity profile for Newtonian fluid are smaller when compared with six constant Jeffreys model of fluid.

Trapping phenomena

The trapping phenomena for different values of volume flow rate Q , width of the channel d , relaxation time λ_1 and retardation time λ_2 are shown in Figs. 6.16 to 6.19. It is observed from Fig. 6.16 that the size of the trapped bolus increases in both lower and upper half of the channel with an increase in volume flow rate Q . It is seen from Fig. 6.17 that with an increase in the width of the channel d the size of the trapped bolus decreases in the lower half of the channel while in the upper half the size increases. Fig. 6.18 illustrate the stream lines for different values of relaxation time λ_1 . It is observed from the figure that with an increase in relaxation time λ_1 the number and size of the trapping bolus increases. Fig. 6.19 illustrate the stream lines for different values of λ_2 . It is observed from the figure that with an increase in λ_2 the size of the trapping bolus decreases.

In order to show the comparison between Newtonian and six constant Jeffreys model of fluid table 6.3 is presented. It is observed from the table 3 that with an increase in volume flow rate Q the magnitude value of the velocity profile decreases. The comparison shows that the velocity profile for Newtonian fluid are smaller when compared with six constant Jeffreys model of fluid.

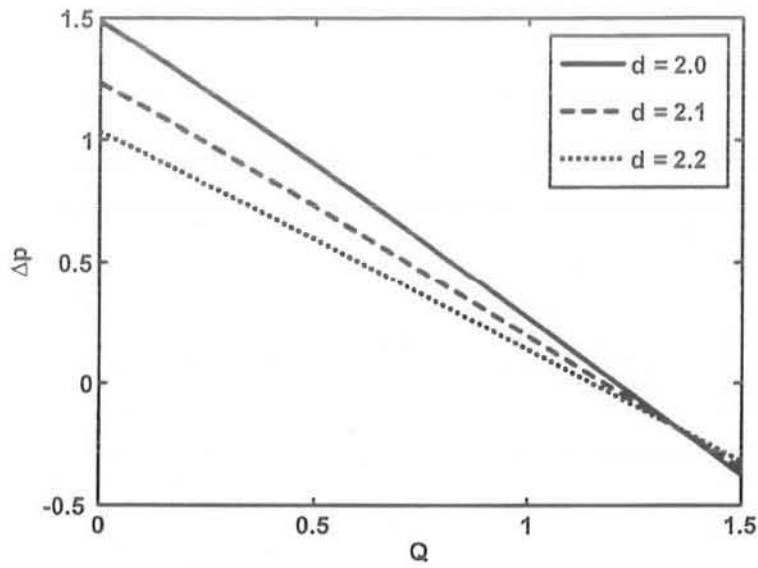


Fig.(6.1) : Variation of Δp with Q for different values of d at $a = 0.5$, $b = 1.2$, $\phi = \frac{\pi}{8}$, $\alpha = 0.04$, $\lambda_1 = 0.4$, $\lambda_2 = 0.9$.

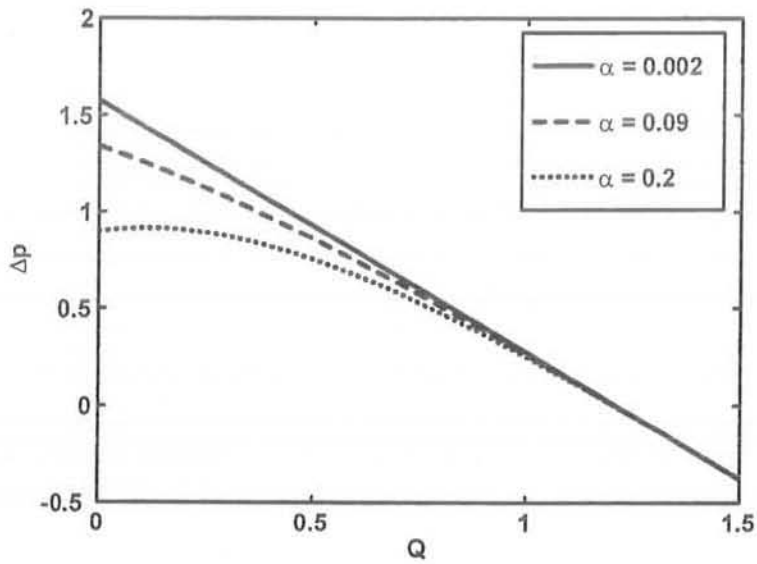


Fig. (6.2) : Variation of Δp with Q for different values of α at $a = 0.5$, $b = 1.2$, $\phi = \frac{\pi}{8}$, $d = 2$, $\lambda_1 = 0.4$, $\lambda_2 = 0.9$.

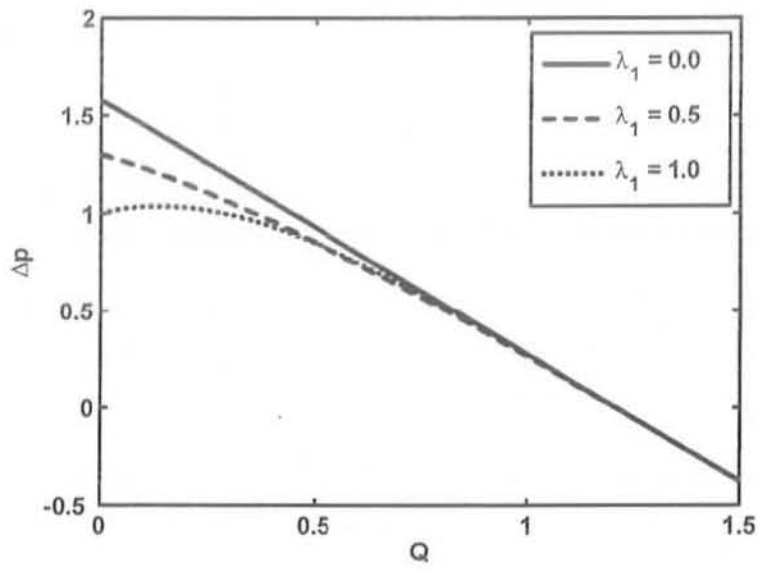


Fig. (6.3) : Variation of Δp with Q for different values of λ_1 at $a = 0.5$, $b = 1.2$, $\phi = \frac{\pi}{8}$, $d = 2$, $\alpha = 0.09$, $\lambda_2 = 0.9$.

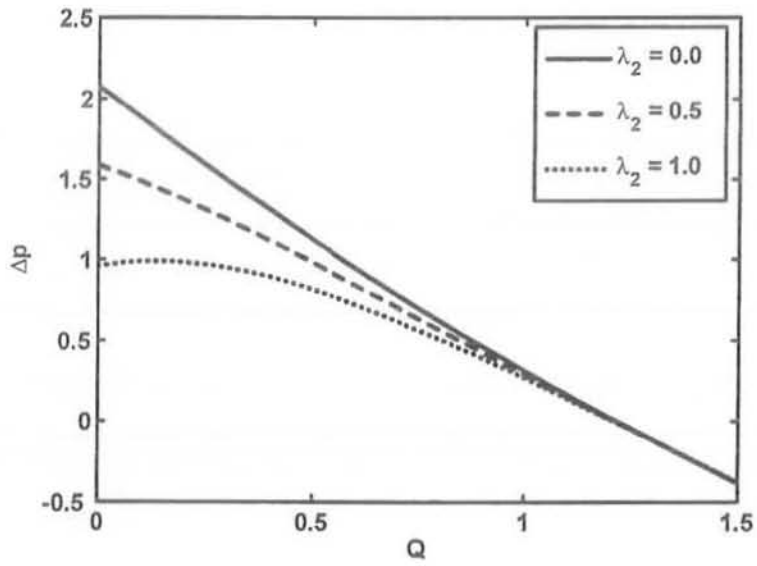


Fig. (6.4) : Variation of Δp with Q for different values of λ_2 at $a = 0.5$, $b = 1.2$, $\phi = \frac{\pi}{8}$, $d = 2$, $\alpha = 0.09$, $\lambda_1 = 0.9$.

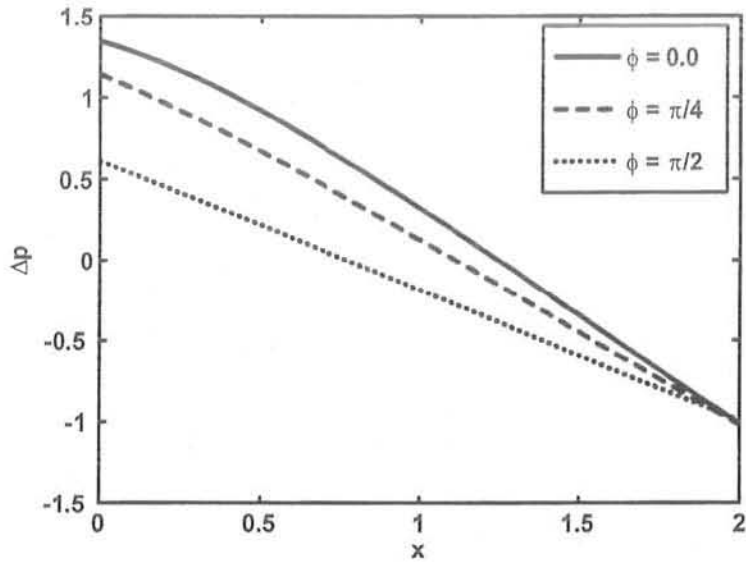


Fig. (6.5) : Variation of Δp with Q for different values of ϕ at $a = 0.5$, $b = 1.2$, $\lambda_2 = 0.9$, $d = 2$, $\alpha = 0.09$, $\lambda_1 = 0.5$.

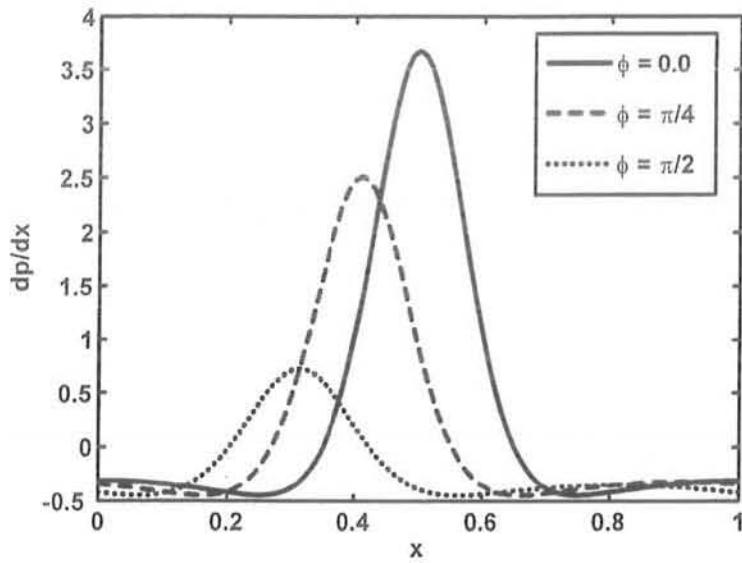


Fig. (6.6) : Variation of $\frac{dp}{dx}$ with x for different values of ϕ at $a = 0.5$, $b = 1.2$, $\alpha = 0.09$, $d = 2$, $\lambda_1 = 0.5$, $Q = 1$, $\lambda_2 = 0.9$.

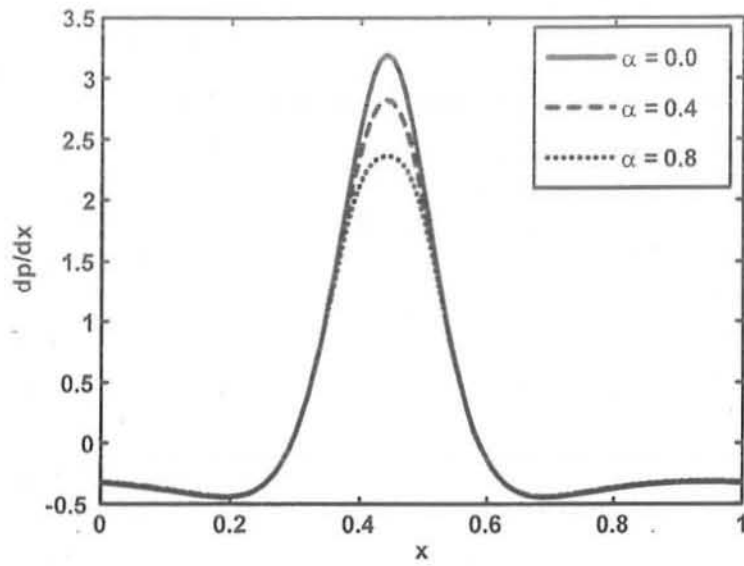


Fig.(6.7) : Variation of $\frac{dp}{dx}$ with x for different values of α at $a = 0.5$, $b = 1.2$, $\phi = \frac{\pi}{8}$, $d = 2$, $\lambda_1 = 0.3$, $Q = 1$, $\lambda_2 = 0.9$.

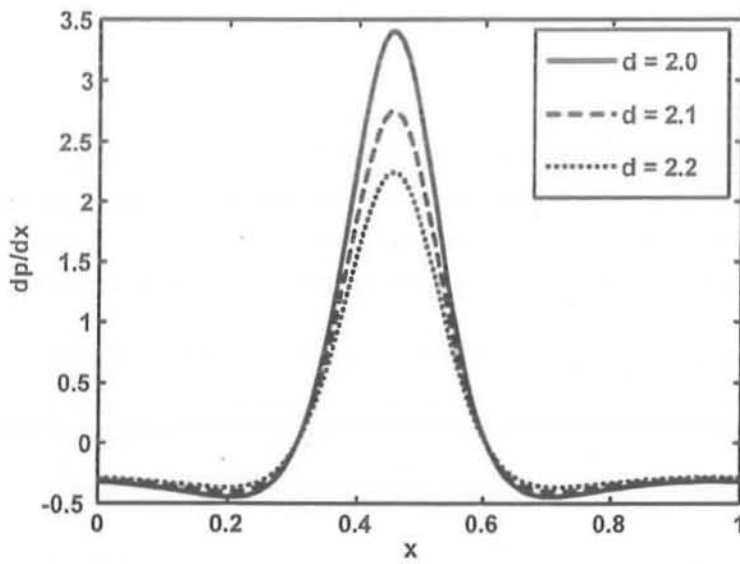


Fig.(6.8) : Variation of $\frac{dp}{dx}$ with x for different values of d at $a = 0.5$, $b = 1.2$, $\phi = \frac{\pi}{8}$, $\alpha = 0.04$, $\lambda_1 = 0.4$, $Q = 1$, $\lambda_2 = 0.9$.

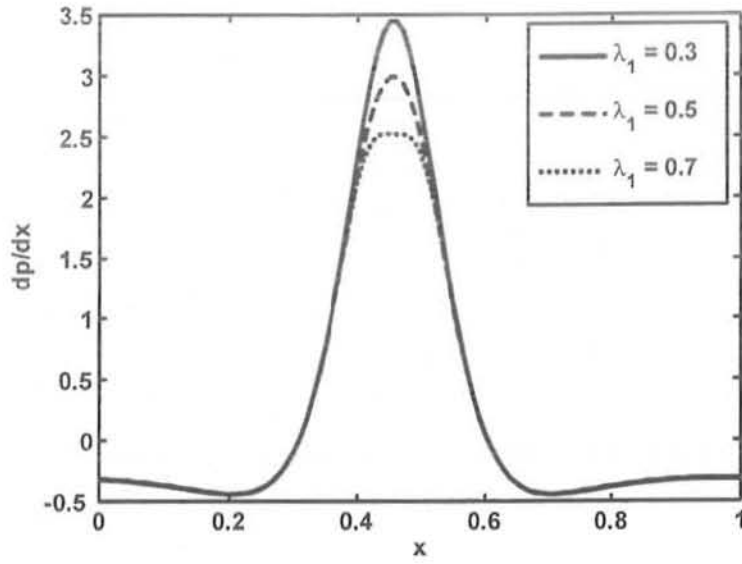


Fig. (6.9) : Variation of $\frac{dp}{dx}$ with x for different values of λ_1 at $a = 0.5$, $b = 1.2$, $\phi = \frac{\pi}{8}$, $d = 2$, $\alpha = 0.4$, $Q = 1$, $\lambda_2 = 0.9$.

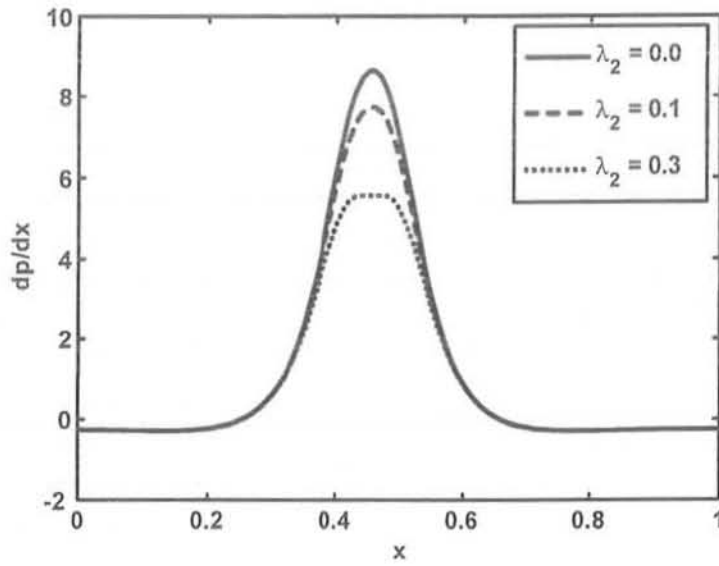


Fig.(6.10) : Variation of $\frac{dp}{dx}$ with x for different values of λ_2 at $a = 0.5$, $b = 1.2$, $\phi = \frac{\pi}{8}$, $d = 2$, $\alpha = 0.4$, $Q = 0.5$, $\lambda_1 = 0.7$.

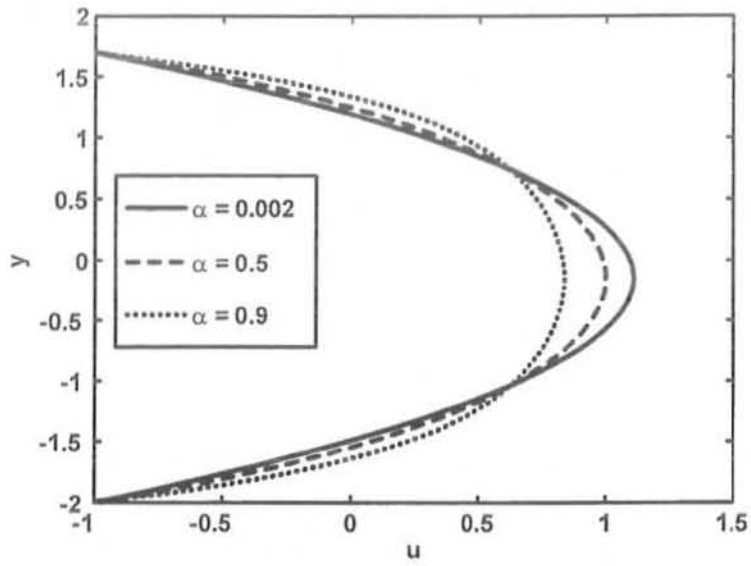


Fig.(6.11) : Velocity profile for different values of α at $a = 0.7$, $b = 1.2$, $\phi = \frac{\pi}{2}$, $d = 2$, $\lambda_1 = 0.5$, $Q = 4.5$, $x = 0$, $\lambda_2 = 0.9$.

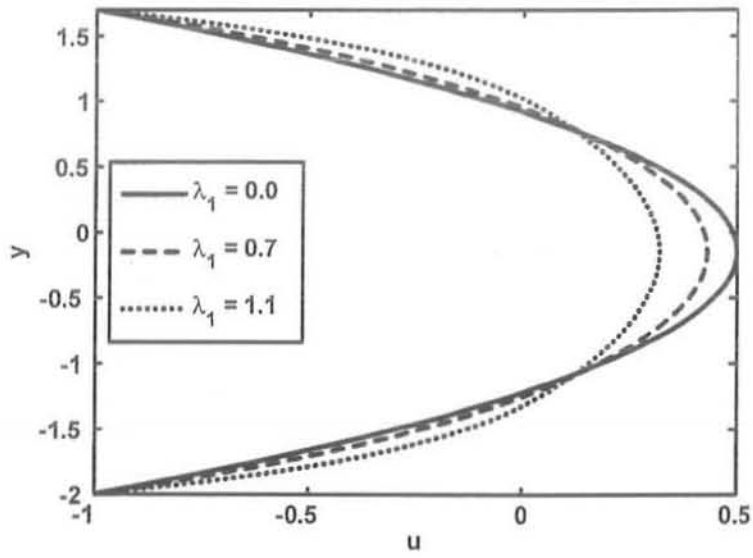


Fig. (6.12) : Velocity profile for different values of λ_1 at $a = 0.7$, $b = 1.2$, $\phi = \frac{\pi}{2}$, $d = 2$, $\alpha = 0.9$, $Q = 3$, $x = 0$, $\lambda_2 = 0.8$.

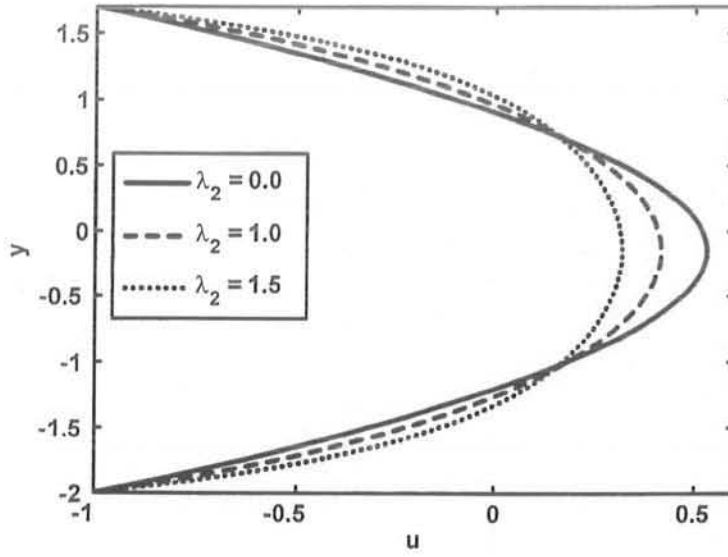


Fig.(6.13) : Velocity profile for different values of λ_2 at $a = 0.7, b = 1.2, \phi = \frac{\pi}{2}, d = 2, \alpha = 0.9, Q = 3, x = 0, \lambda_1 = 0.5$.

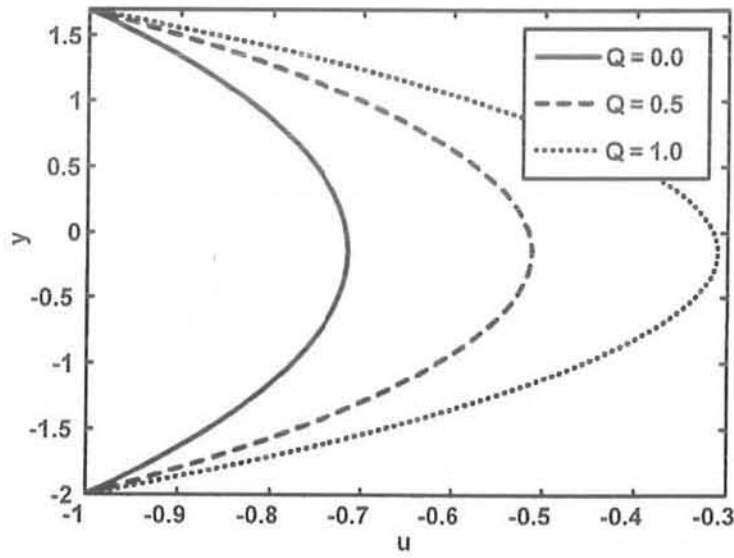


Fig. (6.14) : Velocity profile for different values of Q at $a = 0.7, b = 1.2, \phi = \frac{\pi}{2}, d = 2, \alpha = 0.02, \lambda_1 = 0.5, x = 0, \lambda_2 = 0.9$.

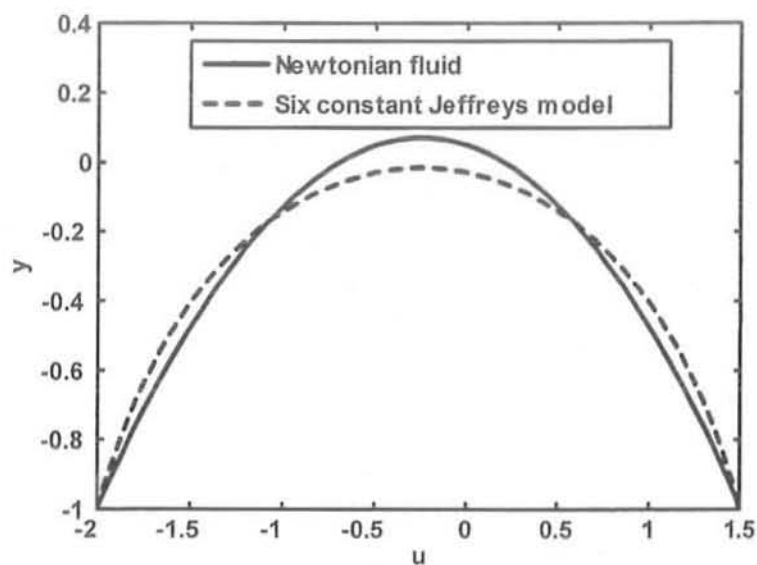


Fig. (6.15) : Velocity profile at $a = 0.5$, $b = 1.2$, $\phi = \frac{\pi}{2}$, $d = 2$, $\alpha = 0.02$, $\lambda_1 = 1.0$, $\lambda_2 = 1.3$, $x = 0$.

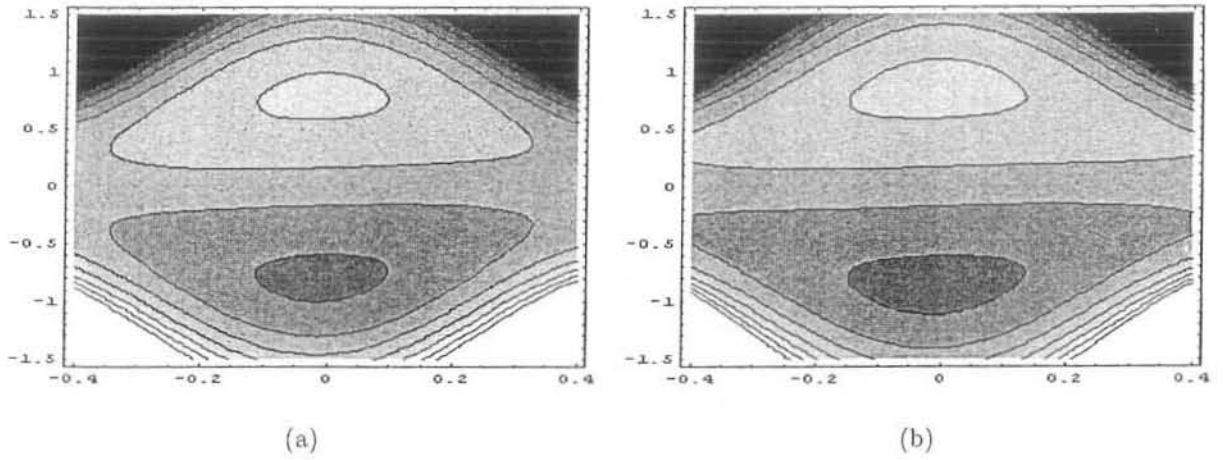


Fig.(6.16) : Stream lines for different values of Q . (a) for $Q = 1.8$, (b) for $Q = 2.0$. The other parameters are $a = 0.5$, $b = 0.5$, $\phi = 0.1$, $d = 1$, $\alpha = 0.9$, $\lambda_1 = 0.5$, $\lambda_2 = 0.45$.

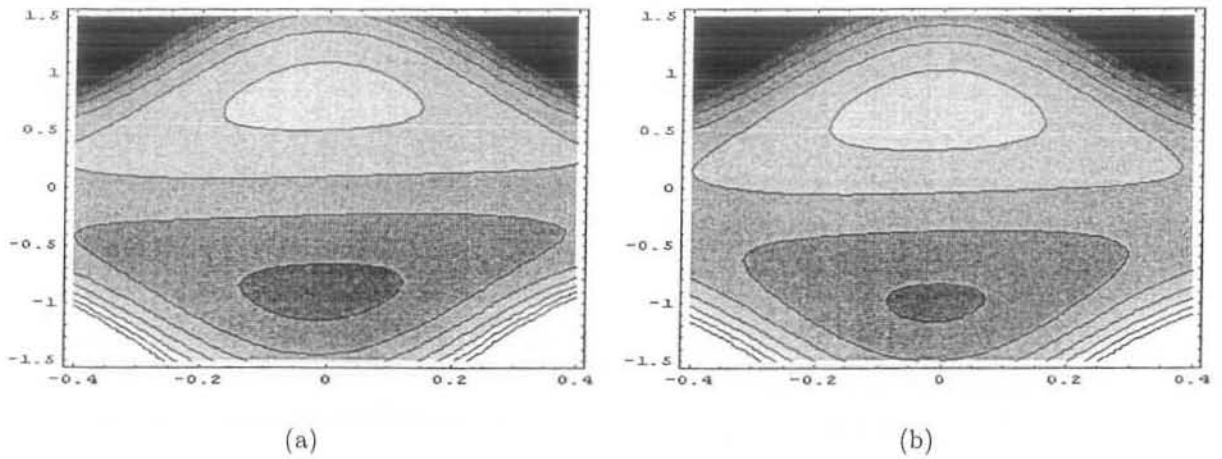
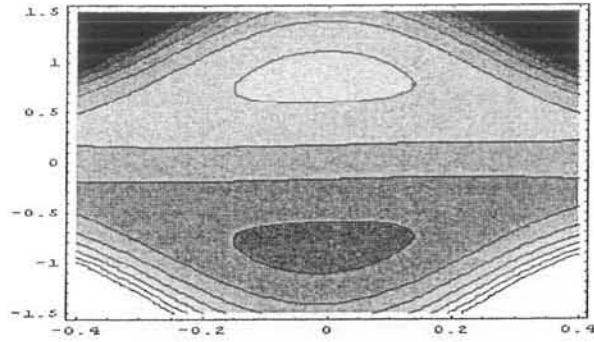
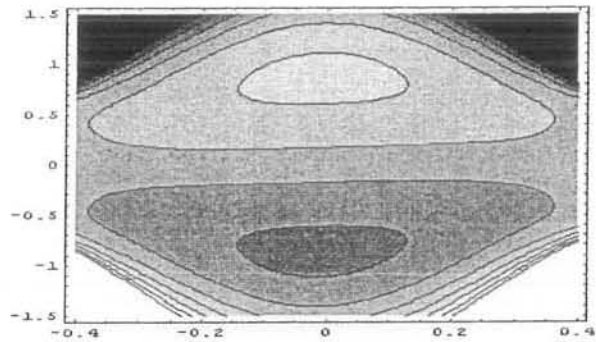


Fig.(6.17) : Stream lines for different values of d . (a) for $d = 1.1$, (b) for $d = 1.3$. The other parameters are $a = 0.5$, $b = 0.5$, $\phi = 0.1$, $Q = 2$, $\alpha = 0.9$, $\lambda_1 = 0.1$, $\lambda_2 = 0.45$.

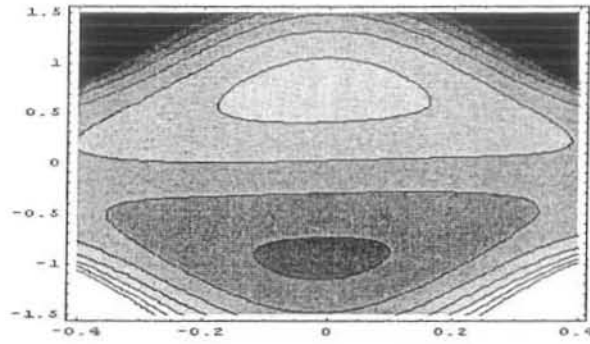


(a)

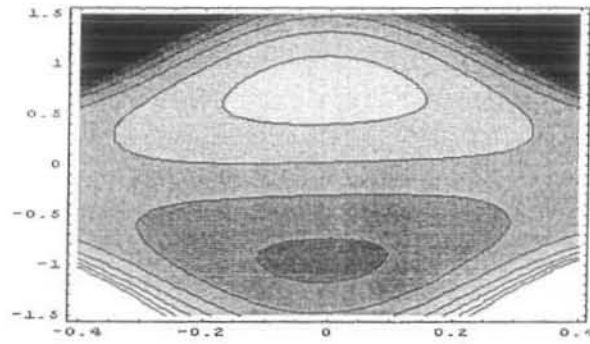


(b)

Fig.(6.18) : Stream lines for different values of λ_1 . (a) for $\lambda_1 = 0.0$, (b) for $\lambda_1 = 0.3$. The other parameters are $a = 0.5$, $b = 0.5$, $\phi = 0.1$, $d = 1$, $\alpha = 0.9$, $Q = 2$, $\lambda_2 = 0.45$.



(a)



(b)

Fig.(6.19) : Stream lines for different values of λ_2 . (a) for $\lambda_2 = 0.0$, (b) for $\lambda_2 = 0.6$. The other parameters are $a = 0.5$, $b = 0.5$, $\phi = 0.1$, $d = 1.5$, $\alpha = 0.9$, $Q = 2$, $\lambda_1 = 0.4$.

Table 6.3: Values of volume flow rate Q for Newtonian and six constant Jeffreys model of fluid for fixed $a = 0.5$, $b = 1.2$, $d = 2$, $x = 1$, $y = 0.5$, $\phi = \frac{\pi}{2}$, $\lambda_1 = 0.5$, $\lambda_2 = 0.8$, $\alpha = 0.02$.

volume flow rate Q	$ u(x, y) $ for Newtonian fluid	$ u(x, y) $ for six constant Jeffreys model
0.0	-0.825142	-2.61906
1.0	-0.475277	-1.67261
1.5	-0.300299	-1.19937
2	-0.125352	-0.726091

6.5 Conclusion

This chapter present the peristaltic flow of a six constant Jefferys model of fluid in an asymmetric channel. The governing two dimensional equations are simplified using long wave length and low Reynolds number approximation. The analytical and numerical solutions of simplified equations are calculated. The results are discussed through graphs. The main finding can be summarized as follows:

1. It is observed that in the peristaltic pumping region the pressure rise decreases with an increase in d , α , and λ_2 , while it increases with an increase in λ_1 .
2. The pressure gradient increases with an increase in α and λ_1 , while it decreases with an increase in d (width of the channel) and λ_2 .
3. The velocity field decreases with an increase in α and Q (volume flow rate), while with an increase in λ_1 and λ_2 the amplitude of the velocity decreases in the center and near the channel wall the velocity increases.
4. The size of the trapped bolus increases with an increase in volume flow rate Q .
5. The number of the trapped bolus decreases with an increase in the width of the channel d .
6. With an increase in relaxation time λ_1 the number and size of the trapped bolus increases.
7. When $\lambda_1 \rightarrow 0$ and $\lambda_2 \rightarrow 0$ the results of Mishra and Rao [14] can be recovered.

Chapter 7

Peristaltic motion of a Walter's B fluid in a symmetric or asymmetric channel

7.1 Introduction

This chapter deals with the modelling of Walter's B fluid for two dimensional incompressible flow. An analytical solution of Walter's B fluid in an asymmetric channel with sinusoidal wave variation have been calculated. The expressions for stream function and pressure gradient have been computed. The expression for pressure rise has been computed performing numerical integration. The pumping characteristics and axial pressure gradient have been discussed to highlight the physical features of emerging parameters of Walter's B fluid.

7.2 Mathematical formulation

Let us consider the peristaltic transport of an incompressible Walter's B' fluid in a two-dimensional channel of width $d_1 + d_2$. The geometry of the symmetric or asymmetric channel is defined in Chapter one. However, for Walter's B fluid the Cauchy stress tensor is different

which is defined as [67].

$$\mathbf{S} = -P\mathbf{I} + 2\eta_0\mathbf{e} - 2k_0\frac{\delta\mathbf{e}}{\delta t}, \quad (7.1)$$

where

$$\begin{aligned} 2\mathbf{e} &= \nabla\mathbf{V} + (\nabla\mathbf{V})^T, \\ \frac{\delta\mathbf{e}}{\delta t} &= \left(\frac{\partial}{\partial t} + \mathbf{V} \cdot \nabla\right)\mathbf{e} - \mathbf{e}\nabla\mathbf{V} - (\nabla\mathbf{V})^T\mathbf{e}. \end{aligned} \quad (7.2)$$

With the help of Eq. (1.6), Eqs. (1.2), (6.1) and (7.1) for Walter's B fluid take the following form

$$\frac{\partial U}{\partial X} + \frac{\partial V}{\partial Y} = 0, \quad (7.3)$$

$$\rho \left(\frac{\partial U}{\partial t} + U \frac{\partial U}{\partial X} + V \frac{\partial U}{\partial Y} \right) = -\frac{\partial P}{\partial X} + \frac{\partial S_{XX}}{\partial X} + \frac{\partial S_{XY}}{\partial Y}, \quad (7.4)$$

$$\rho \left(\frac{\partial V}{\partial t} + U \frac{\partial V}{\partial X} + V \frac{\partial V}{\partial Y} \right) = -\frac{\partial P}{\partial Y} + \frac{\partial S_{XY}}{\partial X} + \frac{\partial S_{YY}}{\partial Y}, \quad (7.5)$$

where

$$\begin{aligned} S_{XX} &= 2\eta_0\frac{\partial U}{\partial X} - k_0 \left[2 \left(\frac{\partial}{\partial t} + U \frac{\partial}{\partial X} + V \frac{\partial}{\partial Y} \right) \frac{\partial U}{\partial X} - 4 \left(\frac{\partial U}{\partial X} \right)^2 - 2 \frac{\partial V}{\partial X} \left(\frac{\partial V}{\partial X} + \frac{\partial U}{\partial Y} \right) \right], \\ S_{XY} &= \eta_0 \left(\frac{\partial U}{\partial Y} + \frac{\partial V}{\partial X} \right) - k_0 \left[\left(\frac{\partial}{\partial t} + U \frac{\partial}{\partial X} + V \frac{\partial}{\partial Y} \right) \left(\frac{\partial U}{\partial Y} + \frac{\partial V}{\partial X} \right) - 2 \frac{\partial U}{\partial X} \frac{\partial U}{\partial Y} \right. \\ &\quad \left. - \frac{\partial V}{\partial Y} \left(\frac{\partial U}{\partial Y} + \frac{\partial V}{\partial X} \right) - \frac{\partial U}{\partial X} \left(\frac{\partial U}{\partial Y} + \frac{\partial V}{\partial X} \right) - 2 \frac{\partial V}{\partial X} \frac{\partial V}{\partial Y} \right], \\ S_{YY} &= 2\eta_0\frac{\partial V}{\partial Y} - k_0 \left[2 \left(\frac{\partial}{\partial t} + U \frac{\partial}{\partial X} + V \frac{\partial}{\partial Y} \right) \frac{\partial V}{\partial Y} - 4 \left(\frac{\partial V}{\partial Y} \right)^2 - 2 \frac{\partial U}{\partial Y} \left(\frac{\partial V}{\partial X} + \frac{\partial U}{\partial Y} \right) \right] \end{aligned} \quad (7.6)$$

Defining the scales

$$\begin{aligned} \bar{x} &= \frac{x}{\lambda}, \quad \bar{y} = \frac{y}{d_1}, \quad \bar{u} = \frac{u}{c}, \quad \bar{v} = \frac{v}{c}, \quad \bar{t} = \frac{ct}{\lambda}, \quad \bar{h}_1 = \frac{h_1}{d_1}, \quad \bar{h}_2 = \frac{h_2}{d_1}, \quad \bar{S}_{\bar{x}\bar{x}} = \frac{\lambda}{\eta_0 c} S_{xx}, \\ \bar{S}_{\bar{x}\bar{y}} &= \frac{d_1}{\eta_0 c} S_{xy}, \quad \bar{S}_{\bar{y}\bar{y}} = \frac{d_1}{\eta_0 c} S_{yy}, \quad \delta = \frac{d_1}{\lambda}, \quad \text{Re} = \frac{\rho c d_1}{\eta_0}, \quad \alpha_1 = \frac{k_0 c}{d_1 \eta_0}, \quad \bar{p} = \frac{d_1^2}{c \lambda \eta_0} p. \end{aligned} \quad (7.7)$$

Using Eqs. (1.11) and (7.7), Eqs. (7.3) to (7.6) in terms of a stream function Ψ ($u = \frac{\partial \Psi}{\partial y}$, $v = -\delta \frac{\partial \Psi}{\partial x}$ after dropping bars), can be written as

$$\delta \operatorname{Re} \left[\left(\frac{\partial \Psi}{\partial y} \frac{\partial}{\partial x} - \frac{\partial \Psi}{\partial x} \frac{\partial}{\partial y} \right) \frac{\partial \Psi}{\partial y} \right] = -\frac{\partial p}{\partial x} + \delta^2 \frac{\partial S_{xx}}{\partial x} + \frac{\partial S_{xy}}{\partial y}, \quad (7.8)$$

$$-\delta^3 \operatorname{Re} \left[\left(\frac{\partial \Psi}{\partial y} \frac{\partial}{\partial x} - \frac{\partial \Psi}{\partial x} \frac{\partial}{\partial y} \right) \frac{\partial \Psi}{\partial x} \right] = -\frac{\partial p}{\partial y} + \delta^2 \frac{\partial S_{xy}}{\partial x} + \delta \frac{\partial S_{yy}}{\partial y}, \quad (7.9)$$

where

$$\begin{aligned} S_{xx} &= 2\Psi_{xy} - \alpha_1 \left[2\delta \left(\Psi_y \frac{\partial}{\partial x} - \Psi_x \frac{\partial}{\partial y} \right) \Psi_{xy} - 4\delta \Psi_{xy}^2 + 2\delta \Psi_{xx} (\Psi_{yy} - \delta^2 \Psi_{xx}) \right], \\ S_{xy} &= (\Psi_{yy} - \delta^2 \Psi_{xx}) - \alpha_1 \left[\delta \left(\Psi_y \frac{\partial}{\partial x} - \Psi_x \frac{\partial}{\partial y} \right) (\Psi_{yy} - \delta^2 \Psi_{xx}) - 2\delta \Psi_{xy} \Psi_{yy} - 2\delta^3 \Psi_{xy} \Psi_{xx} \right], \\ S_{yy} &= -2\delta \Psi_{xy} - \alpha_1 \left[-2\delta^2 \left(\Psi_y \frac{\partial}{\partial x} - \Psi_x \frac{\partial}{\partial y} \right) \Psi_{xy} - 4\delta^2 \Psi_{xy}^2 - 2\Psi_{yy} (\Psi_{yy} - \delta^2 \Psi_{xx}) \right], \end{aligned} \quad (7.10)$$

in which $\delta, \operatorname{Re}$ represent the wave and Reynolds numbers, respectively. Elimination of pressure from Eqs. (7.8) and (7.9) yields

$$\delta \operatorname{Re} \left[\left(\frac{\partial \Psi}{\partial y} \frac{\partial}{\partial x} - \frac{\partial \Psi}{\partial x} \frac{\partial}{\partial y} \right) \left(\frac{\partial^2 \Psi}{\partial y^2} + \delta^2 \frac{\partial^2 \Psi}{\partial x^2} \right) \right] = \delta^2 \left(\frac{\partial^2 S_{xx}}{\partial x \partial y} - \frac{\partial^2 S_{xy}}{\partial x^2} \right) + \frac{\partial^2 S_{xy}}{\partial y^2} - \delta \frac{\partial^2 S_{yy}}{\partial y \partial x}. \quad (7.11)$$

The boundary conditions in terms of stream function Ψ are defined in Eq. (6.26)

The average volume flow rate Q over one period of the peristaltic wave is defined in chapter one.

7.3 Solution of the problem

Since Eq. (7.11) is highly non-linear, therefore, we seek the perturbation solution in small δ ($\delta \ll 1$). We expand Ψ , F and P as follow

$$\Psi = \Psi_0 + \delta \Psi_1 + O(\delta^2), \quad (7.12)$$

$$q = q_0 + \delta q_1 + O(\delta^2), \quad (7.13)$$

$$p = p_0 + \delta p_1 + O(\delta^2). \quad (7.14)$$

Substituting the above expressions in Eqs.(7.11), and (6.26) collecting the like powers of δ , we obtain the following systems

7.3.1 System of order δ^0 :

$$\frac{\partial^4 \Psi_0}{\partial y^4} = 0, \quad (7.15)$$

$$\frac{\partial p_0}{\partial x} = \frac{\partial^3 \Psi_0}{\partial y^3}, \quad (7.16)$$

$$\frac{\partial p_0}{\partial y} = 0, \quad (7.17)$$

$$\Psi_0 = \frac{q_0}{2}, \quad \frac{\partial \Psi_0}{\partial y} = -1 \quad \text{on} \quad y = h_1(x), \quad (7.18)$$

$$\Psi_0 = -\frac{q_0}{2}, \quad \frac{\partial \Psi_0}{\partial y} = -1 \quad \text{on} \quad y = h_2(x). \quad (7.19)$$

7.3.2 System of order δ^1 :

$$\begin{aligned} \frac{\partial^4 \Psi_1}{\partial y^4} = & \operatorname{Re} \left[\left(\frac{\partial \Psi_0}{\partial y} \frac{\partial}{\partial x} - \frac{\partial \Psi_0}{\partial x} \frac{\partial}{\partial y} \right) \left(\frac{\partial^2 \Psi_0}{\partial y^2} \right) \right] \\ & + \alpha_1 \left[\frac{\partial^2}{\partial y^2} \left(\frac{\partial \Psi_0}{\partial y} \frac{\partial^3 \Psi_0}{\partial x \partial y^2} - \frac{\partial \Psi_0}{\partial x} \frac{\partial^3 \Psi_0}{\partial y^3} - 2 \frac{\partial^2 \Psi_0}{\partial x \partial y} \frac{\partial^2 \Psi_0}{\partial y^2} \right) + 2 \frac{\partial^2}{\partial y \partial x} \left(\frac{\partial^2 \Psi_0}{\partial y^2} \right)^2 \right], \end{aligned} \quad (7.20)$$

$$\begin{aligned} \frac{\partial p_1}{\partial x} = & -\operatorname{Re} \left[\left(\frac{\partial \Psi_0}{\partial y} \frac{\partial}{\partial x} - \frac{\partial \Psi_0}{\partial x} \frac{\partial}{\partial y} \right) \left(\frac{\partial \Psi_0}{\partial y} \right) \right] \\ & + \frac{\partial}{\partial y} \left[\frac{\partial^2 \Psi_1}{\partial y^2} - \alpha_1 \left(\left(\Psi_{0y} \frac{\partial}{\partial x} - \Psi_{0x} \frac{\partial}{\partial y} \right) \Psi_{0yy} - 2 \Psi_{0xy} \Psi_{0yy} \right) \right], \end{aligned} \quad (7.21)$$

$$\frac{\partial p_1}{\partial y} = 2\alpha_1 \frac{\partial}{\partial y} \left(\frac{\partial^2 \Psi_0}{\partial y^2} \right)^2, \quad (7.22)$$

$$\Psi_1 = \frac{q_1}{2}, \quad \frac{\partial \Psi_1}{\partial y} = 0 \quad \text{on} \quad y = h_1(x), \quad (7.23)$$

$$\Psi_1 = -\frac{q_1}{2}, \quad \frac{\partial \Psi_1}{\partial y} = 0 \quad \text{on} \quad y = h_2(x). \quad (7.24)$$

Higher order solutions are not sought.

7.3.3 Solution for system of order δ^0

Solution of Eq. (7.15) satisfying the boundary conditions (7.18) and (7.19) can be written as

$$\begin{aligned} \Psi_0 = & \frac{q_0 + h_1 - h_2}{(h_2 - h_1)^3} (2y^3 - 3(h_1 + h_2)y^2 + 6h_1h_2y) - y \\ & + \frac{1}{(h_2 - h_1)^3} \left[\left(\frac{q_0}{2} + h_1 \right) (h_2^3 - 3h_1h_2^2) - \left(h_2 - \frac{q_0}{2} \right) (h_1^3 - 3h_2h_1^2) \right]. \end{aligned} \quad (7.25)$$

The axial pressure gradient at this order is

$$\frac{dp_0}{dx} = \frac{12(q_0 + h_1 - h_2)}{(h_2 - h_1)^3}. \quad (7.26)$$

For one wavelength the integration of Eq. (7.26), yields

$$\Delta p_0 = \int_0^1 \frac{dp_0}{dx} dx. \quad (7.27)$$

7.3.4 Solution for system of order δ^1

Substituting the zeroth-order solution (7.25) into (7.20), the solution of the resulting problem satisfying the boundary conditions take the following form

$$\Psi_1 = C_{31}y^7 + C_{32}y^6 + C_{33}y^5 + C_{34}y^4 + G_1 \frac{y^3}{3!} + G_2 \frac{y^2}{2!} + G_3y + G_4, \quad (7.28)$$

where the coefficients appearing in Eq. (7.28) are defined as

$$\begin{aligned} A_{00} &= \frac{12(q_0 + h_1 + h_2)}{(h_2 - h_1)^3}, & A_{01} &= \frac{(h_1 + h_2)}{2}, & A_{02} &= \frac{h_1h_2}{2}, \\ A_{21} &= \frac{(2h_2 - q_0)(h_2 - h_1)^3 + 2h_2^2(h_2 - 3h_1)(h_1 - h_2 + q_0)}{2(h_2 - h_1)^3}, \\ B_{00} &= \frac{6(q_0 + h_1 + h_2)(h_1 + h_2)}{(h_2 - h_1)^3}, & B_1 &= \frac{6(q_0 + h_1 + h_2)h_1h_2}{(h_2 - h_1)^3}, \\ B_2 &= \frac{72(q_0 + h_1 + h_2)^2(h_1 + h_2)}{(h_2 - h_1)^6}, & B_3 &= \left(\frac{12(q_0 + h_1 + h_2)}{(h_2 - h_1)^3} \right)^2, \end{aligned}$$

$$\begin{aligned}
B_4 &= A'_{00} \frac{12(q_0 + h_1 + h_2)}{(h_2 - h_1)^3}, & B_5 &= B'_{00} \frac{12(q_0 + h_1 + h_2)}{(h_2 - h_1)^3}, \\
B_6 &= B'_1 \frac{12(q_0 + h_1 + h_2)}{(h_2 - h_1)^3}, & B_7 &= A'_{21} \frac{12(q_0 + h_1 + h_2)}{(h_2 - h_1)^3}, \\
G_1 &= \frac{(q_1 - C_{48})}{C_{49}}, & G_2 &= C_{54} + q_1 C_{55}, & G_3 &= C_{52} + q_1 C_{53}, \\
G_4 &= C_{51} + q_1 C_{50}, & C_{55} &= -\frac{6(h_1 + h_2)}{(h_2 - h_1)^3}, & C_{54} &= C_{39} + A_{01} \frac{C_{48}}{C_{49}}, \\
C_{53} &= \frac{6(h_1 h_2)}{(h_2 - h_1)^3}, & C_{52} &= C_{43} - \frac{C_{44} C_{48}}{C_{49}}, & C_{51} &= \frac{C_{47} C_{48}}{C_{49}} - C_{46}, \\
C_{50} &= \frac{-1}{2} - \frac{C_{47}}{C_{49}}, & C_{49} &= \frac{(h_2 - h_1)^3}{12}, \\
C_{48} &= C_{31} h_1^7 + C_{32} h_1^6 + C_{33} h_1^5 + C_{34} h_1^4 + \frac{h_1^2}{2} C_{39} + h_1 C_{43} - C_{46}, \\
C_{47} &= \frac{h_2^2 (3h_1 - h_2)}{12}, & C_{46} &= C_{45} + \frac{h_2^2}{6} C_{39} + h_2 C_{43}, \\
C_{45} &= C_{31} h_2^7 + C_{32} h_2^6 + C_{33} h_2^5 + C_{34} h_2^4, & C_{44} &= h_2 A_{01} - \frac{h_2^2}{2}, \\
C_{43} &= C_{39} + C_{40} + C_{41} + C_{42}, & C_{42} &= -h_2 C_{39}, \\
C_{41} &= -5C_{33} h_2^4 - 4C_{34} h_2^3, & C_{40} &= -7C_{31} h_2^6 - 6C_{32} h_2^5, \\
C_{39} &= C_{35} + C_{36} + C_{37} + C_{38}, & C_{38} &= \frac{4C_{34} (h_2^3 - h_1^3)}{(h_1 - h_2)}, \\
C_{37} &= \frac{5C_{33} (h_2^4 - h_1^4)}{(h_1 - h_2)}, & C_{36} &= \frac{6C_{32} (h_2^5 - h_1^5)}{(h_1 - h_2)}, \\
C_{35} &= \frac{7C_{31} (h_2^6 - h_1^6)}{(h_1 - h_2)}, & C_{34} &= \frac{C_{30}}{24}, & C_{33} &= \frac{C_{29}}{120}, \\
C_{32} &= -\frac{C_{24}}{360}, & C_{31} &= \frac{C_{23}}{840}, & C_{30} &= C_{28} + C_{26}, & C_{29} &= C_{25} + C_{27}, \\
C_{28} &= (2B_4 A_{01} - 4B'_2) \alpha_1, & C_{27} &= (-2B_4 + 4B'_3) \alpha_1, \\
C_{26} &= (-B_5 A_{02} - B'_{00} - B_7) \text{Re}, & C_{25} &= (B_4 A_{02} - A'_{00} + B_5 A_{01} - B_6) \text{Re}, \\
C_{24} &= B_4 A_{01} \text{Re}, & C_{23} &= \frac{1}{3} B_4 \text{Re}.
\end{aligned} \tag{7.29}$$

The axial pressure gradient at this order is obtained from Eqs. (7.21) and (7.22) using Eq.

(7.25)

$$\begin{aligned}\frac{dp_1}{dx} &= D_0y^3 + D_1y^2 + D_2y + D_3 + D_4y^4, \\ \frac{dp_1}{dy} &= \frac{144\alpha_1(q_0 + h_1 - h_2)^2}{(h_2 - h_1)}(2y - h_1 - h_2).\end{aligned}\quad (7.30)$$

where

$$\begin{aligned}D_4 &= -a_3 \text{Re} + 210C_{31}, \quad D_3 = -\text{Re} a_7 + G_1 - \alpha_1 a_2, \quad D_2 = -a_6 \text{Re} + 24C_{34} - \alpha_1 a_1, \\ D_1 &= -a_5 \text{Re} + 6C_{33} - \alpha_1 a_0, \quad D_0 = -a_4 \text{Re} + 120C_9, \quad a_0 = -240A'_{00}, \\ a_1 &= 3A_{00}B'_{00} + A_{00}B_{00}, \quad a_2 = A'_{00}B_1 - A'_{00} - 3A_{00}B'_1 - B_{00}^2, \quad a_3 = \frac{A_{00}A'_{00}}{12}, \\ a_4 &= \frac{-1}{3}B_{00}A'_{00}, \quad a_5 = \frac{-1}{2}B'_1A_{00} - \frac{A_{00}}{2} + \frac{1}{2}B_{00}B'_{00} + \frac{B_1A'_{00}}{2} - \frac{A'_{00}}{2}, \\ a_6 &= B_{00} - B_1B'_{00} + B'_{00} - A'_{21}A_{00}, \quad a_7 = B_1B'_1 - B_1 - B'_1 + 1 + A'_{21}B_{00}.\end{aligned}\quad (7.31)$$

The first order non dimensional pressure rise per wavelength is

$$\Delta p_1 = \int_0^1 \frac{dp_1}{dx} \Big|_{y=0} dx. \quad (7.32)$$

Define

$$q = q_0 + \delta q_1. \quad (7.33)$$

Summarizing the perturbation results up to first order for Ψ , dp/dx , and Δp as

$$\Psi = \Psi_0 + \delta\Psi_1, \quad \frac{dp}{dx} = \frac{dp_0}{dx} + \delta\frac{dp_1}{dx}, \quad \Delta p = \Delta p_0 + \delta\Delta p_1. \quad (7.34)$$

Using $q_0 = q - \delta q_1$ and then neglecting the terms greater than $O(\delta)$ the results given by Eq. (7.34) can be explicitly computed.

7.4 Results and discussion

In this section graphical results are displayed to see the effects of various physical parameters on pressure rise and pressure gradient. The expression for pressure rise is calculated numerically

using the mathematics software Mathematica. Figs. 7.1 to 7.4 are prepared to see the effects of pressure rise for different values of amplitude ratio ϕ , wave number δ , Walter's B fluid parameter α_1 and width of the channel d . In Fig. 7.1 it is observed that the pressure rise decreases with an increase of the amplitude ratio ϕ . Further, the peristaltic pumping occurs in the region $0 \leq \Theta \leq 1.2$, and augmented pumping occurs in the region $1.2 \leq \Theta \leq 1.5$ for different values of ϕ . It is observed from Figs. 7.2 and 7.3 that for peristaltic pumping ($\Delta p > 0, \Theta > 0$), free pumping ($\Delta p = 0$) and the copumping region ($\Delta p < 0, \Theta > 0$), pumping increases when the wave number δ and Walter's B fluid parameter α_1 increases. The effects of the width of the channel d , on the pumping characteristic is plotted in Fig. 7.4. It is observed that for peristaltic pumping ($\Delta p > 0, \Theta > 0$) and for free pumping ($\Delta p = 0$), pumping decreases as the width of the channel d increases, while the behavior is opposite in the copumping region ($\Delta p < 0, \Theta > 0$); here pumping increases as d increases. Figs. 7.5 to 7.8 are displayed to see the effects of various physical parameters on the pressure gradient (dp/dx). The pressure gradient against x for different values of α_1 , d , δ and ϕ are presented in Figs. 7.5 to 7.8. It is observed that the pressure gradient increases with increase in α_1 (see Fig. 7.5). It is seen that the minimum value of the pressure gradient is at about $x = 0.45$ and the maximum occurs at $x = 0.62$. The pressure gradient for different values of d are shown in Fig. 7.6. It is observed that with an increase in d , the pressure gradient increases in the regions $x \in [0, 0.5]$ and $[0.7, 1]$ and decreases in the region $x \in [0.5, 0.7]$. The pressure gradient for different values of δ are seen in Fig. 7.7. It is observed that the pressure increases with an increases in δ in the whole region and the maximum occurs at the center. The pressure gradient for various values of ϕ are shown in Fig. 7.8. The pressure gradient decreases in the center of the channel with an increase in ϕ and the maximum value occurs at the center for small ϕ .

Figs. 7.9 to 7.11 illustrate the trapping phenomena for different values of volume flow rate Q , width of the channel d and amplitude ratio ϕ . It is observed from Fig. 7.9 that the size of the trapping bolus increases with an increase of volume flow rate Q in both upper and lower half of the channel. It is also observed from Fig. 7.10 that with an increase in width of the channel d the size of the trapped bolus decreases. Fig. 7.11 shows the stream lines for different values of the amplitude ratio ϕ . It is observed from Fig. 7.11 that the size of the trapping bolus decreases with an increase in amplitude ratio ϕ .

Table 7.1 shows the comparison of present solution with those available in the literature when some of parameters are replaced to be zero in our problem.

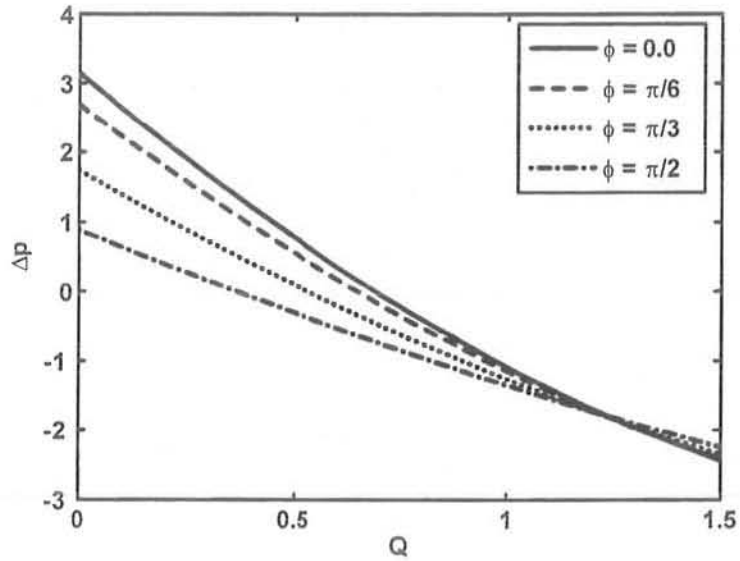


Fig.(7.1) : Variation of Δp with Q for different values of ϕ at $a = 0.5$, $b = 0.5$, $d = 1$, $Re = 10$, $\delta = 0.01$, $\alpha_1 = 4$.

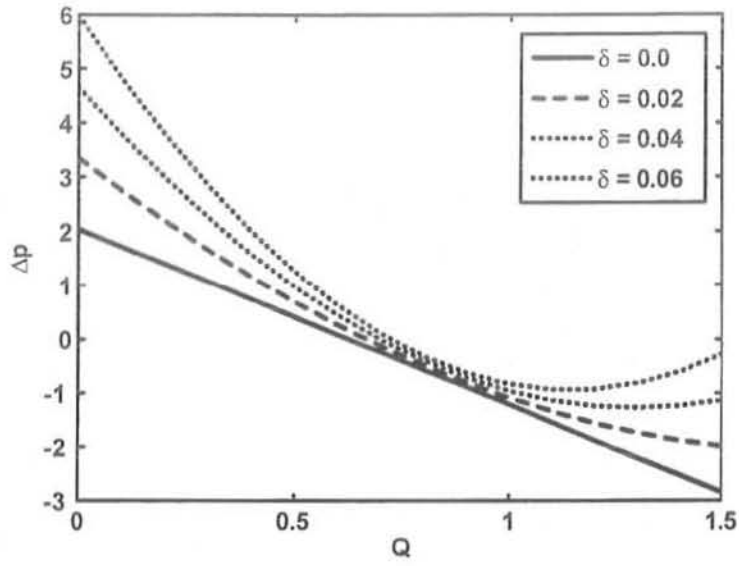


Fig.(7.2) : Variation of Δp with Q for different values of δ at $a = 0.5, b = 0.5, d = 1, \text{Re} = 10,$
 $\phi = \frac{\pi}{6}, \alpha_1 = 4.$

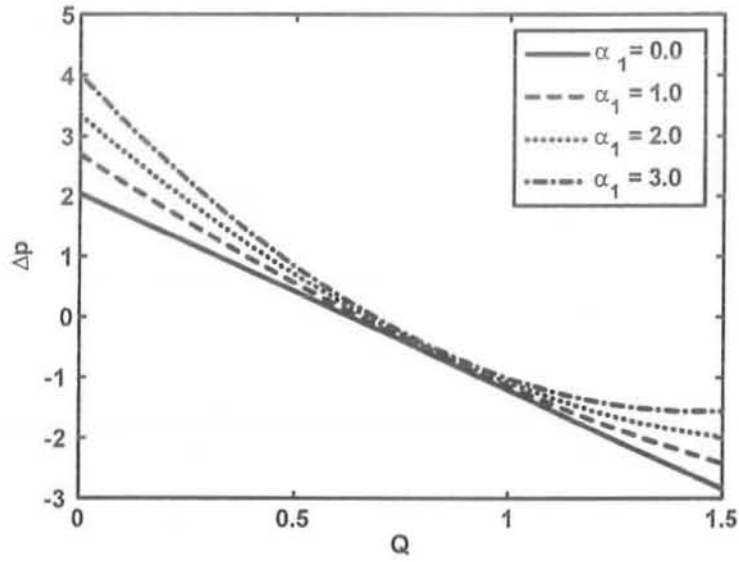


Fig.(7.3) : Variation of Δp with Q for different values of α_1 at $a = 0.5, b = 0.5, d = 1, \text{Re} = 10,$
 $\delta = 0.01, \phi = \frac{\pi}{6}.$

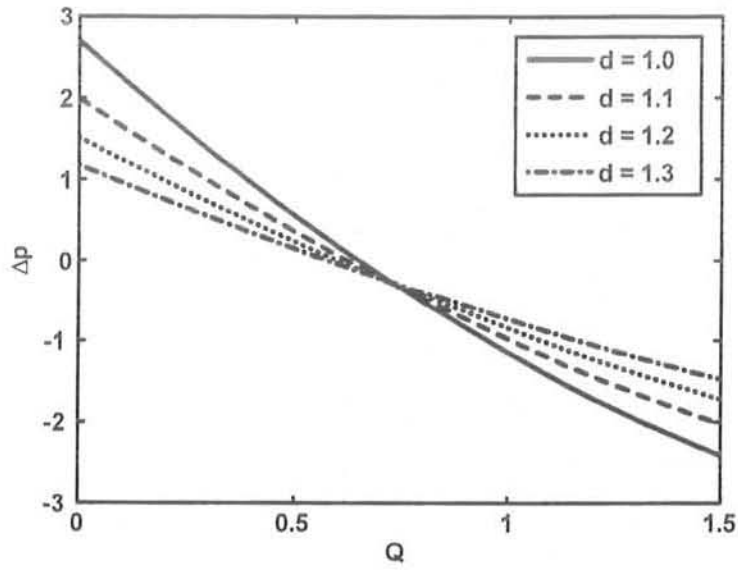


Fig.(7.4) : Variation of Δp with Q for different values of d at $a = 0.5$, $b = 0.5$, $\alpha_1 = 4$, $Re = 10$, $\delta = 0.01$, $\phi = \frac{\pi}{6}$.

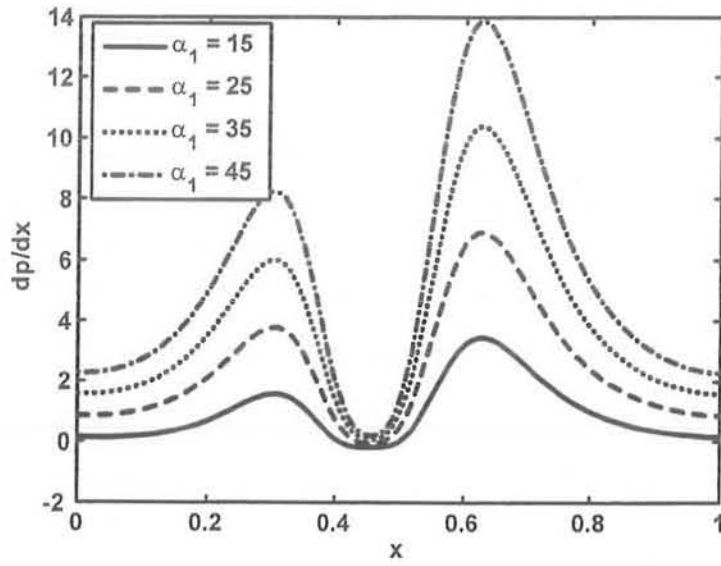


Fig.(7.5) : Variation of dp/dx with x for different values of α_1 at $a = 0.5$, $b = 0.5$, $d = 1$, $Re = 10$, $Q = 1$, $\delta = 0.01$, $\phi = \frac{\pi}{6}$.

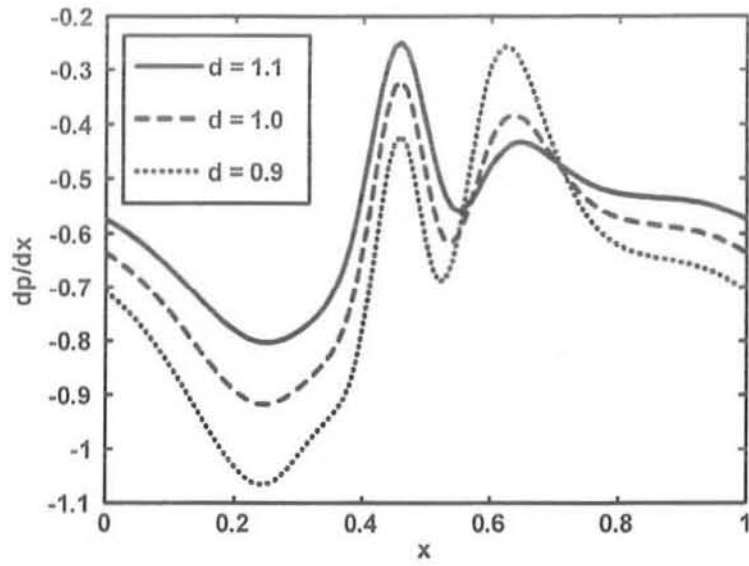


Fig.(7.6) : Variation of dp/dx with x for different values of d at $a = 0.5$, $b = 0.5$, $Re = 10$, $\delta = 0.01$, $Q = 1$, $\alpha_1 = 4$, $\phi = \frac{\pi}{6}$.

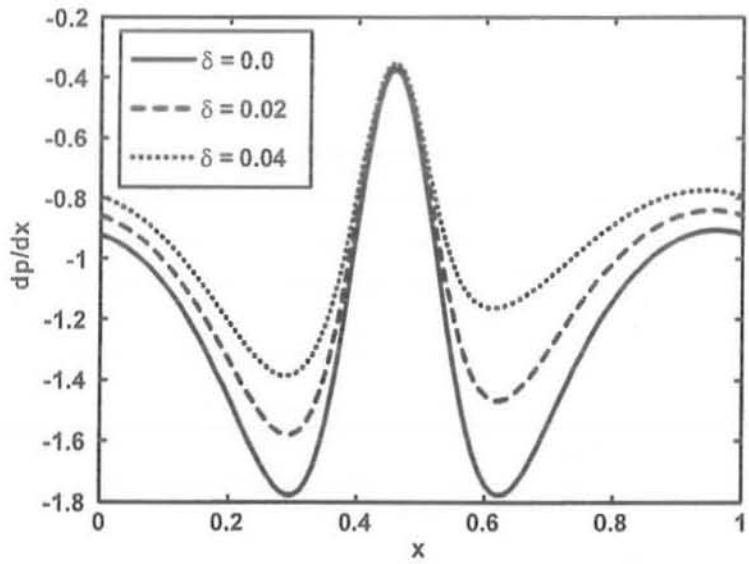


Fig.(7.7) : Variation of dp/dx with x for different values of δ at $a = 0.5$, $b = 0.5$, $d = 1$, $Re = 10$, $Q = 1$, $\alpha_1 = 4$, $\phi = \frac{\pi}{6}$.

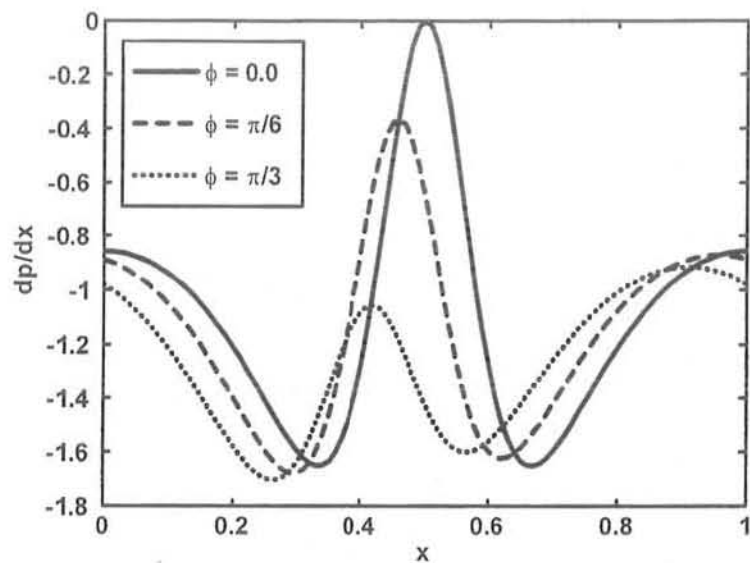
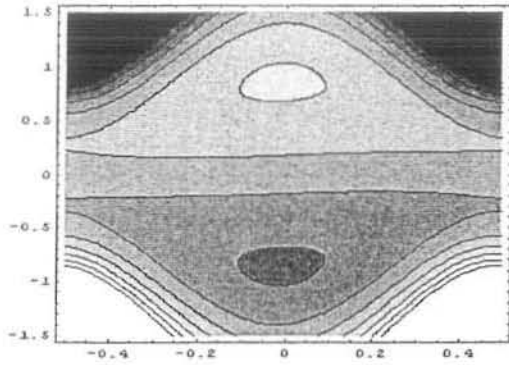
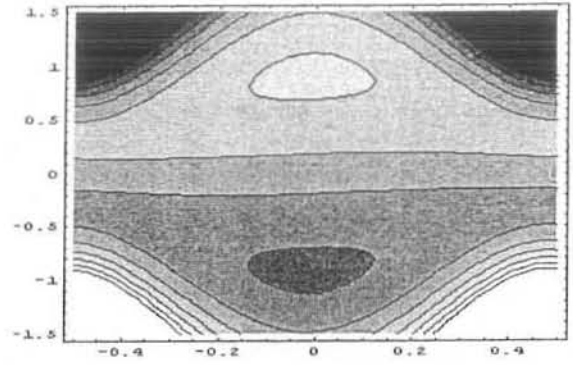


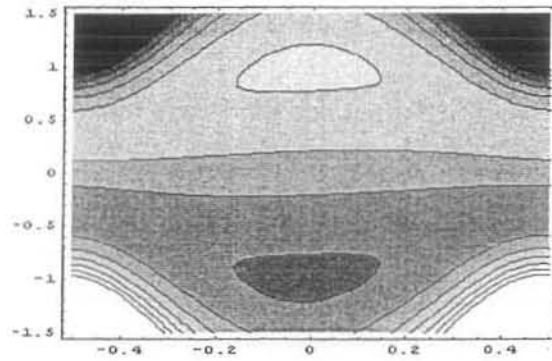
Fig.(7.8) : Variation of dp/dx with x for different values of ϕ at $a = 0.5$, $b = 0.5$, $d = 1$, $Re = 10$, $Q = 1$, $\delta = 0.01$, $\alpha_1 = 4$.



(a)

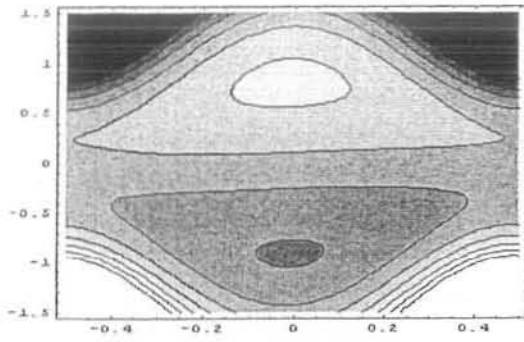


(b)

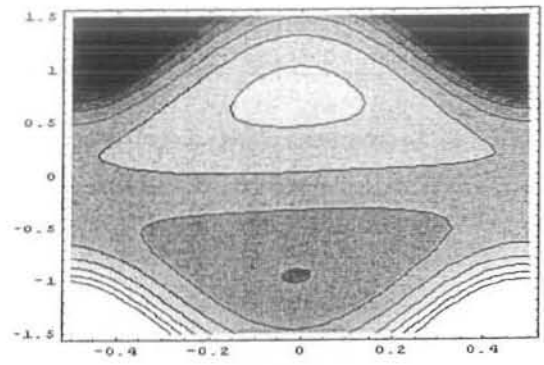


(c)

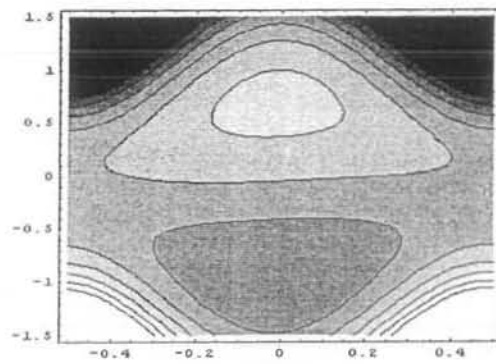
Fig.(7.9) : Stream lines for different values of volume flow rate Q . (a) for $Q = 2.0$, (b) for $Q = 2.2$. (c) for $Q = 2.4$. The other parameters are $a = 0.5$, $b = 0.5$, $\phi = 0.1$, $d = 1$, $\alpha_1 = 4$, $\delta = 0.07$.



(a)

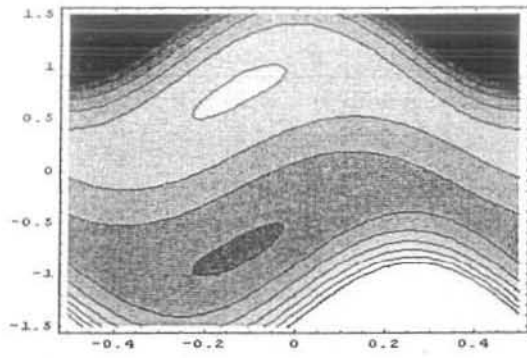


(b)

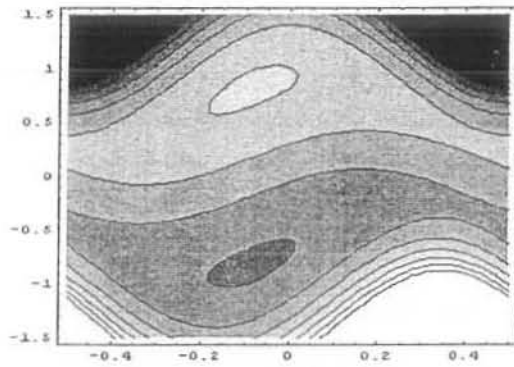


(c)

Fig.(7.10) : Stream lines for different values of width of the channel d . (a) for $d = 1.1$, (b) for $d = 1.2$. (c) for $d = 1.3$. The other parameters are $a = 0.5$, $b = 0.5$, $\phi = 0.1$, $Q = 2.0$, $\alpha_1 = 4$, $\delta = 0.07$.



(a)



(b)

Fig.(7.11) : Stream lines for different values of volume flow rate ϕ . (a) for $\phi = \frac{\pi}{2}$, (b) for $\phi = \frac{\pi}{3}$.
The other parameters are $a = 0.5$, $b = 0.5$, $Q = 2.0$, $d = 1.0$, $\alpha_1 = 4$, $\delta = 0.07$.

Table 7.1: Pressure rise with volume flow rate for fixed $a = 0.5$, $b = 0.5$, $d = 1$, $\phi = \frac{\pi}{6}$.

Q	Mishra et al [14] ΔP for $\alpha_1 = Re = \delta = 0$	Present work ΔP for $\alpha_1 = 1, Re = 10, \delta = 0.04$
0	2.03888	2.30219
0.1	1.71353	1.91822
0.2	1.38817	1.53906
0.3	1.06282	1.16472
0.4	0.737464	0.795195
0.5	0.41211	0.430483
0.6	0.0867558	0.0705845
0.7	-0.238599	-0.2845
0.8	-0.563953	-0.634769
0.9	-0.889307	-0.980225
1	-1.21466	-1.32087
1.1	-1.54002	-1.65669
1.2	-1.86537	-1.9877
1.3	-2.19072	-2.3139
1.4	-2.51608	-2.63529
1.5	-2.84143	-2.95185

7.5 Conclusion

This chapter presents the modelling of Walter's B fluid for two dimensional incompressible flow. An analytical solution of Walter's B fluid in an asymmetric channel have been calculated. The expression for pressure rise has been computed performing numerical integration. The pumping characteristics and axial pressure gradient have been discussed to highlight the physical features of emerging parameters of Walter's B fluid. The main finding can be summarized as follows:

1. The pressure rise decreases with an increase of the amplitude ratio ϕ for small values of volume flow rate and for large values the behavior is quite opposite.

2. For peristaltic pumping, free pumping and the copumping regions, pumping rate increases with an increase in wave number δ and Walter's B fluid parameter α_1 .
3. The pumping rate decreases in peristaltic pumping, free pumping regions with an increase in width of the channel d , while the behavior is opposite in the copumping region.
4. The pressure gradient increases with an increase in α_1 .
5. The pressure gradient increases in the regions $x \in [0, 0.5]$ and $x \in [0.7, 1]$ and decreases in the region $x \in [0.5, 0.7]$ with an increase in d .
6. The pressure gradient increases with an increase in δ in the whole region and the maximum occurs at the center.
7. The pressure gradient decreases in the center of the channel with the increase in ϕ and the maximum value occurs at the center for small ϕ .
8. The size of the trapped bolus increases with an increase of volume flow rate Q .
9. The size of the trapped bolus decreases with an increase in width of the channel d and amplitude ratio ϕ .

Chapter 8

Peristaltic transport of a hyperbolic tangent fluid model in an asymmetric channel

8.1 Introduction

This chapter presents the modeling of the two dimensional hyperbolic tangent fluid model. Using the assumption of long wavelength and low Reynold number, the governing equations of hyperbolic tangent fluid for an asymmetric channel have been solved using regular perturbation method. The expression for pressure rise has been calculated using numerical integrations. At the end, various physical parameters have been shown pictorially. It is found that the narrow part of the channel required large pressure gradient, also in the narrow part the pressure gradient decreases with an increase in Weissenberg number We and channel width d .

8.2 Mathematical formulation

The constitutive equation for hyperbolic tangent fluid is given by Ai and Vafai [68]

$$\tau = -PI + S, \tag{8.1}$$

$$\mathbf{S} = - [[\mu_\infty + (\mu_0 + \mu_\infty) \tanh(\Gamma\dot{\gamma})^n] \dot{\gamma}], \quad (8.2)$$

in which $-PI$ is the spherical part of the stress due to constraint of incompressibility, \mathbf{S} is the extra stress tensor, μ_∞ is the infinite shear rate viscosity, μ_0 is the zero shear rate viscosity, Γ is the time constant, n is the power law index and $\dot{\gamma}$ is defined as

$$\dot{\gamma} = \sqrt{\frac{1}{2} \sum_i \sum_j \dot{\gamma}_{ij} \dot{\gamma}_{ji}} = \sqrt{\frac{1}{2} \Pi}. \quad (8.3)$$

where $\Pi = \frac{1}{2} \text{trac} \left(\text{grad } \mathbf{V} + (\text{grad } \mathbf{V})^T \right)^2$.

Here Π is the second invariant strain tensor. We consider the constitutive Eq. (8.2), the case for which $\mu_\infty = 0$ and $\Gamma\dot{\gamma} < 1$. The component of extra stress tensor therefore, can be written as

$$\begin{aligned} \mathbf{S} &= -\mu_0 [(\Gamma\dot{\gamma})^n] \dot{\gamma} = -\mu_0 [(1 + \Gamma\dot{\gamma} - 1)^n] \dot{\gamma} \\ &= -\mu_0 [1 + n(\Gamma\dot{\gamma} - 1)] \dot{\gamma}. \end{aligned} \quad (8.4)$$

Invoking Eq. (1.6) into Eqs. (6.1) and (8.4), we get

$$\rho \left(\frac{\partial U}{\partial t} + U \frac{\partial U}{\partial X} + V \frac{\partial U}{\partial Y} \right) = -\frac{\partial P}{\partial X} - \frac{\partial S_{XX}}{\partial X} - \frac{\partial S_{XY}}{\partial Y}, \quad (8.5)$$

$$\rho \left(\frac{\partial V}{\partial t} + U \frac{\partial V}{\partial X} + V \frac{\partial V}{\partial Y} \right) = -\frac{\partial P}{\partial Y} - \frac{\partial S_{XY}}{\partial X} - \frac{\partial S_{YY}}{\partial Y}, \quad (8.6)$$

where

$$\begin{aligned} S_{XX} &= -2\mu_0 (1 + n(\Gamma\dot{\gamma} - 1)) \frac{\partial U}{\partial X}, \\ S_{XY} &= -\mu_0 (1 + n(\Gamma\dot{\gamma} - 1)) \left(\frac{\partial U}{\partial Y} + \frac{\partial V}{\partial X} \right), \\ S_{YY} &= -2\mu_0 (1 + n(\Gamma\dot{\gamma} - 1)) \frac{\partial V}{\partial Y}, \\ \dot{\gamma} &= \left(2 \left(\frac{\partial U}{\partial X} \right)^2 + \left(\frac{\partial U}{\partial Y} + \frac{\partial V}{\partial X} \right)^2 + 2 \left(\frac{\partial V}{\partial Y} \right)^2 \right)^{1/2}, \end{aligned} \quad (8.7)$$

Defining

$$\begin{aligned}\bar{x} &= \frac{x}{\lambda}, \quad \bar{y} = \frac{y}{d_1}, \quad \bar{u} = \frac{u}{c}, \quad \bar{t} = \frac{ct}{\lambda}, \quad \bar{h}_1 = \frac{h_1}{d_1}, \quad \bar{h}_2 = \frac{h_2}{d_1}, \quad \bar{S}_{\bar{x}\bar{x}} = \frac{\lambda}{\mu_0 c} S_{xx}, \quad \bar{S}_{\bar{x}\bar{y}} = \frac{d_1}{\mu_0 c} S_{xy}, \\ \bar{S}_{\bar{y}\bar{y}} &= \frac{d_1}{\mu_0 c} S_{yy}, \quad \delta = \frac{d_1}{\lambda}, \quad \text{Re} = \frac{\rho c d_1}{\mu_0}, \quad \text{We} = \frac{\Gamma c}{d_1}, \quad \bar{p} = \frac{d_1^2}{c \lambda \mu_0} p, \quad \bar{\gamma} = \frac{\dot{\gamma} d_1}{c}.\end{aligned}\quad (8.8)$$

Using Eqs. (1.11) and (8.8) the Eqs. (8.5) to (8.7) in terms of stream function $\Psi(u = \frac{\partial \Psi}{\partial y}, v = -\delta \frac{\partial \Psi}{\partial x}$ after dropping bars), can be written as

$$\delta \text{Re} \left[\left(\frac{\partial \Psi}{\partial y} \frac{\partial}{\partial x} - \frac{\partial \Psi}{\partial x} \frac{\partial}{\partial y} \right) \frac{\partial \Psi}{\partial y} \right] = -\frac{\partial p}{\partial x} - \delta^2 \frac{\partial S_{xx}}{\partial x} - \frac{\partial S_{xy}}{\partial y}, \quad (8.9)$$

$$-\delta^3 \text{Re} \left[\left(\frac{\partial \Psi}{\partial y} \frac{\partial}{\partial x} - \frac{\partial \Psi}{\partial x} \frac{\partial}{\partial y} \right) \frac{\partial \Psi}{\partial x} \right] = -\frac{\partial p}{\partial y} - \delta^2 \frac{\partial S_{xy}}{\partial x} - \delta \frac{\partial S_{yy}}{\partial y}, \quad (8.10)$$

where

$$\begin{aligned}S_{xx} &= -2(1 + n(\text{We}\dot{\gamma} - 1)) \frac{\partial^2 \Psi}{\partial x \partial y}, \\ S_{xy} &= -(1 + n(\text{We}\dot{\gamma} - 1)) \left(\frac{\partial^2 \Psi}{\partial y^2} - \delta^2 \frac{\partial^2 \Psi}{\partial x^2} \right), \\ S_{yy} &= 2\delta(1 + n(\text{We}\dot{\gamma} - 1)) \frac{\partial^2 \Psi}{\partial x \partial y}, \\ \dot{\gamma} &= \left(2\delta^2 \left(\frac{\partial^2 \Psi}{\partial x \partial y} \right)^2 + \left(\frac{\partial^2 \Psi}{\partial y^2} - \delta^2 \frac{\partial^2 \Psi}{\partial x^2} \right)^2 + 2\delta^2 \left(\frac{\partial^2 \Psi}{\partial x \partial y} \right)^2 \right)^{1/2},\end{aligned}\quad (8.11)$$

in which δ , Re , We represent the wave, Reynolds and Weissenberg numbers, respectively. Under the assumptions of long wavelength $\delta \ll 1$ and low Reynolds number, neglecting the terms of order δ and higher, Eqs. (8.9) and (8.10) take the form

$$\frac{\partial p}{\partial x} = \frac{\partial}{\partial y} \left[1 + n(\text{We} \frac{\partial^2 \Psi}{\partial y^2} - 1) \right] \frac{\partial^2 \Psi}{\partial y^2}, \quad (8.12)$$

$$\frac{\partial p}{\partial y} = 0. \quad (8.13)$$

Elimination of pressure from Eqs. (8.12) and (8.13) yield

$$\frac{\partial^2}{\partial y^2} \left(\left[1 + n(\text{We} \frac{\partial^2 \Psi}{\partial y^2} - 1) \right] \frac{\partial^2 \Psi}{\partial y^2} \right) = 0. \quad (8.14)$$

The relevant boundary conditions for asymmetric channel in stream function Ψ are already defined in Eq. (6.26).

The dimensionless mean flow Q is defined in Eq. (1.29).

8.3 Solution of the problem

8.3.1 Perturbation solution

For perturbation solution, we expand Ψ , q and p as

$$\Psi = \Psi_0 + We\Psi_1 + O(We^2), \quad (8.15)$$

$$q = q_0 + Weq_1 + O(We^2), \quad (8.16)$$

$$p = p_0 + We p_1 + O(We^2). \quad (8.17)$$

Substituting above expressions in Eqs. (8.12), (8.14) and (6.26), collecting the powers of We , we obtain the following systems

8.3.2 System of order We^0

$$\frac{\partial^4 \Psi_0}{\partial y^4} = 0, \quad (8.18)$$

$$\frac{\partial p_0}{\partial x} = (1-n) \frac{\partial^3 \Psi_0}{\partial y^3}, \quad (8.19)$$

$$\Psi_0 = \frac{q_0}{2}, \quad \frac{\partial \Psi_0}{\partial y} = -1 \quad \text{on} \quad y = h_1(x), \quad (8.20)$$

$$\Psi_0 = -\frac{q_0}{2}, \quad \frac{\partial \Psi_0}{\partial y} = -1 \quad \text{on} \quad y = h_2(x). \quad (8.21)$$

8.3.3 System of order We^1

$$\frac{\partial^4 \Psi_1}{\partial y^4} = \frac{n}{n-1} \frac{\partial^2}{\partial y^2} \left(\frac{\partial^2 \Psi_0}{\partial y^2} \right)^2, \quad (8.22)$$

$$\frac{\partial p_1}{\partial x} = (1-n) \frac{\partial^3 \Psi_1}{\partial y^3} + n \frac{\partial}{\partial y} \left(\frac{\partial^2 \Psi_0}{\partial y^2} \right)^2, \quad (8.23)$$

$$\Psi_1 = \frac{q_1}{2}, \quad \frac{\partial \Psi_1}{\partial y} = 0 \quad \text{on} \quad y = h_1(x), \quad (8.24)$$

$$\Psi_1 = -\frac{q_1}{2}, \quad \frac{\partial \Psi_1}{\partial y} = 0 \quad \text{on} \quad y = h_2(x). \quad (8.25)$$

8.3.4 Solution for system of order We^0

Solution of Eq. (8.18) satisfying the boundary conditions (8.20) and (8.21) can be written as

$$\begin{aligned} \Psi_0 = & \frac{q_0 + h_1 - h_2}{(h_2 - h_1)^3} (2y^3 - 3(h_1 + h_2)y^2 + 6h_1h_2y) - y \\ & + \frac{1}{(h_2 - h_1)^3} \left[\left(\frac{q_0}{2} + h_1 \right) (h_2^3 - 3h_1h_2^2) - \left(h_2 - \frac{q_0}{2} \right) (h_1^3 - 3h_2h_1^2) \right]. \end{aligned} \quad (8.26)$$

The axial pressure gradient at this order is

$$\frac{dp_0}{dx} = \frac{12(1-n)(q_0 + h_1 - h_2)}{(h_2 - h_1)^3}. \quad (8.27)$$

For one wavelength the integration of Eq. (8.27), yields

$$\Delta p = \int_0^1 \frac{dp_0}{dx} dx. \quad (8.28)$$

8.3.5 Solution for system of order We^1

Substituting the zeroth-order solution (8.26) into (8.22), the solution of the resulting problem satisfying the boundary conditions take the following form

$$\Psi_1 = D_5 + D_6y + D_7 \frac{y^2}{2!} + D_8 \frac{y^3}{3!} + \frac{288n}{n-1} \left(\frac{q_0 + h_1 - h_2}{(h_2 - h_1)^3} \right)^2 \frac{y^4}{4!}, \quad (8.29)$$

where

$$\begin{aligned}
D_5 &= -\frac{6}{(h_2 - h_1)^3} \left(q_1 - \frac{D_9}{4!} (h_1^3(2h_2 - h_1) - h_2^3(2h_1 - h_2)) \right) \left(\frac{h_1 h_2^2}{2} - \frac{h_2^3}{6} \right) \\
&\quad - \frac{D_9}{3!} \left(\frac{h_1^2 h_2^2}{2} + \frac{h_1 h_2^3}{2} - \frac{h_2^4}{4} \right) - \frac{q_1}{2}, \\
D_6 &= \frac{6h_1 h_2 q_1}{(h_2 - h_1)^3} + \frac{D_9 h_1 h_2}{2} \left(\frac{(h_1 + h_2)}{3} - \frac{1}{2(h_2 - h_1)^3} (h_1^3(2h_2 - h_1) - h_2^3(2h_1 - h_2)) \right), \\
D_7 &= \frac{-6q_1(h_1 + h_2)}{(h_2 - h_1)^3} + D_9 \left(\frac{(h_1 + h_2)}{4(h_2 - h_1)^3} (h_1^3(2h_2 - h_1) - h_2^3(2h_1 - h_2)) - \frac{(h_1^2 + h_1 h_2 + h_2^2)}{3!} \right), \\
D_8 &= \frac{12}{(h_2 - h_1)^3} \left(q_1 - \frac{D_9}{4!} (h_1^3(2h_2 - h_1) - h_2^3(2h_1 - h_2)) \right), \\
D_9 &= \frac{n}{n-1} 288 \left(\frac{q_0 + h_1 - h_2}{(h_2 - h_1)^3} \right)^2. \tag{8.30}
\end{aligned}$$

The axial pressure gradient at this order is

$$\frac{dp_1}{dx} = (1-n)C_3 - 144n(h_1 + h_2) \left[\frac{q_0 + h_1 - h_2}{(h_2 - h_1)^3} \right]^2. \tag{8.31}$$

For one wavelength the integration of Eq. (8.31), yields

$$\Delta p = \int_0^1 \frac{dp_1}{dx} dx. \tag{8.32}$$

Summarizing the perturbation results for small parameter We , the expression for stream functions and pressure gradient can be written as

$$\begin{aligned}
\Psi &= \frac{q + h_1 - h_2}{(h_2 - h_1)^3} (2y^3 - 3(h_1 + h_2)y^2 + 6h_1 h_2 y) - y \\
&\quad + \frac{1}{(h_2 - h_1)^3} \left[\left(\frac{q}{2} + h_1 \right) (h_2^3 - 3h_1 h_2^2) - (h_2 - \frac{q}{2}) (h_1^3 - 3h_2 h_1^2) \right] \\
&\quad + We \left[D_{10} + D_{11}y + D_{12} \frac{y^2}{2!} + D_{13} \frac{y^3}{3!} + D_{14} \frac{y^4}{4!} \right], \tag{8.33}
\end{aligned}$$

$$\begin{aligned}
\frac{dp}{dx} &= \frac{12(1-n)(q + h_1 - h_2)}{(h_2 - h_1)^3} + We \left(-\frac{12(1-n)}{(h_2 - h_1)^3} \frac{D_{14}}{4!} (h_1^3(2h_2 - h_1) - h_2^3(2h_1 - h_2)) \right. \\
&\quad \left. - 144n(h_1 + h_2) \left(\frac{q + h_1 - h_2}{(h_2 - h_1)^3} \right)^2 \right), \tag{8.34}
\end{aligned}$$

where

$$\begin{aligned}
D_{10} &= \frac{6}{(h_2 - h_1)^3} \left(\frac{D_{14}}{4!} (h_1^3(2h_2 - h_1) - h_2^3(2h_1 - h_2)) \right) \left(\frac{h_1 h_2^2}{2} - \frac{h_2^3}{6} \right) \\
&\quad - \frac{D_{14}}{3!} \left(\frac{h_1^2 h_2^2}{2} + \frac{h_1 h_2^3}{2} - \frac{h_2^4}{4} \right), \\
D_{11} &= \frac{D_{14} h_1 h_2}{2} \left(\frac{(h_1 + h_2)}{3} - \frac{1}{2(h_2 - h_1)^3} (h_1^3(2h_2 - h_1) - h_2^3(2h_1 - h_2)) \right), \\
D_{12} &= D_{14} \left(\frac{(h_1 + h_2)}{4(h_2 - h_1)^3} (h_1^3(2h_2 - h_1) - h_2^3(2h_1 - h_2)) - \frac{(h_1^2 + h_1 h_2 + h_2^2)}{3!} \right), \\
D_{13} &= \frac{-12}{(h_2 - h_1)^3} \left(\frac{D_{14}}{4!} (h_1^3(2h_2 - h_1) - h_2^3(2h_1 - h_2)) \right), \\
D_{14} &= \frac{n}{n-1} 288 \left[\frac{q + h_1 - h_2}{(h_2 - h_1)^3} \right]^2. \tag{8.35}
\end{aligned}$$

In the above solution when $\dot{\gamma} \rightarrow 0$ then $\mu \rightarrow \mu_0$, (or $n = 0$) the solutions of Mishra and Rao [14] are special case of our problem.

The non-dimensional pressure rise over one wavelength Δp for the axial velocity are

$$\Delta p = \int_0^1 \frac{dp}{dx} dx, \tag{8.36}$$

where dp/dx is defined in Eq. (8.34).

8.4 Results and discussion

The analytical solution of the hyperbolic tangent model is presented. The expression for pressure rise Δp is calculated numerically using mathematics software. The effects of various parameters on the pressure rise Δp are shown in Figs. 8.1 to 8.6 for various values of Weissenberg number We , amplitude ratio ϕ , tangent hyperbolic power law index n , channel width d and wave amplitudes a, b . It is observed from Fig. 8.1 that pressure rise decreases for small values of Q ($0 \leq Q \leq 1.45$) with an increase in We and for large Q ($1.45 \leq Q \leq 2$), the pressure rise increases. We also observe that for different values of We , there is a linear relation between Δp and Q , i.e, the pressure rise decreases for small Q and increases for large Q . The pressure rise Δp for different values of ϕ are illustrated in Fig. 8.2. It is shown that Δp decreases with an increase in ϕ for $Q \in [0, 1.9]$ and after that Δp increases. The graphs of Δp for different

values of power law index n are presented in Fig. 8.3. It is seen that with an increase in n , Δp decreases for $Q \in [0, 1.6]$ and for $Q \in [1.6, 2]$, it increases. It is observed that the pressure rise decreases with an increase in d and increases with an increase in a and b for small Q and for large Q , the results are opposite (see Figs. 8.4 to 8.6). Figs. 8.7 and 8.8 represent that for $x \in [0, 0.2]$ and $[0.6, 1]$ the pressure gradient is small, we say that the flow can easily pass without imposition of large pressure gradient, while in the narrow part of the channel $x \in [0.2, 0.6]$, to retain same flux, large pressure gradient is required. Moreover, in the narrow part of the channel, the pressure gradient decreases with an increase in We and d .

Trapping phenomena

Another interesting phenomena in peristaltic motion is trapping. It is basically the formation of an internally circulating bolus of fluid by closed stream lines. This trapped bolus pushed a head along a peristaltic waves. Figs. 8.9 to 8.11 illustrate the stream lines for different values of Q , We and a . The stream lines for different values of volume flow rate Q are shown in Figs. 8.9 a to c. It is found that with an increase in volume flow rate Q , the size and the number of trapping bolus increases. In Figs. 8.10 a to c. the stream line are prepared for different value of Weissenberg number We . It is depicted that the size of the trapped bolus increases with an increase in We . It is observed from Figs. 8.11 a to c that the size and the number of the trapping bolus increases with an increase in amplitude of the wave a .

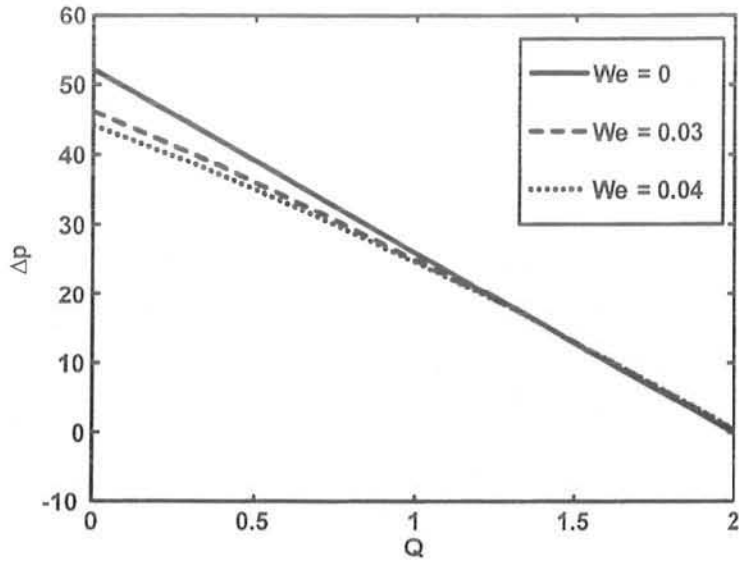


Fig.(8.1) : Variation of Δp with Q for different values of We at $a = 0.5$, $b = 0.5$, $d = 0.4$, $n = 0.04$ and $\phi = \frac{\pi}{6}$.

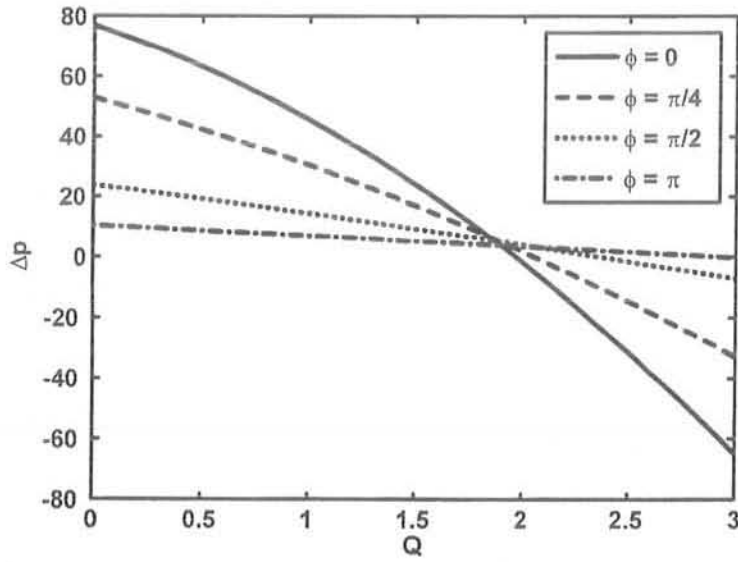


Fig.(8.2) : Variation of Δp with Q for different values of ϕ at $a = 0.5$, $d = 0.5$, $We = 0.03$, $n = 0.04$ and $b = 0.7$.

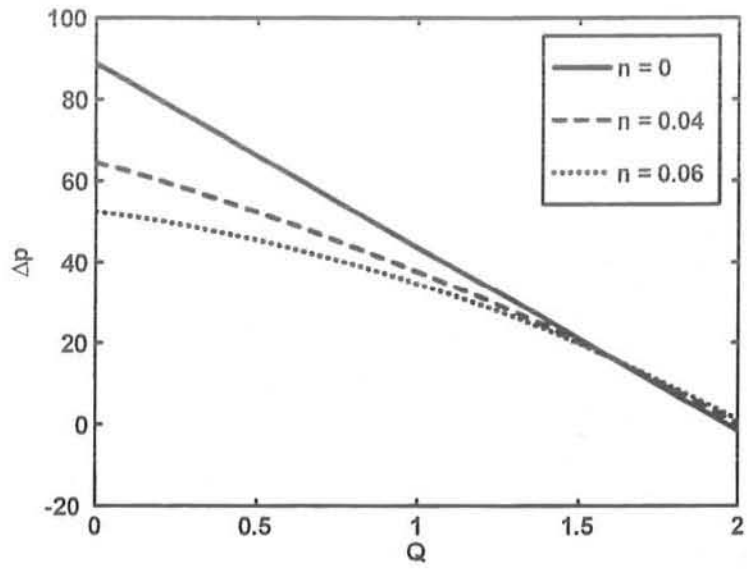


Fig.(8.3) : Variation of Δp with Q for different values of n at $a = 0.5, d = 0.5, We = 0.03, b = 0.7$ and $\phi = \frac{\pi}{6}$.

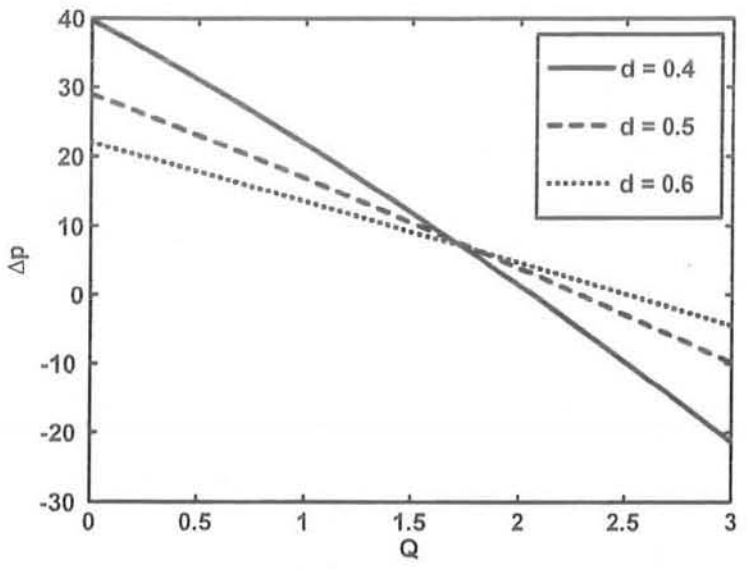


Fig.(8.4) : Variation of Δp with Q for different values of d at $a = 0.5, b = 0.5, We = 0.03, n = 0.04$ and $\phi = \frac{\pi}{4}$.

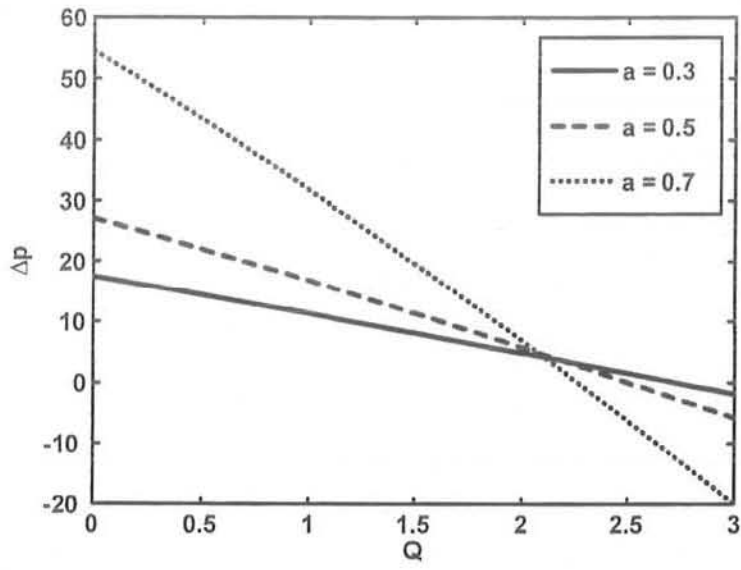


Fig.(8.5) : Variation of Δp with Q for different values of a at $b = 0.7, d = 0.7, We = 0.03, n = 0.04$ and $\phi = \frac{\pi}{4}$.

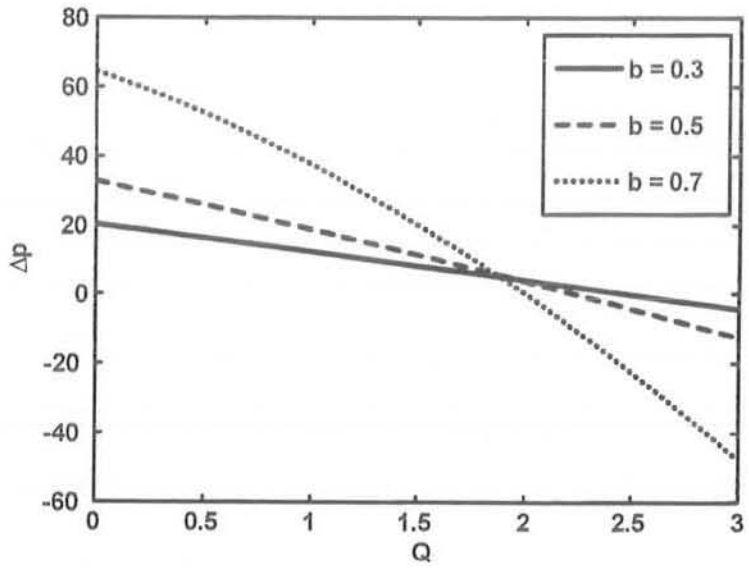


Fig.(8.6) : Variation of Δp with Q for different values of b at $a = 0.5, d = 0.5, We = 0.03, n = 0.04$ and $\phi = \frac{\pi}{6}$.

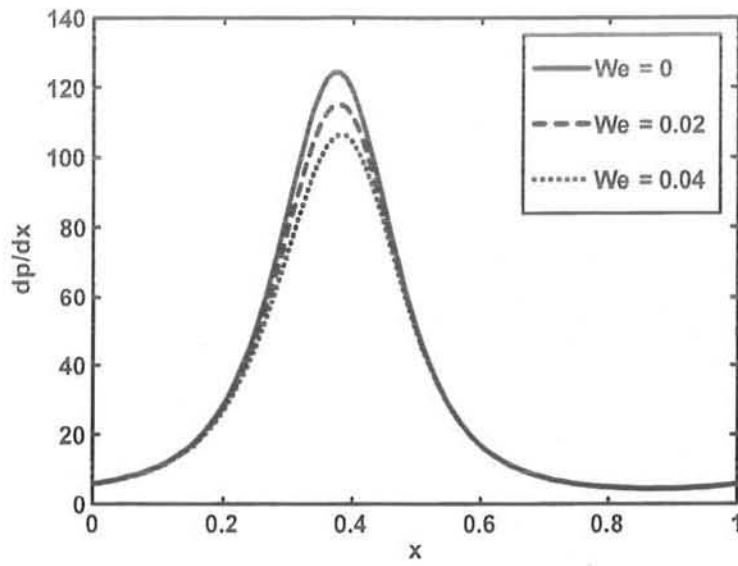


Fig.(8.7) : Variation of $\frac{dp}{dx}$ with x for different values of We at $a = 0.5$, $b = 0.5$, $d = 0.2$, $n = 0.04$, $Q = 0.4$ and $\phi = \frac{\pi}{2}$.

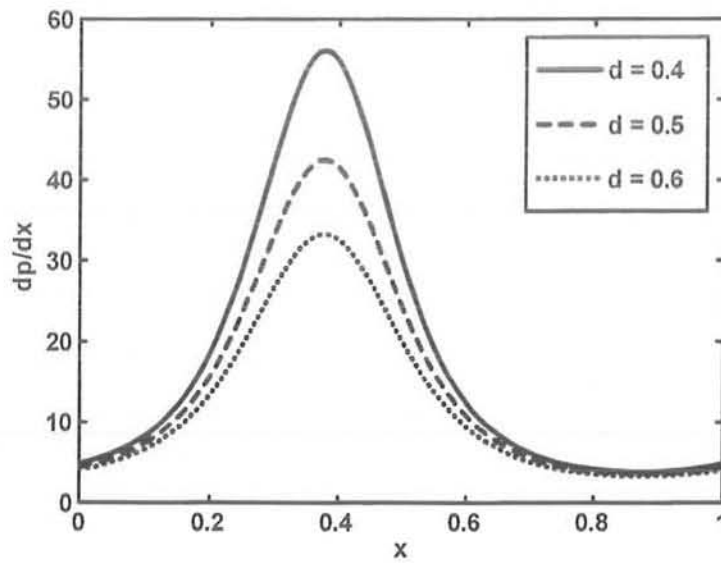
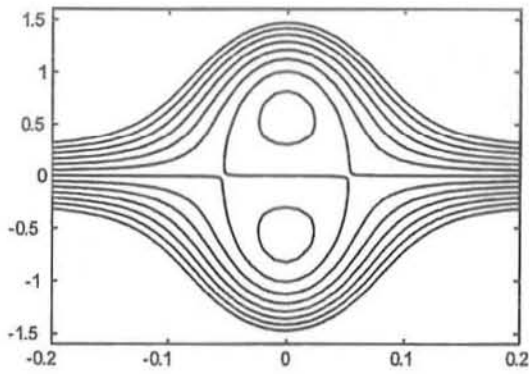
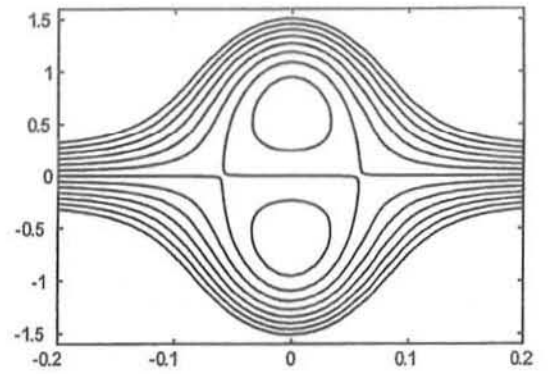


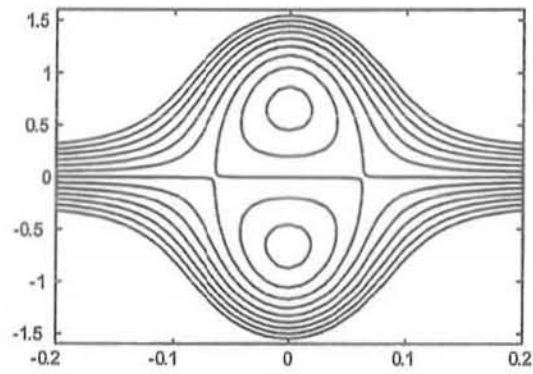
Fig.(8.8) : Variation of $\frac{dp}{dx}$ with x for different values of d at $a = 0.5$, $b = 0.5$, $We = 0.03$, $n = 0.04$, $Q = 0.4$ and $\phi = \frac{\pi}{2}$.



(b)

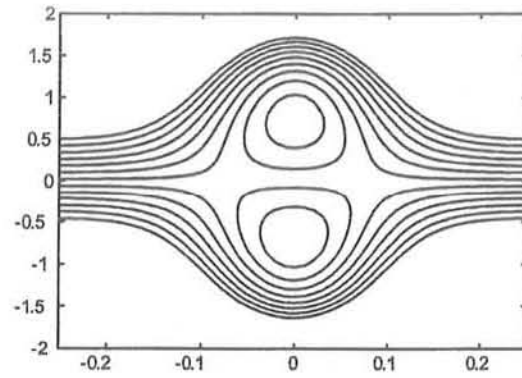


(b)

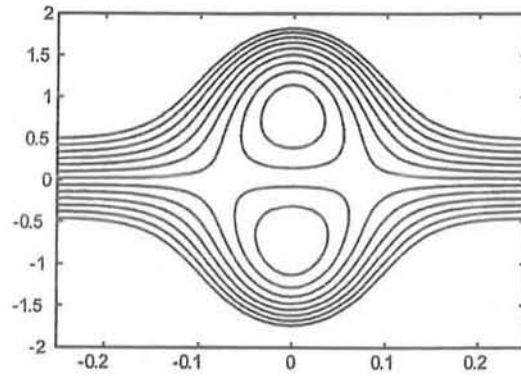


(c)

Fig. (8.9) : Stream lines for three different values of Q . (a) for $Q = 0.24$, (b) for $Q = 0.25$, (c) for $Q = 0.26$. The other parameters are chosen as $a = 0.5$, $b = 0.5$, $d = 1.0$, $n = 0.09$, $We = 0.04$, $\phi = 0.01$.

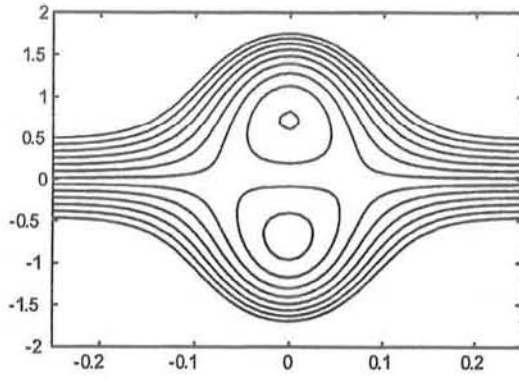


(a)

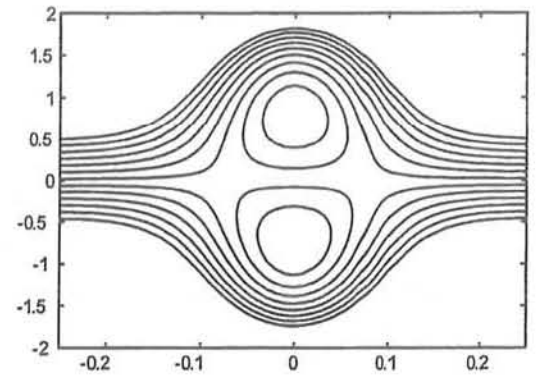


(b)

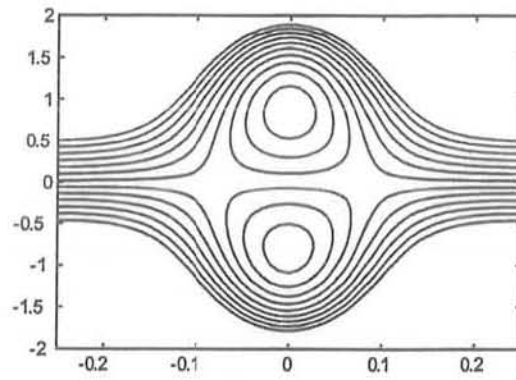
Fig.(8.10) : Stream lines for two different values of We . (a) for $We = 0.4$, (b) for $We = 0.04$. The other parameter are chosen as $a = 0.54$, $b = 0.5$, $d = 1.0$, $n = 0.09$, $Q = 0.25$, $\phi = 0.01$.



(a)



(b)



(c)

Fig. (8.11) : Stream lines for three different values of a . (a) for $a = 0.52$, (b) for $a = 0.54$, (c) for $a = 0.56$. The other parameters are chosen as $b = 0.5$, $d = 1.0$, $Q = 0.3$, $\phi = 0.01$, $We = 0.04$, $n = 0.09$.

8.5 Conclusion

This chapter presents the peristaltic flow of tangent hyperbolic fluid in an asymmetric channel. The governing two dimensional equations have been modeled and then simplified using long wave length approximation. The simplified equations are solved analytically using regular perturbation method. The results are discussed through graphs. The main finding can be summarized as follows:

1. It is observed that in the peristaltic pumping region the pressure rise decreases with an increase in We , ϕ , n and d , and increases with an increases in a and b .
2. The pressure gradient decreases with an increases in both We and d .
3. The size of the trapping bolus increases with an increases in Q , We and decreases with an increase in a .

Chapter 9

Effects of partial slip on the peristaltic transport of a hyperbolic tangent fluid model in an asymmetric channel

9.1 Introduction

This chapter presents the effects of partial slip on the peristaltic transport of a hyperbolic tangent fluid model in an asymmetric channel. The governing equations of two dimensional hyperbolic tangent fluid model are simplified under the assumptions of long wavelength and low Reynolds number. The flow is investigated in a wave frame of reference moving with the velocity of the wave. The governing equations of hyperbolic tangent fluid have been solved using regular perturbation method. The expression for pressure rise has been calculated using numerical integrations. The behavior of different physical parameters have been discussed graphically.

9.2 Mathematical formulation

The governing equations for the present case are same as discussed in previous chapter, however, due to partial slip condition the boundary conditions are different which are defined as

$$\begin{aligned}\Psi &= \frac{q}{2}, \quad \frac{\partial \Psi}{\partial y} = -LS_{xy} - 1 \quad \text{for } y = h_1(x), \\ \Psi &= -\frac{q}{2}, \quad \frac{\partial \Psi}{\partial y} = LS_{xy} - 1 \quad \text{for } y = h_2(x).\end{aligned}\quad (9.1)$$

The dimensionless mean flow Q is defined as in Eq. (1.29).

9.3 Solution of the problem

To avoid the repetition, the solution of Eqs. (8.14) subject to the boundary conditions (9.1) using the similar procedure as discussed in chapter eight can be directly written as

$$\begin{aligned}\Psi &= \frac{-1}{2(h_1 - h_2)^2(-6A + h_1 - h_2)} \left(-6qD_{15}(h_1^2 - h_2^2) + q(h_1^3 + h_2^3) \right. \\ &\quad \left. - 3qh_1h_2(h_1 + h_2) - 2h_1h_2(h_1^2 - h_2^2) \right) + \frac{6(q + h_1 - h_2)(h_1 + h_2)}{(h_1 - h_2)^2(-6D_{15} + h_1 - h_2)} \frac{y^2}{2!} \\ &\quad + \frac{-1}{(h_1 - h_2)^2(6D_{15} - h_1 + h_2)} \left(-6qD_{15}(h_1 - h_2) + (h_2^3 - h_1^3) - 6D_{15}qh_1h_2 - 3h_1h_2(h_1 - h_2) \right) y \\ &\quad + \frac{12(q + h_1 - h_2)}{(h_1 - h_2)^2(6D_{15} - h_1 + h_2)} \frac{y^3}{3!} + We \left(D_{22} + D_{21}y + D_{20} \frac{y^2}{2!} + D_{19} \frac{y^3}{3!} + BD_{18} \frac{y^4}{4!} \right).\end{aligned}\quad (9.2)$$

The axial pressure is defined as

$$\begin{aligned}\frac{dp}{dx} &= \frac{12(1-n)(q + h_1 - h_2)}{(h_1 - h_2)^2(6D_{15} - h_1 + h_2)} + We \left(\frac{-72(1-n)D_{16}(q + h_1 - h_2)^2(h_1 + h_2)}{(h_1 - h_2)^4(6D_{15} - h_1 + h_2)^2} \right. \\ &\quad \left. + \frac{144n(q + h_1 - h_2)^2(h_1 + h_2)}{(h_1 - h_2)^4(6D_{15} - h_1 + h_2)(-6D_{15} + h_1 - h_2)} \right).\end{aligned}\quad (9.3)$$

where

$$\begin{aligned}
D_{15} &= L(1-n), & D_{16} &= \frac{2n}{n-1}, & D_{17} &= Ln. \\
D_{18} &= \frac{12(q+h_1-h_2)}{(h_1-h_2)^2(6D_{15}-h_1+h_2)}, \\
D_{19} &= \frac{12}{(h_1-h_2)^4(6D_{15}-h_1+h_2)^2} \left(-6D_{16}(q+h_1-h_2)^2(h_1+h_2) \right), \\
D_{20} &= \frac{1}{(h_1-h_2)^4(6D_{15}-h_1+h_2)^2(-2D_{15}+h_1-h_2)} \left(72D_{17}(h_1-h_2)^2(q+h_1-h_2)^2 \right. \\
&\quad \left. +12D_{16}(q+h_1-h_2)^2(h_1^3+3h_1^2h_2-h_2^3-3h_1h_2(4D_{15}+h_2)) \right), \\
D_{21} &= \frac{1}{(h_1-h_2)^4(6D_{15}-h_1+h_2)^2(-2D_{15}+h_1-h_2)} \left(-12D_{17}(h_1-h_2)^2(q+h_1-h_2)^2(h_1+h_2) \right. \\
&\quad \left. -12D_{16}(q+h_1-h_2)^2(h_1+h_2)(h_1h_2(h_1-h_2)+(h_1^2-4h_1h_2+h_2^2)) \right), \\
D_{22} &= \frac{1}{2(h_1-h_2)^4(6D_{15}-h_1+h_2)^2(-2D_{15}+h_1-h_2)} \left(12h_1h_2(h_1-h_2)(q+h_1-h_2)^2 \right. \\
&\quad \left. (6D_{17}h_1-6D_{17}h_2+D_{16}h_1h_2)+24D_{15}D_{16}h_1h_2(q+h_1-h_2)^2(h_1^2-3h_1h_2+h_2^2) \right). \tag{9.4}
\end{aligned}$$

The non-dimensional pressure rise over one wavelength Δp for the axial velocity are

$$\Delta p = \int_0^1 \frac{dp}{dx} dx, \tag{9.5}$$

where dp/dx is defined in Eq. (9.3).

9.4 Results and discussion

In this section, the graphical results are displayed to see the effects of various physical parameters on pressure rise, pressure gradient, velocity profile and streamlines. The expression for the pressure rise over one wave length is calculated numerically using a Mathematics software. Figs. 9.1 to 9.6 are plotted for pressure rise against volume flow rate Q . It is observed that the relation between pressure rise and volume flow rate is inversely proportional to each other. In Fig. 9.1 it is observed that in pumping region ($\Delta p > 0$), the pressure rise increases with an increase in Weissenberg number We . It is also observed from Figs. 9.2 and 9.3, that the pressure rise decreases with an increase of power law index n and width of the channel d in the pumping ($\Delta p > 0$) and free pumping ($\Delta p = 0$) region while in copumping ($\Delta p < 0$) region the pressure rise increases with an increase in n and d . It is also depicted from Figs. 9.4 to 9.6 that in the pumping ($\Delta p > 0$) and free pumping ($\Delta p = 0$) regions the pressure rise increases with an increase in slip parameter L , and amplitudes of wave a and b , while the behavior is opposite in copumping ($\Delta p < 0$) region. The pressure gradient for different values of L , n and a are prepared in Figs. 9.7 to 9.9. It is observed that magnitude of pressure gradient increases with an increase in L and decreases with an increase in n (see Figs. 9.7 and 9.8). However, with an increase in a the magnitude of pressure gradient decreases in the region $x \in [0, 0.2]$ and $[0.8, 1]$, where as in the region $x \in [0.2, 0.8]$ it is increases. The velocity profiles for different values of Weissenberg number We , volume flow rate Q , and slip parameter L are shown in Figs. 9.10 to 9.12. It is observed from Fig. 9.10 that the magnitude value of the velocity field increases with an increase in Weissenberg number We . From Fig. 9.11 it is shown that the magnitude value of the velocity field decreases with an increase in volume flow rate Q . It is depicted from Fig. 9.12 that due to slip parameter L the velocity near the channel walls are not same but it is slipping and also the velocity increases with an increase in L .

The trapping phenomena for different values of Weissenberg number We , power law index n , slip parameter L and volume flow rate Q are shown in Figs. 9.13 to 9.16. It is seen from Figs. 9.13 and 9.14 that the size of the trapping bolus increases with an increase of Weissenberg number We and power law index n in the upper half of the channel, while in the lower half the size of the bolus decreases. From Figs. 9.15 a to c , it is observed that with an increase of slip parameter L the size of the trapping bolus increases in lower and upper half of the channel. It is

also observed from Fig. 9.16 that with an increase in Q , the size of the trapped bolus decreases in the upper half of the channel, while in the lower half the behavior is opposite as compared to the upper half, here size of the trapping bolus increases.

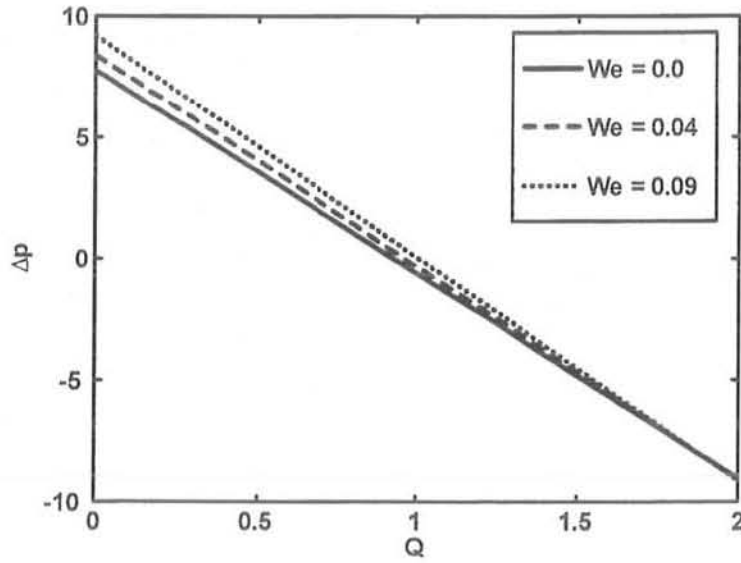


Fig.(9.1) : Variation of Δp with Q for different values of We . The other parameters are $a = 0.7$, $b = 0.5$, $d = 0.9$, $\phi = \frac{\pi}{6}$, $n = 0.06$, $L = 0.04$.

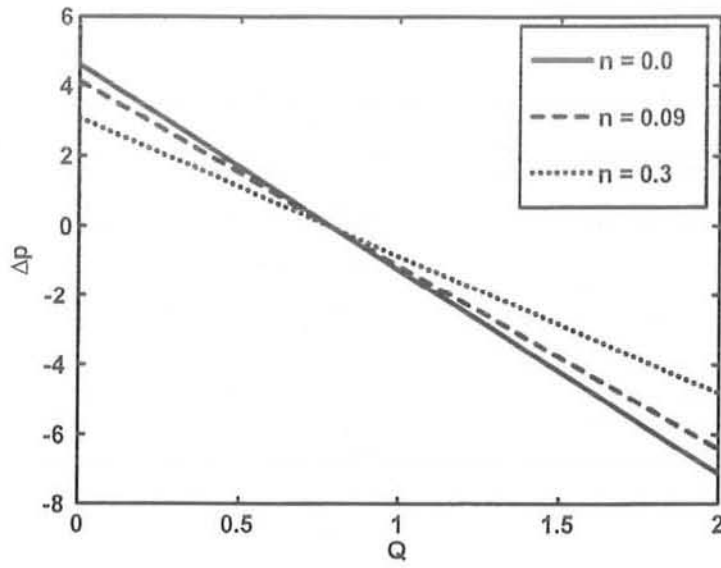


Fig.(9.2) : Variation of Δp with Q for different values of n . The other parameters are $a = 0.6$, $b = 0.5$, $d = 0.9$, $\phi = \frac{\pi}{6}$, $We = 0.06$, $L = 0.02$.

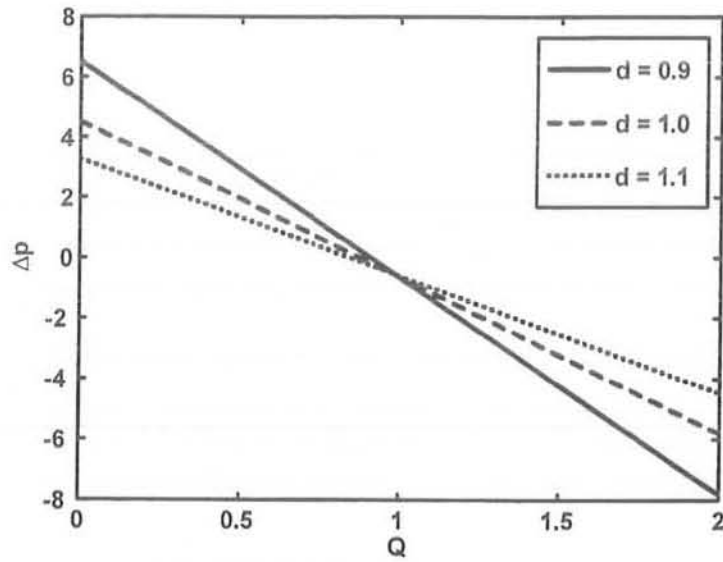


Fig.(9.3) : Variation of Δp with Q for different values of d . The other parameters are $a = 0.5$, $b = 0.5$, $We = 0.04$, $\phi = \frac{\pi}{6}$, $n = 0.06$, $L = 0.02$.

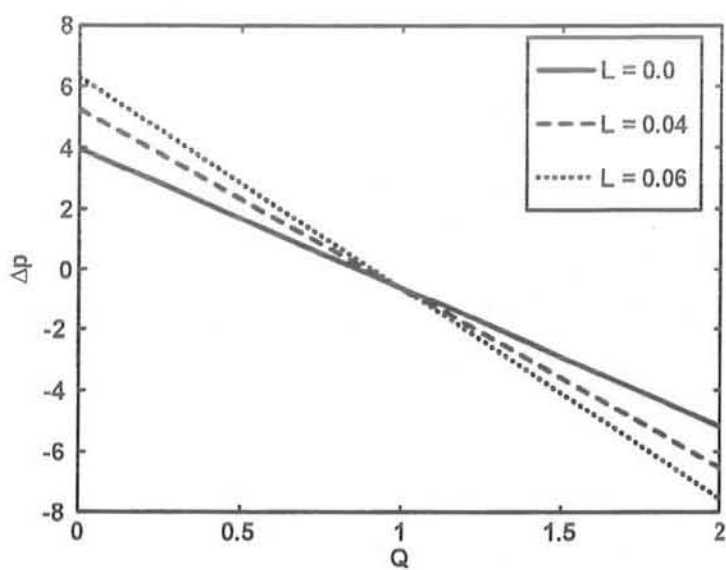


Fig.(9.4) : Variation of Δp with Q for different values of L . The other parameters are $a = 0.7$, $b = 0.5$, $d = 1$, $\phi = \frac{\pi}{6}$, $n = 0.06$, $We = 0.04$.

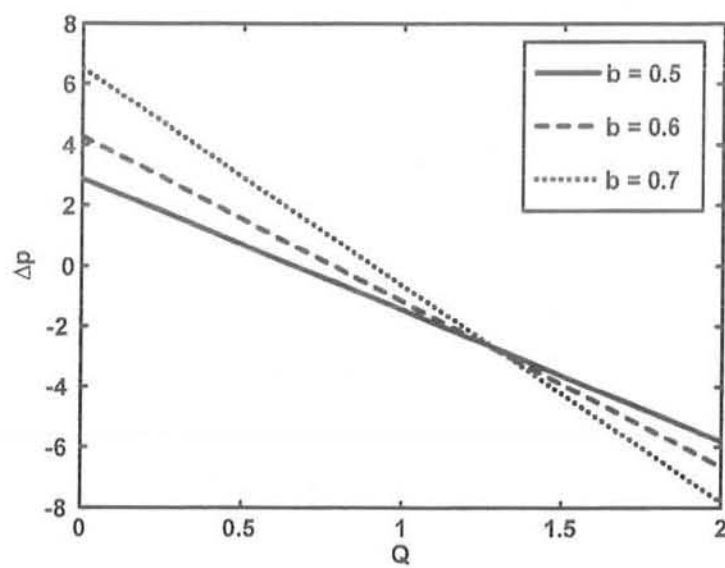


Fig.(9.5) : Variation of Δp with Q for different values of b . The other parameters are $a = 0.5$, $We = 0.04$, $d = 0.9$, $\phi = \frac{\pi}{6}$, $n = 0.04$, $L = 0.02$.

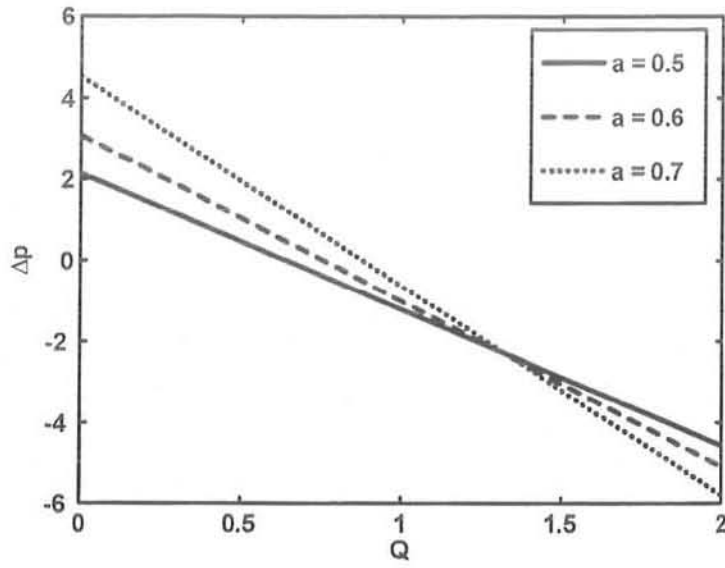


Fig.(9.6) : Variation of Δp with Q for different values of a . The other parameters are $We = 0.04$, $b = 0.5$, $d = 1$, $\phi = \frac{\pi}{6}$, $n = 0.06$, $L = 0.02$.

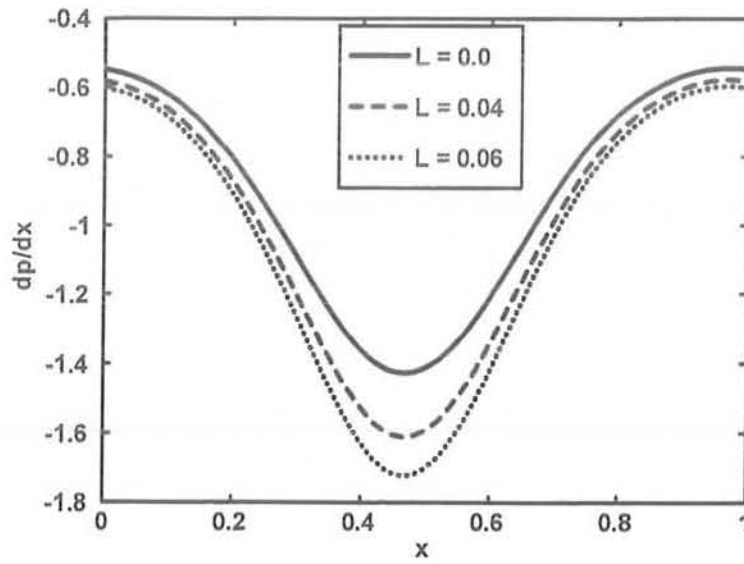


Fig.(9.7) : Variation of dp/dx with x for different values of L . The other parameters are $a = 0.5$, $b = 0.5$, $d = 2$, $\phi = \frac{\pi}{8}$, $Q = 2$, $n = 0.04$, $We = 0.04$.

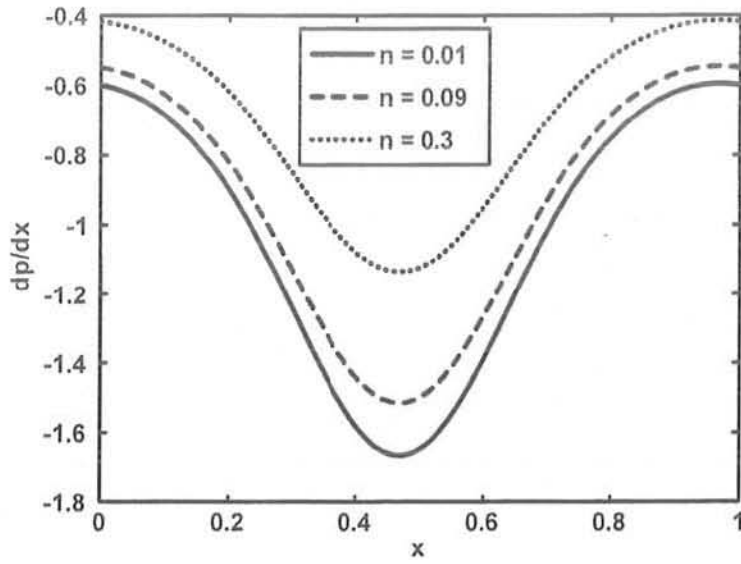


Fig.(9.8) : Variation of dp/dx with x for different values of n . The other parameters are $a = 0.5$, $b = 0.5$, $d = 2$, $\phi = \frac{\pi}{8}$, $Q = 2$, $We = 0.04$, $L = 0.04$.

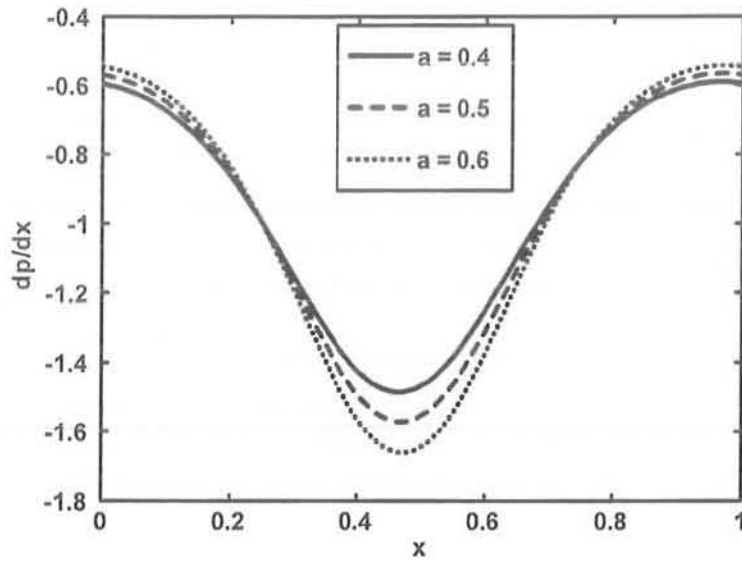


Fig.(9.9) : Variation of dp/dx with x for different values of a . The other parameters are $We = 0.04$, $b = 0.5$, $d = 2$, $\phi = \frac{\pi}{8}$, $Q = 2$, $n = 0.06$, $L = 0.04$.

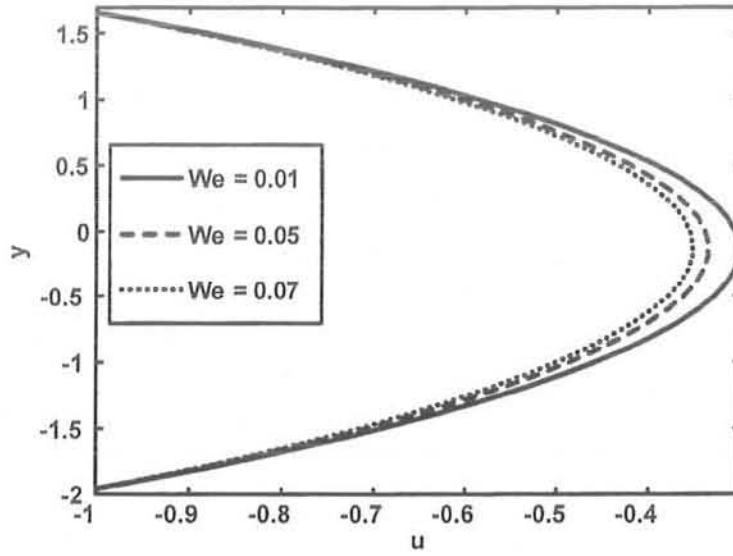


Fig.(9.10) : Velocity profile for different values of We . The other parameters are $a = 0.7$, $b = 1.2$, $d = 2$, $\phi = \frac{\pi}{2}$, $Q = 1$, $n = 0.3$, $L = 0.06$.

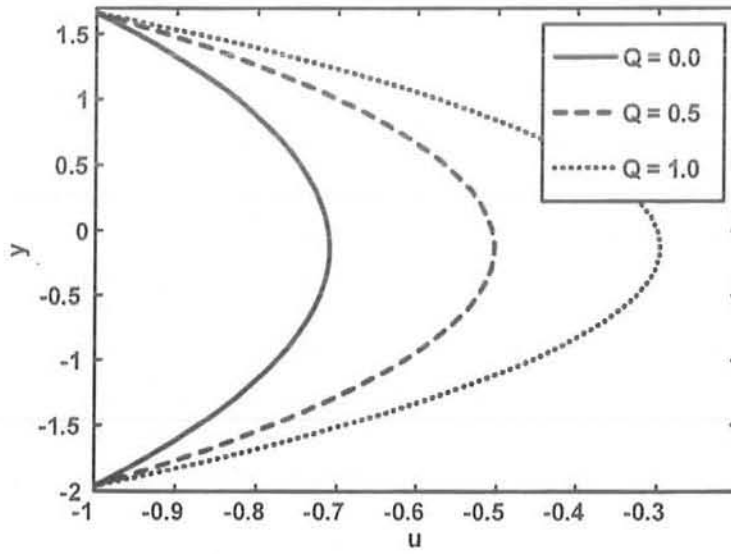
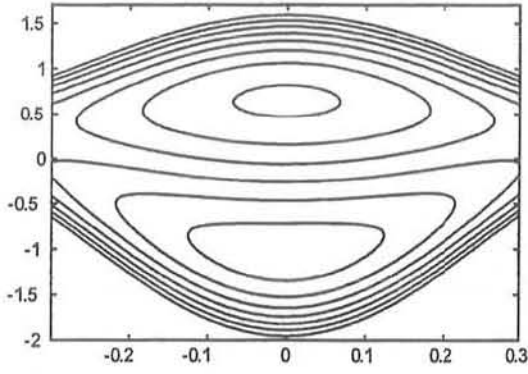
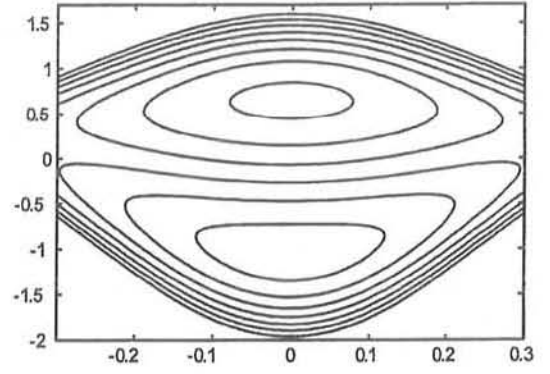


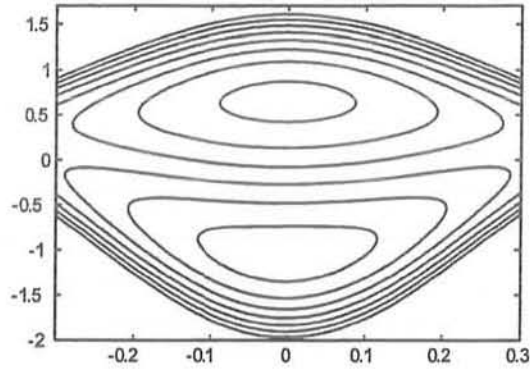
Fig.(9.11) : Velocity profile for different values of Q . The other parameters are $a = 0.7$, $b = 1.2$, $d = 2$, $\phi = \frac{\pi}{2}$, $We = 0.06$, $n = 0.4$, $L = 0.06$.



(a)

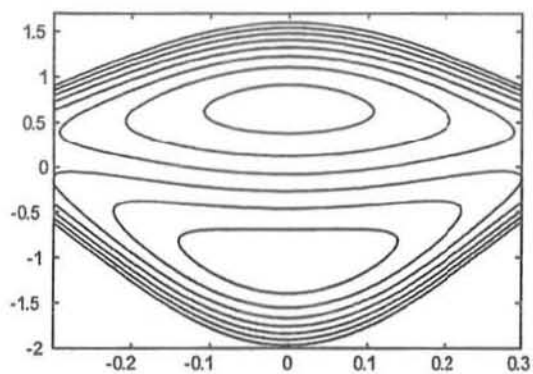


(b)

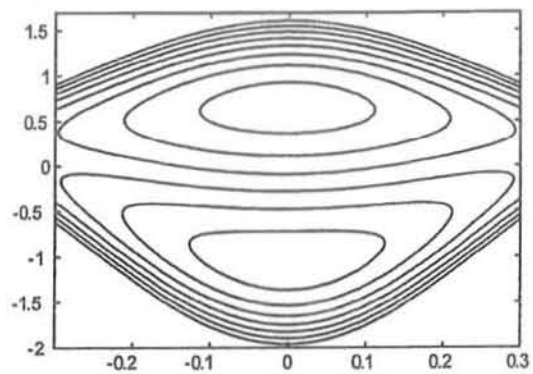


(c)

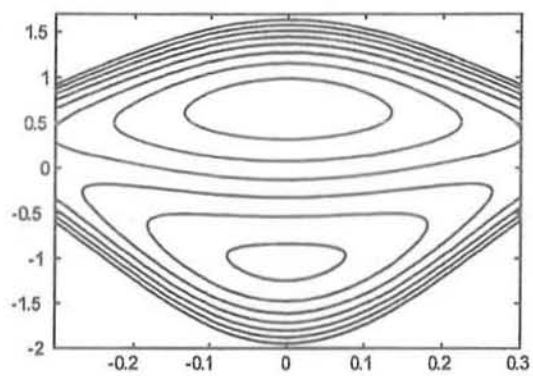
Fig.(9.13) : Stream lines for different values of We . (a) for $We = 0.01$, (b) for $We = 0.05$, (c) for $We = 0.07$. The other parameters are $\phi = 0.01$, $Q = 1.5$, $a = 0.5$, $n = 0.04$, $d = 0.9$, $b = 1.0$, $L = 0.02$.



(a)

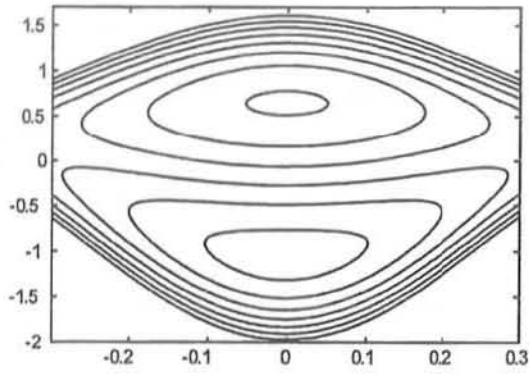


(b)

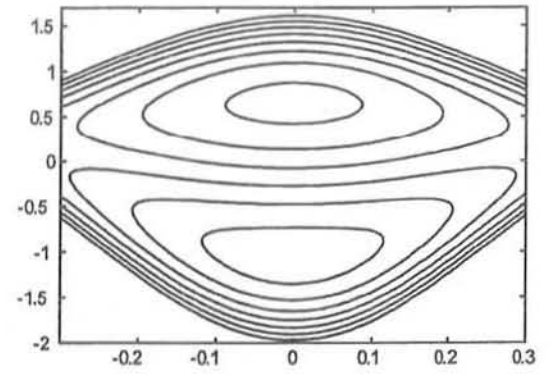


(c)

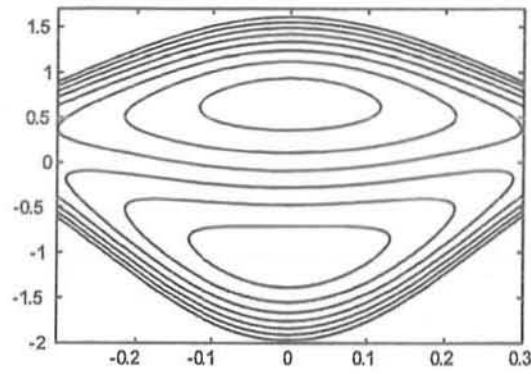
Fig.(9.14) : Stream lines for different values of n . (a) for $n = 0.01$, (b) for $n = 0.09$, (c) for $n = 0.3$. The other parameters are $\phi = 0.01$, $Q = 1.5$, $a = 0.5$, $We = 0.06$, $d = 0.9$, $b = 1.0$, $L = 0.06$.



(a)

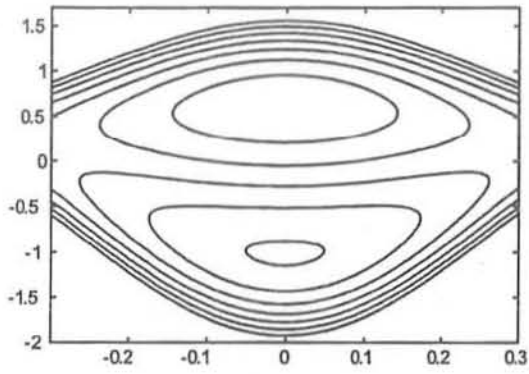


(b)

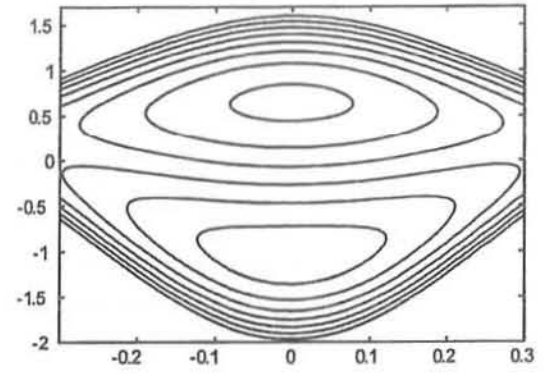


(c)

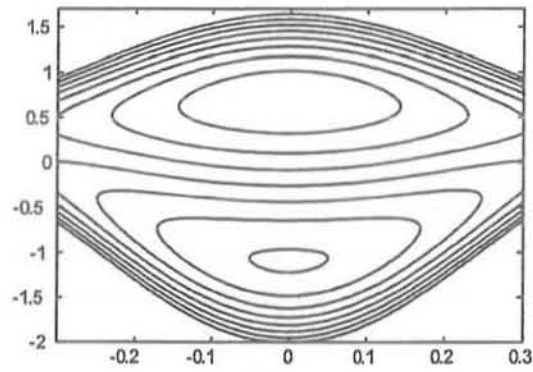
Fig.(9.15) : Stream lines for different values of L . (a) for $L = 0.02$, (b) for $L = 0.04$, (c) for $L = 0.06$. The other parameters are $\phi = 0.01$, $Q = 1.5$, $a = 0.5$, $We = 0.09$, $d = 0.9$, $b = 1.0$, $n = 0.04$.



(a)



(b)



(c)

Fig.(9.16) : Stream lines for different values of Q . (a) for $Q = 1.4$, (b) for $Q = 1.5$, (c) for $Q = 1.6$. The other parameters are $\phi = 0.01$, $L = 0.04$, $a = 0.5$, $We = 0.06$, $d = 0.9$, $b = 1.0$, $n = 0.02$.

9.5 Conclusion

This chapter presents the slip effects on the peristaltic flow of tangent hyperbolic fluid in an asymmetric channel. The governing two dimensional equations have been modeled and then simplified under long wave length and low Reynolds number approximation. The simplified equations are solved analytically using regular perturbation method. The results are discussed through graphs. The main finding can be summarized as follows:

1. It is observed that in the peristaltic pumping region ($\Delta p > 0$), the pressure rise increases with an increase in We , L , a and b .
2. It is also observed that the pressure rise decreases with an increase of power law index n and width of the channel d in the pumping ($\Delta p > 0$) and free pumping ($\Delta p = 0$) region, while in copumping ($\Delta p < 0$) region the pressure rise increases with an increase in n and d .
3. The pressure gradient increases with an increase in both L and a , while it decreases with an increase in n .
4. It is observed that the velocity field increases with an increase in Weissenberg number We and decreases with an increase in volume flow rate Q .
5. It is also observed that due to slip parameter L the velocity near the channel walls are not same but it is slipping and also the velocity increases with an increase in L .
6. The size of the trapping bolus increases in the upper half of the channel and decreases in the lower half of the channel with an increase of We and n , while the behavior is opposite in the case when volume flow rate Q increases.
7. With an increase of slip parameter L the size of the trapping bolus increases.

Chapter 10

Peristaltic flow of a Williamson fluid in an asymmetric channel

10.1 Introduction

This chapter presents a peristaltic flow of a Williamson model in an asymmetric channel. The governing equations of Williamson model in two dimensional peristaltic flow phenomena are constructed under long wave length and low Reynolds number approximations. A regular perturbation expansion method is used to obtain the analytical solution of the non linear problem. The expressions for stream function, pressure gradient and pressure rise have been computed. The pertinent feature of various physical parameters have been discussed graphically. It is observed that, (the non dimensional Williamson parameter) for large We , the curves of the pressure rise are not linear but for very small We it behave like a Newtonian fluid.

10.2 Mathematical formulation

Let us consider the peristaltic transport of an incompressible Williamson fluid in a two dimensional channel of width $d_1 + d_2$. The constitutive equation for Williamson fluid is given by [69]

$$\tau = -PI + S, \quad (10.1)$$

$$\mathbf{S} = - \left[\mu_\infty + (\mu_0 + \mu_\infty) (1 - \Gamma\dot{\gamma})^{-1} \right] \dot{\gamma}, \quad (10.2)$$

in which $-PI$ is the spherical part of the stress due to constraint of incompressibility, \mathbf{S} is the extra stress tensor, μ_∞ is the infinite shear rate viscosity, μ_0 is the zero shear rate viscosity, Γ is the time constant and $\dot{\gamma}$ is defined as

$$\dot{\gamma} = \sqrt{\frac{1}{2} \sum_i \sum_j \dot{\gamma}_{ij} \dot{\gamma}_{ji}} = \sqrt{\frac{1}{2} \Pi}, \quad (10.3)$$

where $\Pi = \frac{1}{2} \text{trac} \left(\text{grad } \mathbf{V} + (\text{grad } \mathbf{V})^T \right)^2$.

Here Π is the second invariant strain tensor. We consider the constitution Eq. (10.2), the case for which $\mu_\infty = 0$ and $\Gamma\dot{\gamma} < 1$. The component of extra stress tensor therefore, can be written as

$$\mathbf{S} = -\mu_0 [(1 - \Gamma\dot{\gamma})^{-1}] \dot{\gamma} = -\mu_0 [(1 + \Gamma\dot{\gamma})] \dot{\gamma}. \quad (10.4)$$

Invoking Eq. (1.11) in Eqs. (6.1) and (10.1) to (10.4), we get

$$\rho \left(\frac{\partial U}{\partial t} + U \frac{\partial U}{\partial X} + V \frac{\partial U}{\partial Y} \right) = -\frac{\partial P}{\partial X} - \frac{\partial S_{XX}}{\partial X} - \frac{\partial S_{XY}}{\partial Y}, \quad (10.5)$$

$$\rho \left(\frac{\partial V}{\partial t} + U \frac{\partial V}{\partial X} + V \frac{\partial V}{\partial Y} \right) = -\frac{\partial \bar{P}}{\partial Y} - \frac{\partial S_{XY}}{\partial X} - \frac{\partial S_{YY}}{\partial Y}, \quad (10.6)$$

where

$$\begin{aligned} S_{XX} &= -2\mu_0 (1 + \Gamma\dot{\gamma}) \frac{\partial U}{\partial X}, \\ S_{XY} &= -\mu_0 (1 + \Gamma\dot{\gamma}) \left(\frac{\partial U}{\partial Y} + \frac{\partial V}{\partial X} \right), \\ S_{YY} &= -2\mu_0 (1 + \Gamma\dot{\gamma}) \frac{\partial V}{\partial Y}, \\ \dot{\gamma} &= \left(2 \left(\frac{\partial U}{\partial X} \right)^2 + \left(\frac{\partial U}{\partial Y} + \frac{\partial V}{\partial X} \right)^2 + 2 \left(\frac{\partial V}{\partial Y} \right)^2 \right)^{1/2}. \end{aligned} \quad (10.7)$$

Using Eqs. (1.11) and (8.8), Eqs. (10.5) to (10.7) in terms of stream function $\Psi(u = \frac{\partial \Psi}{\partial y}, v =$

$-\delta \frac{\partial \bar{\Psi}}{\partial x}$ after dropping bars), can be written as

$$\delta \operatorname{Re} \left[\left(\frac{\partial \Psi}{\partial y} \frac{\partial}{\partial x} - \frac{\partial \Psi}{\partial x} \frac{\partial}{\partial y} \right) \frac{\partial \Psi}{\partial y} \right] = -\frac{\partial p}{\partial x} - \delta^2 \frac{\partial S_{xx}}{\partial x} - \frac{\partial S_{xy}}{\partial y}, \quad (10.8)$$

$$-\delta^3 \operatorname{Re} \left[\left(\frac{\partial \Psi}{\partial y} \frac{\partial}{\partial x} - \frac{\partial \Psi}{\partial x} \frac{\partial}{\partial y} \right) \frac{\partial \Psi}{\partial x} \right] = -\frac{\partial p}{\partial y} - \delta^2 \frac{\partial S_{xy}}{\partial x} - \delta \frac{\partial S_{yy}}{\partial y}, \quad (10.9)$$

where

$$\begin{aligned} S_{xx} &= -2(1 + We\dot{\gamma}) \frac{\partial^2 \Psi}{\partial x \partial y}, \\ S_{xy} &= -(1 + We\dot{\gamma}) \left(\frac{\partial^2 \Psi}{\partial y^2} - \delta^2 \frac{\partial^2 \Psi}{\partial x^2} \right), \\ S_{yy} &= 2\delta(1 + We\dot{\gamma}) \frac{\partial^2 \Psi}{\partial x \partial y}, \\ \dot{\gamma} &= \left(2\delta^2 \left(\frac{\partial^2 \Psi}{\partial x \partial y} \right)^2 + \left(\frac{\partial^2 \Psi}{\partial y^2} - \delta^2 \frac{\partial^2 \Psi}{\partial x^2} \right)^2 + 2\delta^2 \left(\frac{\partial^2 \Psi}{\partial x \partial y} \right)^2 \right)^{1/2}, \end{aligned} \quad (10.10)$$

in which δ , Re , We represent the wave, Reynolds and Weissenberg numbers, respectively. Under the assumptions of long wavelength $\delta \ll 1$ and low Reynolds number, neglecting the terms of order δ and higher, Eqs. (10.8) and (10.9) take the form

$$\frac{\partial p}{\partial x} = \frac{\partial}{\partial y} \left(\left[1 + We \frac{\partial^2 \Psi}{\partial y^2} \right] \frac{\partial^2 \Psi}{\partial y^2} \right), \quad (10.11)$$

$$\frac{\partial p}{\partial y} = 0. \quad (10.12)$$

Elimination of pressure from Eqs. (10.11) and (10.12) yield

$$\frac{\partial^2}{\partial y^2} \left(\left[1 + We \frac{\partial^2 \Psi}{\partial y^2} \right] \frac{\partial^2 \Psi}{\partial y^2} \right) = 0. \quad (10.13)$$

The boundary conditions in terms of stream function Ψ are defined in Eq. (6.26). The dimensionless mean flow Q is defined in Eq. (1.29).

10.3 Solution of the problem

10.3.1 Perturbation solution

Since, Eq.(10.13) is non linear equation, its exact solution may be not possible, therefore, we employ the regular perturbation to find the solution.

For perturbation solution, we expand Ψ , q and p as

$$\Psi = \Psi_0 + We\Psi_1 + O(We^2), \quad (10.14)$$

$$q = q_0 + Weq_1 + O(We^2), \quad (10.15)$$

$$p = p_0 + Wep_1 + O(We^2). \quad (10.16)$$

With the help of Eqs. (10.14) to (10.16), the solution of Eqs. (10.13) and (10.11) with the corresponding boundary conditions (6.26) can be directly written as

$$\begin{aligned} \Psi = & \frac{q + h_1 - h_2}{(h_2 - h_1)^3} (2y^3 - 3(h_1 + h_2)y^2 + 6h_1h_2y) - y \\ & + \frac{1}{(h_2 - h_1)^3} \left(\left(\frac{q}{2} + h_1 \right) (h_2^3 - 3h_1h_2^2) - (h_2 - \frac{q}{2}) (h_1^3 - 3h_2h_1^2) \right) \\ & + We \left(D_{23} + D_{24}y + D_{25} \frac{y^2}{2!} + D_{26} \frac{y^3}{3!} + D_{27} \frac{y^4}{4!} \right), \end{aligned} \quad (10.17)$$

$$\begin{aligned} \frac{dp}{dx} = & \frac{12(q + h_1 - h_2)}{(h_2 - h_1)^3} + We \left(-\frac{12}{(h_2 - h_1)^3} \frac{D_{27}}{4!} (h_1^3(2h_2 - h_1) - h_2^3(2h_1 - h_2)) \right. \\ & \left. - 144(h_1 + h_2) \left[\frac{q + h_1 - h_2}{(h_2 - h_1)^3} \right]^2 \right), \end{aligned} \quad (10.18)$$

where

$$\begin{aligned}
D_{23} &= \frac{6}{(h_2 - h_1)^3} \left(\frac{D_{27}}{4!} (h_1^3(2h_2 - h_1) - h_2^3(2h_1 - h_2)) \right) \left(\frac{h_1 h_2^2}{2} - \frac{h_2^3}{6} \right) \\
&\quad - \frac{D_{27}}{3!} \left(\frac{h_1^2 h_2^2}{2} + \frac{h_1 h_2^3}{2} - \frac{h_2^4}{4} \right), \\
D_{24} &= \frac{D_{27} h_1 h_2}{2} \left(\frac{(h_1 + h_2)}{3} - \frac{1}{2(h_2 - h_1)^3} (h_1^3(2h_2 - h_1) - h_2^3(2h_1 - h_2)) \right), \\
D_{25} &= D_{27} \left(\frac{(h_1 + h_2)}{4(h_2 - h_1)^3} (h_1^3(2h_2 - h_1) - h_2^3(2h_1 - h_2)) - \frac{(h_1^2 + h_1 h_2 + h_2^2)}{3!} \right), \\
D_{26} &= \frac{-12}{(h_2 - h_1)^3} \left(\frac{D_{27}}{4!} (h_1^3(2h_2 - h_1) - h_2^3(2h_1 - h_2)) \right), \\
D_{27} &= -288 \left(\frac{q + h_1 - h_2}{(h_2 - h_1)^3} \right)^2. \tag{10.19}
\end{aligned}$$

The non-dimensional pressure rise over one wavelength Δp for the axial velocity are

$$\Delta p = \int_0^1 \left(\frac{dp}{dx} \right) dx, \tag{10.20}$$

where dp/dx is defined in Eq. (10.18).

10.4 Results and discussion

The analytical solution of the Williamson fluid model is presented. The expression for pressure rise Δp is calculated numerically using mathematics software. The effects of various parameters on the pressure rise Δp are shown in Figs. 10.1 to 10.4 for various values of Weissenberg number We , channel width d and wave amplitudes a, b . It is observed from Fig. 10.1 that pressure rise decreases for small values of Q ($-1 \leq Q \leq 1.3$) with an increase in We and for large Q ($1.3 \leq Q \leq 2$), the pressure rise increases. For $\Delta p > 7$ increasing We gives a better pumping performance and for $\Delta p = 7$ there is no difference between Newtonian and Williamson fluid as the pumping curves coincide with each other. It is depicted that the pressure rise decreases with an increase in d and increases with an increase in a and b for small Q and for large Q , the results are opposite (see Figs. 10.2 to 10.4). Here we also see that the better pumping regions are $\Delta p > 5$ and almost $\Delta p = 0$, there is no difference between Newtonian and non-Newtonian fluids. Figs. 10.5 and 10.6 represent that for $x \in [0, 0.1]$ and $[0.75, 1]$, the pressure gradient is

small, we can say that the flow can easily pass without imposition of large pressure gradient, while in the narrow part of the channel $x \in [0.1, 0.75]$, to retain same flux large pressure gradient is required. Moreover in the narrow part of the channel, the pressure gradient decreases with an increase in We and d . It is also observed that the behavior of We and d on the pressure gradient are similar. The pressure rise Δp for different values of b are shown in Fig. 10.7. It is seen that the curves for the pressure rise are not linear and in the region $Q \in [-1, 0.4]$, the pressure rise decreases with an increase in b while in the region $Q \in [0.41, 1]$, the pressure rise increases with an increase in b .

Trapping phenomena

Another interesting phenomena in peristaltic motion is trapping. It is basically the formation of an internally circulating bolus of fluid by closed stream lines. This trapped bolus pushed a head along a peristaltic waves. Figs. 10.8 to 10.10 illustrate the stream lines for different values of We , Q and a . The stream lines for different values of We are shown in Fig. 10.8. It is found that with an increase in Weissenberg number We the size of the trapping bolus decreases in the upper half of the channel and increases in the lower half of the channel. In Fig. 10.9 the stream lines are prepared for different values of volume flow rate Q . It is depicted that the size of the trapped bolus increases in the upper half of the channel with an increase in Q , while the size and the number of the trapped bolus increases in the lower half of the channel. It is observed from Fig. 10.10 that the size of the trapping bolus increases in the lower and upper half of the channel with an increase in amplitude of the wave a .

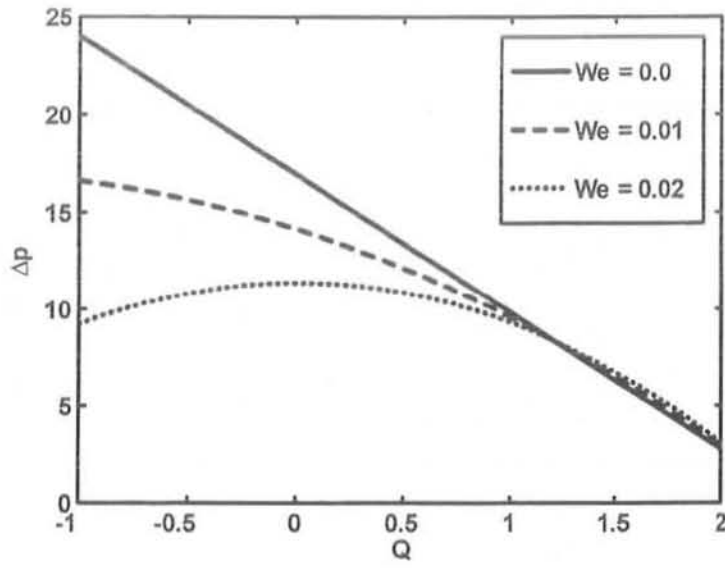


Fig.(10.1) : Variation of Δp with Q for different values of We at $a = 0.1, b = 0.2, d = 0.2$ and $\phi = \pi$.

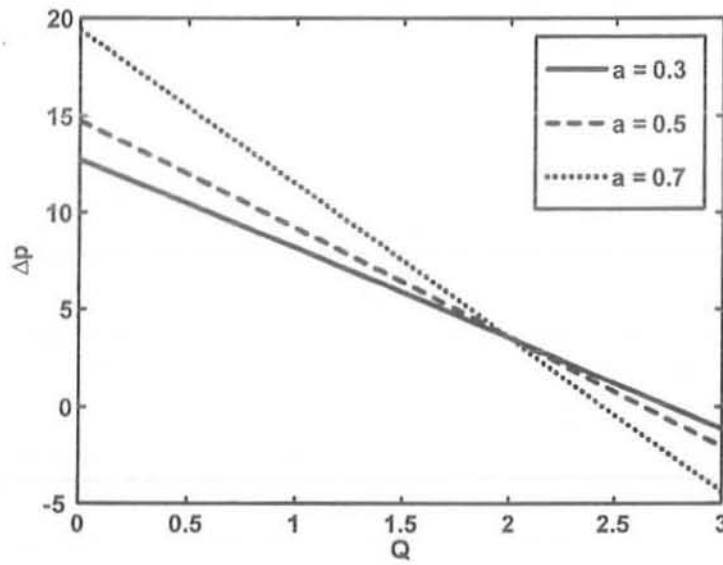


Fig.(10.2): Variation of Δp with Q for different values of a at $We = 0.001, b = 0.1, d = 0.4$ and $\phi = \pi$.

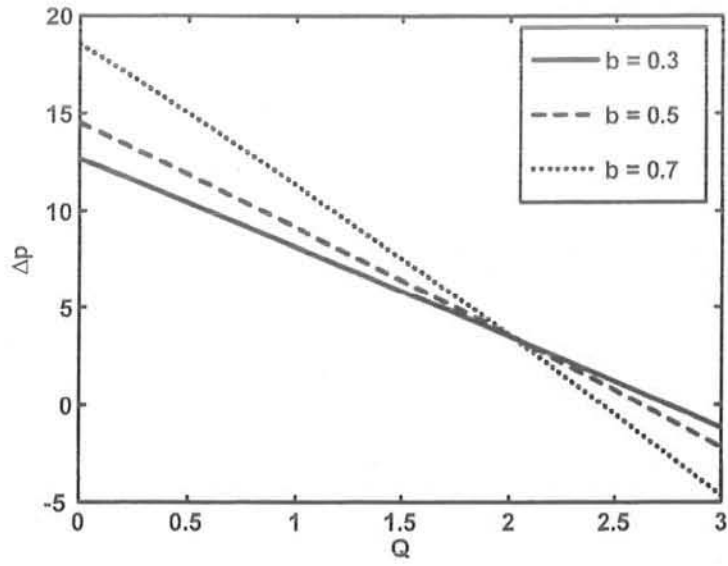


Fig.(10.3): Variation of Δp with Q for different values of b at $We = 0.001, a = 0.1, d = 0.1$ and $\phi = \pi$.

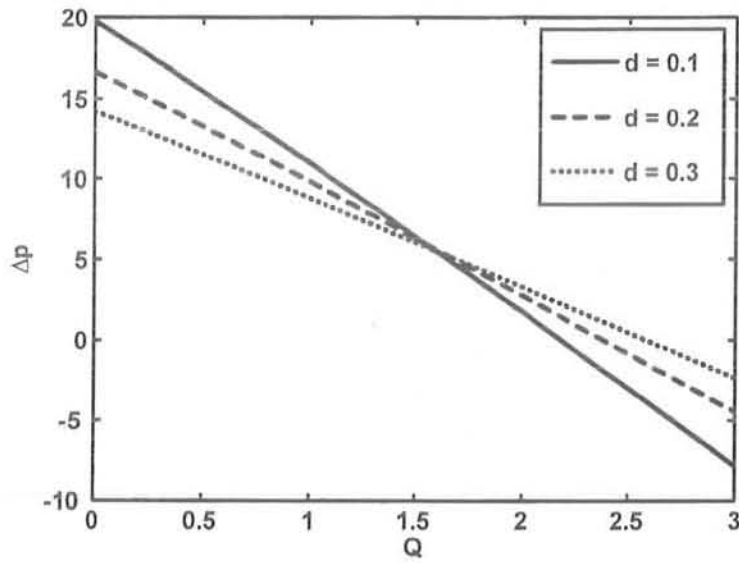


Fig.(10.4): Variation of Δp with Q for different values of d at $We = 0.001, b = 0.2, a = 0.1$ and $\phi = \pi$.

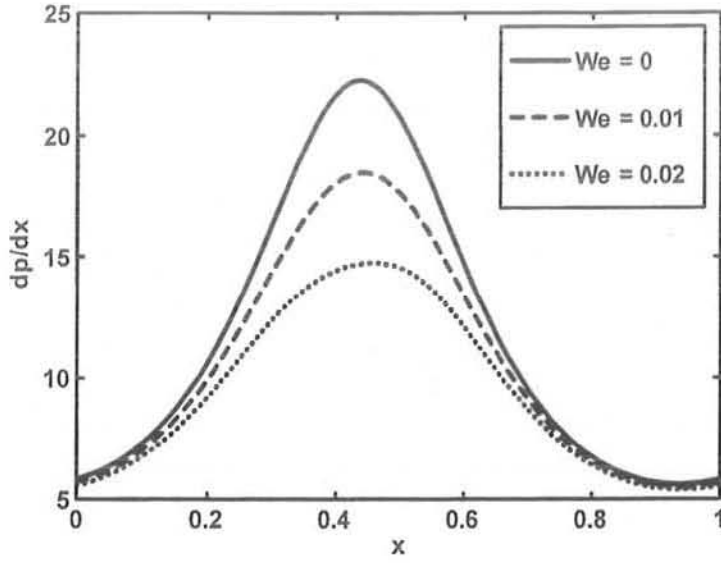


Fig.(10.5): Variation of dp/dx with x for different values of We at $a = 0.1, b = 0.3, d = 0.4, \phi = \frac{\pi}{6}$ and $Q = 0.5$.

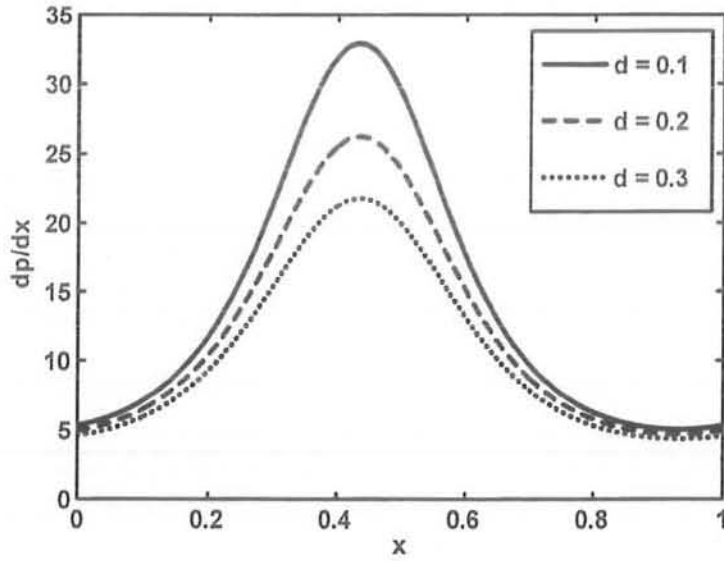


Fig.(10.6) : Variation of dp/dx with x for different values of d at $a = 0.1, b = 0.4, We = 0.01, \phi = \frac{\pi}{6}$ and $Q = 1$.

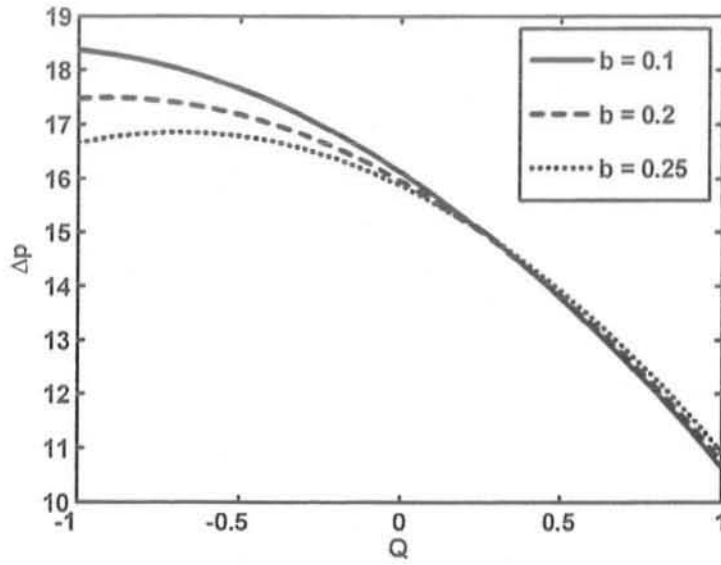
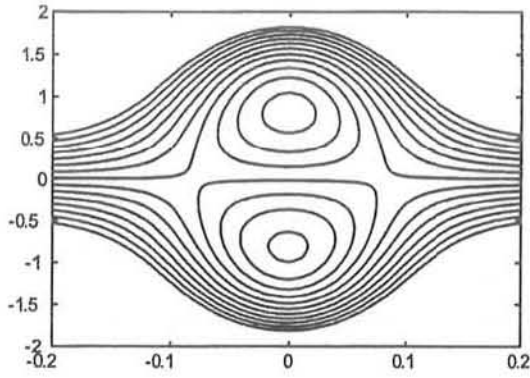
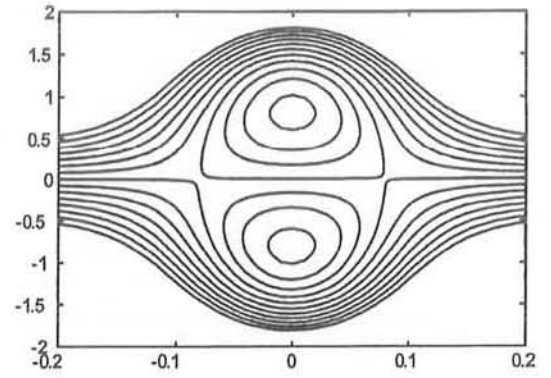


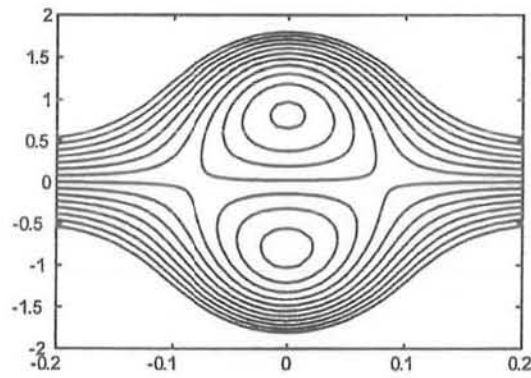
Fig.(10.7): Variation of Δp with Q for different values of b at $We = 0.01$, $a = 0.1$, $d = 0.1$ and $\phi = \pi$.



(a)

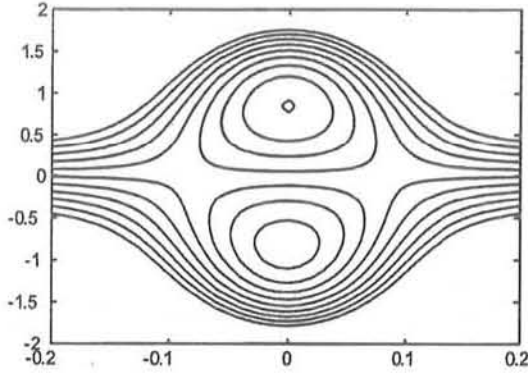


(b)

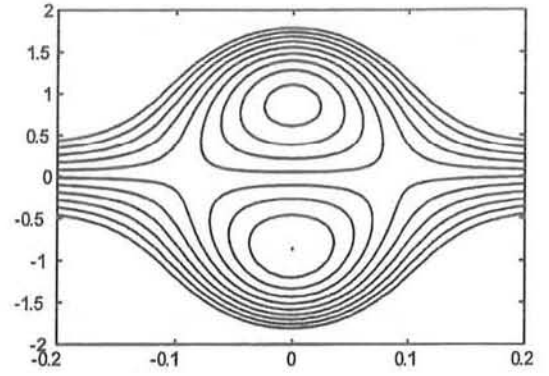


(c)

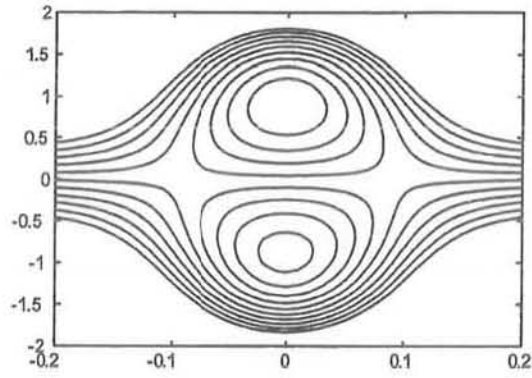
Fig.(10.8) : Stream lines for three different values of We . (a) for $We = 0.01$, (b) for $We = 0.03$, (c) for $We = 0.05$. The other parameters are chosen as $a = 0.5$, $b = 0.5$, $d = 1.0$, $Q = 0.3$, and $\phi = 0.01$.



(a)

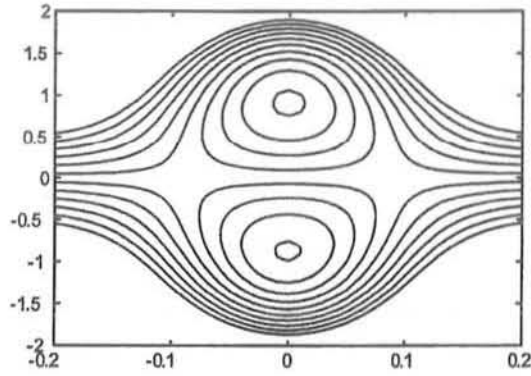


(b)

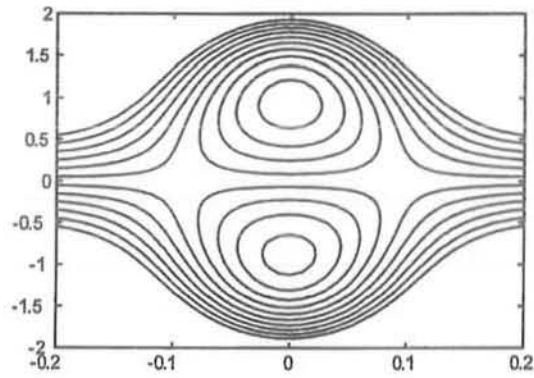


(c)

Fig.(10.9) : Stream lines for three different values of Q . (a) for $Q = 0.31$, (b) for $Q = 0.32$, (c) for $Q = 0.33$. The other parameters are chosen as $a = 0.5$, $b = 0.5$, $d = 1.0$, $We = 0.06$, and $\phi = 0.01$.



(a)



(b)

Fig.(10.10) : Stream lines for three different values of a . (a) for $a = 0.53$, (b) for $a = 0.54$. The other parameters are chosen as $b = 0.5$, $d = 1.0$, $We = 0.05$, $Q = 0.3$ and $\phi = 0.01$.

10.5 Conclusion

This chapter presents the peristaltic flow of Williamson fluid in an asymmetric channel. The governing two dimensional equations have been modeled and then simplified using long wave length approximation. The simplified equations are solved analytically using regular perturbation method. The results are discussed through graphs. The main finding can be summarized as follows:

1. It is observed that for large We , the curves of the pressure rise are not linear but for small We it behave like a Newtonian fluid.
2. It is observed that in the peristaltic pumping region the pressure rise decreases with an increase in We and d and increases with an increase in a and b .
3. The pressure gradient decreases with an increase in both We and d .
4. The size of the trapping bolus decreases in the upper half of the channel and increases in the lower half of the channel with an increase in We .
5. The size of the trapping bolus increases in the upper and lower half of the channel with an increase in Q and a .

References

1. F. Kill, The function of the ureter and the renal pelvis-Saunders: Philadelphia. (1957).
2. S. Boyarsky, Surgical physiology of the renal pelvis, Monogr. Surg. Sci. **1**, 173(1964).
3. T. W. Latham, Fluid motion in a peristaltic pump, M.Sc. Thesis, MIT, Cambridge, MA. (1966).
4. J. C. Burns, T. Parkes, Peristaltic motion, J. Fluid Mech. **29**, 731 (1967).
5. C. Barton, S. Raynor, Peristaltic flow in tubes, Bull. Math. Biophys. **30**, 663 (1968).
6. A. H. Shapiro, M. Y. Jaffrin, S. L. Weinberg, Peristaltic pumping with long wavelengths and low Reynolds number, J. Fluid Mech. **37**, 799 (1969).
7. M. Y. Jaffrin, A. H. Shapiro, Peristaltic puming, Ann. Rev. Fluid Mech. **3**, 13 (1971).
8. G. Bohme, R. Friedrich, Peristaltic flow of a viscoelastic liquids, J. Fluid Mech. **128**, 109 (1983).
9. L. M. Srivastava, V. P. Srivastava, Peristaltic transport of a non-Newtonian fluid (Application to the vas deferens at small intestine), Ann. BioMed. Eng. **13**, 137 (1985).
10. S. Takabatake, K. Ayukawa, A. Mori, Peristaltic pumping in circular cylindrical tubes: a numerical study of fluid transport and its efficiency, J. Fluid Mech. **193**, 267 (1988).
11. O. Eytan, A. J. Jaffa, J. Har-Toov, E. Dalach, D. Elad, Dynamics of the intrauterine fluid-wall interface, Ann. BioMed. Eng. **27**, 372 (1999).
12. O. Eytan, D. Elad, Analysis of intra-uterine fluid motion induced by uterine contractions, Bull. Math. Biol. **61**, 221 (1999).
13. C. Pozrikidis, A study of peristaltic flow, J. Fluid. Mech. **180**, 515 (1987).
14. M. Mishra, A. R. Rao, Peristaltic transport of a Newtonian fluid in an asymmetric channel, ZAMP. **54**, 532 (2003).

15. A. R. Rao, M. Mishra, Nonlinear and curvature effects on peristaltic flow of a viscous fluid in an asymmetric channel, *Acta Mech.* **168**, 35 (2004).
16. M. H. Haroun, Effect of wall compliance on peristaltic transport of a Newtonian fluid in an asymmetric channel, *Math. Prob. Eng.* **2006**, 1 (2006).
17. E. F. Elshehawey, N. T. Eldabe, E. M. Elghazy, A. Ebaid, Peristaltic transport in an asymmetric channel through a porous medium, *Appl. Math. Comp.* **182**, 140 (2006).
18. T. Hayat, Q. Hussain, N. Ali, Influence of partial slip on the peristaltic flow in a porous medium, *Physica A.* **387**, 3399 (2008).
19. K. K. Raju, R. Devanathan, Peristaltic motion of a non-Newtonian fluid; Part II, viscoelastic fluids, *Rheol. Acta.* **13**, 944 (1974).
20. A. M. Siddiqui, M. H. Schwarz, Peristaltic flow of a second order fluid in tubes, *J. non-Newtonian Fluid Mech.* **53**, 257 (1994).
21. F. M. Mahomed, S. Asghar, Peristaltic flow of magnetohydrodynamic Johnson-Segalman fluid, *Nonlinear Dynam.* **40**, 375 (2005).
22. T. Hayat, Y. Wang, A. M. Siddiqui, K. Hutter, Peristaltic motion of a Johnson-Segalman fluid in a planar channel, *Math Prob. Eng.* **1**, 1 (2003).
23. T. Hayat, Y. Wang, K. Hutter, S. Asghar, A. M. Siddiqui, Peristaltic transport of an Oldroyd-B fluid in a planar channel, *Math. Prob. Eng.* **4**, 347 (2004).
24. Kh. S. Mekheimer, E. F. El Shehawey, A. M. Elaw, Peristaltic motion of a particle-fluid suspension in a planar channel, *Int. J. Theor. Phy.* **37**, 2895 (1998).
25. T. Hayat, M. Khan, A. M. Siddiqui, S. Asghar, Non-linear peristaltic flow of a non-Newtonian fluid under effect of a magnetic field in a planar channel, *Commun. Nonlinear Sci. Numer. Simulation.* **12**, 910 (2007).
26. Kh. S. Mekheimer, Non-linear peristaltic transport through a porous medium in an inclined planar channel, *J. Porous Med.* **6**, 189 (2003).

27. J. C. Mishra, S. K. Pandey, Peristaltic transport of a non-Newtonian fluid with a peripheral layer, *Int. J. Engng Sci.* **37**, 1841 (1999).
28. A. M. Siddiqui, W. H. Schwarz, Peristaltic pumping of a third order fluid in a planar channel, *Rheol Acta.* **32**, 47 (1993).
29. D. Srinivasacharya, M. Mishra, A. R. Rao, Peristaltic pumping of a micropolar fluid in a tube, *Acta Mech.* **161**, 165 (2003).
30. P. Hariharan, V. Seshadri, R. K. Banerjee, Peristaltic transport of non-Newtonian fluid in a diverging tube with different wave forms, *Math. Comp. Model.* **48**, 998 (2008).
31. T. Hayat, Y. Wang, A. M. Siddiqui, K. Hutter, S. Asghar, Peristaltic transport of a third-order fluid in a circular cylindrical tube, *Math. Model Meth. Appl. Sci.* **12**, 1691 (2002).
32. M. H. Haroun, Non-linear peristaltic flow of a fourth grade fluid in an inclined asymmetric channel, *Comput. Mater. Sci.* **39**, 324 (2007).
33. S. Srinivas, V. Pushparaj, Non-linear peristaltic transport in an inclined asymmetric channel, *Commun. Nonlinear. Sci. Numer. Simulat.* **13**, 1782 (2008).
34. M. H. Haroun, Effect of Deborah number and phase difference on peristaltic transport of a third-order fluid in an asymmetric channel, *Commun. Nonlinear. Sci. Numer. Simulat.* **12**, 1464 (2007).
35. M. Kothandapani, S. Srinivas, Peristaltic transport of a Jeffrey fluid under the effect of magnetic field in an asymmetric channel, *Inter. J. Non-linear Mech.* **43**, 915 (2008).
36. T. Hayat, M. Umar Qureshi, N. Ali, The influence of slip on the peristaltic motion of a third order fluid in an asymmetric channel, *Phys. Lett A.* **372**, 2653 (2008).
37. T. Hayat, A. Afsar, N. Ali, Peristaltic transport of a Johnson–Segalman fluid in an asymmetric channel, *Math. Compt. Modell.* **47**, 380 (2008).
38. T. Hayat, N. Alvi, N. Ali, Peristaltic mechanism of a Maxwell fluid in an asymmetric channel, *Nonlinear. Anayl. Real world Appl.* **9**, 1474 (2008).

39. Y. Wang, T. Hayat, N. Ali, M. Oberlack, Magnetohydrodynamic peristaltic motion of a Sisko fluid in a symmetric or asymmetric channel, *Physica A.* **387**, 347 (2008).
40. N. Ali, T. Hayat, Peristaltic flow of a micropolar fluid in an asymmetric channel, *Compt. Math. Appl.* **55**, 589 (2008).
41. N. Ali, T. Hayat, Peristaltic motion of a Carreau fluid in an asymmetric channel, *Appl. Math. Compt.* **193**, 535 (2007).
42. V. K. Stud, G. S. Sephon, R. K. Mishra, Pumping action on blood flow by a magnetic field, *Bull. Math. Biol.* **39**, 385 (1977).
43. L. M. Srivastava, R. P. Agrawal, Oscillating flow of a conducting fluid with suspension of spherical particles, *J. Appl. Mech.* **47**, (1980).
44. H. L. Agrawal, B. Anwaruddin, Peristaltic flow of blood in a branch, *Ranchi Uni. Math. J.* **15**, 111 (1984).
45. Kh.S. Mekheimer Peristaltic transport of a couple stress fluid in a uniform and non-uniform channels, *Biorheology.* **39**, 755 (2009).
46. M. Kothandapani, S. Srinivas, On the influence of wall properties in the MHD peristaltic transport with heat transfer and porous medium, *Phys. Lett. A.* **372**, 4586 (2008).
47. V. I. Vishnyakov, K. B. Pavlov, Peristaltic flow of a conductive liquid in a transverse magnetic field, *Magnetohydrodynamics.* **8**, 174 (1972).
48. Kh.S. Mekheimer, Effect of induced magnetic field on peristaltic flow of a couple stress fluid, *Phys. Lett. A.* **372**, 4271 (2008).
49. N. T. M. Eldabe. M. F. El-Sayed, A. Y. Galy, H. M. Sayed, Peristaltically induced transport of a MHD biviscosity fluid in a non-uniform tube, *Physica A.* **383**, 253 (2007).
50. Kh. S. Mekheimer, Peristaltic flow of a Magneto-Micropolar fluid:Effect of induced magnetic field, *J. Appl. Math.* **2008**, 23 (2008).
51. V. Radhakrishnamurty, G. Radhakrishnamacharya, P. Chandra, *Advances in Physio. Fluid Dynamics*, Narosa Publishing house, India. 1995.

52. K. Vajravelu, G. Radhakrishnamacharya, V. Radhakrishnamurty, Peristaltic flow and heat transfer in a vertical porous annulus, with long wave approximation, *Int. J. Non-Linear Mech.* **42**, 754 (2007).
53. S. Nadeem, Noreen Sher Akbar, Effects of heat transfer on the peristaltic transport of MHD Newtonian fluid with variable viscosity: Application of Adomian decomposition method, *Commun. Nonlinear. Sci. Numer. Simulat.* **14**, 3844 (2009).
54. Kh. S. Mekheimer, Y. Abd. elmaboud, The influence of heat transfer and magnetic field on peristaltic transport of a Newtonian fluid in a vertical annulus: Application of an endoscope, *Phys. Lett. A.* **372**, 1657 (2008).
55. S. Nadeem, Noreen Sher Akbar, influence of heat transfer on a peristaltic transport of Herschel-Bulkley fluid in a non-uniform inclined tube, *Commun. Nonlinear. Sci. Numer. Simulat.* **14**, 4100 (2009).
56. S. Nadeem, T. Hayat, Noreen Sher Akbar, M.Y. Malik, On the influence of heat transfer in peristalsis with variable viscosity, *Inter. J. Heat and Mass Trans.* **52**, 4722 (2009).
57. R.J. Goldstein, W.E. Ibele, S.V. Patankar, T.W. Simon, T.H. Kuehn, P.J. Strykowski, K.K. Tamma, J.V.R. Heberlein, J.H. Davidson, J. Bischof, F.A. Kulacki, U. Kortshagen, S. Garrick, V. Srinivasan, Heat transfer-A review of 2003 literature, *Inter. J. Heat and Mass Trans.* **49**, 451 (2006).
58. Kh.S. Mekheimer, S. Z. A. Husseny, Y. Abd Elmaboud, Effects of heat transfer and space porosity on peristaltic flow in a vertical asymmetric channel, *Numer. Meth. PDE.* 10.1002/num.20451.
59. S. Srinivas, M. Kothandapani, Peristaltic transport in an asymmetric channel with heat transfer-A note, *Inter. Commun. Heat Mass Transf.* **35**, 514 (2008).
60. S. Nadeem, Noreen Sher Akbar, Influence of heat transfer on peristaltic transport of a Johnson-segalman fluid in an inclined asymmetric channel, *Commun. Nonlinear. Sci. Numer. Simulat.* *Doi* : 10.1016/j.cnsns.2009.10.030.

61. S. Srinivas, R. Gayathri, Peristaltic transport of a Newtonian fluid in a vertical asymmetric channel with heat transfer and porous medium, *Appl. Math. Comp.* **215**, 185 (2009).
62. N. T. Eldabe, E. M. Elghazy, A. Ebaid, Closed form solution to a second order boundary value problem and its application in fluid mechanics, *Phys. Lett. A.* **363**, 257 (2007).
63. A. M. Wazwaz, Adomian decomposition method for a reliable treatment of the Emden-Fowler equation, *Appl. Math. Comput.* **61**, 543 (2005).
64. G. Adomian, *Non-linear Stochastic Operator Equations.* Academic Press Orlando, FL. 1986.
65. A. M. Wazwaz, A new method for solving singular initial value problems in the second order ordinary differential equations, *Appl. Math. Comput.* **128**, 47 (2002).
66. S. N. Aristov, O. I. Skul'skii, Exact solution of the problem on a six-constant Jeffrey Model of fluid in a plane channel, *J. Appl. Mech. Tech. Phys.* **44**, 817 (2002).
67. Serdar Baris, Steady Three- Dimensional flow of a Walter's B' fluid in a vertical channel, *Turkish J. Eng. Eniv. Sci.* **26**, 385 (2002).
68. L. Ai, K. Vafai, An investigation of Stoke's second problem for non-Newtonian fluids, *Numer. Heat Trans. part A.* **47**, 955 (2005).
69. I. Dapra, G. Scarpi, Perturbation solution for pulsatile flow of a non-Newtonian Williamson fluid in a rock fracture, *Inter. j. Rock Mech. Mining Sci.* **44**, 271 (2007).



Heat transfer in a peristaltic flow of MHD fluid with partial slip

S. Nadeem *, Safia Akram

Department of Mathematics, Quaid-i-Azam University 45320, Islamabad 44000, Pakistan

ARTICLE INFO

Article history:

Received 26 June 2008

Received in revised form 26 February 2009

Accepted 31 March 2009

Available online 22 April 2009

PACS:

44.05.+e

Keywords:

Newtonian fluid

Heat transfer

Peristaltic flow

Adomian decomposition method

ABSTRACT

In the present note, we have discussed the effects of partial slip on the peristaltic flow of a MHD Newtonian fluid in an asymmetric channel. The governing equations of motion and energy are simplified using a long wave length approximation. A closed form solution of the momentum equation is obtained by Adomian decomposition method and an exact solution of the energy equation is presented in the presence of viscous dissipation term. The expression for pressure rise is calculated using numerical integration. The trapping phenomena is also discussed. The graphical results are presented to interpret various physical parameter of interest. It is found that the temperature field decreases with the increase in slip parameter L , and magnetic field M , while with the increase in P_r and E_c , the temperature field increases.

© 2009 Published by Elsevier B.V.

1. Introduction

Recently, Elshehawey et al. [1] discussed the problem of peristaltic transport of an incompressible viscous fluid in an asymmetric channel through a porous medium. They found an explicit form of stream function using Adomian decomposition method. More recently, Hayat et al. [2] extended the idea of Elshehawey et al. [1] for partial slip condition. According to [2] for large values of slip parameter the size of trapped bolus decreases and symmetry disappears. Number of researchers have discussed the peristaltic flow problems in different flow geometries, like [3–14]. But a limited attention has been focused to the study of peristaltic flow in the presence of heat transfer analysis. Mention may be made to the interesting works by Radhakrishnamacharya and co-workers [15–18]. The aim of the present note is to highlight the importance of MHD and heat transfer analysis in an asymmetric channel under the influence of slip condition. The governing equations of momentum and energy are simplified using long wave length approximation. The simplified momentum equation is solved by Adomian decomposition method and a closed form solution subject to partial slip boundary conditions have been calculated. An impressive bibliography on the Adomian decomposition method is presented in the works by Eldabe and co-workers [19–25]. With the closed form solution obtained from momentum equation, the exact solution of the energy equation is obtained in the presence of viscous dissipation terms. It is found that when $M = 0$ in the momentum equation, the results of Hayat et al. [2] has been recovered as a special case of our problem. Moreover when $L = M = 0$, the solution of Elshehawey et al. [1] are recovered as a special case of our problem. At the end, the results of flow characteristics are analyzed by plotting graphs.

2. Mathematical formulation and solution of the problem

We consider MHD flow of an electrically conducting viscous fluid in an asymmetric channel through porous medium. The lower wall of the channel is maintained at temperature T_1 while the upper wall has temperature T_0 . We assume that the fluid

* Corresponding author.

E-mail address: snqau@hotmail.com (S. Nadeem).

Sohail Nadeem · Safia Akram

Peristaltic flow of a couple stress fluid under the effect of induced magnetic field in an asymmetric channel

Received: 13 January 2009 / Accepted: 4 November 2009 / Published online: 28 November 2009
© Springer-Verlag 2009

Abstract The present paper investigates the peristaltic transport of a couple stress fluid in an asymmetric channel with the effect of the induced magnetic field. The exact solutions of momentum and the magnetic field equations have been calculated under the assumptions of long wave length and low but finite Reynolds number. The expression for pressure rise has been computed numerically using mathematics software Mathematica. The graphical results have been presented to discuss the physical behavior of various physical parameters of interest. Finally, the trapping phenomena have been discussed for various physical parameters.

Keywords Peristaltic flow · Couple stress fluid · Induced magnetic field · Asymmetric channel

1 Introduction

Numerous applications of non-Newtonian fluids in engineering and industry have led to renewed interest among the researchers. Such applications include extraction of crude oil from petroleum products, food mixing and chyme movement in the intestine, flow of plasma, flow of blood, flow of nuclear fuel slurries, flow of liquid metals and alloys, and flow of mercury amalgams. In non-Newtonian fluid models, couple stress fluid model has distinct features, such as polar effects in addition to possessing large viscosity. The theory of couple stress was first developed by Stokes [1] and represents the simplest generalization of classical theory which allows for polar effects such as presence of couple stress and body couples. A number of studies containing couple stress have been investigated in Refs. [2–4].

Recently, Peristaltic problems have gained a considerable importance because of its applications in physiology, engineering, and industry. Such applications include urine transport from kidney to bladder, swallowing food through the esophagus, movement of chyme in the gastrointestinal tract, transport of spermatozoa in the ducts efferentes of the male reproductive tract, movement of ovum in the female fallopian tubes, vasomotion of small blood vessels, transport of slurries, corrosive fluids, sanitary fluids, and noxious fluids in nuclear industry. In view of these applications, a number of researchers have discussed the peristaltic flows involving Newtonian and non-Newtonian fluids with different kinds of geometries [5–24]. Very recently, Mekheimer [25] has discussed the effects of the induced magnetic field on peristaltic flow of a couple stress fluid in a slit channel. According to him, the magnetohydrodynamic flow of a fluid in channel in connection with peristaltic flow has applications in physiological fluids, e.g., the blood, blood pump machines and with the need for theoretical research on the operation of peristaltic MHD compressor. Srivastava and Agrawal [26] and Agrawal and Anwaruddin [27] discussed the effects of MHD on blood flow. Further, the application of magnetic field occurs in the form of a device Magnetic Resonance Imaging (MRI) [28], which is used for diagnosis of brain, vascular diseases, and all the human body.

Influence of Heat Transfer and Magnetic Field on a Peristaltic Transport of a Jeffrey Fluid in an Asymmetric Channel with Partial Slip

Sohail Nadeem and Safia Akram

Department of Mathematics, Quaid-i-Azam University 45320, Islamabad 44000, Pakistan

Reprint requests to S. N.; Fax: +92 92512275341; E-mail: snqau@hotmail.com

Z. Naturforsch. **65a**, 483–494 (2010); received March 3, 2009 / revised September 15, 2009

In the present paper, we have studied the influence of heat transfer and magnetic field on a peristaltic transport of a Jeffrey fluid in an asymmetric channel with partial slip. The complicated Jeffrey fluid equations are simplified using the long wave length and low Reynolds number assumptions. In the wave frame of reference, an exact and closed form of Adomian solution is presented. The expressions for pressure drop, pressure rise, stream function, and temperature field have been calculated. The behaviour of different physical parameters has been discussed graphically. The pumping and trapping phenomena of various wave forms (sinusoidal, multisinusoidal, square, triangular, and trapezoidal) are also studied.

Key words: Exact Solution; Adomian Solution; Partial Slip; Peristaltic Flow; Asymmetric Channel; Heat Transfer Analysis.

1. Introduction

Recently, Kothandapani and Srinivas [1] have discussed the peristaltic flow of a Jeffrey fluid in an asymmetric channel in the presence of a transverse magnetic field. They employ for the Jeffrey fluid a relatively simple linear model using time derivatives instead of convective derivatives. Their observation was that the size of trapped bolus in the Jeffrey fluid is much smaller than in the Newtonian fluid. Due to the large number of applications, the peristaltic flows for different fluids and different geometries have been discussed by a number of researchers [1–15]. Only a limited attention has been focused on the study of peristaltic flows in the presence of heat transfer analysis. Mention may be made to the works of [16–23]. No attempt has been made to discuss the slip effects on the peristaltic transport of a Jeffrey fluid in an asymmetric channel in the presence of heat transfer analysis. Therefore the aim of the present paper is to discuss the influence of heat transfer and magnetic field on a peristaltic transport of a Jeffrey fluid (non-Newtonian) with partial slip in an asymmetric channel. The exact and closed form of Adomian solutions are obtained under the assumptions of long wave length and low Reynolds number. Many existing solutions in the literature are found to be subcases of our problem. The influence of physical parameters on the pressure rise,

temperature, and stream function have been studied for five types of wave forms, namely sinusoidal, multisinusoidal, square, trapezoidal, and triangular.

2. Mathematical Formulation

We consider magneto-hydrodynamic (MHD) flow of an electrically conducting Jeffrey fluid in an asymmetric channel. The lower wall of the channel is maintained at temperature T_1 while the upper wall has temperature T_0 . We assume that the fluid is subject to a constant transverse magnetic field \mathbf{B} . A very small magnetic Reynolds number is assumed and hence the induced magnetic field can be neglected. When the fluid moves into the magnetic field two major physical effects arise. The first one is that an electric field \mathbf{E} is induced in the flow. We shall assume that there is no excess charge density and therefore, $\nabla \cdot \mathbf{E} = 0$. Neglecting the induced magnetic field implies that $\nabla \times \mathbf{E} = 0$ and therefore, the induced electric field is negligible. The second effect is dynamically in nature, i.e., a Lorentz force ($\mathbf{J} \times \mathbf{B}$), where \mathbf{J} is the current density. This force acts on the fluid and modifies its motion resulting in the transfer of energy from the electromagnetic field to the fluid. In the present study, the relativistic effects are neglected and the current density \mathbf{J} is given by Ohm's law as

$$\mathbf{J} = \sigma(\mathbf{V} \times \mathbf{B}).$$

Slip effects on the peristaltic flow of a Jeffrey fluid in an asymmetric channel under the effect of induced magnetic field

S. Nadeem^{*,†} and Safia Akram

Department of Mathematics, Quaid-i-Azam University 45320, Islamabad 44000, Pakistan

SUMMARY

In the present study, we investigated the effects of slip and induced magnetic field on the peristaltic flow of a Jeffrey fluid in an asymmetric channel. The governing two-dimensional equations for momentum, magnetic force function and energy are simplified by using the assumptions of long wavelength and low but finite Reynolds number. The reduced problem has been solved by Adomian decomposition method (ADM) and closed form solutions have been presented. Further, the exact solution of the proposed problem has also been computed and the mathematical comparison shows that both solutions are almost similar. The effects of pertinent parameters on the pressure rise per wavelength are investigated using numerical integration. The expressions for pressure rise, friction force, velocity, temperature, magnetic force function and the stream lines against various physical parameters of interest are shown graphically. Moreover, the behavior of different kinds of wave shape are also discussed. Copyright © 2009 John Wiley & Sons, Ltd.

Received 20 November 2008; Revised 19 March 2009; Accepted 6 April 2009

KEY WORDS: Adomian decomposition method; exact solution; Jeffrey fluid; heat transfer; partial slip; induced magnetic field; peristaltic motion

1. INTRODUCTION

A flow phenomena in which the fluid velocity indirectly contacts with a solid boundary having the same velocity as the boundary itself is known as no slip condition. However, in some situations, such as fluid flow past a permeable walls [1], slotted plates [2], rough and coated surfaces [3], emulsion, suspensions, foam, polymer solutions, gas and liquid flow in microdevices [4], the traditional no slip condition does not hold valid and should be replaced by a partial slip boundary condition. The slip boundary condition was first discussed by Navier [5], in which the velocity is proportional to the shear stress at the boundary. After the initiation of Navier, a number of researchers have discussed the partial slip boundary condition for different kinds of fluids with different geometries [6–9].

^{*}Correspondence to: S. Nadeem, Department of Mathematics, Quaid-i-Azam University 45320, Islamabad 44000, Pakistan.

[†]E-mail: snqau@hotmail.com

Peristaltic Transport of a Hyperbolic Tangent Fluid Model in an Asymmetric Channel

Sohail Nadeem and Safia Akram

Department of Mathematics, Quaid-i-Azam University 45320, Islamabad 44000, Pakistan

Reprint requests to S. N; E-mail: snqau@hotmail.com

Z. Naturforsch. 64a, 559–567 (2009); received August 18, 2008 / revised December 4, 2008

In the present analysis, we have modeled the governing equations of a two dimensional hyperbolic tangent fluid model. Using the assumption of long wavelength and low Reynolds number, the governing equations of hyperbolic tangent fluid for an asymmetric channel have been solved using the regular perturbation method. The expression for pressure rise has been calculated using numerical integrations. At the end, various physical parameters have been shown pictorially. It is found that the narrow part of the channel requires a large pressure gradient, also in the narrow part the pressure gradient decreases with the increase in Weissenberg number We and channel width d .

Key words: Modeling of Hyperbolic Tangent Fluid Model; Asymmetric Channel; Analytical Solutions.

1. Introduction

Peristaltic transport is a well known process of a fluid transport which is induced by a progressive wave of area contraction or expansion along the length of distensible tube containing the fluid. It is used by many systems in the living body to propel or to mix the contents of a tube. The peristalsis mechanism usually occur in urine transport from kidney to bladder, swallowing food through the esophagus, chyme motion in the gastrointestinal tract, vasomotion of small blood vessels and movement of spermatozoa in the human reproductive tract. There are many engineering processes as well in which peristaltic pumps are used to handle a wide range of fluids particularly in chemical and pharmaceutical industries. It is also used in sanitary fluid transport, blood pumps in heart lung machine, and transport of corrosive fluids, where the contact of the fluid with the machinery parts is prohibited. Because most of the physiological fluids behave like a non-Newtonian fluid, therefore, some interesting studies dealing with the flows of non-Newtonian fluids are given in [1–15].

Motivated by possible applications in industry and physiology and previous studies regarding the peristaltic flows of Non-Newtonian fluid models, we discussed the tangent hyperbolic fluid model. The governing equations of hyperbolic tangent fluid model for peristaltic fluid flow in a two dimensional asymmet-

ric channel has been modeled in the present paper. To the best of the authors knowledge no attempt has been made to study the hyperbolic tangent fluid model for peristaltic problems. The governing equations are reduced using long wave length approximation and then the reduced problem has been solved by the regular perturbation method. The expression for pressure rise is computed numerically using mathematics software Mathematica. At the end, the graphical results are presented to discuss the physical behaviour of various parameters of interest.

2. Fluid Model

For an incompressible fluid the balance of mass and momentum are given by

$$\operatorname{div} V = 0, \quad (1)$$

$$\rho \frac{dV}{dt} = \operatorname{div} S + \rho f, \quad (2)$$

where ρ is the density, V is the velocity vector, S is the Cauchy stress tensor, f represents the specific body force and d/dt represents the material time derivative. The constitutive equation for hyperbolic tangent fluid is given by [10–11]

$$S = -PI + \tau, \quad (3)$$

$$\tau = -[\eta_{\infty} + (\eta_0 + \eta_{\infty}) \tanh(\Gamma \dot{\gamma})^n] \dot{\gamma}, \quad (4)$$



Short communication

Peristaltic flow of a Williamson fluid in an asymmetric channel

S. Nadeem*, Safia Akram

Department of Mathematics, Quaid-i-Azam University 45320, Islamabad 44000, Pakistan

ARTICLE INFO

Article history:

Received 26 August 2008

Received in revised form 18 June 2009

Accepted 22 July 2009

Available online 12 August 2009

Keywords:

Williamson fluid model

Asymmetric channel

Peristaltic flow

Analytical solution

ABSTRACT

In this work, we have presented a peristaltic flow of a Williamson model in an asymmetric channel. The governing equations of Williamson model in two dimensional peristaltic flow phenomena are constructed under long wave length and low Reynolds number approximations. A regular perturbation expansion method is used to obtain the analytical solution of the non-linear problem. The expressions for stream function, pressure gradient and pressure rise have been computed. The pertinent features of various physical parameters have been discussed graphically. It is observed that, (the non-dimensional Williamson parameter) for large We , the curves of the pressure rise are not linear but for very small We it behave like a Newtonian fluid.

© 2009 Elsevier B.V. All rights reserved.

1. Introduction

Since, the pioneer work done by Latham [1], numerous researchers have discussed the peristaltic flows due its increasing importance's, specially in physiology, biological systems and engineering [2–6]. These includes urine transport from kidney to bladder, movement of chyme in the gastrointestinal tract, transport of spermatozoa, in the ducts efferent of the male reproductive tracts and in the cervical canal, in movement of ovum in the female fallopian tube, in the vasomotion of small blood vessels and in biomedical systems including roller and finger pumps etc. In realistic prospective number of phenomenons such as food mixing and chyme movement in the intestine, flow of plasma, flow of blood, a Bingham fluid, flow of nuclear fuel slurries, flow of liquid metals and alloys, flow of mercury amalgams and lubrication with heavy oil and greases would not follow the Newtonian laws of viscosity. Therefore, for such kind of applications it would be more appropriate if the non-Newtonian behaviors of the fluids are taken into account. Due to complexity of non-Newtonian fluids various researchers have taken different kinds of fluids. Some interesting studies dealing different kinds of non-Newtonian fluid models are given in Refs. [7–21]. Keeping in mind the applications of non-Newtonian fluid model and the non-linear nature of the governing equation, the aim of the present paper is to consider the constitutive equation of a fluid model known as Williamson model. To the best of the author's knowledge, the peristaltic flow of a Williamson model has not been discussed by anyone. In the Williamson model, the apparent viscosity varies gradually between μ_0 at zero shear rate, and μ_∞ as the shear rate tends to infinity [22]. The governing equations for two dimension flow are modeled and have been solved using regular perturbation for an asymmetric channel. It is found that the solutions of the viscous fluid can be recovered from our analysis. The pertinent parameters have been discussed pictorially.

* Corresponding author.

E-mail address: snqau@hotmail.com (S. Nadeem).